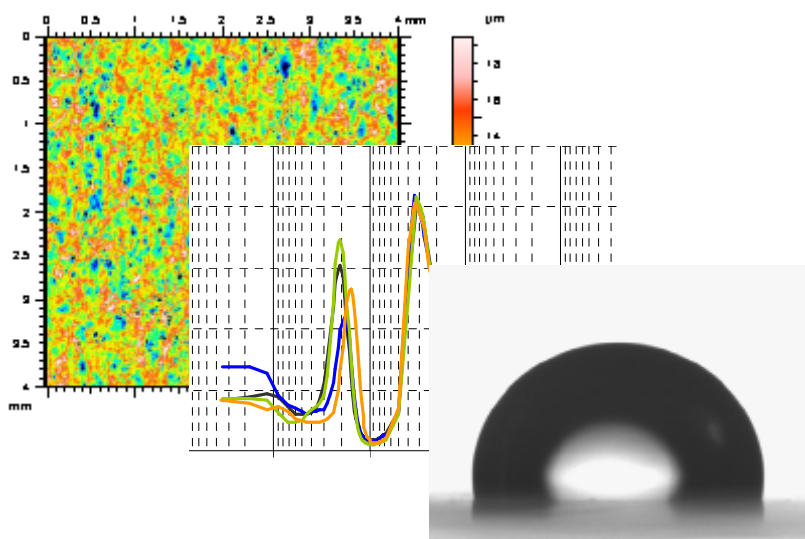


Physical & Chemical Interactions on Paper Surface – Impact on the Printability of Papers Produced with *E. globulus* Kraft Pulps

Isabel Maria Teixeira Moutinho



Physical & Chemical Interactions on Paper Surface –
Impact on the Printability of Papers Produced with E.
globulus Kraft Pulps

Isabel Maria Teixeira Moutinho

UNIVERSIDADE DE COIMBRA
Faculdade de Ciências e Tecnologia
2009

Dissertation submitted to Coimbra University for the degree of Doctor of Philosophy in
Chemical Engineering (Chemical Processes)

...

Tese submetida à Universidade de Coimbra para a obtenção do grau de Doutor em
Engenharia Química – Especialidade de Processos Químicos.

Coimbra – Portugal

2009

ACKNOWLEDGMENTS

I would like to express my warmest thanks to all those who contributed, in one way or another, to the conclusion of this work, but especially to:

- Prof. Margarida Figueiredo and Prof. Paulo Ferreira. Without their guidance, academic insight and patience, such a study would never have been accomplished.
- Prof. Graça Carvalho, Prof. Helena Gil and Prof. Jorge Coelho for their help and critical thinking during the various phases of the work.
- Eng. José Luis Amaral, Eng. Paulo Mendes Sousa and Dra. Fernanda Paula from RAIZ for their support and contribution for the execution of some stages of the experimental work.
- FCT (Fundação para a Ciência e a Tecnologia) and *grupo* Portucel Soporcel for the financial support and valuable information shared, vital for this work.
- The staff of the Chemical Engineering Department of the Coimbra University for their help throughout the several years that I have been developing my experimental work.
- Nuno Oliveira for his important help and support during all the work.
- My new co-workers, particularly to Vitor Crespo, João Breda, Maria José Heitor and Marta Fortunato for their encouragement during the final stage of the work.

Finally, I would like to express my gratitude and infinite thanks to:

- My parents, my sister and my brother, for their continued support during this important stage of my education and my life.
- André, for his help and support during most of the duration of this work.
- Sónia, for her help, companionship, friendship and endless patience and support during all these years.
- Carla, for her important help, support, friendship and for the great years of co-work.
- Gus, Marco and PASO, for their friendship, help and infinite support.

RESUMO

Actualmente assiste-se a uma crescente exigência dos consumidores relativamente à qualidade dos papéis de impressão e escrita (P&W), especialmente no que respeita à sua imprimabilidade. As interacções tinta-papel são afectadas quer pelas propriedades físico-químicas da superfície do papel quer pelas propriedades da matriz fibrosa, pelo que não apenas o tratamento final da superfície mas, em geral, todas as operações do processo de produção condicionam o desempenho do papel em termos de impressão. Neste contexto, a modificação química da superfície do papel é hoje em dia uma prática comum para aumentar a qualidade de impressão, sendo a colagem superficial uma operação corrente em qualquer fábrica de papel.

Tradicionalmente, é utilizada uma solução de amido para o tratamento superficial de papéis de impressão e escrita, a fim de melhorar propriedades como a resistência superficial ou imprimabilidade. No entanto, recentemente têm vindo a ser usadas formulações de colagem superficial à base de misturas de amido catiónico com pequenas percentagens de copolímeros sintéticos, de modo a realçar os efeitos da colagem superficial, particularmente no que diz respeito à energia de superfície, carácter hidrofílico e afinidade para com diferentes tipos de tinta. O objectivo principal é o de otimizar os processos de absorção e espalhamento das tintas de impressão, e assim favorecer a qualidade de impressão.

O principal objectivo do presente trabalho é precisamente analisar o impacto da aplicação de diferentes formulações de colagem superficial, constituídas por misturas de amido e um agente de colagem, tanto nas propriedades superficiais do papel como na qualidade de impressão. Para tal foram utilizadas misturas de amido catiónico com 10 copolímeros distintos, em três percentagens diferentes de copolímero (5%, 10% e 20% w/w), num total de 30 formulações. Estas formulações foram devidamente caracterizadas e depois aplicadas na superfície de folhas de papel não revestido produzido com base em pasta kraft branqueada de *E. globulus* e procedeu-se à análise exaustiva das respectivas superfícies, designadamente em termos de lisura, porosidade e algumas propriedades químicas, como a energia de superfície e o carácter ácido-base da superfície. O papel tratado com 100% de amido catiónico foi tomado como amostra de referência. Foram utilizadas diversas técnicas de caracterização, como perfilometria óptica, porosimetria de mercúrio, medição dos ângulos de contacto e cromatografia gasosa de fase inversa (IGC).

Complementarmente, usou-se ainda Microscopia de Força Atómica, Espectroscopia Electrónica para Análise Química e Espectroscopia de Lão Secundário, a fim de esclarecer aspectos mais específicos em algumas das amostras. Por fim, procedeu-se à avaliação da qualidade de impressão inkjet nas diferentes amostras, através quer da determinação de vários parâmetros de qualidade de impressão quer da análise das amostras impressas por um painel de utilizadores finais deste tipo de papéis. Estes resultados foram correlacionados com os provenientes da caracterização da superfície do papel, recorrendo a PLS (*Partial Least Squares*). Todos os resultados experimentais foram sujeitos a uma análise de variância (ANOVA) e análise de componentes principais (PCA - *Principal Component Analysis*) por forma a avaliar a variabilidade intra e inter-amostras. Esta variabilidade foi analisada de modo sistemático tendo em conta os tratamentos de superfície aplicados.

O estudo desenvolvido revelou que os tratamentos de colagem na superfície do papel têm um impacto pouco significativo em parâmetros físicos, como os determinados por perfilometria ou por porosimetria de mercúrio, mas influenciam decisivamente as propriedades químicas da superfície das amostras. Com efeito, as diferentes formulações testadas conduziram a níveis de energia de superfície e de carácter ácido-base, avaliados pela medição dos ângulos de contacto e por IGC, significativamente diferentes. Estas diferenças permitiram detectar e interpretar os efeitos quer da natureza quer da quantidade de copolímero incorporado nas formulações, conduzindo ainda a uma melhor compreensão das interações de natureza físico-química que ocorrem à superfície do papel quando este é sujeito a tratamentos de colagem superficial para optimização do processo de impressão inkjet.

Por último, é de sublinhar que os resultados obtidos neste trabalho se revestem do maior interesse para a indústria papeleira nacional, na medida em envolvem o seu mais importante produto – os papéis não revestidos para impressão e escrita –, para o qual não há estudos sistemáticos publicados com as formulações testadas. Além disso, a selecção das formulações e dos copolímeros teve em conta a viabilidade da sua aplicação industrial.

ABSTRACT

The consumer's demand for quality in printing and writing paper grades (P&W) is increasing, especially in what concerns printability.

Paper-ink interactions are strongly dependent on the structural and chemical properties of the paper surface. These properties are the result not only of specific surface treatments but also of the properties of the fibrous matrix, namely the quality of the pulp fibers. Therefore final printing quality performance of the paper is influenced, in general, by all the operations in the papermaking process. For this reason the chemical modification of the paper surface in order to improve printing quality is nowadays a common practice in papermaking, and surface sizing is a standard operation in many paper mills.

Typically – and especially for P&W papers - starch is used for surface sizing, with the main goal of improving paper surface resistance and printability. However, there is an increasing tendency to use blends of cationic starch and synthetic copolymers to enhance surface sizing effects by controlling the paper surface energy, the corresponding hydrophilic character and the affinity towards different types of ink. The main objective of this approach is to improve print quality by optimizing the balance between the absorption and spreading phenomena.

This work targets the analysis of the impact of the application of different surface sizing formulations, composed of blends of cationic starch and minor quantities of distinct copolymers, in the chemical and physical surface characteristics of the modified paper samples and in the final printing quality. Ten distinct copolymers were blended with cationic starch in three different percentages of copolymer (5%, 10% and 20% w/w), resulting in a total of 30 different formulations. These formulations were characterized and applied to the surface of an *E. globulus* bleached kraft pulp based uncoated paper, and the corresponding paper surfaces were fully characterized with respect to some structural properties, namely roughness and porosity, as well as some chemical properties, namely surface energy and acid-base character. A sample surface sized only with cationic starch was taken as reference. Several characterization techniques were used, namely laser profilometry, mercury porosimetry, contact angle measurements and inverse gas chromatography (IGC). Selected samples were additionally analyzed by Atomic Force Microscopy, Electron Spectroscopy for Chemical Analysis and Time-of-Flight Secondary Ion Mass Spectroscopy, in order to clarify specific aspects. Finally, the influence of the different sizing agents on the printing quality of the samples was investigated by quantifying several parameters in a

specific inkjet printed mask and also by using the results of an evaluating panel composed of several end users of this type of papers.

The results from the printing tests were correlated to those obtained from the characterization of the paper surfaces by using Partial Least Squares. All the data were submitted to an analysis of variance (ANOVA) and Principal Component Analysis (PCA) in order to evaluate inter and intra-samples variability. This variability was thoroughly analyzed and interpreted in terms of the corresponding surface treatments.

The results revealed that the surface sizing treatments used in this study have a minor impact on the surface roughness and porosity, but a substantial influence on surface energetics. In fact, relevant differences were detected in the surface energy and acid-base character of the sized samples, as measured by contact angle and IGC. These differences enabled the interpretation of the influence of the nature and quantity of the copolymers used in the sizing formulations and simultaneously a better understanding of the physical and chemical interactions that occur at paper surface when it is subjected to a sizing treatment in order to optimize the inkjet printing process.

Finally, it should be pointed out that the results are of the utmost importance to the national paper industry as they relate to its most relevant product – the eucalyptus based printing and writing uncoated papers – for which there are no published results involving the tested formulations. Furthermore, both the copolymers and the formulations used were selected having in mind the feasibility of their application in the paper industry.

INDEX

ACKNOWLEDGMENTS	VII
RESUMO	IX
ABSTRACT	XI
INDEX	XIII
NOMENCLATURE AND UNITS	XIX
CHAPTER 1	1
1 INTRODUCTION	3
1.1 HISTORY.....	3
1.2 PAPER PRODUCTION	6
1.3 PAPER SURFACE TREATMENTS	7
1.3.1 Surface Sizing.....	8
1.4 CHARACTERIZATION OF PAPER SURFACE	13
1.5 PRINTING	13
1.5.1 Printing Quality	17
1.6 ABOUT THE WORK	17
CHAPTER 2	21
MATERIALS AND METHODS	21
2 MATERIALS AND METHODS	23
2.1 SURFACE SIZING	24
2.1.1 Equipment and Methodology	24
2.1.2 Sizing Formulations	26
2.2 CHARACTERIZATION OF THE SURFACE SIZING AGENTS.....	27

2.3	PHYSICOCHEMICAL CHARACTERIZATION OF THE PAPER SAMPLES	27
2.4	PRINTING QUALITY EVALUATION.....	30
CHAPTER 3	31
3	CHARACTERIZATION OF THE SIZING CHEMICALS	33
3.1	SIZING AGENTS COMPOSITION	34
3.2	SIZING AGENTS PROPERTIES.....	38
CHAPTER 4	41
4	PROFILOMETRY	43
4.1	THEORY.....	43
4.1.1	Roughness Parameters Definition.....	44
4.1.1.1	Amplitude Parameters	45
4.1.1.2	Spatial Parameters.....	48
4.1.1.3	Hybrid Parameters.....	49
4.1.2	Roughness Measurement Techniques and Equipments.....	51
4.1.2.1	Equipment - Altisurf® 500	53
4.2	RESULTS.....	58
CHAPTER 5	65
5	MERCURY POROSIMETRY.....	67
5.1	THEORY.....	67
5.1.1	Measurement Techniques.....	67
5.1.1.1	Mercury Porosimetry	68
5.1.1.2	Equipment - AutoPore IV 9500	69
5.2	RESULTS.....	71

CHAPTER 6	77
6 CONTACT ANGLE MEASUREMENTS	79
6.1 THEORY.....	79
6.1.1 Fundamental Interactions.....	79
6.1.2 Surface Energy Calculation Theories	81
6.1.2.1 Zisman	81
6.1.2.2 Owens, Wendt, Rabel and Kaelble.....	82
6.1.2.3 Fowkes	83
6.1.2.4 van Oss & Good	84
6.1.3 Contact Angle Measurements.....	85
6.1.3.1 Equipment – OCA 20.....	86
6.1.4 Topography Influence in Contact Angle Values.....	89
6.1.5 Dynamic Parameters	91
6.2 RESULTS.....	92
6.2.1 Effect of Topography.....	93
6.2.2 Static Contact angles	94
6.2.3 Surface Energies	97
6.2.4 Dynamic Contact Angles.....	102
CHAPTER 7	115
7 INVERSE GAS CHROMATOGRAPHY (IGC)	117
7.1 THEORY.....	119
7.1.1 Dispersive Component of the Surface Free Energy.....	120
7.1.2 Acid-Base Character	121
7.1.3 Equipment - DANI GC 1000.....	123
7.2 RESULTS.....	126
7.2.1 Retention Times.....	127
7.2.2 Dispersive Component of the Surface Energy.....	130

7.2.3	IGC versus Contact Angle in the Determination of σ_s^D	134
7.2.4	Acid-Base Character	136
CHAPTER 8	141
8 PRINTING QUALITY	143
8.1	THEORY.....	143
8.1.1	Inkjet Printing	143
8.1.2	Printing Quality Evaluation	147
8.1.2.1	Inkjet Printing Quality Parameters.....	148
8.1.2.2	Methodology	151
8.2	RESULTS.....	154
8.3	CORRELATIONS AND MODELS	161
CHAPTER 9	167
9 COMPLEMENTARY STUDIES	169
EFFECT OF SURFACE SIZING ON THE SURFACE CHEMISTRY OF PAPER CONTAINING EUCALYPTUS PULP.....		
CLXXI		
ON THE EVALUATION OF THE TOPOGRAPHY OF SURFACE SIZED EUCALYPTUS BASED PAPERS		
CXCI		
CHAPTER 10	205
10 CONCLUSIONS	207
CHAPTER 11	213
11 REFERENCES	215
FIGURES INDEX	I

TABLES INDEX	IX
APPENDIX	I
APPENDIX A	III
DATASHEETS OF THE SYNTHETIC SURFACE SIZING AGENTS.....	III
APPENDIX B	XXXV
SURFACE SIZING FORMULATIONS.....	XXXV
APPENDIX C	XXXVII
PROFILOMETRY RESULTS	XXXVII
APPENDIX D	XLI
1 1.1 MERCURY POROSIMETRY RESULTS	XLI
APPENDIX E	XLVII
CONTACT ANGLE MEASUREMENTS.....	XLVII
APPENDIX F	LVII
INVERSE GAS CHROMATOGRAPHY.....	LVII
APPENDIX G	LXXV
PRINTING QUALITY PARAMETERS	LXXV

NOMENCLATURE AND UNITS

a – Cross-section area of the probe

AFM – Atomic Force Microscopy

AN – Gutmann's acceptor number

AN* - Gutmann's modified acceptor number

ANOVA – Analysis of Variance

BD – Drop base diameter

CA – Contact angle ($^{\circ}$)

ΔG – Free energy of adsorption

ΔH – Enthalpy of Adsorption

DN – Gutmann's donor number

ΔS – Entropy of adsorption

ESCA - Electronic Spectroscopy for Chemical Analysis

IGC – Inverse Gas Chromatography

IR – Infra Red

J – Correction factor for gas compressibility

K_a – Acidic constant

K_b – Basic constant

N – Avogadro's number

OBA – Optical Brightening Agent

OD – Optical density

OWRK – Owens Wendt Raelbe and Kaelbe

P – Pressure

PA – Printed Area

P&W – Printing and Writing

PCA – Principal Components Analysis

Pick-up – Amount of Surface Sizing applied (g/m^2)

PLS – Partial Least Squares

θ – Contact angle ($^\circ$)

R – Ideal gas constant

R^* – Correction factor for the topography influence in the contact angle values

σ – Surface energy/tension (mN/m)

S_a – Roughness average (μm)

S_{dq} – Root-mean-square slope of the surface ($\mu\text{m}/\mu\text{m}$)

S_{dr} – Developed interfacial area ratio (%)

S_{ds} – Density of summits of the surface (pks/mm^2)

S_{ku} – Kurtosis of the height Distribution

S_p – Maximum height of summits (μm)

S_q – Root-mean-square deviation of the surface (μm)

S_{sc} – Arithmetic mean summit curvature of the surface ($1/\mu\text{m}$)

S_{sk} – Skewness of the height distribution

S_t – Total height of the surface (μm)

S_{tr} – Surface texture isotropy

Subscript _L – Liquid

Subscript _s – Solid

Subscript _{sl} – Solid-liquid interface

Superscript ^{AB} – Acid-base

Superscript ^D - Dispersive

Superscript ^P – Polar

Superscript ^S – Specific

S_v – Maximum depth of the surface (μm)

Sz – Ten point height of the surface (μm)

T – Temperature

TA – Target Area

ToF-SIMS – Time of Flight Secondary Ion Mass Spectroscopy

Tr – Retention time (min)

Vn – Retention volume (ml)

Vol – Drop volume

Wa – Work of adhesion (mN/m)

WV – Wetting velocity

CHAPTER 1

INTRODUCTION

1 INTRODUCTION

Paper has played a vital role in the cultural development of mankind, being used mainly for writing, printing, and packaging. It plays a key role in communication; printed communication is almost synonymous with paper. Papermaking is a vast, multidisciplinary technology that has expanded tremendously in recent years. Significant advances have been made in all areas of papermaking, including raw materials, production technology, process control and end products. The complexity of the processes, the scale of operation, and production speeds leave little room for error or malfunction. Modern papermaking would not be possible without a proper command of a great variety of technologies. Along the years not only has the technology progressed and new technology emerged, but also the understanding of the fundamentals of unit processes, raw materials and product properties have also deepened considerably. Paper products are complex in structure and contain many different components. The requirements placed on the way these products perform are wide, varied and often conflicting. Product development and improvements is thus a constant need and requires a profound understanding of the chemistry and physics of both raw materials and product structures (Oittinen and Saarelma 1998; Lehtinen 2000; Levlin and Söderhjelm 2000)

1.1 HISTORY

Following the evolution of the human intelligence, the graphical representations became increasingly complex, and together with an increase in the ability to create tools, took to the development of more adequate supports. The history tells about the use of boards, cooked clay, tissues of various fibers, papyrus, parchment and finally paper (Oittinen and Saarelma 1998; Lehtinen 2000; Paulapuro 2000).

Clay seems to have been the first material used explicitly for writing, by Sumerians, 6 millennia B.C.. The manuscripts on dry palm leaves appeared after the invention of the alphabet, and they were used mainly in India and Southeast Asia until the 19th century. In Greece appeared the waxed boards, which the Romans have also adopted. About 3 thousand years B.C. it was found out the possibility of the adaptation for writing of thick stem plants, which grew in the margins of the Nile River and were called “Papyrus”. Many years after, the Romans improved the papyrus quality, by pasting the fibers to each other with

starch glues. Papyrus was in fact the main mean for writing communication until the 8th century. (Oittinen and Saarelma 1998; Lehtinen 2000; Paulapuro 2000).

The primacy of paper production is assigned to Ts'ai Lun of china in the year 105 After Christ, who made paper of fishing nets and rags pulp, and later using vegetable fibers. In Europe, paper was first manufactured in Spain and Sicily, and gradually its use spread northward (Lehtinen 2000; Paulapuro 2000).

When the paper demand rapidly increased in the eighteenth century, papermakers in Continental Europe came up with the idea of developing a machine for forming the paper.

Nicolas-Louis Robert (1761-1828) has gone down in history as the inventor of a continuously moving belt of wire cloth on which the fiber suspension was spread and the water was allowed to drain away, leaving an endless sheet of paper on the wire. The first trials were made as early as 1793, but only in 1798 a construction on which a continuous web of paper could be made. The wooden machine was 260 cm long, and the width of the paper was 64 centimeters (Lehtinen 2000; Paulapuro 2000).

In 1807, a patent for a machine with the essential features of the "fourdrinier" machine we know today was procured in the names of the Fourdrinier brothers (Henry and Sealy) and John Gamble (Lehtinen 2000; Paulapuro 2000).

In the 1820s in England, machine-produced paper surpassed in quantity the hand-paper production. Around 1840, there were about 250 paper machines in operation in England, 125 in France, and 50 in Germany, the majority of which were of English origin (Lehtinen 2000; Paulapuro 2000).

Along the years many individuals and companies obtained patents on the basic components in the process. Improvements at each stage of the papermaking process have contributed to the exceptional speed, runnability, and reliability of today's paper machines. Figure 1.1 shows the exponential increase in maximum operating speeds of paper machines (Lehtinen 2000; Paulapuro 2000).

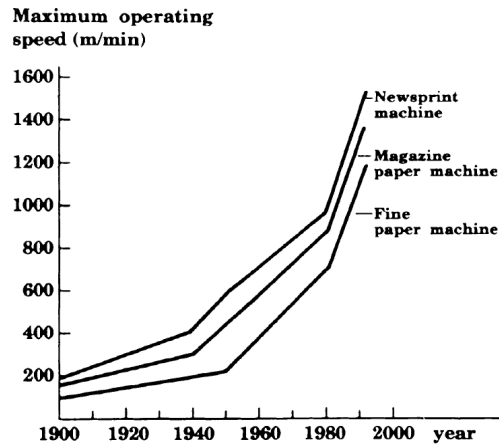


Figure 1.1 - Trends in maximum operating speeds of paper machines (Paulapuro 2000).

Papers can be graded in several ways, some of the main criteria used to classify papers include basis weight, fiber furnish, type of surface finish or end use, as depicted in Table 1.1 (Oittinen and Saarelma 1998; URL 4 2009).

Table 1.1 – Classification of papers according to different criteria.

Criteria	Papers
Basis weight	<i>Tissue</i> : Low weight, <40 g/m ² <i>Paper</i> : Medium weight, 40 - 120 g/m ² <i>Paperboard</i> : Medium High weight, 120-200 g/m ² <i>Board</i> : High weight, >200 g/m ²
Color	<i>Brown</i> : Unbleached <i>White</i> : Bleached <i>Colored</i> : Bleached and dyed or pigmented
Usage	<i>Industrial</i> : Packaging, wrapping, filtering, electrical etc. <i>Cultural</i> : Writing, printing, Newspaper, currency etc. <i>Food</i> : Food wrapping, candy wrapping Coffee filter, tea bag etc.
Raw Material	<i>Wood</i> : Contain fibers from wood <i>Wood Free</i> : Bleached <i>Agricultural residue</i> : Fibers from straw, grass or other annual plants <i>Recycled</i> : Recycle or secondary Fiber
Surface Treatment	<i>Coated</i> : Coated with clay or other mineral. <i>Uncoated</i> : No coating <i>Laminated</i> : aluminum, poly etc

The present work is focused on printing and writing paper (P&W), which is, according to the above table, an Uncoated Wood Free paper.

1.2 PAPER PRODUCTION

Paper is obtained by a mixture of fibers, typically from vegetal origin composed by cellulose, which are kept together by hydrogen bridges. The most common source of natural fibers is the pulp obtained from the wood of threes. Vegetal fibers such as cotton, hemp, flax and rice can also be used. Usually, and regarding printing and writing (P&W) papers in particular, composition also includes filler and additives (Oittinen and Saarela 1998; Lehtinen 2000; Paulapuro 2000).

The papermaking process contains a great number of different unit processes, which work through different mechanisms to produce the desired effects on the fiber suspension, and subsequently, on the fibrous web. It starts with slushing of fibers and other raw materials in water, continues through paper machine and finishing operations and ends with packaging of the paper. The papermaking process is essentially a very large drainage operation. Figure 7.12 presents the main sections of a paper mill, which comprise the stock preparation, paper machine and finishing and the typical layout of a P&W paper machine.

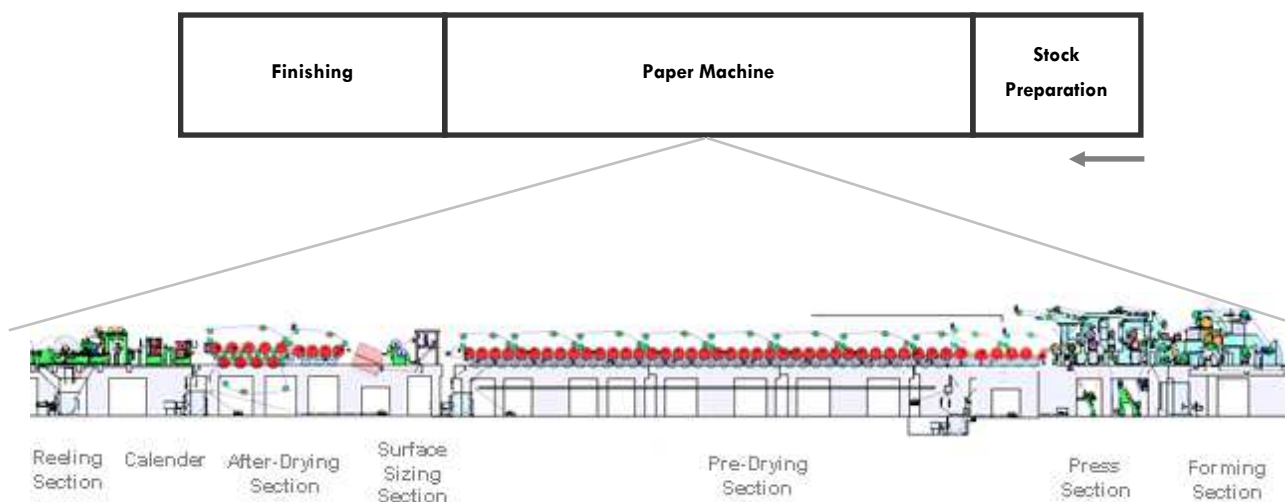


Figure 1.2 – Schematic representation of the production process for printing and writing papers.

Consistency of the stock flow entering the paper machine forming section is typically between 0.2% and 1.0% (2 - 10 g fiber per kg water). After drainage on the wire of the forming section using gravitation, pulsation, or vacuum, the web consistency increases to 15% - 25%. Mechanical compression removes water on the press section. The web consistency (now called dry solids content) then increases to 33% - 55% depending on the paper grade and press section design. After the press section, the web enters the pre-dryer section where evaporation, removes the remaining water. However, a small amount of moisture (2% - 5%)

remains in the paper before the surface sizing operation, after which the paper web enters in the after-drying section, to achieve the final moisture content typically between 5% and 7% (Oittinen and Saarelma 1998; Lehtinen 2000; Paulapuro 2000).

Although the principles of paper manufacturing are similar to the ones developed many centuries ago, significant advances have been made in all areas of papermaking, including raw materials, production technology, process control and end products. As mentioned in the very beginning of this work, at the present time, the complexity of the processes, the scale of operation, and the production speeds leave little room for error or malfunction. Paper must maintain its competitiveness through continuous product development in order to meet the ever-increasing demands on its performance. This framework is the main driving force for many studies on paper, with a great focus on paper surface in the most recent years, mainly due to the increasing importance given to paper ink interactions, which are mainly ruled by the paper surface properties (Oittinen and Saarelma 1998; Lehtinen 2000; Paulapuro 2000).

1.3 PAPER SURFACE TREATMENTS

Currently, paper surface has been the subject of many attentions, since it is one of the crucial factors affecting the final performance of the paper. Paper surface treatments are thus increasingly used in every paper mill to control and improve the surface properties of its product. These surface treatments may be physical (calendering) or chemical (surface sizing or coating) (Keskitalo 2000; Levlin and Söderhjelm 2000).

In the production of P&W papers, the physical treatment of the surface by calendering and the chemical treatment by surface sizing are generally always used. Coating is a chemical surface treatment rarely applied for this type of papers; it is currently used for many other paper grades such as magazine paper or photographic paper (Lehtinen 2000).

Calendering consists in submitting the paper to pressure, by passing it between rolling cylinders. The main target of calendering is to modify the surface structure and/or the sheet thickness. In the case of printing, the main calendering targets are to reduce surface roughness and compress the pore structure to obtain a good printing result. Two different options can be used for calendering: hard rolls, made from cast iron or soft rolls, with polymer coverage. The latter distribute the calendering pressure more evenly creating a

more uniform surface finish and are currently the option preferably used in the industry (Oittinen and Saarelma 1998).

Regarding the chemical treatment, it should be mentioned that the main difference between coating and surface sizing is that the former involves pigments in the solution that is applied to the paper surface, in concentrations that are in general larger than 3.5 g/m². Pigments such as clay, talc, and calcium carbonate are often used to produce the coating formulations in order to further enhance the printability of fibrous sheets (Oittinen and Saarelma 1998) (Donigian et al. 1997; Nissi et al. 1999; Lohmander and Rigdahl 2000; Ahlroos and grön 2001; Fardim 2002; Conceição et el. 2003; Forsström et al. 2003; Ridgway and Gane 2003; Garcia 2004; Putkisto et al. 2004; Engström 2005).

Surface sizing is the subject this work and will be detailed in the following section.

1.3.1 SURFACE SIZING

Surface sizing is a common operation in any paper mill of P&W papers. It consists in the application of an aqueous suspension composed of several functional chemicals at the surface of the paper, mainly to improve surface resistance, increase paper stiffness and improve paper printability.

There are two types of formulations that can be used in surface sizing: starch alone or starch combined with a synthetic surface sizing agent. The most common option in the industry is to perform surface sizing by using starch alone (usually modified starch - cationic), however there is an increasing tendency, already applied in several paper mills, to combine the cationic starch with some synthetic surface sizing agents (Browning 1977; Bauer et al. 1999; Sequera 1999; Keskitalo 2000; Lehtinen 2000; Lee et al. 2002; Carceller and Juppo2004; Andersson et al. 2006; Prinz and Schultz 2007).

When both starch and synthetic surface sizing agents are used, the most important function of the starch is to act as a binder, in order to produce an even blend. As for the synthetic surface sizing agents, their use is often necessary because the primary raw material of paper and paperboard is the hydrophilic component cellulose. As these synthetic surface sizing agents are usually polymers with some degree of hydrophobicity, the paper surface becomes water resistant, which is crucial for many printing processes (Oittinen and Saarelma 1998; Keskitalo 2000; Lehtinen 2000; Glittenberg and Leonhardt 2007).

It should be pointed out that besides starch (usually cationic) and, in some cases, the synthetic surface sizing agents, the sizing formulations include additional compounds, such as salt, optical brightener agents (OBA) and defoaming agents.

Starch is a natural polymer consisting of glucose monomers. It is the second most abundant biologically produced organic material after cellulose. Chemically, the starch polymer is much like cellulose. The difference lies in the structure which gives these two materials different properties, as illustrated in Figure 1.3 (Bauer et al. 1999; Lehtinen 2000).

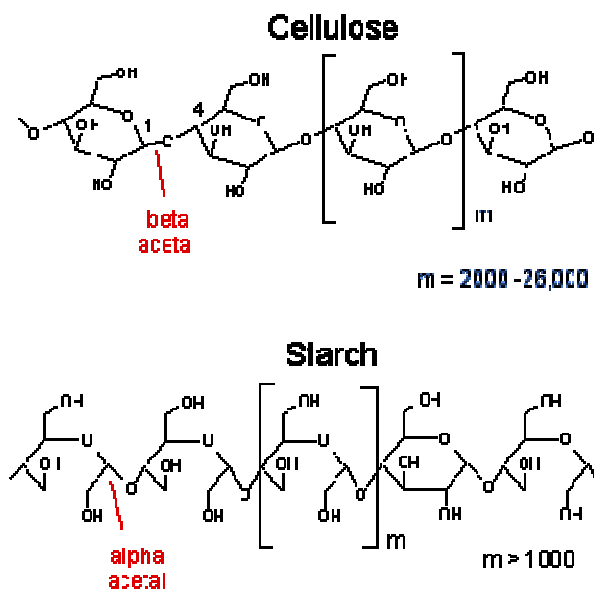


Figure 1.3 - Structure of starch and cellulose.

As indicated in Figure 1.3, the difference relies in the way glucose monomers are bonded. The bonds between glucose units are called glycosidic bonds, and their orientation is different in cellulose and starch. In starch, all glycosidic bonds are oriented in the same direction whereas, in cellulose, the orientation of two consecutive bonds is opposite. This is the reason for cellulose being a straight polymer while starch is coiled. Cellulose forms fibers, which are partly crystalline, while starch is totally amorphous and forms granules with different shapes and sizes depending on which plant they come from (corn, wheat, potato, and tapioca are common sources) (Bauer et al. 1999; Lehtinen 2000).

In the paper industry, the starch is previously cooked by steam. During the cooking process, the starch granules start to swell, at $40^{\circ}\text{C} - 50^{\circ}\text{C}$, and after that, the starch polymers start to

dissolve. Starch has binding properties only in the dissolved form (see Figure 1.4) (Bauer et al. 1999; Lehtinen 2000).

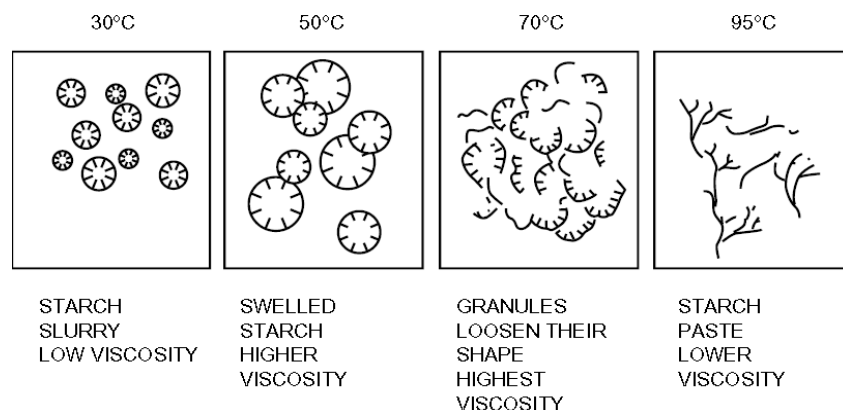


Figure 1.4 - Starch during cooking.

Cooked native starch tends to be very viscous and forms gels at very low dry solids. This behavior is called retrogradation because the starch polymers strive to rebind to each other and to form irreversible gels. Thus, starch for surface sizing is usually modified to ensure its good functionality, by improving and/or controlling its binding power, rheology, viscosity-temperature stability, and tendency to degradation. In the particular case of the starch modified for application in surface sizing, the most important modification that it is submitted is cationization, making it positively charged, by the addition of H^+ functional groups, in order to increase the affinity for the anionic surface of the cellulose fibers (Bauer et al. 1999; Lehtinen 2000; Glittenberg and Leonhardt 2007).

The synthetic surface sizing agents are usually polymeric compounds, totally or partially hydrophobic. Typically the chemical bases used to produce synthetic surface sizing agents are styrene, maleic anhydride, acrylic acid, ester or polyurethanes (Brandão 1999; Exner 2001; Sreekumar et al. 2007; Prinz and Schultz 2007).

When combined with starch, a thin reticular film is formed at the paper surface, as depicted in Figure 1.5. This film influences several paper properties such as smoothness, surface resistance, surface free energy and hydrophobicity.

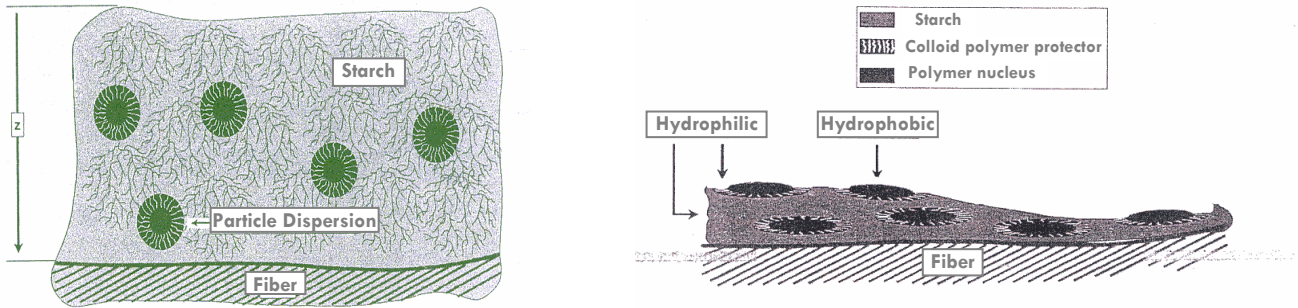


Figure 1.5 - Polymer-starch film formation on paper surface.

In terms of industrial application of surface sizing, a revolutionary change over the years has undergone in terms of equipments. Until the beginning of the 1980's, the pond size press technology was the most used. In this system, the paper passes through a pond with the sizing blend and after, between two cylinders, as depicted in Figure 1.6 (Lehtinen 2000).

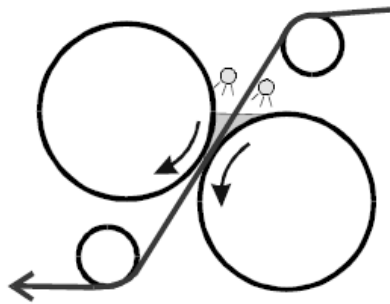


Figure 1.6 – Schematic representation of a pond size press.

This main advantage of this technology presented is the penetration depth of the sizing blend, giving z-directional strength to the paper. However, it limited paper machine speeds to approximately 1000 m/min. The main breakthrough in surface sizing technology, introduced in the 1980's, was the appearance of the film size press technology. In this method, the sizing blend is applied in the rolls, in the desired amount, and not directly onto the paper. The paper is passed through those rolls to allow the transfer of the blend, as depicted in Figure 1.7 (Oittinen and Saarelma 1998; Lehtinen 2000).

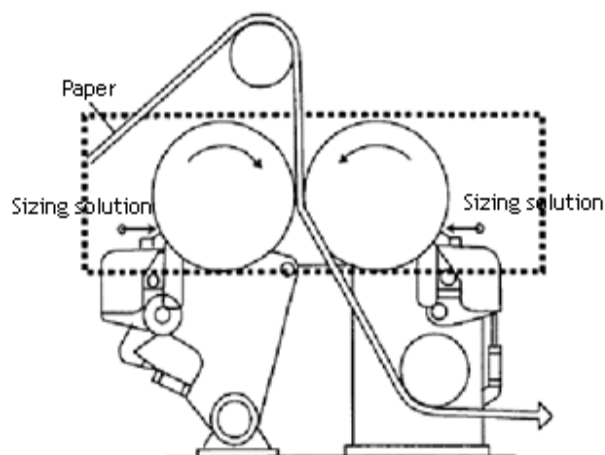


Figure 1.7 – Schematic representation of a film size press.

One of the main advantages of the film press technology is the metering elements that allow uniform films to be formed on the transfer roll surface. During the last years, film presses were the technology selected for the new woodfree paper machines installed and at the same time, most pond size presses on larger machines have been converted into film presses. The introduction of the film press technique has improved surface properties, such as dusting of the paper surface, due to reduced sizing penetration (Keskitalo 2000; Lehtinen 2000).

Regardless the technology used, the surface sizing operation is affected by the sizing formulation properties (composition, viscosity, pH, temperature) as well as the base paper properties (basis weight, bulk, internal sizing, water content and surface energy, porosity and roughness). Thus, these properties must be adequately controlled, mainly in order to control the penetration of the surface sizing blend in the sheet structure.

Currently, this is an area of the papermaking process where many attention has been focused, due to the increasing importance attributed to the surface properties of the paper. Thus, this is a research area under high development and many related studies have been published in the open literature (Borch 1982; Aspler et al. 1987; Aspler et al. 1993; Mangin 1993; Lee et al. 2002; Ajerschi et al. 2004; Carceller and Juppo 2004; Laleg 2004; Lertsutthiwong et al. 2004; Mešić et al. 2004; Andersson et al. 2006; Glittenberg and Leonhardt 2007; Gu et al. 2007; Moutinho et al. 2007b; Olkkonen and Lipponen 2007; Prinz and Schultz 2007; Sreekumar et al. 2007; Ashori et al. 2008; Moutinho et al. 2008a).

1.4 CHARACTERIZATION OF PAPER SURFACE

The evaluation of the effect of any surface modification requires a deep knowledge of the paper surface characteristics. Surface characterization can be undertaken either from the physical or the chemical point of view, and many techniques have been used for that purpose.

Physical characterization of the paper surface is a more explored subject, since it is long established that properties such as porosity or roughness decisively influence paper performance. Thus profilometry (Gadelmawla et al. 2002; Wågberg and Johansson 2002; Barros 2004; Ashori et al. 2008; TrueGage 2008), mercury porosimetry (Knauf and Doshi 1986; Johnson et al. 1999; Moura et al. 2005), Scanning Electron Microscopy (SEM) (Chinga and Helle 2002b), Confocal microscopy (Conners and Banerjee 1995), and more recently, Atomic Force Microscopy (AFM) (Chhabra et al. 2005; Das et al. 2006), are now currently used to investigate the characterize paper.

Regarding the surface chemical properties, modern and sophisticated techniques have been implemented (or adapted) for the chemical characterization of paper sheets, namely contact angle measurements (Roe et al. 1967; Brigs et al. 1989; Marmur 2006), Fourier Transform Infrared Spectroscopy (FTIR) (Liu et al. 1998; Ernstsson 2005; Fardim and Durán 2005), Electronic Spectroscopy for Chemical analysis (ESCA/XPS) (Brinen 1993; Belgacem et al. 1995; Kangas and Kleen 2004), Inverse Gas Chromatography (IGC) (Gutierrez et al. 1999; Kunaver et al. 2004; Wang and Sain 2007), Time of Flight – Second Ion Mass Spectroscopy (ToF-SIMS) (Kleen et al. 2003; Koljonen 2004; Lee et al. 2006) and Raman Spectroscopy (Vyörykkä 2005). Most of these techniques were used in the present work, although some of them were only applied in some specific studies on a few samples, in order to complement this study. In both cases the main objective is to provide information about paper surface that enables a better knowledge of the surface performance, in particular the paper-ink interactions, most relevant for P&W papers. The basic principle of the techniques used for the majority of the samples will be described in later chapters together with the corresponding results.

1.5 PRINTING

Paper is definitely the most important raw material in printing. The techniques and procedures used to produce printed products have evolved tremendously specially over the

last century, as summarized in Table 1.2. The Chinese invented the oldest known printing method, letterpress, in the year 700. Since then, many and revolutionary steps have been given, especially in the 20th century, from flexography, gravure, and offset to the modern digital printing and techniques (Oittinen and Saarelma 1998; Keskitalo 2000).

Table 1.2 - Development of printing and other visualization methods.

Visualization Method	Year
Letterpress	700
Letterpress, metal type	1450
Lithography	1800
Photography	1820
Motion picture	1895
Gravure	1900
Flexography	1900
Television	1926
Photo copying	1940
Computer display	1973
Electronic printing	1980
Networked printing	1990
Electronic publishing on display	1990
Distributed color printing	1995

The traditional methods are usually called mechanical printing, in order to express the fact that the energy for image formation in the printing step is pressure. The term “mechanical” distinguishes conventional printing methods from electronic or digital printing methods, which are based on computer output.

Mechanical printing uses the rotary principle in which printing ink transfers to the paper in a nip between two rotating cylinders. The imaging steps during mechanical printing procedures include transfer of the ink to a plate, ink transfer from the plate to the paper, and ink drying (Oittinen and Saarelma 1998). Figure 1.8, Figure 1.9 and Figure 1.10 describe the basic principles of flexography, rotogravure and offset printing, respectively.

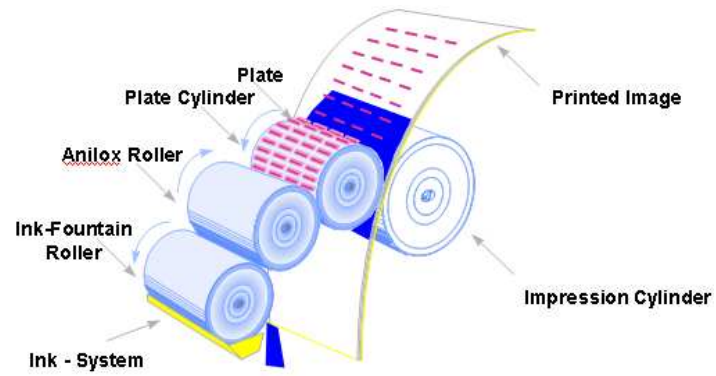


Figure 1.8 - Schematic representation of flexography printing principle.

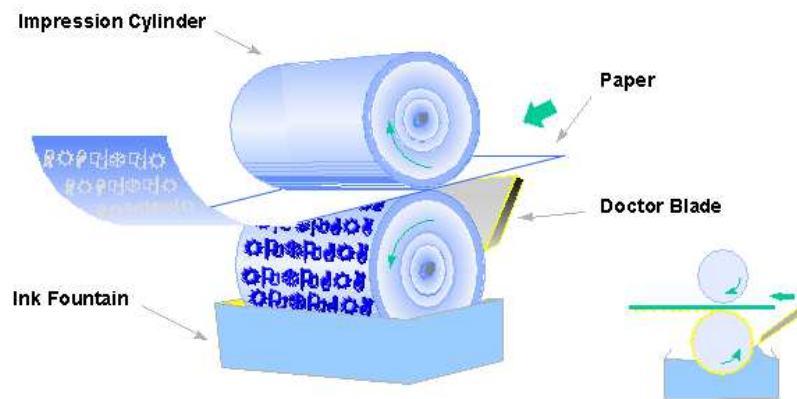


Figure 1.9 – Schematic representation of rotogravure printing principle.

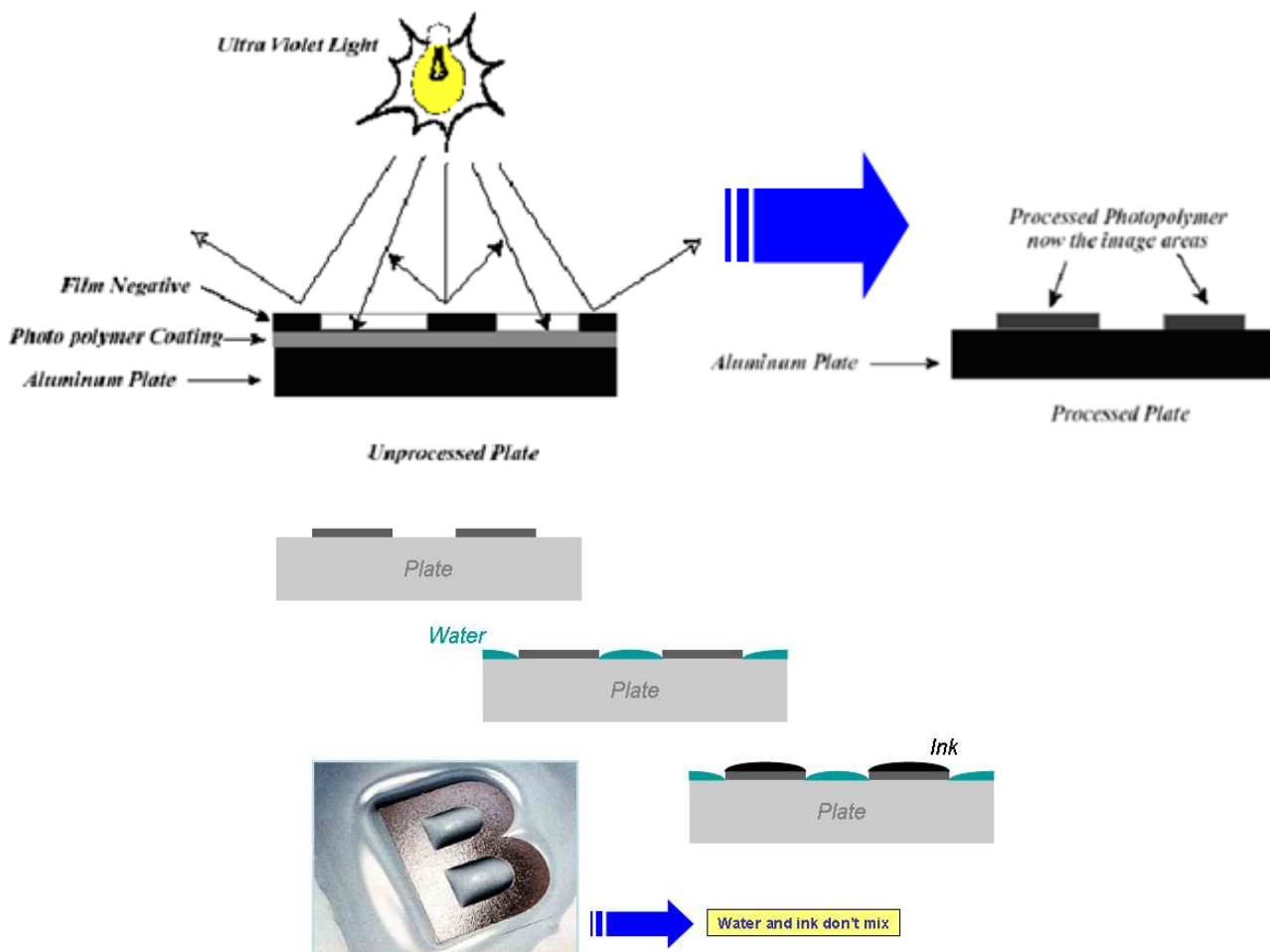


Figure 1.10 - Schematic representation of offset printing principle.

The term digital printing refers to printing methods where the page data is input directly from a computer system to the printing device, without intermediate steps, and the printed information can be varied from sheet to sheet (Oittinen and Saarelma 1998).

In digital printing methods, such as laser or inkjet printing there is no physical contact between the printing device and the paper. Laser printing, uses a laser to expose the non-image areas of a charged photoconductive drum, and the image areas, which remain charged, pick up a thin layer of oppositely charged toner particles. The drum then transfers the toner particles to the paper. In Inkjet printing by directing individual drops to a paper surface an image is created (Keskitalo 2000). Because of its ability to print on a variety of substrates, inkjet technology is also increasingly used in industrial printing and in the package printing industry (Svanholm 2004). And thus, due to its current and increasing importance in the printing market related to the paper type under study in this work, inkjet printing was the

method selected to perform printing quality evaluation in this work, and thus it will be further developed in Chapter 8.

1.5.1 PRINTING QUALITY

Regardless the printing method involved and the purpose of the printed material, printing quality evaluation is always done, as a control tool or at least by the final user of the printed material. Print quality definition does not have absolute terms it depends on interactions between paper and printing ink and the printing process variables (Oittinen and Saarelma 1998; Levlin and Söderhjelm 2000).

The performance of paper in printing depends on its runnability and printability. Runnability relates to the factors that determine how the paper runs in the press. Printability factors concern to quality of paper in relation to ink and printing (Oittinen and Saarelma, 1998). Thus, the final performance of a paper, in terms of printing quality achieved depends on the properties of the fibrous matrix and on the characteristics of the paper surface, which are influenced by the quality of the pulp fibers, the refining process, the chemicals added in the preparation of the furnish, the operations at the paper machine and the modifications of the paper surface (Levlin and Söderhjelm, 2000; Moutinho et al. 2007b).

Quantitative evaluation of printing quality is very difficult but very important, that is why in the last years the number of studies regarding this subject has increased substantially (Varnella 1998; Donigian et al. 1999; Keskitalo 2000; Chen et al. 2002; Donderi et al. 2003; Mattila et al. 2003; Rosenberger 2003; Glittenberg and Voigt 2004; Danby and Zhou 2004; Svanholm 2004; Lee et al. 2005; Yang et al. 2005; Olsson et al. 2006; Mäkenen et al. 2007; Sreekumar et al. 2007; Ungh et al. 2007)

1.6 ABOUT THE WORK

The work described in this thesis was motivated by the need of increasing the knowledge in specific fields related to paper ink interactions. This need was driven by the growing importance of the printing quality in the customer demands and by the recognition of paper surface modification as a major tool to improve the quality of many paper products as described in Section 1.3

Besides the scarce information on this topic in the open literature, the available information is not focused in printing and writing papers produced with eucalyptus *globulus* fibers, which is the core of the Portuguese papermaking industry. Thus this study is pioneer in the surface studies of paper and also and in particular in the context the Portuguese paper industry and research.

Before embracing this larger and longer work, a previous one was performed, as undergraduate student, whose main purpose was to compare the impact of different surface sizing agents on the surface properties and printing quality of paper sheets prepared in the laboratory. Despite the limitation of using handsheets, this work pointed out many aspects that required further investigation (Moutinho et al. 2004). Furthermore, it provided a first contact with this field, namely with the phenomena related to the interactions between paper and sizing formulation and/or printing inks as well as with techniques currently used to characterize the surface of the paper samples. This constituted the main incentive for this project that includes the present thesis, whose main objective is to analyze the effect of the addition of different types of synthetic surface sizing agents to the more classical surface sizing blend (composed of cationic starch) on the properties of commercial paper sheets, in particular, on inkjet printing performance. In order to apply the obtained results and conclusions to the industry, all the steps of the work followed as close as possible the industrial practice. Furthermore the selection of the surface sizing was also performed having this point in mind.

Finally, it is important to stress that this work is focused on surface sizing and not on coating. The main difference between these two surface treatments lies on the fact that the coating blends include pigments and the amount applied is usually above 6 g/m². Moreover printing and writing papers (P&W) are not usually coated.

The experimental work carried out in order to achieve these goals involves the following main steps:

- ✓ **Characterization/identification of the compounds used in the surface sizing blends.** These were composed of cationic starch and different proportions of synthetic sizing agents. The sizing agents used ranged from styrene acrylate copolymers that have been recently applied for surface sizing at industrial level, to melamine copolymers that are not usually used for this purpose. The formulation constituted only by cationic starch was taken as reference, as it is the most commonly used. It should be highlighted that some of the sizing agents tested possessed distinct

chemical composition whereas others had identical composition but different molecular configurations. Additionally, the influence of their incorporation percentage was also investigated, using incorporation percentages of 5, 10 and 20%.

- ✓ **Production of the surface sized samples.** Preliminary studies were undertaken in order to optimize the surface sizing procedure. These included the selection of the formulations to be applied and the identification of the variables to be controlled, as will be detailed in Section 2.1.2. Additionally, also a methodology to guarantee the traceability of each paper sheet used was set.
- ✓ **Physical and Chemical characterization of the samples.** As the major concern is about surface behavior, the characterization techniques focus mainly surface energetics (contact angle e inverse gas chromatography), surface topography (profilometry), and porosity (mercury porosimetry). It should be pointed out that these techniques are not used as routine and thus, a previous work was needed regarding each one of them, to establish the most adequate operating conditions and to fully interpret their results. Additionally, some of the samples were analyzed with more sophisticated techniques as AFM or ESCA in order to investigate specific details.
- ✓ **Evaluation of the inkjet printing performance of the samples.** This is not a simple issue as it is a subject not usually disclosed in the open literature, and thus all the methodology was developed specifically for this work, using the available technologies.

The surface sizing operation, which is the focus of this work, represents at the most 5% of the paper structure, depending on the paper basis weight, and the differences between the samples are necessarily limited by this fact. Thus it should be highlighted that previously to any analysis of the characterization results, these were subjected to Analysis of Variance (ANOVA), to guarantee that the differences between the samples were statistically valid.

This document is organized in 11 Chapters:

In this chapter (Introduction) some generic information regarding the papermaking process, surface sizing, paper surface characterization and printing is presented. It is also given a general overview of the work in order to frame the reader into its purpose and methodology.

Chapter 2 (Materials and Methods) describes the experimental procedures used in the work, in what concerns to the surface sizing operation, the paper surface characterization and the printing quality evaluation. However the characterization techniques are fully detailed in further chapters together with the corresponding results.

Chapter 3 (Characterization of the Sizing Chemicals) covers the methodology developed to determine the composition and the properties of the compounds used in the sizing formulations (starch and synthetic surface sizing agents).

The following chapters concern the physical and chemical characterization of the paper surface of all 31 samples produced. Chapters 4, 5, 6, 7 regard, respectively, to profilometry, mercury porosimetry, contact angle measurements, and inverse gas chromatography (IGC). The structure of these chapters is similar. They are all divided in two sub-sections: firstly the principles of the technique, details and the methodology used are described and, secondly, the corresponding results are presented and analyzed.

Chapter 8 (Printing Quality) covers the method used to evaluate the inkjet printing performance of the samples and the corresponding results. Mathematical models were implemented in order to correlate the values of the printing parameters with the surface properties determined in the previous chapters.

Chapter 9 (Complementary Studies) is a compilation of scientific papers (published and submitted) regarding specific aspects of the work. These papers involve either only a few samples and/or a particular characterization technique which were found adequate to point out a particular aspect of the work.

Chapter 10 (Conclusions) summarizes the main conclusions that can be withdrawn from this study and points out some suggestions for future work.

Chapter 11 (References) is used to list the most relevant publications consulted to accomplish this work, where detailed information on a given subject can be consulted.

The thesis is also complemented by a series of appendices (Appendix A to G.) where additional information is presented, mainly in tables and plots. This was done to avoid making the main text too extensive and too hard to follow.

CHAPTER 2

MATERIALS AND METHODS

2 MATERIALS AND METHODS

As detailed in Section 1.6, this work aims at modifying the surface properties of printing and writing paper sheets through surface sizing. For that, different surface sizing formulations (previously characterized) will be tested and the corresponding sized samples characterized in terms of their physical and chemical properties. Finally the impact of the surface modifications into the inkjet printing quality will also be evaluated.

Figure 2.1 represents schematically the methodology used to achieve these objectives.

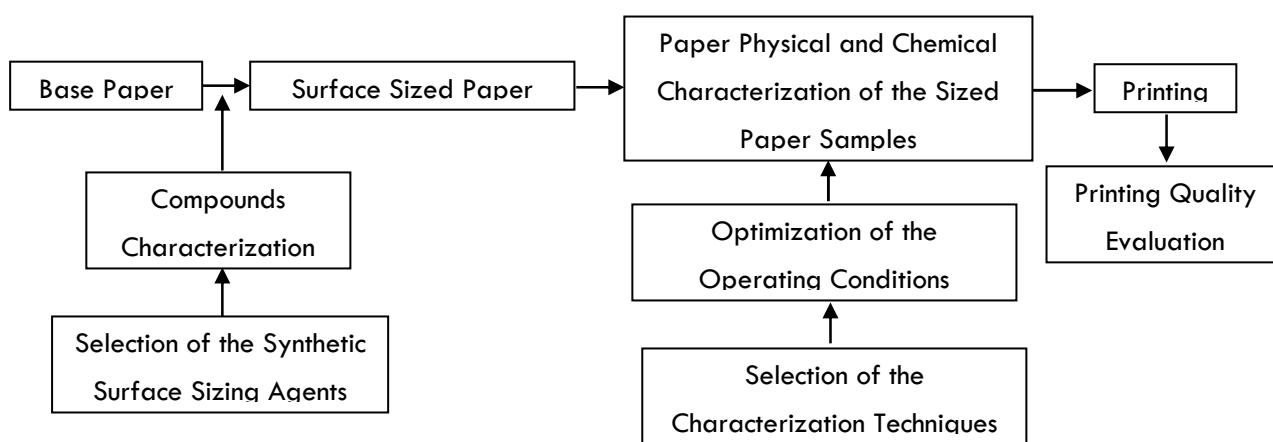


Figure 2.1 – Schematic representation of the methodology used in this work

The compounds and techniques involved in this work will be described in this chapter, in four different sections: Section 2.1 that not only describes the sizing equipment but also the sizing formulations, which will be followed by an explanation of the techniques used to characterize the sizing agents (Section 2.2) and to characterize the sized paper sheets (Section 2.3). Finally, information on how printing quality is evaluated will be given in Section 2.4. More extensive descriptions will be provided regarding the surface sizing process and the sizing formulations, whereas only a brief explanation of the techniques used to characterize the sized paper samples will be presented, since these will be supplied in subsequent chapters along with the corresponding experimental results (Chapters 4 to 8).

2.1 SURFACE SIZING

2.1.1 EQUIPMENT AND METHODOLOGY

The surface sizing formulations were applied to a base paper (79 ± 0.5 g/m² basis weight), produced in a paper mill with an *Eucalyptus globulus* Kraft pulp. This paper was calendered (20 KN/m calendering pressure) and had no surface chemical treatment of any kind.

The Mathis laboratory device, model SVA-IR-B (illustrated in Figure 2.2), was used for paper sheet surface sizing. It operates automatically with velocities ranging from 1 to 10 m/min and can be used with three applicator rolls of different diameters. A preliminary study was undertaken in order to optimize the sizing procedure. The main goal was to obtain a sizing amount (pick-up) similar to that of industrial scale (usually approximately between 2 and 5 g/m²). This was achieved using the 0.15 mm roll in conjunction with a velocity of 6 m/min. A pick-up of 3.5 ± 0.3 g/m² (including both faces) was reached for these operating conditions.

Additionally, and to minimize the migration of the sizing formulations into the fibrous matrix paper samples were subsequently dried (Figure 2.2) using the maximum intensity available for the IR dryer (1.0 kW).

Due to equipment limitations, the sizing process was performed separately for each side of the paper sheets. The uniformity of the application with the selected conditions was confirmed using a colored blend (by sizing the paper sheet with a colored blend it is easily observed the evenness for the color distribution at the surface, indicating that the equipment allows good uniformity). The surface sized samples produced were no further calendered since this mechanical operation could mask the effect of the different sizing formulations in what concerns the physical properties of the paper surface.

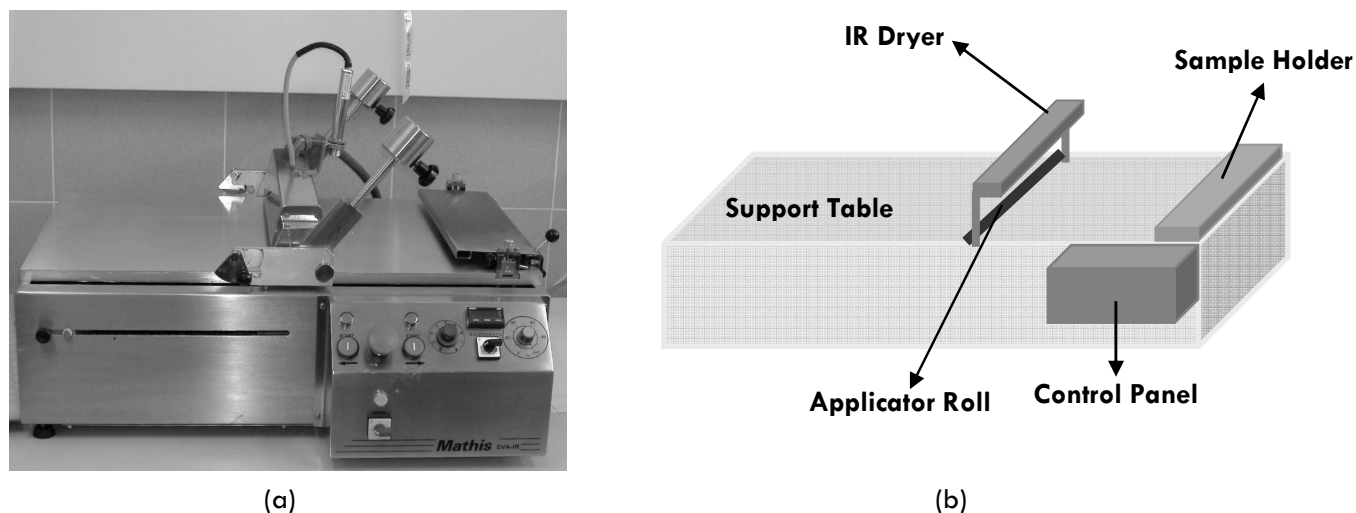


Figure 2.2 – Equipment used in the surface sizing process (a) picture; (b) schematic representation. The paper sheet is placed in the support table and secured with the sample holder, after, using a syringe, a straight line of sizing blend is manually spread in front of the applicator roll, with it in the start position (right in front of the sample holder) by pressing the start bottom on the control panel, the applicator roll spreads the sizing blend at the paper surface and the IR dryer dries it partially immediately after the application.

At least 20 paper sheets (A3 size) were sized with each sizing formulation in order to obtain enough appropriate samples for further analysis. For each set the following was observed:

- ✓ Identification of each of the A3 paper sheets used;
- ✓ Determination of the exact net basis weight of each unsized paper sheet (weight of each paper sheet and basis weight calculation according to the dimensions);
- ✓ Sizing of a set of 20 paper sheets for each sizing formulation, according to the procedure described above;
- ✓ Determination of the net basis weight after surface sizing and consequent determination of the surface sizing pick-up (from the weight difference).
- ✓ Selection of the paper sheets with adequate pick-up ($3.5 \pm 0.3 \text{ g/m}^2$ in both sides);

For each surface sizing formulation, an average of 10 paper sheets with the required pick-up was obtained.

2.1.2 SIZING FORMULATIONS

As mentioned before (Chapter 1), the most common sizing formulation applied in papermaking is cationic starch alone; however there is an increasing tendency, already applied in several paper mills, of combine the cationic starch with some synthetic surface sizing agents.

Thus and in order to be as close as possible to the industrial practice, the first sizing formulation used in the present work was also cationic starch, which was taken as reference. The cationic starch suspension was collected immediately before the size press of the paper machine and consequently includes all the size press additives (such as OBA, salt, biocide and anti-foam). Subsequently other sizing formulations were tested, in a total 30, consisting of blends of cationic starch and small amounts of synthetic surface sizing agents (up to 20% w/w). The latter were not only copolymers containing styrene and acrylate, also commonly used in the paper industry, but also included styrene, acrylate and melamine based compounds in order to expand the chemical variability of the sizing agents tested. Table 2.1 lists the compounds used in the preparation of the surface sizing formulations and the corresponding abbreviations.

Table 2.1 – Compounds used in the surface sizing formulations.

Compound	Reference
Cationic starch (used as reference)	S1
Co-styrene-acrylate*	S1
Co-styrene-maleic anhydride	S2
Co-acrylonitrile-acrylate	S3
Co-styrene-maleic anhydride	S4
Quaternary ditallow methyl epoxypropyl ammonium	S5
Methylated Melamine	S6
Co-styrene-dimethylaminopropylamine maleimide	S7
Co-styrene-butyl acrylate	S8
Co-styrene-acrylate*	S9
Co-styrene-acrylate*	S10

* Different monomers proportion

Although cationic starch was the predominant component of the blends, concentrations of 5, 10 and 20% of the different synthetic surface sizing agents were used. An incorporation of 10% is usually found in the paper mills for this kind of formulations, being 20% the maximum allowed in a paper machine, namely due to white water contamination problems. In the present work 5% incorporation percentage was additionally selected in order to

expand the concentration range of the surface sizing agent providing a better picture of its influence.

The nomenclature used to identify the sizing formulations was:

StSi-j

Meaning **St** that the blend contains cationic starch, taken as standard (St), while **Si-j** indicates that the blend includes surface sizing agent **Si** (i varies from 1 to 10, see Table 2.1), in the percentage j (j equals 5, 10 or 20 w/w). For instance, formulation **StS2-10** is composed of cationic starch and surface sizing agent **S2** (Co-styrene-maleic anhydride, Table 3.1) in a percentage of 10 of S2 and (consequently) 90% of cationic starch. In Appendix B are summarized the blends composition.

2.2 CHARACTERIZATION OF THE SURFACE SIZING AGENTS

The knowledge of the characteristics of the compounds used to prepare the surface sizing formulations, in what concerns either their chemical composition or their physical and chemical properties, as this information is crucial to relate the resultant surface modifications with the performance of the sized paper sheets, namely in terms of printing quality.

Since most of the co-polymers used as surface sizing agents were commercial products, the information about their chemical characteristics, provided by the corresponding datasheets (Appendix A), was rather limited (or confidential). Thus, it was necessary to carry out some additional measurements namely density, elemental analysis, particle size, pH, solids content and total surface tension. As described later (Chapter 3) this information enabled the schematic representation of the compounds molecules.

2.3 PHYSICOCHEMICAL CHARACTERIZATION OF THE PAPER SAMPLES

The characterization of the paper samples produced was performed by using several techniques, listed in Table 2.2. Some of these techniques (profilometry, mercury porosimetry, contact angle and IGC) were applied for all samples, while others (AFM, ESCA, ToF-SIMS and SEM) could only be applied in some samples (mainly because they are not available in our laboratories). Detailed considerations about all these techniques will be presented in the

next chapters (Chapter 4 to Chapter 7) together with the analysis of the corresponding results.

Table 2.2 – Characterization techniques used to characterize paper surface.

Characterization Technique	Type of Characterization	Output	Equipment	Institution	Chapter/Section
Profilometry	Physical	Roughness parameters	Profilometer Altisurf 500 from AltiMet & PaperMap software	RAIZ	4
Mercury Porosimetry	Physical	Total porosity and Pore size distribution	AutoPore IV 9500 from Micromeritics	LABGRAN	5
Scanning Electron Microscopy (SEM)	Physical	Surface Images	JSM-5310 Scanning Microscope from Jeol	IPN	9
Atomic force Microscopy (AFM)	Physical	Roughness parameters Surface images	Nanoscope IIIa microscope from Digital Instruments Inc.	Åbo Akademy University (Finland)	9
Contact Angle Measurements	Chemical	Initial wetting Total surface free energy, Dispersive and polar components Static and dynamic contact angle Wetting velocity	OCA20 from Data Physics	DEQ	6
Inverse Gas Chromatography (IGC)	Chemical	Dispersive component of surface energy Surface acid-base character	GC 1000 from DANI	DEQ /Soporcel)	7
Electron Spectroscopy for Chemical analysis (ESCA)	Chemical	Surface chemical composition Carbon bonding structure	AXIS 165 high-resolution electron spectrometer	Helsinki University (Finland)	9
Time-of-Flight Secondary Ion Mass Spectrometry (ToF-SIMS)	Chemical	Identification of elemental and molecular species And their distribution at the surface	PHI TRIFT II time-of-flight secondary ion mass spectrometer	Top Analytica (Finland)	9

2.4 PRINTING QUALITY EVALUATION

To evaluate the printing quality all the samples were printed with a specific mask (Figure 2.3) using the inkjet printer HP5652. Inkjet printing quality was evaluated both by quantitative measurements and by subjective evaluation. The quantitative measurements include: Optical Density, measured by the spectrophotometer Gretag D19C; Gamut Area, determined through the CIE Lab color coordinates obtained for six colors by using the AvaMouse spectrophotometer (Avantes); and Line quality, evaluated using the Personal Image Analysis system PIA BASF – 8042319 for the black line with yellow background. Subjective evaluation was based on the observation of a panel members and subsequent classification of the printed images depicted in Figure 2.3.

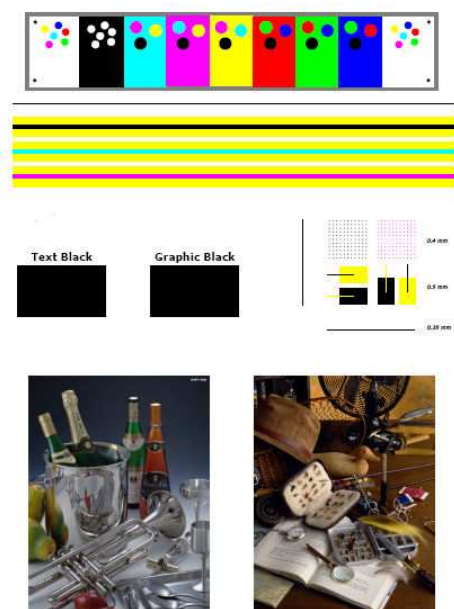


Figure 2.3 – Mask used to evaluate inkjet printing quality.

The theoretical and technical details as well as definitions and results regarding printing quality are given in Chapter 8.

CHAPTER 3

CHARACTERIZATION OF THE SIZING CHEMICALS

3 CHARACTERIZATION OF THE SIZING CHEMICALS

As mentioned before, most of the surface sizing agents used in this work were not prepared in the lab but were supplied by industrial producers and the information available was limited to the respective compound datasheet. Figure 3.1 illustrates, as an example, the typical information available in a datasheet (a copy of all the available datasheets used is given in Appendix A)

As it can be seen, besides the name of the compound (monomer), the data provided in those datasheets is rather vague (frequently corresponding to a range rather than to an accurate value).

xxx xxx xxx

Surface sizing agent

Chemical Description	Chemische Basis	Styrene acrylate copolymer Styrol-Acrylat-Copolymer	
Ionicity	Ladungscharakter	Weakly anionic Schwach anionisch	
Solids	Feststoffgehalt	%	23,5–25,5
Form supplied	Lieferform	Aqueous polymer dispersion Wäßrige Polymerdispersion	
Density	Dichte	g/cm ³ (20 °C)	1,02–1,06
pH value (as supplied)	pH-Wert Lieferform)		4,0–6,0
Viscosity	Viskosität	mPa · s (Brookfield RV; spindle 1; 100 rpm; 20 °C (Brookfield RV; Spindel 1; 100 min ⁻¹ ; 20 °C)	< 30
Storage stability	Lagerbeständigkeit	12 months ex Bayer works The product must be protected from freezing. 12 Monate ab Lieferung Werk Bayer Das Produkt muß frostfrei gelagert werden	
Recommended for	Haupteinsatzgebiete	Surface sizing agent for paper and board. Application in the size press with fluorescent whiteners. Surface coloring with anionic direct and acid dyestuffs as well as anionic color	

Figure 3.1 – Example of the information available in a product datasheet

The following sections report the measurements and calculations undertaken to gather a relevant set of properties of the sizing agents, which will be most useful for the interpretation of the paper surface properties and printing quality results.

3.1 SIZING AGENTS COMPOSITION

As mentioned before, the compounds datasheets give information on the monomers that constitute each copolymer. However, nothing is revealed about the monomers proportion. Although several attempts were made to experimentally determine this parameter, a trial and error procedure was found to be necessary to establish this proportion for each sizing agent used.

The methodology followed, described in Figure 3.2 in the form of a flowchart, was based on three types of inputs:

- ✓ Identification of the monomers present in each copolymer (given in the datasheet);
- ✓ Chemical composition of each monomer (NIST database, 2004)
- ✓ Elemental composition (N, C, H, O) experimentally determined by elemental analysis (Table 3.1).

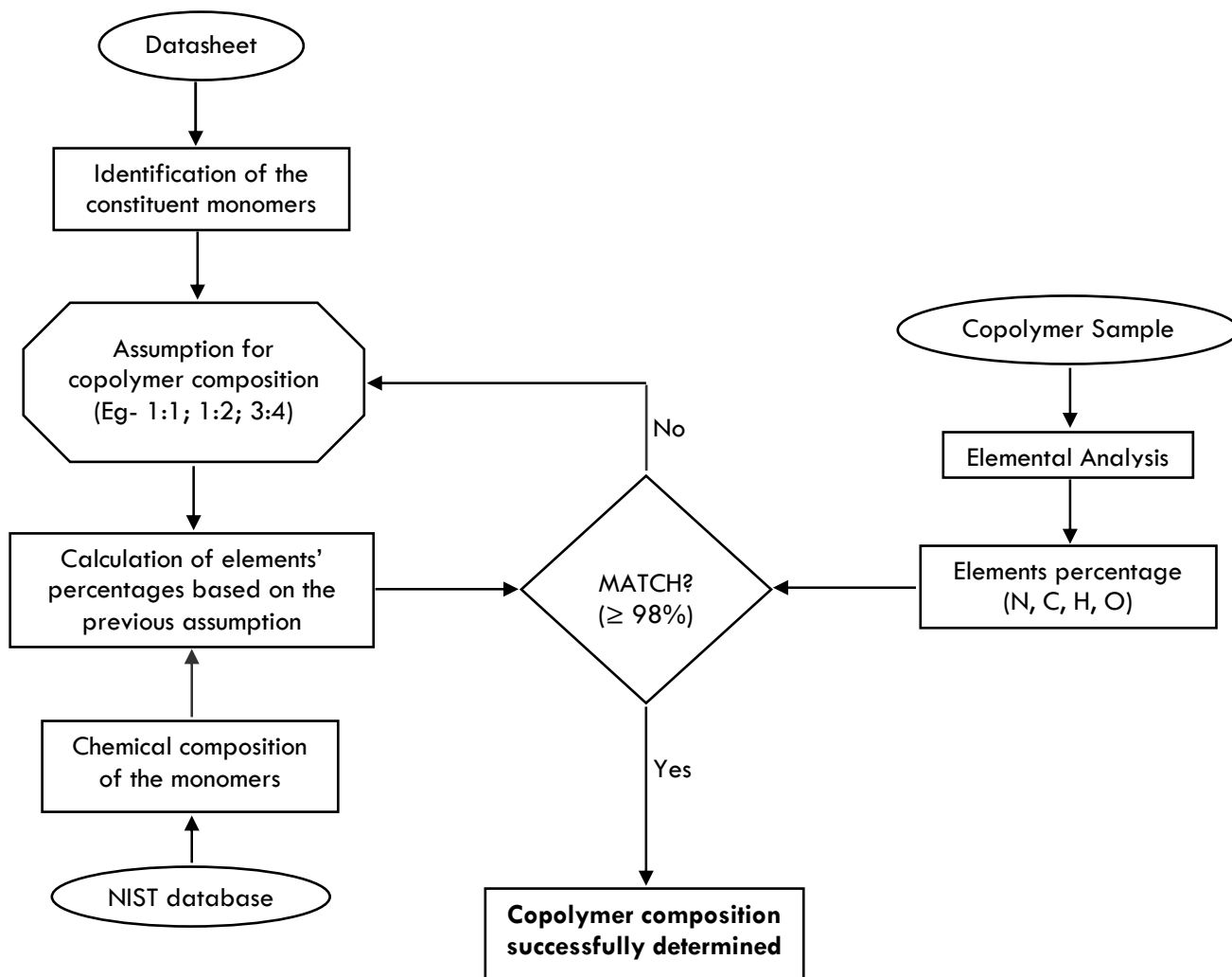


Figure 3.2 – Algorithm used for the determination of the monomers' proportion of each of the copolymers used.

Essentially, this methodology consists of a first estimation of the monomers proportion, from which, based on the corresponding chemical formula (NIST database), it is possible to calculate the elements percentage (N, C, H, O). These are then compared to the results obtained from sample elemental analysis (Table 4.1) and adjusted until both match. The proportion of the monomers estimated in this way is listed in Table 3.2.

Table 3.1 – Elemental analysis results

Compound	Element Amount (%)			
	Nitrogen	Carbon	Hydrogen	Oxygen
S1	---	71.82	7.48	20.70
S2	1.79	79.50	6.21	12.49
S3	11.56	61.35	7.60	19.48
S4	1.18	76.37	6.22	16.23
S5	1.98	68.93	12.23	6.82
S6	37.76	40.53	4.73	16.98
S7	6.88	72.44	7.25	8.98
S8	1.10	79.15	8.55	11.21
S9	---	71.92	7.31	20.78
S10	0.08	67.70	8.03	23.91

Table 3.2 – Composition of the surface sizing agents.

Sizing Agent	Base Compound	Composition
S1	Co-styrene-acrylate	styrene : acrylate 3 : 4
S2	Co-styrene-maleic anhydride	styrene : maleic anhydride 3 : 1
S3	Co-acrylonitrile-acrylate	acrylonitrile : acrylate 1 : 1
S4	Co-styrene-maleic anhydride	styrene : maleic anhydride 2 : 1
S5	Quaternary ditallow methyl epoxypropyl ammonium	quaternary ditallow methyl epoxypropyl ammonium
S6	Methylated Melamine	melamine : methyl group 1 : 1
S7	Co-styrene-dimethylaminopropylamine maleimide	styrene : dimethylaminopropylamine maleimide 2 : 1
S8	Co-styrene-butyl acrylate	styrene : butyl acrylate 2 : 3
S9	Co-styrene-acrylate	styrene : acrylate 3 : 4
S10	Co-styrene-acrylate	styrene : acrylate 1 : 2

Knowing the chemical composition of the compounds, a schematic representation of the molecules structure was drawn, using the freeware software ChemSketch (Figure 3.3). When necessary (**S1** and **S9**), additional information of the compounds properties, such as particle size and surface tension was considered to validate the structure drawn.

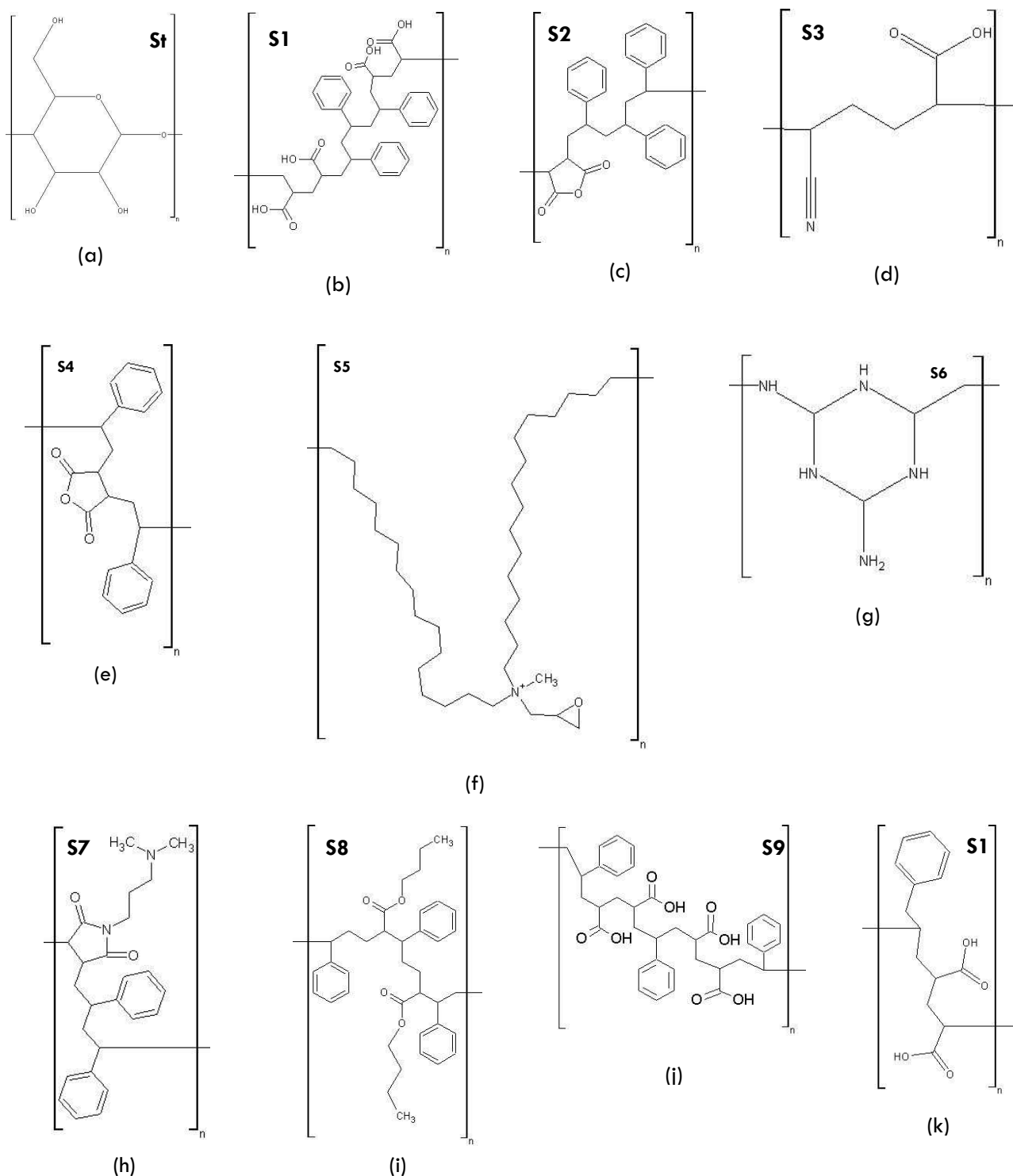


Figure 3.3 – Schematic representation of the molecules' structure of the compound used in the surface sizing: (a) cationic starch; (b) Co-styrene-acrylate; (c) Co-styrene-maleic anhydride; (d) Co-acrylonitrile-acrylate; (e) Co-styrene-maleic anhydride; (f) Quaternary ditallow methyl epoxypropyl ammonium; (g) Methylated Melamine; (h) Co-styrene-dimethylaminopropylamine maleimide; (i) Co-styrene-butyl acrylate; (j) Co-styrene-acrylate; (k) Co-styrene-acrylate.

From Figure 3.3 it is clear that there are visible differences either in the composition as in the structure of the compounds that will most certainly led to distinct chemical properties.

3.2 SIZING AGENTS PROPERTIES

Additionally to the chemical composition, some other relevant properties of the compounds used in the sizing formulations (both cationic starch and synthetic surface sizing agents) had to be determined, as described below:

- ✓ Density was measured by liquid picnometry, following ISO 758 method.
- ✓ Particle size was determined, from a dilute suspension previously sonicated, by photon correlation spectroscopy using the COULTER® N4 Plus. Three independent samples were prepared and three measurements were taken for each one.
- ✓ pH measurements were performed following ISO 787-9 method (Lehtinen, 2000).
- ✓ Solids content determination was carried out at 105 °C (SCAN-P 39:80) (Lehtinen, 2000).
- ✓ The total surface tension was determined using the contact angle measurement device OCA20 from Dataphysics (as described in detail in Chapter 6) using the pendant drop method.

The results obtained for the several properties are gathered in Table 3.3. However, in some cases, these properties could not be measured due to experimental restrictions (eg. Some surface tension values could not be achieved due to the viscosity of some sizing agents).

Table 3.3 – Compounds Properties.

Compound	Solids (%)	pH	Particle Size (nm)	Density (g/cm ³)	Surface Tension (mN/m)
St	12.0	5.0	298.8 ± 8.4	1.049 ± 0.05	32.90 ± 0.11
S1	25.2	5.0	66.8 ± 0.9	1.009 ± 0.03	64.38 ± 0.18
S2	15.0	8.4	37.2 ± 5.2	---	---
S3	35.2	3.2	254.5 ± 8.6	1.051 ± 0.03	49.61 ± 0.05
S4	14.6	7.6	25.4 ± 3.6	1.008 ± 0.05	38.51 ± 0.02
S5	6.60	9.2	---	---	---
S6	73.0	7.3	---	---	---
S7	99.1	10.0	---	---	---
S8	30.7	2.8	88.9 ± 1.7	1.022 ± 0.02	43.22 ± 0.03
S9	25.7	4.3	83.6 ± 0.5	1.008 ± 0.10	49.99 ± 0.07
S10	25.5	4.7	73.8 ± 0.8	0.998 ± 0.11	64.33 ± 0.04

As can be seen from this table, the compounds exhibit relevant differences in terms of particle size, surface tension and pH. This was not surprising considering the significant diversity of the constituent molecules.

The values of these properties will be used in combination with the composition and structure of the compounds to interpret some surface properties and behaviors of the sized papers.

CHAPTER 4

PROFILOMETRY

4 PROFILOMETRY

4.1 THEORY

Surface texture is a property naturally associated to any material, from the large scale of a mountain to the small scale measured by a microscope. Paper is no exception for this rule of nature, since its surface is always textured (Thomas 1998).

The surface texture, most commonly called topography, is often crucial for the end-use properties of any type of paper. For printing and writing papers (P&W), surface texture is a physical characteristic which results from the production process itself and it is an important factor affecting printability (Ashori et al. 2007).

In the surface topography of P&W papers, four components can be distinguished, according to the scale: form, waviness, roughness and micro-roughness, as depicted in Figure 4.1 (Wagberg and Johansson 2002; URL 2; URL 3):

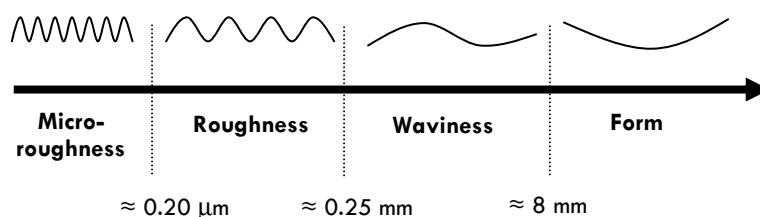


Figure 4.1 – Different surface texture components (URL 2; URL 3).

Among the components of the surface topography of P&W papers, roughness and micro-roughness stand out from the remaining, since due to the topographic range to which it corresponds it becomes the most relevant to be considered for printing processes. From this point on, the term roughness will include these two components of surface texture.

Roughness directly controls gloss and also has a major role in determining printing quality and uniformity. Thus, it is an important property to be accessed in order to adequately characterize paper surface. From its measurements several parameters are obtained, which are usually called topographical parameters.

Topographical parameters can be computed from two-dimensional (2D) or three-dimensional (3D) profile analysis of the paper surface. The calculation of 2D parameters has widely been carried out in science and engineering for almost a century. However, in more recent years, there has been evidence of an increasing need for 3D surface analysis.

This need arises partially as a result of the recognition that all surfaces interact in three rather than two dimensions. In some cases 2D parameters introduced in many national and international standards are inadequate to give a comprehensive description of 3D surfaces and thus unable to meet the need of a wide variety of applications (Stout et al. 1993; Dong et al. 1994a; Dong et al. 1994b; Wågberg 2002).

The functional applications of the materials in fields like wear, friction, lubrication, fatigue, sealing, painting, etc., are deeply influenced by the amplitude and spatial characteristics of the 3D surface topography of the materials (Dong et al. 1994a).

4.1.1 ROUGHNESS PARAMETERS DEFINITION

3D topography is complex and cannot be described completely by a single or a few parameters.

Each one of the roughness parameters reduce all the information in a profile to a single number which is calculated using a specific formula. As each parameter only describes one aspect of the topography, a set of parameters is necessary to accurately characterize surface topography (Dong et al 1994a; Wågberg 2002).

Some of these parameters are naturally extended from their 2D counterparts; others are uniquely defined for 3D topography. Currently, in order to distinguish 2D and 3D parameters, a capital letter “S” (meaning that it is calculated from an area (or surface) rather than a line) is used to identify 3D parameters whereas a capital “R” is traditionally used for 2D parameters (Stout et al. 1993; Dong et al 1994a; Dong et al 1994b; Cohen 2006).

3D measurement systems are all digital height measurement systems. They represent the measured surface with a set of data usually in the form of a x-y matrix of the Cartesian coordinate, where x and y spacing are not necessarily the same (Stout et al. 1993; Dong et al. 1994a; Cohen 2006; TrueGage 2008).

An equally spaced digitalized 3D surface, can be denoted by $z(x_i, y_j)$ ($x_i = i\Delta x$, $y_j = j\Delta y$; $i = 1, 2, \dots, M$; $j = 1, 2, \dots, N$), where Δx and Δy are the sampling intervals, and M and N represent the number of sampling points in the x and y directions, respectively (Stout et al. 1993; Dong et al. 1994a; Cohen 2006; TrueGage 2008).

Parameters used to describe surfaces are mainly statistical indicators that can be divided in amplitude parameters, spacing parameters and hybrid parameters.

4.1.1.1 Amplitude Parameters

Amplitude parameters, defined below, are a class of surface parameters based on the vertical deviations of the roughness profile from the mean plane, i.e. the best fitting plane, also called reference plane (Figure 4.2).

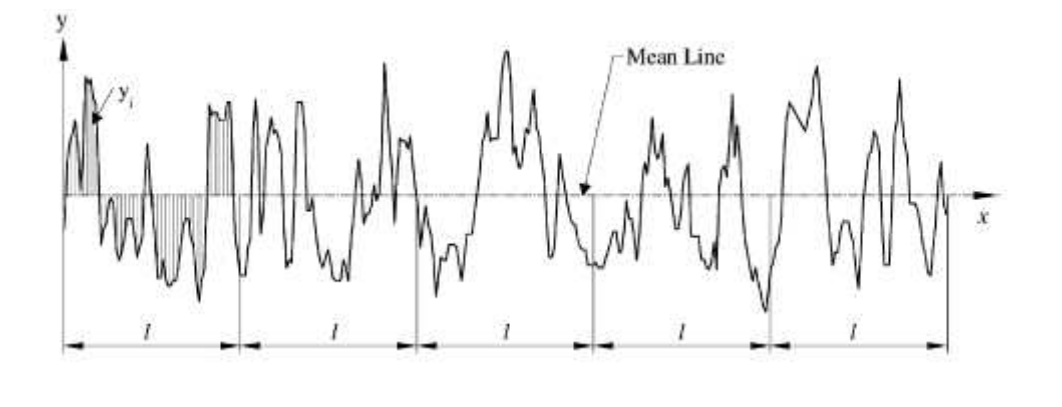


Figure 4.2 – Exemplification of the deviations from the reference plane for a given profile line (Gadelmawla et al. 2002).

Most of them are closely related to the parameters found in statistics for characterizing population samples. The reference plane of the calculation of these parameters is the mean plane of the measured surface (Stout et al. 1993; Gadelmawla et al. 2002; Cohen 2006; TrueGage 2008).

They can be divided in: i) dispersion; ii) asymmetry of the height distribution, and iii) extreme parameters.

i) Dispersion Parameters

Sa - *The roughness average* - is the arithmetic average of the absolute values of the surface height deviations (Figure 4.3) measured from the reference plane, given by:

$$Sa = \frac{1}{NM} \sum_{x=1}^N \sum_{y=1}^M |Z_{x,y}| \quad (4.1)$$

Sa was one of the first parameters used to quantify surface texture and is the most universally recognized roughness parameter for general quality control. It is easy to define,

easy to measure and gives a good general description of height variations (Gadelmawla et al. 2002) However, it only quantifies the “absolute” magnitude of the surface heights, and thus a deep valley or a high peak will result in the same Sa. Moreover, it is insensitive to their spatial distribution, in that two very high peaks will contribute the same to Sa whether the peaks are close to each other or separated. In fact, surfaces with grossly different features may have the same Sa. (Stout et al. 1993; Bastos 2004; Cohen 2006; TrueGage 2008).

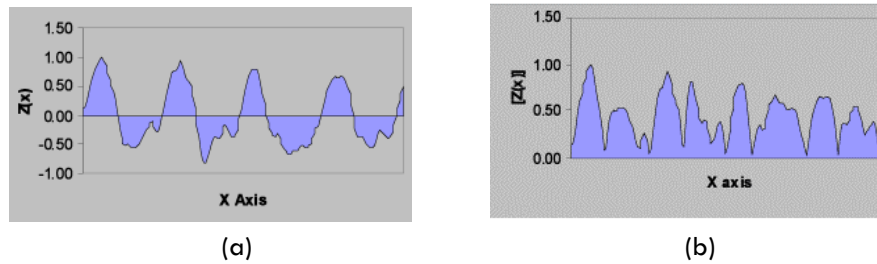


Figure 4.3 – Representation of the surface height deviations for a given profile line: (a) real values; (b) absolute values (Cohen 2006).

Sq - The root-mean-square (RMS) deviation of the surface - is the standard deviation or “first moment” of the height distribution (Figure 4.3) and it is an important parameter to describe the surface roughness by statistical methods.

$$Sq = \sqrt{\frac{1}{NM} \sum_{x=1}^N \sum_{y=1}^M Z^2_{x,y}} \quad (4.2)$$

Sq is very similar to Sa since the surface heights are “squared” prior to being integrated/averaged, and thus peaks and valleys of equal height/depth are indistinguishable. Therefore a series of high peaks or a series of deep valleys of equal magnitude will produce the same Sq value (Stout et al. 1993; Bastos 2004; Cohen 2006; TrueGage 2008).

ii) Asymmetry of the Height Distribution Parameters

Ssk - The skewness is the “second moment” of the height distribution - indicates if the surface is composed of primarily one plateau and how much the valleys and/or peaks deviate from this plateau (Figure 4.4).

$$Ssk = \frac{1}{NMS_q^3} \sum_{x=1}^N \sum_{y=1}^M Z^3_{x,y} \quad (4.3)$$

Since the height values are cubed prior to the integration/averaging, the polarity of the surface is maintained. Thus a surface with predominantly deep valleys will tend to have a negative skew, whereas a surface comprised predominantly of peaks will have positive skew. Due to the big exponent used, this parameter is very sensitive to the sampling and to the noise of the measurement. (Cohen 2006; TrueGage 2008).

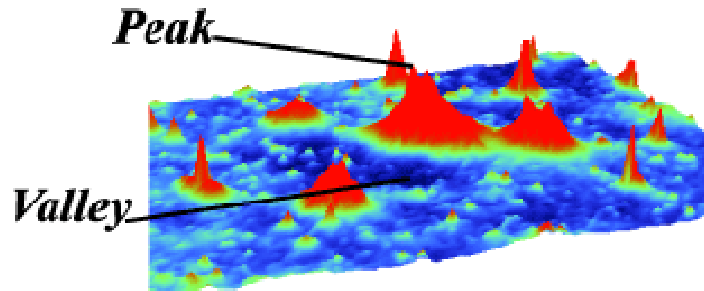


Figure 4.4 – Typical surface structure, demonstrating peaks and valleys (Cohen 2006).

Sku - The kurtosis, is the “third moment” of the height distribution - is the “third moment” of the height distribution and characterizes the anomalies in the surface height distributions in that a normally (i.e. following a Gaussian or Bell curve distribution) disturbed surface texture would tend to have a value of $Sk_u = 3$.

$$Sk_u = \frac{1}{NMS_q^4} \sum_{x=1}^N \sum_{y=1}^M Z_{x,y}^4 \quad (4.4)$$

When the surface texture is composed of non-normally distributed high peaks or deep valleys, the Sk_u becomes very large. When the surface is composed of a slowly varying, “rolling” hill type texture, the Sk_u will be less than 3. Sk_u is a good indicator when an otherwise Gaussian distributed surface may have some defects. Due to the big exponent used, this parameter is very sensitive to the sampling and to the noise of the measurement (Cohen 2006; TrueGage 2008).

ii) Extreme Parameters

These parameters are evaluated from the absolute highest peak and lowest valley found on the surface. A peak is defined as any point above all 8 nearest neighbors. A valley is any point, which is below all 8 nearest neighbors.

Sp - The maximum height of summits - is the distance between the highest peak and the mean plane (Figure 4.5) (Stout et al. 1993; Cohen 2006; TrueGage 2008).

Sv - The maximum depth of the surface - is the distance between the mean plane and the deepest valley (Figure 4.5) (Stout et al. 1993; Cohen 2006; TrueGage 2008).

St - The total height of the surface - is the height between the highest peak and the deepest valley (Figure 4.5) (Stout et al. 1993; Cohen 2006; TrueGage 2008).

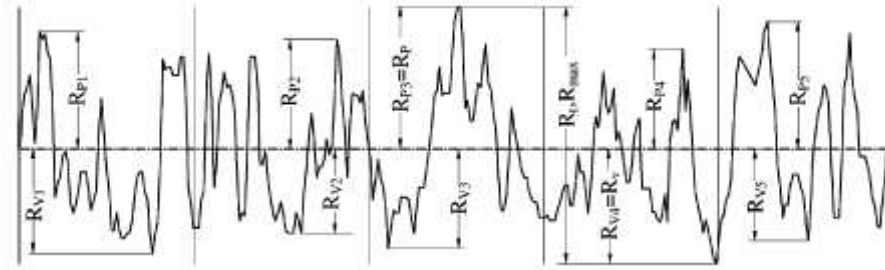


Figure 4.5 - Exemplification of the peaks height and valleys depth measurement for a given profile line (Gadelmawla et al. 2002).

Sz - The ten point height of the surface – is the mean of distance between the 5 highest peaks and the 5 deepest holes. A neighborhood of 3×3 unit areas is taken into account to find out the peaks and the valleys (Stout et al. 1993; Cohen 2006; TrueGage 2008).

$$S_z = \frac{\sum_{1}^{5} |Peak\ Heights| + \sum_{1}^{5} |Valley\ Depths|}{5} \quad (4.5)$$

4.1.1.2 Spatial Parameters

The spatial parameters are those which measure the horizontal characteristics of the surface deviations.

Sds - The density of summits of the surface - that is the number of summits per unit area making up the surface. Summits are derived from peaks. This parameter is expressed in peaks/mm².

$$S_{ds} = \frac{\text{Number of peaks}}{\text{Area}} \Leftrightarrow S_{ds} = \frac{\text{Number of peaks}}{(M-1) \cdot (N-1) \cdot \Delta x \cdot \Delta y} \quad (4.6)$$

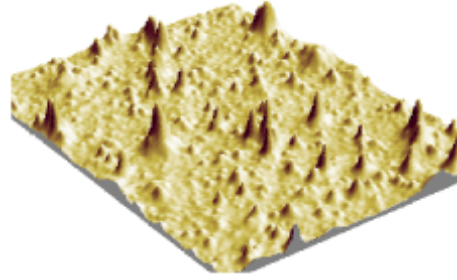


Figure 4.6 – Example of a surface with an Sds value of 2600 peacks/mm² (Cohen 2006).

Peaks are constrained to being separated by at least 1% of the minimum “x” or “y” dimension comprising the 3D measurement areas. Additionally, summits are only found above a threshold that is 5% of Sz above the mean plane (Figure 4.7) (Bastos 2004; Cohen 2006; TrueGage 2008).

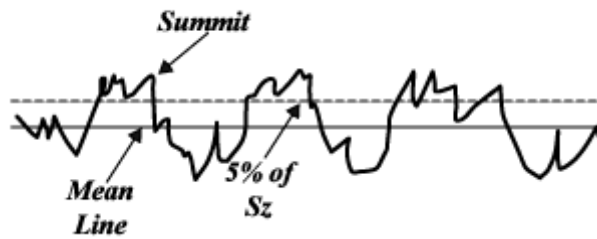


Figure 4.7 – Exemplification of the summits identification (Cohen 2006).

Str - The texture aspect ratio of the surface, is a measure of the spatial isotropy or directionality of the surface texture. This parameter has a value between 0 and 1. If the value is near 1, the surface is isotropic, i.e. has the same characteristics in all directions. If the value is near 0, the surface is anisotropic, i.e. has an oriented and/or periodical structure (Stout et al. 1993; Bastos 2004; Cohen 2006; TrueGage 2008).

$$Str = \frac{\text{Lenght of fastest decay in any direction}}{\text{Lenght of slowest decay in any direction}} \Leftrightarrow Str = \frac{\max \left(\left(\sqrt{\tau_x^2 + \tau_y^2} \right) \right)}{\min \left(\left(\sqrt{\tau_x^2 + \tau_y^2} \right) \right)}, 0 < Str \leq 1 \quad (4.7)$$

4.1.1.3 Hybrid Parameters

Hybrid parameters are a class of surface parameters characterized by depending both on amplitude and spacing, such as slopes, curvatures, etc.

Sdq - The root-mean-square slope of the surface – is the modulus of the decay value, measured in several small segments, through the tangent to the angle formed between each segment and the horizontal direction. Smoother surfaces correspond to small Sdq values (Bastos 2004; Cohen 2006; TrueGage 2008)

$$Sdq = \sqrt{\frac{1}{(M-1)(N-1)} \cdot \sum_{j=2}^N \cdot \sum_{i=2}^M \cdot \left[\left(\frac{z \cdot (x_i, y_j) - z \cdot (x_{i-1}, y_j)}{\Delta x} \right)^2 + \left(\frac{z \cdot (x_i, y_j) - z \cdot (x_i, y_{j-1})}{\Delta y} \right)^2 \right]} \quad (4.8)$$

Sdq is a general measurement of slopes, which comprise the surface and may be used to differentiate surface with similar average roughness, Sa, as demonstrated in Figure 4.8.

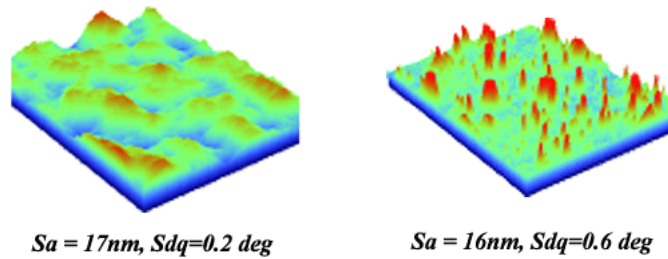


Figure 4.8 – Exemplification of the differentiation between two samples with similar Sa using the Sdq values (Cohen 2006).

Ssc - The arithmetic mean summit curvature of the surface - enables to know the mean form of the peaks: either pointed or rounder, according to the mean value of the curvature of the surface at these points (Bastos 2004; Cohen 2006; TrueGage 2008).

$$Ssc = -\frac{1}{2} \cdot \frac{1}{n} \sum_{k=1}^n \left(\frac{\partial z^2(x, y)}{\partial x^2} + \frac{\partial z^2(x, y)}{\partial y^2} \right) \Bigg|_{\text{For any peak}} \quad (4.9)$$

Sdr - The developed interfacial area ratio - indicates the complexity of the surface due to the comparison of the curvilinear surface and the geometric surface. A completely flat surface will have an Sdr near to 0%. A complex surface will have an Sdr of some percents (Stout et al. 1993; Cohen 2006; TrueGage 2008).

$$Sdr = \frac{(\text{Texture surface area}) - (\text{Cross sectional area})}{\text{Cross sectional area}} \times 100 \Leftrightarrow \quad (4.10)$$

$$\Leftrightarrow Sdr = \frac{\sum_{j=1}^{N-1} \sum_{i=1}^{M-1} A_{ij} - (M-1) \cdot (N-1) \cdot \Delta x \cdot \Delta y}{(M-1) \cdot (N-1) \cdot \Delta x \cdot \Delta y} \times 100$$

$$\text{Where, } A_{ij} = \frac{1}{4} \left\{ \left(\left[\Delta y^2 + (z \cdot (x_i, y_j) - z \cdot (x_i, y_{j+1}))^2 \right]^{\frac{1}{2}} + \left[\Delta y^2 + (z \cdot (x_{i+1}, y_{j+1}) - z \cdot (x_{i+1}, y_j))^2 \right]^{\frac{1}{2}} \right) \cdot \left(\left[\Delta x^2 + (z \cdot (x_i, y_j) - z \cdot (x_{i+1}, y_j))^2 \right]^{\frac{1}{2}} + \left[\Delta x^2 + (z \cdot (x_i, y_{j+1}) - z \cdot (x_{i+1}, y_{j+1}))^2 \right]^{\frac{1}{2}} \right) \right\}$$

Sdr may further differentiate surfaces of similar amplitudes and average roughness. Typically Sdr will increase with the spatial intricacy of the texture whether or not Sa changes. Sdr is useful in applications involving surface coatings and adhesion.

4.1.2 ROUGHNESS MEASUREMENT TECHNIQUES AND EQUIPMENTS

The techniques for paper roughness measurement can be classified in two categories. One type of measurement simulates the printing process under pressure, and the other, called profilometry, determines an effective three-dimensional (3D) surface profile (Barros 2004; Ashori et al, 2008).

Air-leak methods, such as Bendtsen and Parker Print-Surf (PPS), were developed to simulate printing pressure. Unfortunately air-leak meters have some drawbacks in paper surface research. Because the total airflow volume is measured, no information is obtained about the surface structure in detail. In other words, traditional surface roughness assessing instruments give average numbers for the measured area but do not provide any detailed description of the paper surface. This makes such instruments less suitable for revealing details of the surface treatments effect (Barros 2004; Ashori et al, 2008).

As for the determination of the three-dimensional (3D) surface profile, its purpose is to present a surface profile under room conditions as accurately as possible. There are two types of methods to perform profilometry measurements: Contacting methods (Stylus profilometry) and non-contacting methods (Optical profilometry). Laser and electron microscopy can also be applied for profilometry measurements, embracing both contacting and non-contacting methods (Barros 2004; Ashori et al 2008).

The Stylus instruments (Figure 4.9) are easily described as a mechanical instrument that contacts with the surface under analysis and profiles it by following the surface details as accurately as possible. These instruments can have several configurations, particularly in what concerns to the tip that touches the surface. Its simplicity, however, is associated to several limitations: on one hand, since the instrument touches the surface, there is the risk of damaging it. On the other hand, since the stylus is an artifact of finite dimensions, it sometimes fails to follow peaks and valleys faithfully and produces a distorted record of the surface. The “traced profile” (ISO 3274, 1996) recorded by the Stylus instrument is the locus of the centre of the stylus, thus, if the contacting portion of the stylus is assumed to be spherical in section, the radius of curvature of a peak may be exaggerated, while the valley may be represented as a cusp (Thomas, 1998; Barros 2004).

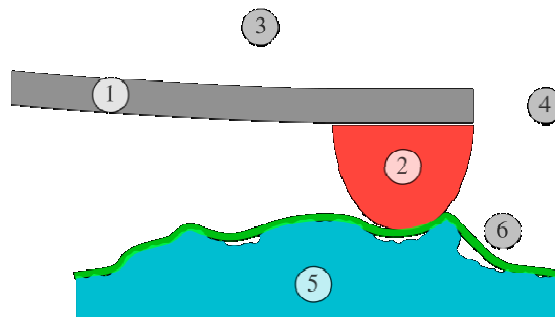


Figure 4.9 - Principle of a contacting stylus instrument profilometer: A cantilever (1) is holding a small tip (2) that is sliding along the horizontal direction (3) over the object's surface (5). Following the profile the cantilever is moving vertically (4). The vertical position is recorded as the measured profile (6) shown in light green.

The optical instruments used to access surface roughness are based in the simple principle that when electromagnetic radiation is incident on a rough surface a portion of its energy, depending on the local physical properties of the surface, will be reflected and the reflected beam will carry information about the roughness (Thomas, 1998). The radiation may be reflected either specularly or diffusely or both (Figure 4.10). Reflection is totally specular when the angle of reflection is equal to the angle of incidence (Snell's law), and a surface that reflects radiation in this manner is said to be smooth. Reflection is totally diffuse when the energy in the incident beam is distributed in all directions (Barros 2004; Thomas, 1998).

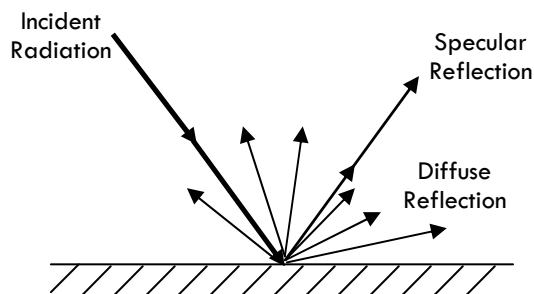


Figure 4.10 – Schematic representation of the different types for reflection of the incident radiation.

According to Vorburger & Teague (1981) the optical techniques can be divided in profiling and parametric. Profiling techniques are associated with specular reflection, whereas parametric techniques are associated mainly with diffuse reflection (Thomas, 1998). One possible method of optical measurement is simply to use the light beam as a non-contacting stylus for profile measurement. The most straightforward method is to detect the change in the angle of specular reflection as the surface is moved under an incident beam.

There are some general aspects that have to be considered in order to choose a specific measuring instrument: cost, ease of operation, size and robustness. There is also the issue of whether a measurement is relative or absolute. In addition, for roughness measuring instruments, it is necessary to decide whether or not the instrument should have a physical contact with the surface, and whether it needs to be able to measure an area of a surface or only a section or profile through it. Most important of all are the horizontal and vertical range and resolution. In fact every instrument or technique presents some limitations of resolution, and the actual values involved will vary from instrument to instrument (Thomas 1998; Barros 2004).

4.1.2.1 Equipment - Altisurf® 500

In this work, and in order to obtain the roughness parameters without the effect of any external force, a non-contact profilometer was chosen, the Altisurf®500 profilometer manufactured by Cotec-Ca (France), coupled with the PaperMap Software. This non-contact device gives accurate height information with the possibility of visual evaluation of the 3D surface structure of paper samples (Bastos 2004; Ashori et al. 2007).

The system consists of a white light source, lens, spectrophotometer, a signal processing system, together with a motorized sample holder and appropriate image analysis software

(Figure 4.11). The white light source (quartz-halogen) is focused through the lens onto the sample to be analyzed. The reflected light is passed through a pinhole into a spectrophotometer where built-in software is used to select the wavelength of maximum intensity, which is used to determine the relative height of that point.

The sample is fixed to the sample holder, which is scanned under an adequately positioned fixed sensor. A 3D surface profile (topographic map) can be created, visualizing the irregularities of the papers surface (two-dimensional line scans can also be measured). The sample holder moves the sample, by pre-programmed steps, under the focused beam. The resolution in the x and y directions (from 0.5 to 100 μm) and the area (up to 10 \times 10 cm) to be measured are selectable. By choosing an appropriate filter (e.g., Gaussian) the roughness of interest can be obtained (Ashori et al. 2008; Levlin and Söderhjelm 2000).

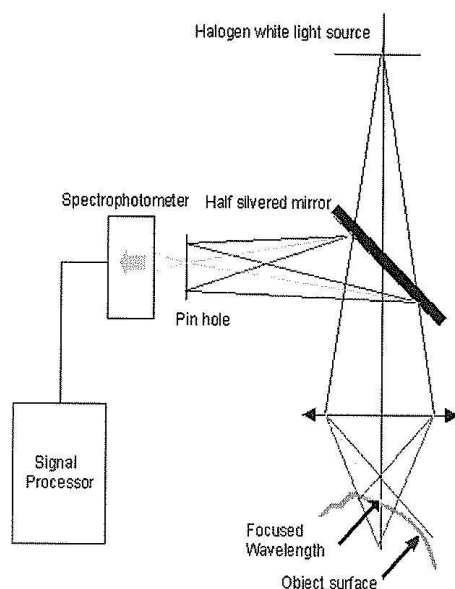


Figure 4.11– Schematic representation of the optical profilometer used in this work (Ashori et al. 2008).

In this study, for each paper sample, 6 pieces of 4 \times 4 mm² were scanned, with a scanning resolution of 2 μm . Therefore 2000 profiles were obtained for each piece. From the data acquisition, a 3D surface profile is obtained (Figure 4.12 (a)), then several mathematical operations are performed in order to apply adequate mathematical filters to the results and to highlight the relevant information, by excluding the surface texture components that are less relevant (Figure 4.12 (b) to Figure 4.12 (e)).

The mathematical treatment includes the following operators:

- ✓ Leveling operation – corresponds to the application of a mathematical filter to remove the general slope of a surface, caused by a measurement that was not strictly horizontal due to the inclination of the sample on the support used to fix it. Figure 4.12 (b) represents the analyzed area after this correction.
- ✓ 4th degree polynomial form removal - This operator consists in mathematically removing the general form of a surface. The remaining information, made up of waviness and roughness, can then be studied separately (Figure 4.12 (c)).
- ✓ Filtering waviness and roughness (0.8 mm filter) - This operator is used to separate the roughness and waviness phenomena of the surface. The quality of the separation depends both on the type of filter and the cut-off value. This process allows obtaining a roughness and a waviness surface that can then be studied individually (Figure 4.12 (d)).
- ✓ Thresholding material ratios 0.5 (corresponding to 99.5%) - This operator allows to artificially truncate the surface at a given altitude (at the top and/or bottom). This operator is especially useful for suppressing peaks that are too large and that therefore hide other relieves, or for simulating a wear process (Figure 4.12 (e)).

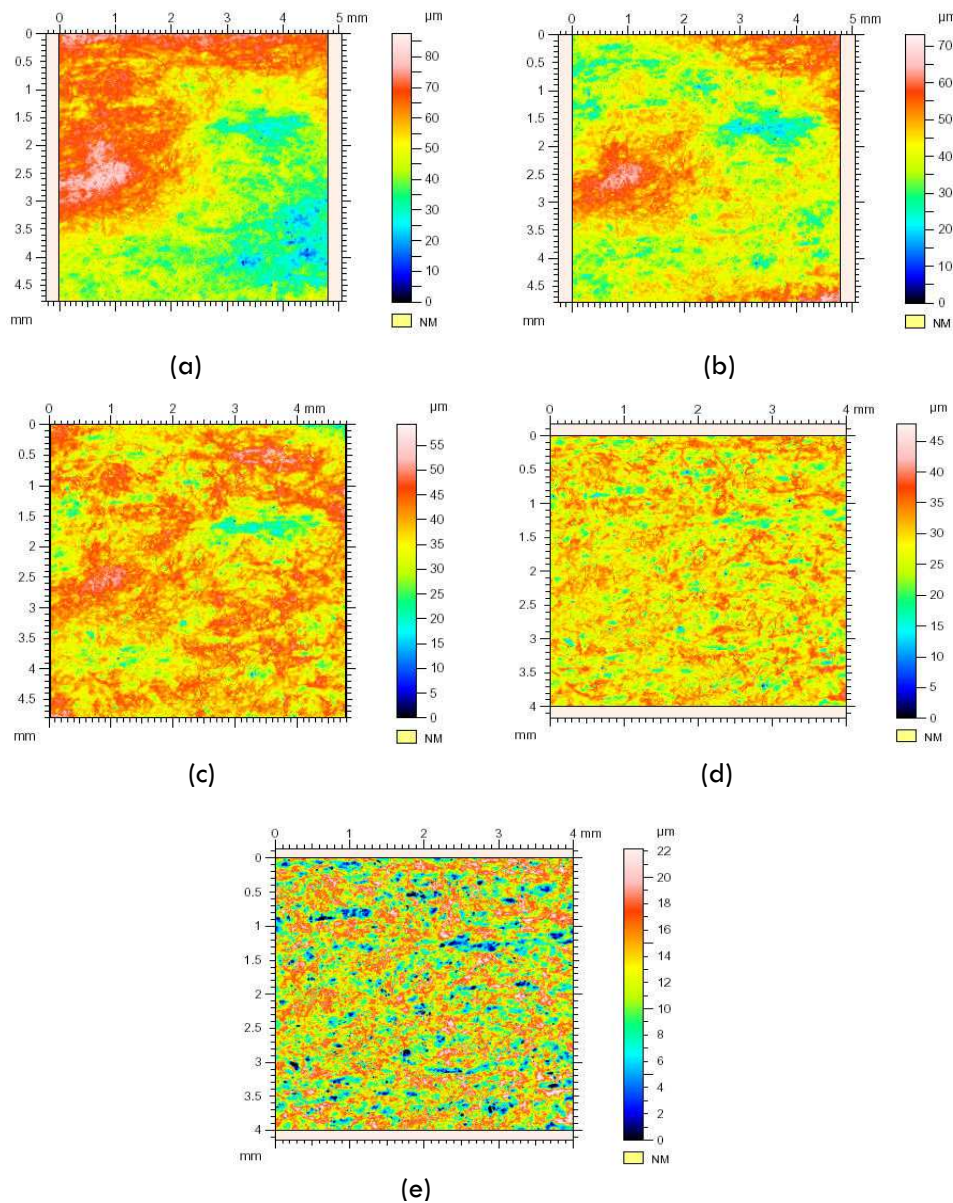


Figure 4.12 – Exemplification of the 3D surface profile (topographic map) obtained from the profilometry measurements for one of the samples tested: (a) profile without any mathematical treatment; (b) profile after the leveling operation; (c) profile after form removal; (d) profile after filtering waviness and roughness; (e) final topographic profile, after thresholding.

The final result being the topographical parameters defined in Section 4.1.1 and presented as illustrated in Figure 4.13.

```
Amplitude Parameters
Sa      = 3.01 µm
Sq      = 3.78 µm
Sp      = 9.23 µm
Sv      = 11.3 µm
St      = 20.6 µm
Ssk     = -0.247
Sku     = 3.02
Sz      = 20.6 µm
Szfid   = 20.6 µm

Spatial Parameters
SPc     = 0 pks/mm2 (1 µm ; 10 µm)
Sds     = 5573 pks/mm2
Str     = 0.445
Sal     = 0.0567 mm
Std     = 5 °
Sfd     = 2.64

Hybrid Parameters
Sdq     = 0.499 µm/µm
Ssc     = 0.186 1/µm
Sdr     = 11.5 %
```

Figure 4.13 – Exemplification, for one of the samples tested, of all the parameters obtained from the profilometry measurements performed with Altisurf® 500.

4.2 RESULTS

Figure 4.14 illustrates the final result of the profilometry measurement procedure, and presents, as an example, the values obtained for one of the measurements performed for samples St.

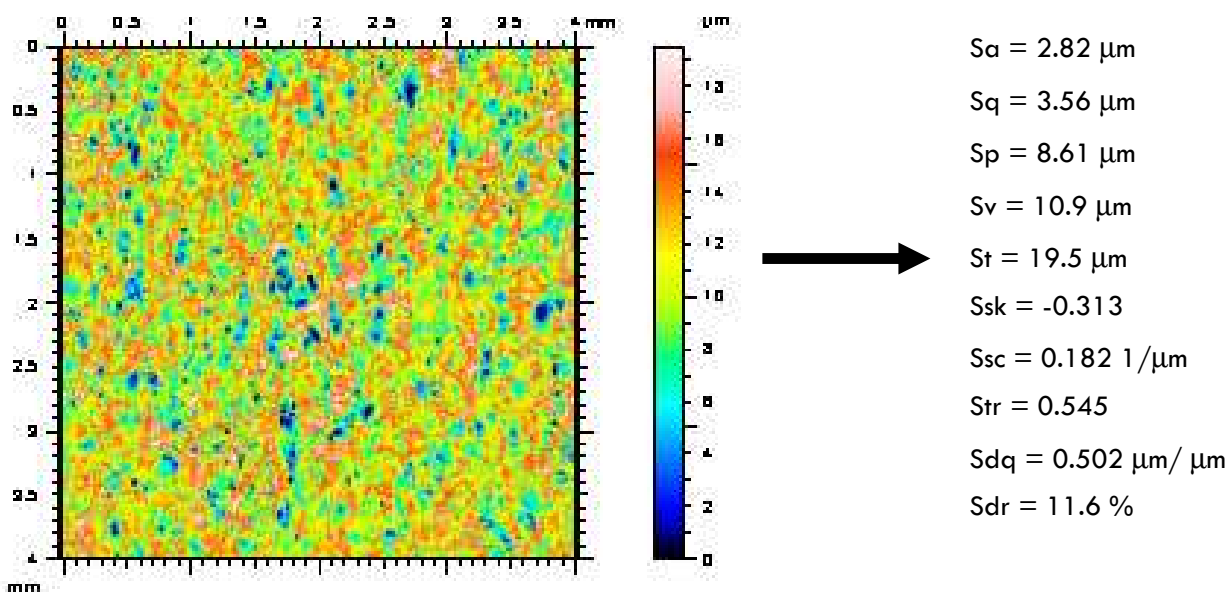


Figure 4.14 - Output obtained from each of the profilometry measurements. In this case, for sample St as an example.

The profilometry measurements were performed for each of the 31 samples. Since 6 measurements per samples were performed, an enormous amount of information was obtained. Thus, the first step to work with valuable and useful information through the profilometry measurements was to isolate the parameters that better characterize the samples. In order to do that, a 2 components PCA was applied. For the purpose of paper surface analysis it is possible to isolate, among all the parameters presented in Section 4.1.1, 10 that may be considered the most relevant as the start point for the PCA analysis: Sa, Sq, Sp, Sv, St, Ssk, Ssc, Str, Sdq and Sdr. The result is presented in Figure 4.15.

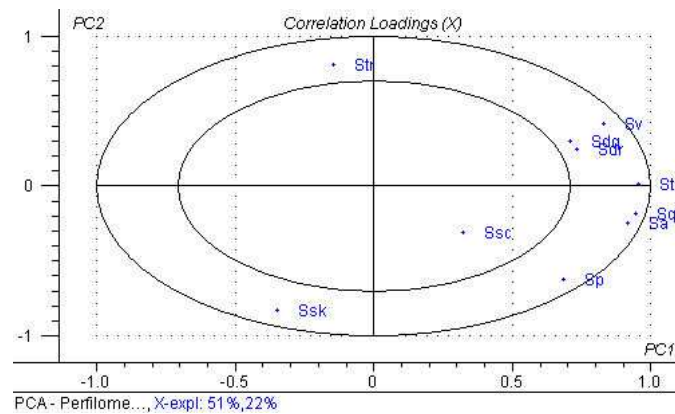


Figure 4.15 - PCA using the descriptive variables obtained by profilometry.

For this set of 10 variables a 73% degree of explanation of the results variability (51% 1st component; 22% 2nd component) was obtained. According to the correlation loadings, the variables Ssc, Sdq and Sdr can be eliminated from the set (as they exhibit the smaller correlation loadings). The resulting PCA analysis is presented in Figure 4.16.

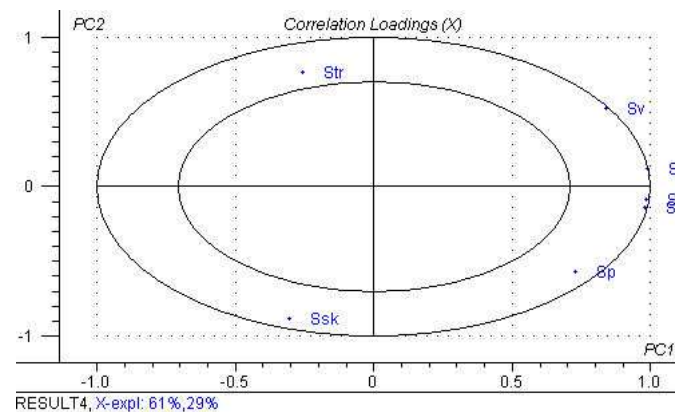


Figure 4.16 - PCA using 7 of the descriptive variables.

This new set, composed by the variables Sa, Sq, Sp, Sv, St, Ssk and Str, explain 90% of the results variability (61% 1st component; 29% 2nd component), and so it is adequate to describe the set of 31 papers. These seven parameters will be the ones used to analyze the effect of surface sizing in topography. It is important to mention that although the variable Sdr was eliminated from this set due to its smaller descriptive power regarding the effect of surface sizing in paper roughness, it will be used later in this work to correct the contact angle values (Section 6.2.1).

By applying ANOVA to the topographical parameters selected by PCA it is possible to analyze in detail the variations in the results of each parameter. The results are presented in Table 4.1.

Table 4.1 – ANOVA results for the profilometry variables selected by PCA.

Variable	Contribution to total variation (%)		Reproducibility Factor (r)	P	F	F _{critical}
	Among samples	Within samples				
Sa	56.72	43.28	0.40	1.7E-14	6.25	1.54
Sq	63.57	36.43	0.45	1.3E-15	7.16	1.55
Sp	53.49	46.51	1.39	9.2E-09	4.29	1.56
Sv	60.53	39.47	1.87	5.7E-17	7.31	1.54
St	57.53	42.47	2.65	5.4E-15	6.46	1.54
Ssk	62.64	37.36	0.23	2.5E-14	6.65	1.56
Str	57.32	42.68	0.22	3.7E-08	4.25	1.58

The quality of this analysis is confirmed by the reduced values of the P factor for all variables analyzed and also because F is much greater than F_{critical}, for all variables. Thus the use of this analysis to perform truthful considerations is validated.

According to results previously published by other authors (Ström 2003; Ashori et al 2008), it is generally believed that a film (surface sizing and/or coating) on the top of a paper sheet reduces roughness by filling the depression irregularities of the paper surface. However, the main observation that can be drawn from Table 4.1 is that there is a large variability within samples, which indicates that the addition of the surface sizing agents to the cationic starch has a reduced impact on the surface topography. This was not totally unexpected, since even considering the largest percentage of surface sizing agent added (20%), the surface sizing blend is composed mainly of starch (80%). It should also be remembered that the main objective of the copolymers addition is to change the chemical rather than the physical properties of the surface. Detailed results corresponding to the several topographic parameters and additional plots can be consulted in Appendix C. Here, the analysis will be illustrated with the most adequate and relevant plots.

In order to have a general understanding of the surface topography of the samples, the most adequate variables, Sa and Sq, corresponding respectively to the average roughness and the root mean square roughness deviation, are represented in Figure 4.17.

Figure 4.17 presents the results according to the percentage of surface sizing agent added to the sizing blend. In these graphs the interval within which the differences from the standard sample are not valid (based on the reproducibility factor) is also represented (the interval between the dashed lines).

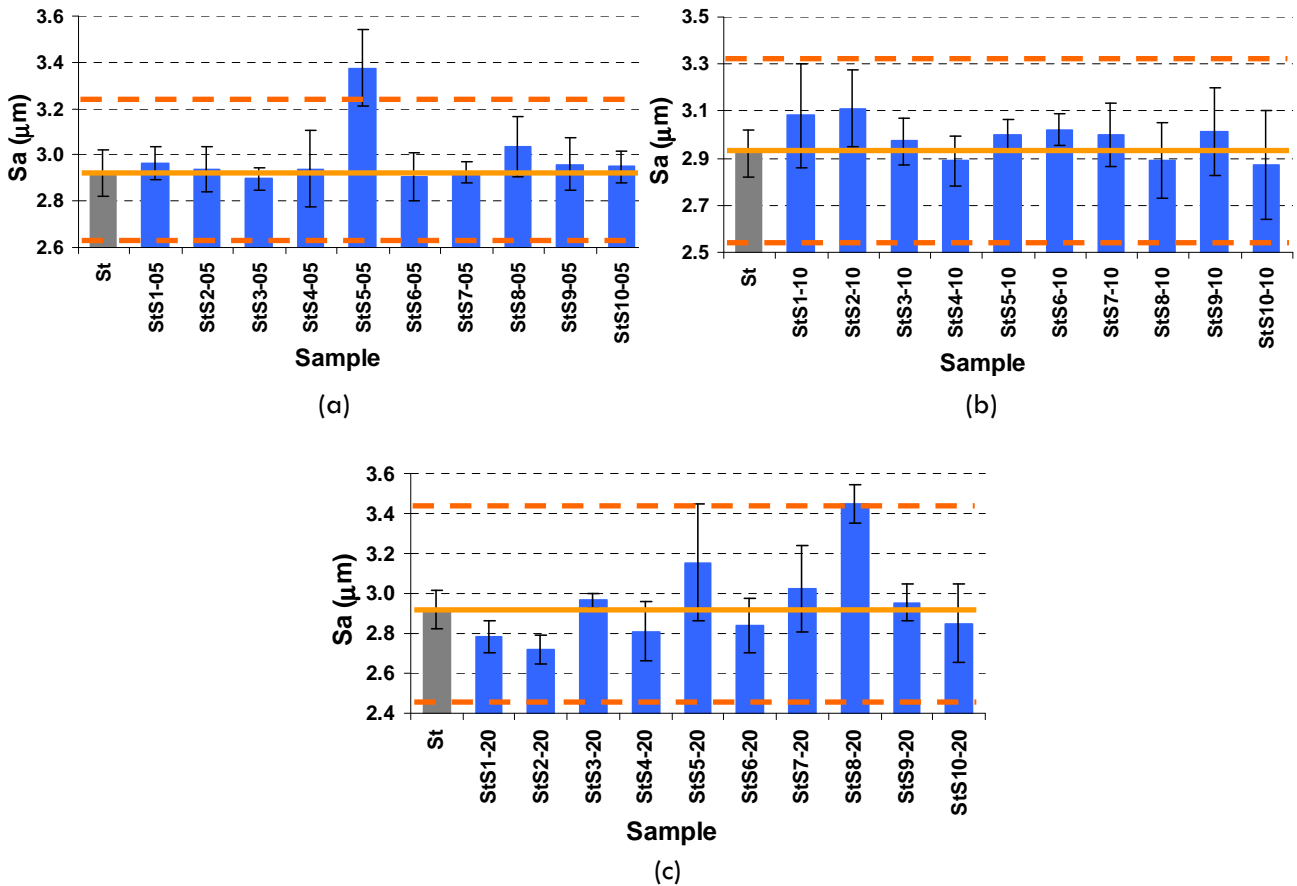


Figure 4.17 – Sa and values obtained for all the paper samples, divided according to the amount of surface sizing agent added; (a) Sa values for samples with 5% of surface sizing agent; (b) Sa values of the samples with 10% of surface sizing agent, (c) Sa values of the samples with 20% of surface sizing agent. Lines — — — — — delimit the interval (based on ANOVA) in which the samples are not distinguishable from the St sample.

From the observation of Figure 4.17 it is possible to notice that there is not a clear tendency among the different samples, for any of the incorporation percentages. In some cases Sa and/or Sq increase when the synthetic copolymers are added to the cationic starch while in others they diminish. However, the Sq values are high, which means that these samples have a large amount of valleys or peaks (this variable does not allow to differentiate valleys from peaks, as mentioned before).

Figure 4.18 illustrates the effect of the concentration increase in the surface topography, using as example some surface sizing agents with quite different behaviors.

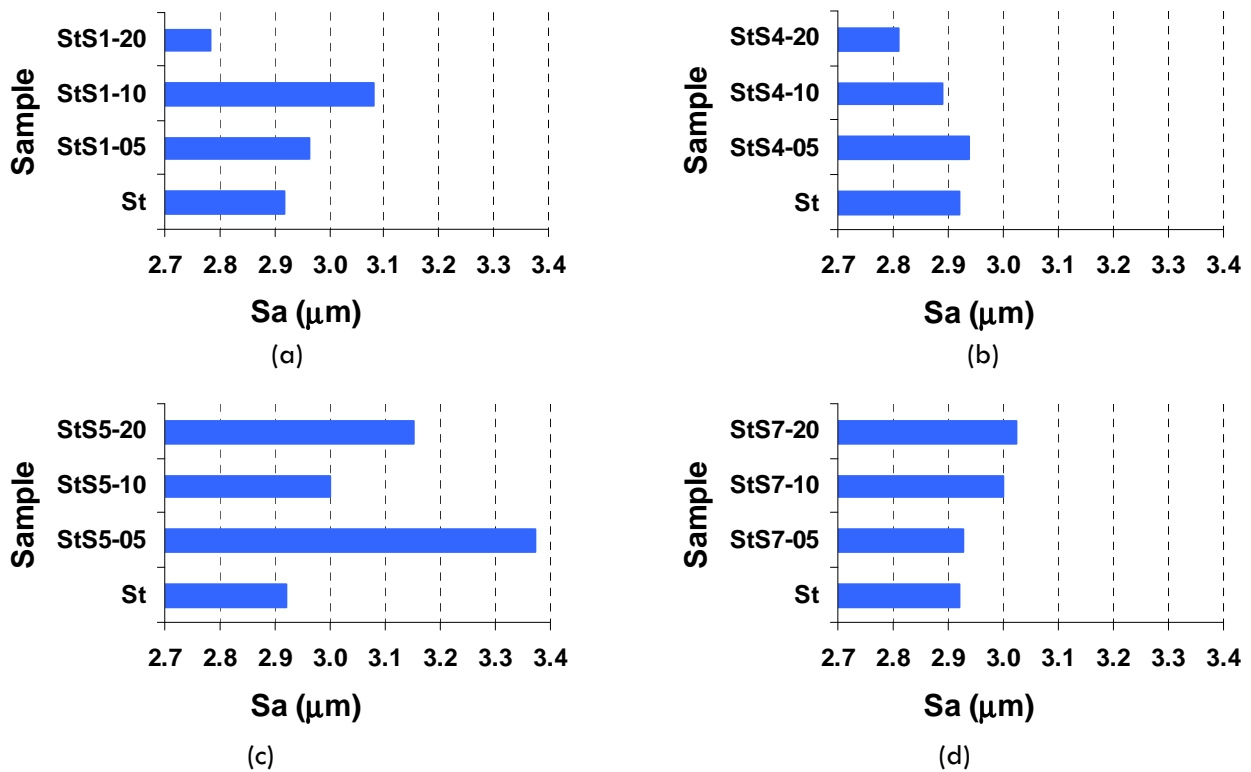


Figure 4.18 – Influence of the surface sizing agent concentration in the Sa values; (a) surface sizing agent S1; (b) surface sizing agent S4, (c) surface sizing agent S5, (d) surface sizing agent S7.

From Figure 4.18 it is clear that the increase of the surface sizing agent amount has not a consistent impact on Sa. Besides, the differences can not be recognized or analyzed as a result of the surface modifications performed, since they are not statistically significant.

From the analysis of the maximum height (S_p), the maximum depth (S_v) and the Skewness (S_{sk}) it is possible to verify whether are the valleys or the peaks that dominate the topography of the samples. The results are presented in Table 4.2.

Table 4.2 – Values of the roughness parameters Sp, Sv and Ssk obtained for the different paper samples.

Sample	Amplitude Parameters		
	Sp (μm)	Sv (μm)	Ssk
St	8.83 \pm 0.31	10.88 \pm 0.33	-0.27 \pm 0.03
StS1-05	8.93 \pm 0.55	11.17 \pm 0.48	-0.25 \pm 0.07
StS1-10	9.07 \pm 0.90	11.72 \pm 0.88	-0.37 \pm 0.18
StS1-20	8.44 \pm 0.15	9.81 \pm 0.41	-0.16 \pm 0.01
StS2-05	8.82 \pm 0.48	11.45 \pm 0.69	-0.41 \pm 0.10
StS2-10	9.00 \pm 1.00	12.05 \pm 0.59	-0.50 \pm 0.14
StS2-20	8.14 \pm 0.21	10.50 \pm 0.21	-0.32 \pm 0.06
StS3-05	8.15 \pm 0.04	11.67 \pm 0.27	-0.45 \pm 0.04
StS3-10	9.35 \pm 0.30	10.16 \pm 0.41	-0.14 \pm 0.05
StS3-20	8.36 \pm 0.08	11.95 \pm 0.21	-0.49 \pm 0.04
StS4-05	9.16 \pm 0.27	10.90 \pm 0.67	-0.27 \pm 0.04
StS4-10	8.48 \pm 0.11	11.12 \pm 0.86	-0.39 \pm 0.09
StS4-20	8.31 \pm 0.19	10.09 \pm 0.47	-0.24 \pm 0.03
StS5-05	9.29 \pm 0.21	13.38 \pm 0.67	-0.46 \pm 0.08
StS5-10	9.21 \pm 0.27	10.48 \pm 0.43	-0.19 \pm 0.02
StS5-20	9.10 \pm 0.37	12.22 \pm 1.77	-0.28 \pm 0.11
StS6-05	8.89 \pm 0.11	10.87 \pm 0.60	-0.25 \pm 0.04
StS6-10	9.17 \pm 0.28	11.00 \pm 0.28	-0.25 \pm 0.04
StS6-20	8.92 \pm 0.18	10.14 \pm 0.32	-0.19 \pm 0.04
StS7-05	8.23 \pm 0.19	11.77 \pm 0.21	-0.43 \pm 0.07
StS7-10	8.59 \pm 0.16	10.93 \pm 0.41	-0.22 \pm 0.07
StS7-20	9.44 \pm 0.83	10.94 \pm 0.75	-0.22 \pm 0.04
StS8-05	8.95 \pm 0.13	11.28 \pm 0.44	-0.27 \pm 0.03
StS8-10	8.66 \pm 0.82	11.38 \pm 0.54	-0.37 \pm 0.16
StS8-20	10.85 \pm 0.26	12.42 \pm 0.67	-0.25 \pm 0.08
StS9-05	8.80 \pm 0.36	11.63 \pm 0.86	-0.38 \pm 0.11
StS9-10	8.93 \pm 0.43	10.87 \pm 0.91	-0.21 \pm 0.04
StS9-20	9.03 \pm 0.05	10.15 \pm 0.07	-0.14 \pm 0.03
StS10-05	8.90 \pm 0.17	10.71 \pm 0.83	-0.32 \pm 0.06
StS10-10	8.58 \pm 0.91	10.85 \pm 0.52	-0.32 \pm 0.09
StS10-20	8.69 \pm 0.58	11.03 \pm 0.83	-0.29 \pm 0.07

For all samples, the Sv values are larger than the Sp values, meaning that these samples have more deep valleys than high peaks. This is also confirmed by the Ssk negative values.

Since the surface sizing formulations were applied in a laboratory device which implies the contact of the sizing roll with the paper surface (Chapter 3), and considering a previous publications on this issue (Bodurtha et al. 2005), it is important to verify whether the

application process induces directionality in the surface of the paper samples. For that the texture aspect ratio of the surface, evaluated by the topographic parameter Str, must be analyzed. From the values of Str presented in Figure 4.19 it is possible to confirm that the paper surfaces exhibit a certain degree of anisotropy, since the Str values are mostly inferior to 0.5. However this anisotropy is not significant since the values are not too close to 0.

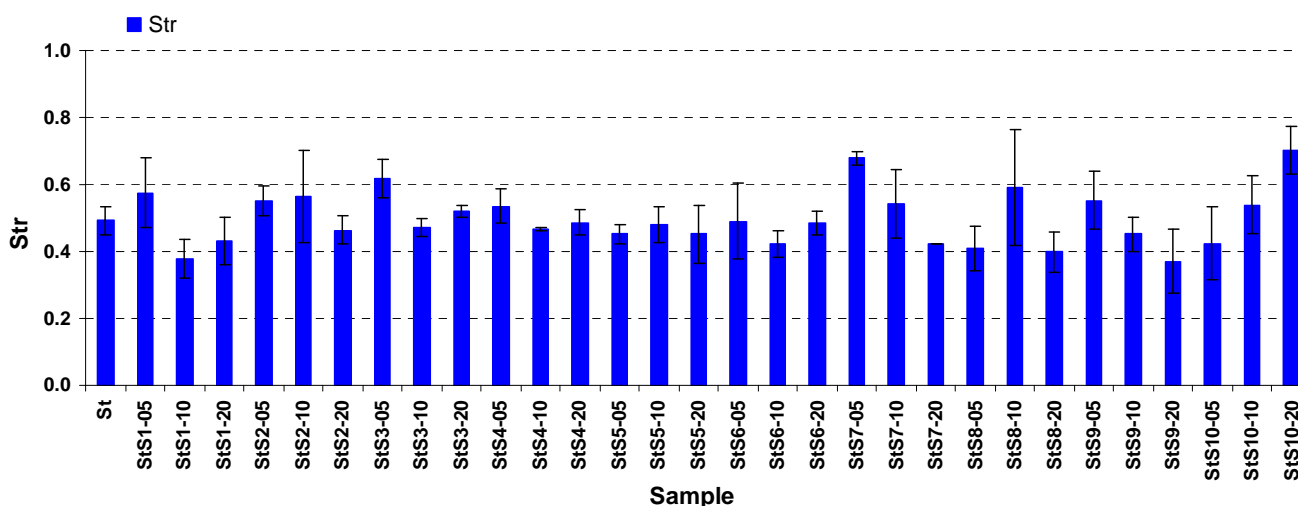


Figure 4.19 – Str values obtained for all the samples.

Despite the impossibility of detailed comparisons between all the samples using the profilometry results, due to the little differences and the lack of statistical significance, some general characteristics of the physical properties of these paper samples can be underlined.

The addition of the synthetic surface sizing agents changes the values of the topographical parameters, but not significantly. The surfaces are moderately rougher with a large predominance of valleys over peaks, and without any significant anisotropy.

The topographical characteristics of the samples will certainly participate in the ink reception process, but since they are identical to all samples, they will not respond for the differences in terms of printing performance.

Thus, any eventual distinct impact of the various sizing agents will only be noticed on the porous structure of the samples and/or on the chemical characteristics of the paper surface, which will be analyzed in the next chapters.

CHAPTER 5

MERCURY POROSIMETRY

5 MERCURY POROSIMETRY

5.1 THEORY

The porosity of any type of material is defined as the ratio of the voids volume to the total volume of the sample:

$$\text{Porosity} = \frac{\text{Volume of voids}}{\text{Total volume of the sample}} = \frac{\text{Pore volume}}{\text{Pore volume} + \text{Solids volume}} \quad (5.1)$$

Paper is a porous material made of a network of fibers with voids in between. Porosity is a critical factor in all sorts of paper, from printing papers, filter papers, cigarette papers to bag papers. In particular for P&W papers, porosity significantly affects opacity, bulk and the ink reception process (Knauf and Doshi 1986; Johnson et al. 1999; Keskitalo 2000). In fact, porosity indicates how paper will react to fluid penetration in coating, sizing and printing operations. Additionally, porosity can also be an important factor in a vacuum feeding operation of a printing press (Johnson et al. 1999)

5.1.1 MEASUREMENT TECHNIQUES

Although easy to define, paper porosity is hard to measure accurately and several techniques can be employed to quantify the volume of voids, whose values greatly depend upon the method and the conditions used (Knauf and Doshi 1986; Murakami and Imamura 1980). However, two types of procedures are frequently used for paper porosity determination: the air resistance and air permeability methods and the methods involving volume or density measurements (Chinga and Helle 2002a; Bordurtha et al. 2005).

The air resistance and air permeability methods are both based on the resistance to the passage of air offered by the paper structure when a pressure difference exists between the two sides of the paper. The air resistance is measured as the time for a given volume of air to flow through a specimen under specified conditions, while the air permeability is measured as the volume of air which flows through the paper for a given time interval, following the Sheffield Method (described in TAPPI T 547) or the Gurley Method (detailed in TAPPI T 460 and TAPPI T 536). Many papermakers rely upon Gurley Densometer tests to evaluate the porous nature of paper. However, it has been shown that the volume fraction available to flow (permeability) is not equal to porosity: papers can have the same

permeability but different porosities (Lindsay 1998; Lindsay 2000; Branton and Baker 2002).

The methods involving volume or density measurements include water saturation and evaporation methods, nitrogen gas adsorption or mercury intrusion porosimetry (Johnson et al. 1999; Alinec et al. 2002).

Among these methods, mercury porosimetry has an increasing use for paper porosity measurements, since it is able to characterize a wide range of pore sizes, from a few hundred micrometers to a few nanometers and a distribution of the pore sizes is also achieved (Alinec et al. 2002).

5.1.1.1 Mercury Porosimetry

Mercury Porosimetry is based on the capillary law governing liquid penetration into small pores. This law, in the case of cylindrical pores and non wetting liquids like mercury is expressed by the Washburn equation (Knauf and Doshi 1986; Bordurtha et al. 2005):

$$D = - \left(\frac{1}{P} \right) \cdot 4\sigma \cos \theta \quad (5.2)$$

where D is the pore diameter, P is the applied pressure, σ the surface tension, and θ the contact angle, all in consistent units. As this equation shows, the larger the pore size, the lower the pressure needed to overcome the capillary forces. Therefore the pore-size distribution can be measured by gradually increasing the pressure on a vessel (called penetrometer, Figure 5.1) containing a piece of paper submerged in mercury and measuring the intake of this by the paper after each increase of pressure. In this way a cumulative pore volume can be determined as a function of the applied pressure (or pore diameter, inversely proportional to pressure as described Washburn eq.), starting with the volume of the largest pores. The output is the so called intrusion curve.

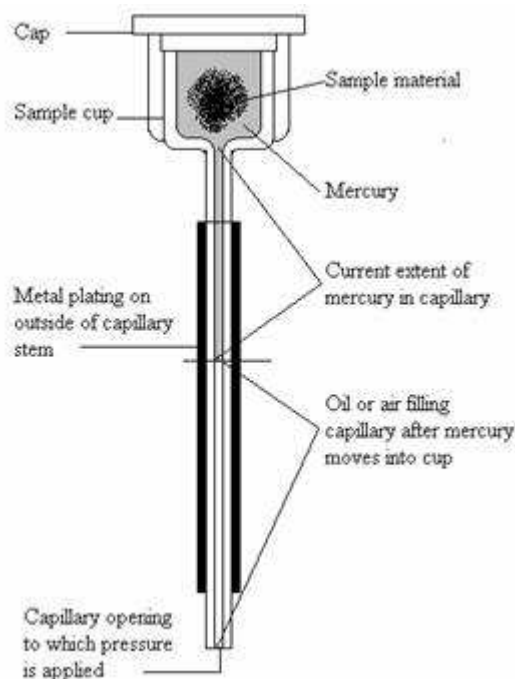


Figure 5.1 – Schematic representation of a penetrometer used in mercury intrusion porosimetry (URL1 2008). It is constituted by a small reservoir where the sample is placed and a long stem. All this is full of mercury at the lowest pressure. As pressure is increased, mercury penetrates into the sample pores (intrusion) and the length of penetrometer stem that is filled with mercury decreases. The difference in mercury level corresponds to the volume intruded in the sample.

However, real pores are never exactly cylindrical, and thus the measured pore radius is an equivalent circular pore radius.

Mercury porosimetry data is not limited to porosity and pore size distribution but this technique also provides information about bulk and skeletal density. Bulk density is the ration between the weight and the bulk volume, which includes the solid volume as well as the volume of all empty spaces. This volume is measured at the lowest intrusion pressure. In opposition the “skeletal” density, corresponding to the “skeletal” volume, refers to the volume of the sample discounting all the voids occupied by the mercury at the highest pressure (Micromeritics 2000).

5.1.1.2 Equipment - AutoPore IV 9500

In this study, the Micromeritics equipment AutoPore IV 9500 (Figure 5.2) was used to perform the mercury porosimetry measurements for all the 31 samples produced. In this apparatus mercury pressure is increased from about 1 psia up to 33 000 psia in two different

chambers: the low pressure port, where the increment in pressure is due to pressured gas (± 2 atm (25 psia)) and the high pressure port where pressure is generated by an hydraulic system.



Figure 5.2 – Mercury porosimeter AutoPore IV 9500.

After submitting the sample to a previous degasification, mercury is admitted to the penetrometer at a pressure of about 1-2 psia, being the pressure continuously increased up to about 25 psia at the low pressure port (covering pore diameters from 360 to 6 μm). The penetrometer is subsequently installed in the high pressure port where pressure is increased up to 33 000 psia, enabling the measurement of pore diameters as small as 5 nm.

The analysis was repeated three times for each paper sample, using pieces of different sheets (approximately 10 pieces of about 1.5 x 1.5 cm^2 per analysis). All the 31 samples were analyzed.

5.2 RESULTS

As mentioned before, mercury data provides information not only about porosity but also about intrusion volume (volume of mercury per sample weight) and density (bulk and skeletal). These values are tabulated in Table 5.1 for one of the measurements performed for the reference sample (sized with cationic starch only) and for sample STS4-20, as an example. All the other values can be found in Appendix D.

Table 5.1 – Exemplification of the mercury porosimetry output, using samples St and StS4-20.

Sample = St	Sample = StS4-20
Total Intrusion Volume = 0.7624 ml/g	Total Intrusion Volume = 0.7851 ml/g
Bulk Density at 0.52 psia = 0.7450 g/ml	Bulk Density at 0.52 psia = 0.7181 g/ml
Apparent (skeletal) Density = 1.7246 g/ml	Apparent (skeletal) Density = 1.6464 g/ml
Porosity = 56.8003 %	Porosity = 56.3830%

As it can be seen, and despite the different sizing formulations, the values obtained for the different parameters are quite similar: intrusion volumes of about 0.77ml/g, bulk densities close to 0.73 g/ml, skeletal densities of 1.65 and 1.72 g/ml and porosities of approximately 56% were obtained. Considering the totality of the samples tested the range of variation remains reduced: 0.68 - 0.85 ml/g for intrusion volume, 0.66 - 0.79 g/ml and 1.45 - 1.80 g/ml for bulk and skeletal densities, respectively, and a variation between 51.71 - 58.69 % regarding porosity. These values are in agreement with those published in literature (Moura et al. 2005)

Regarding the skeletal density, the values measured are in general larger than that of cellulose (1.55 g/ml) which is compatible with the fact that paper contains other denser components besides cellulose fiber, such as fillers.

In Figure 5.3 are represented the intrusion curves (differential and cumulative) of the St Sample, which exhibits two peaks: one at about 3 μm and another at about 20 μm . The same is detected for all the samples tested, whose curves can be consulted in Appendix D.

This result is in agreement with the results obtained by other authors (Moura et al. 2005) for paper sheets and is usually associated to the mercury penetration into smaller pores of the paper internal structure.

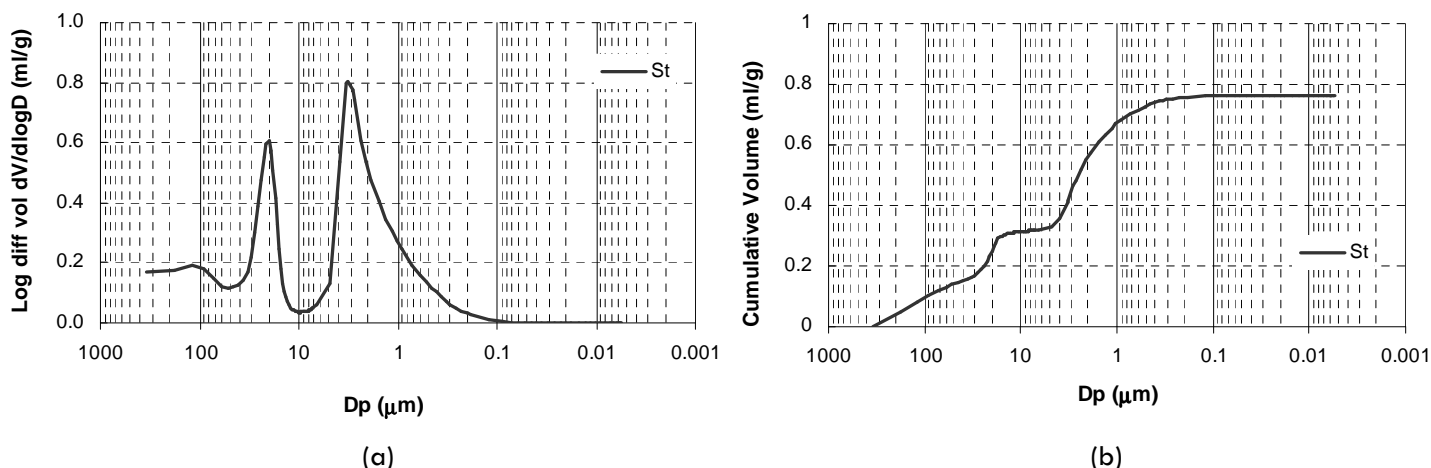


Figure 5.3 - Differential (a) and cumulative (b) pore size distribution diagrams for sample St.

The effect of the surface sizing agent amount is illustrated in Figure 5.4 for StS6-*j* samples, which also includes the curves corresponding to the standard sample (St). This figure shows that although the curves are quite close to each other, those corresponding to the larger copolymer concentrations are slightly but consistently displaced to the right (more evident in the differential curves), denoting a slight decrease in the pores size, as the amount of synthetic sizing agent increases. This was a widespread effect in all samples and is probably due to the filling of the larger pores by the sizing formulation.

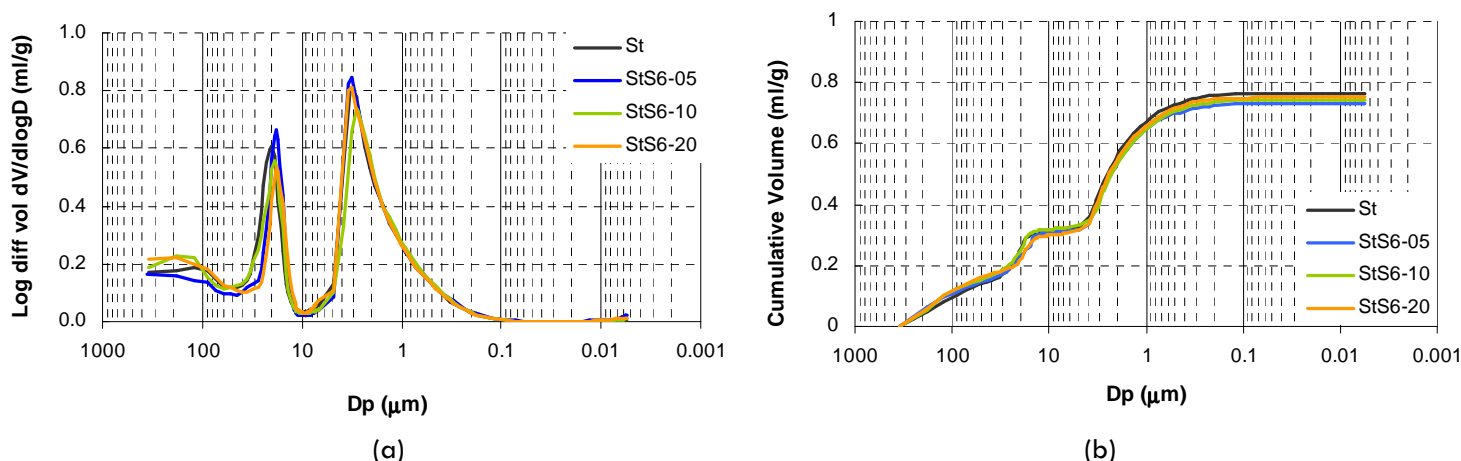


Figure 5.4 – Differential (a) and cumulative (b) pore size distribution diagrams for samples St, StS6-05, StS6-10 and StS6-20.

It should be pointed out that the effect of surface sizing on paper porosity has not been the subject of many studies but the general idea is that it decreases paper porosity (Martin 2008). Moreover regarding the effect of adding distinct copolymers no studies are available in the open literature.

Before continuing the study of the effect surface sizing on paper porosity, ANOVA was applied to the porosimetry data. The results are presented in Table 5.2 for all samples and for each group corresponding to a given concentration of the synthetic agents (5 %, 10 % and 20 %)

Table 5.2 - ANOVA results for porosity.

Variable	Contribution to total variation (%)		Reproducibility Factor (r)	P	F	F _{critical}
	Among samples	Within samples				
Porosity (all Samples)	39.67	60.33	4.65	0.15	1.36	1.64
Porosity (St + StSi-05)	54.31	45.69	4.29	0.03	2.61	2.30
Porosity (St + StSi-10)	41.17	58.83	4.11	0.19	1.54	2.30
Porosity (St + StSi-20)	22.28	77.72	5.14	0.77	0.63	2.30

From Table 5.2 it is possible to observe that the statistical validity of this analysis is not guaranteed, since F is inferior to F_{critical}. Nonetheless, it is worth to mention that, in general, the contribution to the total variation of the variability within samples is larger than that among the different samples. Therefore, the addition of the surface sizing agents does not have a relevant and consistent effect on the samples porosity, as evaluated by mercury intrusion.

Figure 5.5 and

Figure 5.6 represent the average porosities of all paper samples tested and of each copolymer incorporation percentage, respectively, and the corresponding deviations. In these graphs the interval within which the differences from the standard sample are not valid (based on the reproducibility factor) is also represented by the dashed lines.

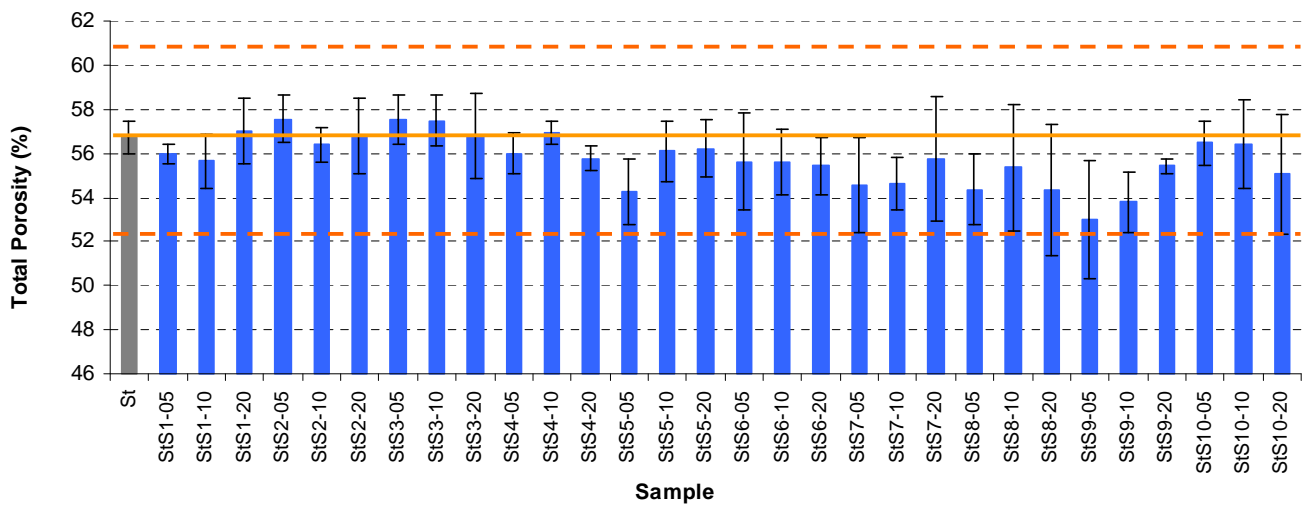


Figure 5.5 – Total porosity values obtained for all paper samples.

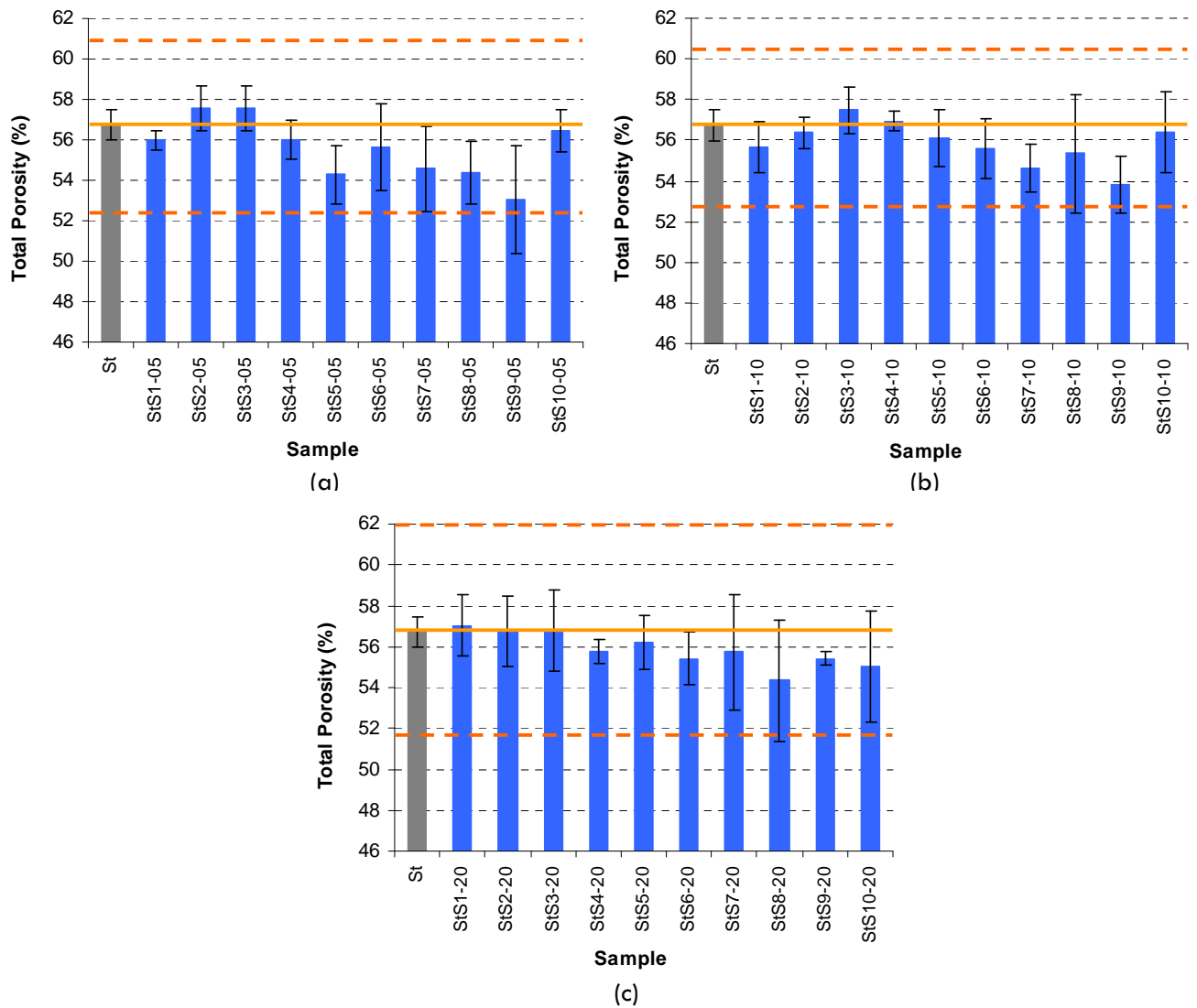


Figure 5.6 – Total porosity values, compared with sample St, of the samples (a) with 5% of surface sizing agent; (b) with 10% of Surface sizing agent; (c) with 20% of surface sizing agent. The dashed lines — — — delimit the interval (based on ANOVA) in which the samples are not distinguishable from the St sample.

In spite of the aforementioned lack of statistical significance, a slight decrease in sample porosity is noticed, in general, as the copolymer amount increases (relatively to the standard sample), in addition to the pore size diminution tendency detected in Figure 5.4.

Furthermore, the small impact of the various surface sizing formulations on sample porosity is in agreement with profilometry data presented in Chapter 4, confirming the reduced influence of the addition of the synthetic surface sizing agents to the surface sizing formulation in the physical properties of the paper. Thus, any eventual distinct impact of the various sizing agents will only be noticed on the chemical characteristics of the paper surface.

CHAPTER 6

CONTACT ANGLE MEASUREMENTS

6 CONTACT ANGLE MEASUREMENTS

6.1 THEORY

6.1.1 FUNDAMENTAL INTERACTIONS

When a liquid is brought into contact with a solid, a solid-liquid interface is formed as a result of the molecular contact between the solid and the liquid. The importance of this interface in lots of applications has led to extensive studies over the past 60 years (Brigs 1989; Adamson 1997). The molecular contact between the solid and the liquid is called wetting and is essential in many applications such as spreading of coatings or adhesion and absorption into porous solids as paper sheets.

The knowledge of the factors controlling the interaction between the paper and the different liquids used in the printing processes is fundamental in order to control and improve paper behavior in printing operations (Aspler 1983; Garret and Lee 1998; Keskitalo 2000; Shen et al. 2000; Wågberg and Westerlind 2000; Hoang et al. 2001; Seppänen et al. 2004; Kannangara et al. 2006; Gu et al. 2007).

In printing techniques where water is used as solvent, such as inkjet printing, the wetting properties of the paper are even more important, since ink does not stay at the surface but it spreads and is absorbed (Figure 6.1) before drying, naturally affecting print quality (Breda 2001; Keskitalo 2000).

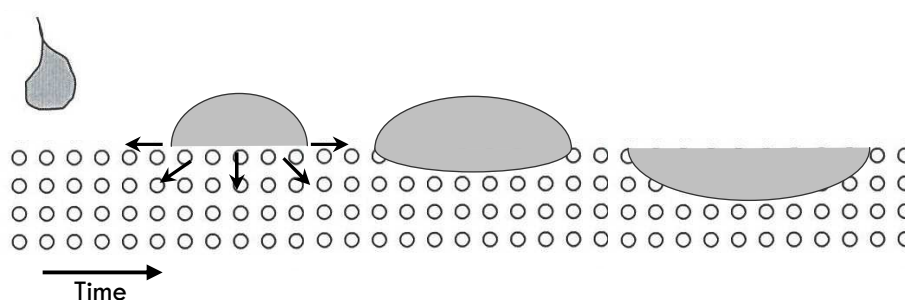


Figure 6.1 – Schematic representation of paper-ink interaction.

Figure 6.2 represents a typical wetting system consisting of a liquid drop on a solid surface. In such systems, the most important measurable characteristic is the contact angle, θ , which results of the equilibrium between the adhesive (σ_{SL}) and cohesive (σ_L and σ_S) forces involved. It is defined as the angle between the tangent to the liquid-gas interface and the

tangent to the solid interface at the contact point between the three phases (Gennes 1985; Brigs et al. 1989; Keskitalo 2000; Levlin and Söderhjelm 2000; Marmur 2006).

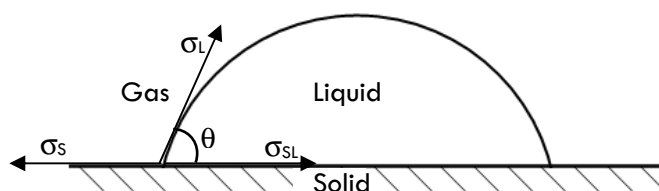


Figure 6.2 – Contact angle formation on a solid surface according to the Young equation

When a wetting system is created, three distinct situations may be found: no wetting (contact angle $> 90^\circ$), partial wetting ($0^\circ < \text{contact angle} < 90^\circ$) or complete wetting (contact angle = 0), as illustrated in Figure 6.3 (Gennes 1985; Brigs et al. 1989; Keskitalo 2000; Levlin and Söderhjelm 2000; Marmur 2006).

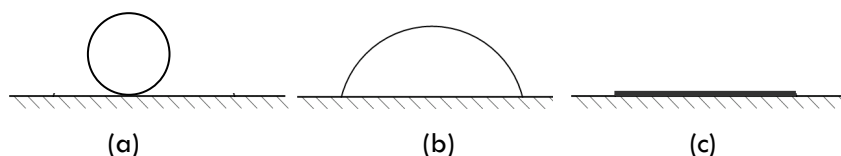


Figure 6.3 – Representation of the possible wetting situations: (a) non wetting, (b) partial wetting and (c) complete wetting.

The main factor ruling wetting is the surface energy (usually called surface tension when referring to liquids) of the components involved, which determines how the liquid phase and the solid phase interact with each other. (Gennes 1985; Brigs et al. 1989; Keskitalo 2000; Levlin and Söderhjelm 2000; Marmur 2006).

To understand the origin of the surface tension/energy of a material it is necessary to examine its surface at a molecular scale. Between the individual molecules there are different attraction forces, such as London-Van der Waals, dipole, hydrogen bonds, ionic forces or even acid-base interactions. In the interior of the material, each molecule is surrounded by others, and a force balance is established. This balance does not exist at the surface of the material, and all forces are directed towards the interior, creating the surface tension of the material, ruled by the type of attraction between the molecules of the surface (Gennes 1985; Brigs et al. 1989; Keskitalo 2000; Levlin and Söderhjelm 2000; Marmur 2006).

When the equilibrium between the liquid and the solid is established, the balance of forces of the system at the contact point between the three phases (Figure 6.2) can be described by the well known Young equation:

$$\sigma_S = \sigma_{SL} + \sigma_L \cdot \cos \theta \quad (6.1)$$

where σ_S is the surface free energy of the solid, σ_{SL} is the interfacial free energy between the liquid and the solid, σ_L is the surface tension of the liquid, and θ is the contact angle.

The new interface formed by the contact between the liquid and the solid surface is characterized by a given energy that would be the one needed to remove the liquid drop from the surface; this energy is called the work of adhesion (Wa), and is computed by (Brigs et al. 1989):

$$Wa = \sigma_S + \sigma_L - \sigma_{SL} \quad (6.2)$$

By combining Equations 6.1 and 6.2 the so called Young-Dupre equation is obtained, which relates the work of adhesion with the contact angle value:

$$Wa = \sigma_L \cdot (1 + \cos \theta) \quad (6.3)$$

These relations, based on force balances and thermodynamic definitions, are applicable to the interactions occurring in any solid-liquid system and several theories have been developed to use them in order to calculate the surface properties of solids, namely the surface free energy, σ_s .

6.1.2 SURFACE ENERGY CALCULATION THEORIES

The most used theories to determine the surface energy of solids from contact angle data using liquids whose surface tensions are known, are those of Zisman (1960's); Owens, Wendt, Rabel and Kaelbe (OWRK) (1960's); Fowkes (1950's) and of van Oss & Good (1980's) (Genes 1985; Brigs et al. 1989; Keskitalo 2000; Levlin and Söderhjelm 2000; Marmur 2006)

6.1.2.1 Zisman

In this theory, at least two liquids with known surface tensions are used and the cosines of the measured contact angles are plotted versus the surface tension of the corresponding liquid.

The straight line obtained is then extrapolated to a value of $\cos\theta=1$ ($\theta=0^\circ$). The extrapolated value is called the critical surface tension (σ_c), and corresponds to complete wetting ($\theta=0$).

The Young equation (6.1) then comes:

$$\sigma_s = \sigma_{sl} + \sigma_c \quad (6.4)$$

when $\sigma_{sl} = 0$, $\sigma_c = \sigma_s$ and thus the critical surface tension equals the solid surface energy.

This method is of limited use since the linear relationship only applies when the relationship between the dispersive and the polar interactions is the same in the solid and in the liquid. This practically only occurs under exceptional circumstances as when purely dispersive interactive solids and liquids are involved (eg. non-polar solids as polymers as polyethylene and Polytetrafluoroethylene).

6.1.2.2 Owens, Wendt, Rabel and Kaelble

This theory distinguishes the dispersive and polar components of the surface energy, which are considered independent and additive for all the constituents of the system:

$$\sigma = \sigma^D + \sigma^P \quad (6.5)$$

Thus, for a liquid:

$$\sigma_L = \sigma_L^D + \sigma_L^P \quad (6.6)$$

where σ_L is the liquid surface tension, σ_L^D is the dispersive component of the liquid surface tension and σ_L^P is the polar component of the liquid surface tension.

Similarly, for the solid:

$$\sigma_s = \sigma_s^D + \sigma_s^P \quad (6.7)$$

In this theory the polar interactions include Coulomb interactions between permanent and induced dipoles.

As for the work of adhesion, this theory also considers the addition of a dispersive and a polar component:

$$W_a = W_a^D + W_a^P \quad (6.8)$$

Each component of the adhesion work is approximated by the geometric mean as:

$$Wa^D = 2 \cdot \sqrt{\sigma_L^D \cdot \sigma_S^D} \quad (6.9)$$

$$Wa^P = 2 \cdot \sqrt{\sigma_L^P \cdot \sigma_S^P} \quad (6.10)$$

Thus

$$Wa = 2 \cdot \sqrt{\sigma_L^D \cdot \sigma_S^D} + 2 \cdot \sqrt{\sigma_L^P \cdot \sigma_S^P} \quad (6.11)$$

Combining Equation 6.11 with Equation 6.3 leads to:

$$\sigma_L \cdot (1 + \cos \theta) = 2 \cdot \sqrt{\sigma_L^D \cdot \sigma_S^D} + 2 \cdot \sqrt{\sigma_L^P \cdot \sigma_S^P} \quad (6.12)$$

Re-arranging this equation it is possible to obtain:

$$\frac{\sigma_L}{\sqrt{\sigma_L^D}} \cdot \frac{(1 + \cos \theta)}{2} = \sqrt{\sigma_S^P} \cdot \frac{\sqrt{\sigma_L^P}}{\sqrt{\sigma_L^D}} + \sqrt{\sigma_S^D} \quad (6.13)$$

By plotting $\frac{\sigma_L}{\sigma_L^D} \cdot \frac{1 + \cos \theta}{2}$ vs $\frac{\sqrt{\sigma_L^P}}{\sqrt{\sigma_L^D}}$ for several liquids with known values of σ_L^D and σ_L^P a

straight line is obtained from which it is possible to calculate σ_S^P (from the slope) and σ_S^D (from the intersection with the vertical axis).

Despite being a universal method, since it can be used for any solid surface, it also presents some drawbacks, namely the poor approximation considered for the polar component ($Wa^P = 2 \cdot \sqrt{\sigma_L^P \sigma_S^P}$) and the fact that the acid-base interactions are neglected.

6.1.2.3 Fowkes

Like in the previous theory, the Fowkes theory also distinguishes the dispersive and non-dispersive parts of the surface energy. The geometric mean is again used to approximate the work of adhesion, but only in the case of the dispersive part. The non dispersive interactions, simply denoted as I^{nd} , are not quantified in this theory. Since no information is available for I^{nd} , this analysis is only used for liquids having merely dispersive interactions with the solid surface under study.

Considering Equation 6.3 and using the approximation for Wa as:

$$Wa = 2 \cdot \sqrt{\sigma_L^D \sigma_S^D} + I^{nd} \quad (6.14)$$

From Eq. 6.3 and considering $I^{nd} = 0$, Eq. 6.14 leads to

$$\sigma_L (1 + \cos \theta) = 2 \cdot \sqrt{\sigma_L^D \cdot \sigma_S^D} \quad (6.15)$$

By plotting $\sigma_L \cdot (1 + \cos \theta)$ vs $\sqrt{\sigma_L^D}$ for several liquids, a straight line is obtained from whose slope the value of σ_S^D is computed.

Similarly to the Zisman theory, only the dispersive interactions are taken into account and thus it is a quite restricted theory, since it is only applicable to non-polar systems.

6.1.2.4 van Oss & Good

In this theory, the interaction between liquid and solid is interpreted as the interaction between an acid and a base. It considers that the surface energy can be decomposed into σ^{LW} and σ^{ab} :

$$\sigma = \sigma^{LW} + \sigma^{ab} \quad (6.16)$$

here the superscript LW stands for Lifshitz - van der Waals interactions, which include London dispersion, Keeson dipole-dipole and Debye induction whereas ab stands for Lewis acid-base interactions.

Once again the geometric mean is used to approximate the several components of the forces considered for the work of adhesion:

$$Wa = 2 \cdot \sqrt{\sigma_L^{LW} \cdot \sigma_S^{LW}} + 2 \cdot \sqrt{\sigma_L^+ \cdot \sigma_S^-} + 2 \cdot \sqrt{\sigma_L^- \cdot \sigma_S^+} \quad (6.17)$$

σ^+ denoting Lewis acid (electron-acceptor) and σ^- Lewis base (electron-donor) character.

Combining Equation 6.17 with Equation 6.3 leads to:

$$\sigma_L \cdot (1 + \cos \theta) = 2 \cdot \left(\sqrt{\sigma_L^{LW} \cdot \sigma_S^{LW}} + \sqrt{\sigma_L^+ \cdot \sigma_S^-} + \sqrt{\sigma_L^- \cdot \sigma_S^+} \right) \quad (6.18)$$

Equation 6.18 has three unknowns (σ_S^{LW} , σ_S^+ and σ_S^-). Thus and unlike the previous methods (based on graphical solving strategies), it is necessary to establish this equation for at least three liquids and solve the corresponding system numerically.

These theories are summarized in Table 6.1 showing that they not only differ in the outputs provided but also on the solving strategy and applicability.

Table 6.1 – Summary of the theories presented for surface energy calculations based on contact angle measurements.

Method	Outputs	Solving Strategy	Applicability	Drawbacks
Zisman	σ_C	Plot $\cos \theta$ vs σ_L	Non-Polar Solids	Little information
OWRK	σ_S^D σ_S^P	Plot $\frac{\sigma_L}{\sqrt{\sigma_L^D}} \cdot \frac{1 + \cos \theta}{2}$ vs $\frac{\sqrt{\sigma_L^P}}{\sqrt{\sigma_L^D}}$	Universal	Poor approximation for polar contribution
Fowkes	σ_S^D	Plot $\sigma_L \cdot (1 + \cos \theta)$ vs $\sqrt{\sigma_L^D}$	Non-polar systems	Little information
van Oss & Good	σ^{LW} σ^+ σ^-	System of equations $\sigma_L \cdot (1 + \cos \theta) =$ $= 2 \cdot \left(\sqrt{\sigma_L^{LW} \cdot \sigma_S^{LW}} + \sqrt{\sigma_L^+ \cdot \sigma_S^-} + \sqrt{\sigma_L^- \cdot \sigma_S^+} \right)$	Universal	Acid and base contributions of liquids are relative to water

Having in mind the materials under test in this study and the universal character of the OWRK theory, it was the one selected for the surface energy calculations in the present work.

6.1.3 CONTACT ANGLE MEASUREMENTS

For the measurements of the contact angle, several methods are available such as the Wilhelmy, the Washburn or the Sessile drop method. The former two methods are not commonly used, mainly because they are indirect methods (Koljonen and Stenius 2005; Gurau et al. 2006).

The sessile drop method is an optical contact angle method, which involves directly measuring the contact angle for a drop of liquid resting on a horizontal solid surface (Figure 6.2). Traditionally, the measurement of the contact angles was carried out using a goniometer eyepiece, being the results quite operator dependent. Nowadays, the measurement is performed through video based systems. Sophisticated CCD cameras are used to capture the drop image which is stored and subsequently analyzed by the equipment software.

Great care is however necessary in the position of the base line (phase boundary solid/liquid) and of the drop contour line. For the latter, different functions can be used, depending upon the software and the computing time available, as described in the next section. The test liquids to be used must be free from evaporation during the measurements and should correspond to a large range of polar and dispersive components. Table 6.2 lists the five test liquids selected for this study (diodomethane, propileneglycol, ethileneglycol, formamide and water), as well as their surface tensions and corresponding dispersive and polar components.

Table 6.2 – Properties of the test liquids used in this work.

Liquid	Surface Tension (mN/m)		
	Total	Dispersive Component	Polar Component
Diodomethane	50.80	50.80	0.00
Propileneglycol	35.40	26.40	9.00
Ethileneglycol	48.28	30.93	17.35
Formamide	58.13	32.28	25.85
Water	72.78	24.73	48.05

6.1.3.1 Equipment – OCA 20

The equipment used for the contact angle measurements was the model OCA 20 from Dataphysics, which can also be used for liquids surface tension measurements.

This equipment, depicted in Figure 6.4, is mainly composed of a light source, a sample holder, a dispense system and a CCD camera for image acquisition. Besides the calculations, the software coupled to the equipment, allows the user to control the dispense mechanism and the image acquisition (picture or video).

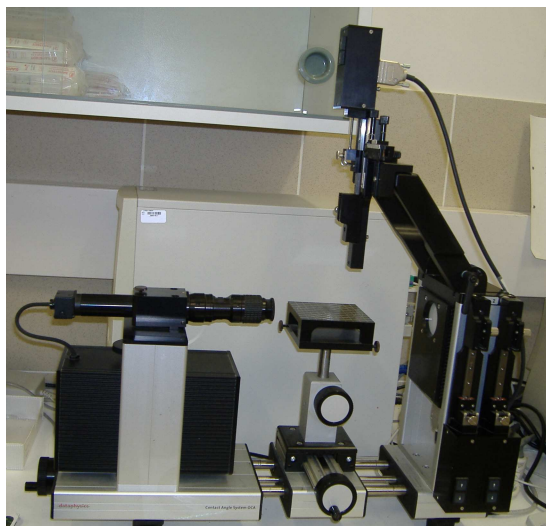


Figure 6.4 – Equipment used for the contact angle measurement - OCA 20 from Dataphysics.

With regard to the contact angle measurements, two distinct types of outputs can be achieved: the “static” contact angle, corresponding to the initial equilibrium contact angle, and the “dynamic” contact angle, corresponding values of the contact angle obtained by measuring the liquid drop contour throughout time.

Both types of results are achieved using the sessile drop method, which comprises five steps: drop dispense, image acquisition, base line detection, drop contour definition and contact angle calculation.

In this method a drop of the liquid under analysis is suspended in the bottom of a capillary. The shape of the drop is the result of two forces: the weight and the force that keeps the drop in a spherical form in order to minimize its surface (Roe et al. 1967).

The drop dispense is performed using an appropriate needle for achieving the static or the dynamic contact angle results: the liquid drop with a specified volume, dependent on the liquid viscosity (Table 6.3), is dispensed over the sample surface.

Table 6.3 – Drop volumes used for different liquids.

Liquid	Drop Volume (μl)
Diodomethane	2.00
Propileneglycol	9.00
Ethileneglycol	9.00
Formamide	8.00
Water	10.00

Regarding image acquisition, the static contact angle measurement is based on a digital image, captured by the CCD camera, of the resting drop immediately after contact with the solid surface (normally corresponding to a time interval inferior to 3 sec), whereas, for the dynamic contact angle, successive images of the liquid drop are acquired during 180 sec with a velocity of 2 frames/sec.

For the static contact angle measurements, at least 10 drops of each of the five test liquids (Table 7.2) were used, using at least two stripes of paper from two different sheets, cut in the diagonal direction in order to avoid any possible effect of fiber orientation. This procedure was repeated for each of the 30 samples. The surface free energy of each samples was computed from the average contact angle values (standard deviation of the measurements $< 2^\circ$). While for the dynamic contact angle measurements, at least three drops were analyzed (water was the test liquid for these measurements), also using at least two stripes of paper from two different sheets, cut in the diagonal direction in order to avoid any possible effect of fiber orientation and it was ensured the reproducibility of the results between tests, by verifying that the same behavior was observed.

The contact angle calculations depend on the accuracy of the baseline of the drop, corresponding to the solid/liquid interface, as well on the drop profile (liquid/air interface).

Distinct mathematical methods are available for fitting the drop contour, resulting in different accuracies and computational times: the height/width method, the Ellipse method and the Laplace-Young method. In the height/width method a segment of circle is fitted to the drop shape, but for large drops leads to considerable errors and thus it is of limited use. In the ellipse method, the drop contour is approximated by an ellipse whereas in the Laplace-Young method a line is fitted exactly to the drop contour which requires a longer computational time. The ellipse method is thus slightly less accurate but faster, being selected when a rapid calculation is necessary (fast absorption by the solid or dynamic contact angle measurements).

Besides the calculation of the contact angle values and corresponding errors associated to the measurement, the equipment software also enables the computation of other drop properties such as the drop volume, drop base diameter and drop age (associating a time to each contact angle value in the dynamic measurements).

6.1.4 TOPOGRAPHY INFLUENCE IN CONTACT ANGLE VALUES

The influence of the surface texture on contact angle measurements is well recognized and has been the subject of various studies (Wenzel 1936; Cassei and Baxter 1944; Cassei 1948; Wenzel 1949; Swain and Lipowsky 1998; Bico et al. 2002; Lai 2003; Marmur 2006). This influence results from the fact that, within a measured (geometric) unit area on a rough surface, the real surface is actually larger and consequently the intensity of the surface energy is greater than in the same (geometric) unit area of a smooth surface. Thus, between one liquid and one solid surface with some degree of roughness, two values of the contact angle are assigned: the apparent contact angle, θ , experimentally determined, and the real contact angle, θ' , derived from Young equation.

Reported results show that high surface roughness increases large contact angles ($> 90^\circ$) and decreases small contact angles ($< 90^\circ$), as schematically represented in Figure 6.5 (Levlin and Söderhjelm 2000; Bico et al. 2002; Marmur 2006).

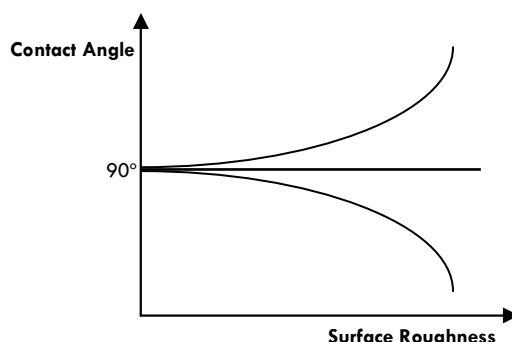


Figure 6.5 – Schematic representation of the surface roughness influence in contact angle values.

The earliest works on the effect of surface roughness on the contact angle measurement are attributed to Wenzel (Wenzel 1936; Wenzel 1949) and to Cassei and Baxter (Cassei and Baxter 1944; Cassei 1948), who provided different expressions for correcting apparent contact angles, based on different average parameters of a rough surface.

Cassei and Baxter assumed that the liquid forms a composite surface on the rough surface, not filling the grooves, as illustrated in Figure 6.6. In this case, the contact area includes a liquid-solid interface and a liquid-air interface (Lai 2003).

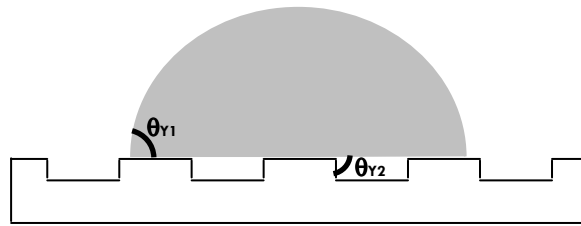


Figure 6.6 – Schematic representation of a drop on a rough surface according to Cassie model.

When a unit area of the surface has a surface fraction, φ_s , corresponding to the solid-liquid interface, with a Young contact angle θ_{Y1} , and a surface fraction, φ_a , corresponding to the air trapped in the hollows with contact angle θ_{Y2} (Figure 6.6), the apparent contact angle, according to Cassie, θ_C , is expressed by:

$$\cos \theta_C = \varphi_s \cdot \cos \theta_{Y1} + \varphi_a \cdot \cos \theta_{Y2} \quad (6.19)$$

Applying this equation to a rough surface trapping air in the hollows, leads to

$$\cos \theta_C = \varphi_s \cdot \cos \theta_{Y1} + (1 - \varphi_s) \cdot \cos 180^\circ = \varphi_s \cdot \cos \theta_{Y1} + \varphi_s - 1 \quad (6.20)$$

The Wenzel approach assumes that the liquid fills up the grooves of the rough surface (Figure 6.7) and considers that for an identically same increase in the free liquid area at the upper surface of the drop (liquid-air interface), a greater amount of actual surface is wetted under the drop in a rough surface when compared to a smooth surface (Lai 2003).

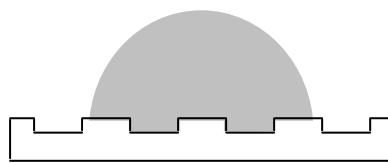


Figure 6.7 - Schematic representation of a drop on a rough surface according to Wenzel.

Therefore, according to Wenzel, a distinction must be made between the total (or actual) surface and the superficial (or geometrical) surface. For that a “roughness factor”, R^* , corresponding to the ratio between the actual surface and the geometric surface, is used in the following relation between the apparent (θ) and the real or Young contact angle (θ'):

$$\cos \theta = R^* \cdot \cos \theta' \quad (6.21)$$

In the present work, the Wenzel correction was selected to account for the influence of topography on the contact angle measurements for the following reasons: i) the material under study is paper, typically hydrophilic in nature, and thus the approach of Wenzel (Figure 6.7) seems a more realistic assumption; ii) the correction factor R^* is easier and more accurately determined than the surface fraction φ_s defined in the Cassie correction (Swain 1998; Wågberg and Westerlind 2000; Bico et al. 2002; Lai 2003; Marmur 2006).

Thus, the contact angle experimentally measured will be corrected using Equation 6.22 with the topographical correction factor R given by:

$$R^* = 1 + \frac{Sdr}{100} \quad (6.22)$$

here Sdr is the interfacial area ratio obtained by profilometry, as previously defined in Section 4.1.1.3

6.1.5 DYNAMIC PARAMETERS

Besides the measurement of the contact angle as a function of time, the software used also provides the values of the drop base diameter and of the drop volume. With this information, it is possible to simultaneously evaluate the spreading and absorption phenomena by computing the following parameters:

- ✓ Wetting velocity
- ✓ Spreading coefficient
- ✓ Absorption coefficient

The wetting velocity is calculated, according to the Tappi standard T458 om-89, using the contact angle values after 5 and 60 seconds (θ_5 and θ_{60} respectively):

$$\text{Wetting velocity } (^\circ/\text{sec}) = \frac{\theta_5 - \theta_{60}}{55} \quad (6.23)$$

6.2 RESULTS

The results obtained for the contact angles measured with the selected liquids, using the above described equipment, will be fully analyzed in this section.

Since inkjet inks are water based, the results obtained for the initial contact angle (known as static contact angle) with water are of special relevance to evaluate printing performance. Nevertheless, the data collected for the five liquids will be used to determine the surface energy and its components. The influence of the various synthetic surface sizing agents as well as of their different proportions will also be discussed. Finally, to complement the results, the evaluation of the contact angles variation throughout time (dynamic contact angle) will be examined.

Similarly to the procedure adopted in previous chapters, the results were firstly analyzed by ANOVA, in order to evaluate the statistical significance of their variability. The results of this analysis are presented in Table 6.4.

Table 6.4 – ANOVA of the contact angle results.

Variables (Contact Angles)*	Contribution for the total variation (%)		Reproducibility Factor (r) (°)	P	F	F _{critical}
	Inter-Samples	Intra-Samples				
Diodomethane	96.81	3.19	3.57	3.5E-263	382.95	1.49
Propilenglycol	97.82	2.18	4.06	7.2E-223	434.52	1.50
Ethilenglycol	98.59	1.41	3.75	1.7E-276	743.27	1.49
Formamide	98.93	1.07	3.69	0.0E+00	1029.46	1.49
Water	98.88	1.12	4.01	0.0E+00	1099.36	1.49

From Table 6.4 table, it is possible to observe that, for all the liquids used, the contribution of the inter-sample differences is much higher than that corresponding to intra-sample variation. This indicates that the differences induced by distinct sizing agents in the various sample surfaces are statistically valid. Table 6.4 also shows that the quality of the statistical analysis is high as denoted by the extremely low value of P and by the fact of F being much larger than F_{critical}. Additionally, the values of the reproducibility factor (r) indicate that, for any liquid, differences larger than 4° in the contact angle values are statistically significant.

Having demonstrated the validity of the differences between samples, the next step is to analyze the effect of sample topography on the contact angle values.

6.2.1 EFFECT OF TOPOGRAPHY

As previously mentioned in this chapter, the contact angle values are claimed to be affected by the sample surface topography. In order to study this effect the Wenzel correction was applied to the measured values, using Equation 6.21, with the corrective factor (R^*) computed from Equation 6.22, by using the Sdr values measured by Profilometry (Appendix C). The values of R^* determined for each sample are compiled in Table 6.5. As it can be seen, all values are close to unity, indicating that the corrections applied are not much relevant.

Table 6.5 – Values of the Sdr parameter (Appendix C) and of the corresponding correction factors, R , calculated for each sample using Equation 6.22.

Sample	SDR (%)	Correction Factor – R^*	Sample	SDR (%)	Correction Factor – R^*
St	11.33	1.113	StS6-05	10.85	1.109
StS1-05	10.75	1.108	StS6-10	10.80	1.108
StS1-10	9.95	1.100	StS6-20	10.92	1.109
StS1-20	9.43	1.094	StS7-05	10.63	1.106
StS2-05	10.83	1.108	StS7-10	10.28	1.103
StS2-10	11.24	1.112	StS7-20	11.40	1.114
StS2-20	9.23	1.092	StS8-05	11.37	1.114
StS3-05	10.46	1.105	StS8-10	11.30	1.113
StS3-10	10.30	1.103	StS8-20	10.93	1.109
StS3-20	10.35	1.104	StS9-05	11.27	1.113
StS4-05	10.96	1.110	StS9-10	10.29	1.103
StS4-10	11.25	1.113	StS9-20	8.67	1.087
StS4-20	9.73	1.097	StS10-05	10.80	1.108
StS5-05	12.20	1.122	StS10-10	10.10	1.101
StS5-10	11.62	1.116	StS10-20	10.43	1.104
StS5-20	10.28	1.103	-----	-----	-----

The differences between the uncorrected values of the contact angle and the corrected values are evident in Figure 6.8, in which the results obtained for water (a) and diodomethane (b) (respectively the more and the less polar of the liquids tested), are plotted.

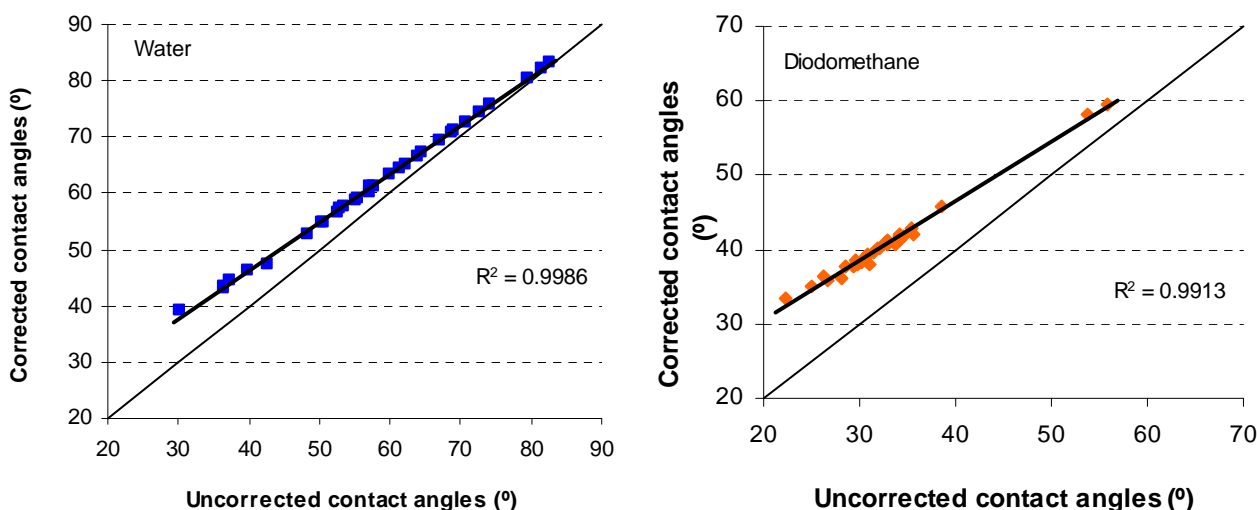


Figure 6.8 - Comparison of the contact angle values before and after the application of the Wenzel correction for water (a) and diodomethane (b).

The analysis of Figure 6.8 indicates that the corrected values are, for all samples, superior to the uncorrected ones (as expected from the values of Table 6.5). However, the relative order between samples is maintained. These observations are equally valid for the other liquids tested (propilenglycol, ethilenehycol and formamide), being the corresponding graphics presented in Appendix E.

The above figures lead to the conclusion that the sample roughness only slightly affects the measurements of the contact angle and consequently the derived parameters as total surface energy and its components. Since good correlations between corrected and uncorrected values were obtained, it can be stated that the above corrections will not alter any conclusion undertaken from raw data in studies where the Sdr measurement is not possible to allow the correction.

6.2.2 STATIC CONTACT ANGLES

As mentioned before, the static contact angles correspond to the initial wetting measurements which are taken for times approximately equal to 3 seconds from the contact of the drop with the sample surface. This time was found to correspond to the average time interval necessary for the system to reach equilibrium. Figure 6.9 illustrates, as an example, the water contact angle values measured for the samples sized with the lowest amount (i.e. 5%) of surface sizing agent. This figure shows that all sized papers are wetted (contact angles

inferior to 90 °) and that the addition of the synthetic sizing agents always increases the water contact angle, when compared to the value obtained for the standard sample (where only starch is applied). In fact, cationic starch has a hydrophilic nature and thus the reduced values of the contact angle with water (< 40 °) are perfectly natural. The increase in paper surface hydrophobicity as a result of adding the sizing agents was also expected regarding the copolymers composition (Section 3.1).

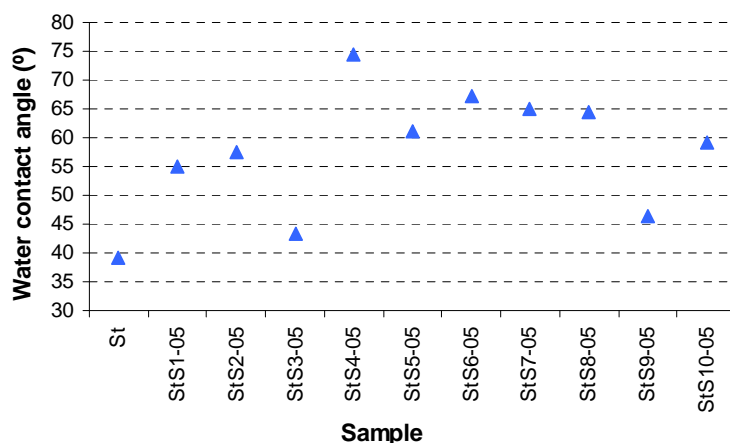


Figure 6.9 - Contact angle values with water, measured for the reference samples and the samples sized with the addition of 5% of synthetic surface sizing agent.

Nonetheless, it is evident that some samples exhibit values close to that of the reference sample (e. g. StS3 and StS9) whereas others present values close to the hydrophobicity barrier (e.g. StS4-05). The latter are, in principle, not favorable for printing performance with based water inks. However, it is important to stress that the final printing quality is the result of the balance of a set of properties and can not be predicted only by the analysis of the contact angle measured for water.

A detailed explanation of these differences will be given when discussing the results obtained for the surface energies and its components since these are the parameters that indeed condition the values of the contact angle. Figure 6.10 presents the average values of the contact angle measured with the five liquids tested and for all the concentrations of the sizing agents (5 %, 10 % and 20 % w/w).

Comparing all the plots, it can be concluded that the contact angle values exhibit in general the following trend:

$$\Theta_{\text{water}} > \Theta_{\text{formamide}} > \Theta_{\text{ethilenglycol}} > \Theta_{\text{propilenglycol}} > \Theta_{\text{diodomethane}}$$

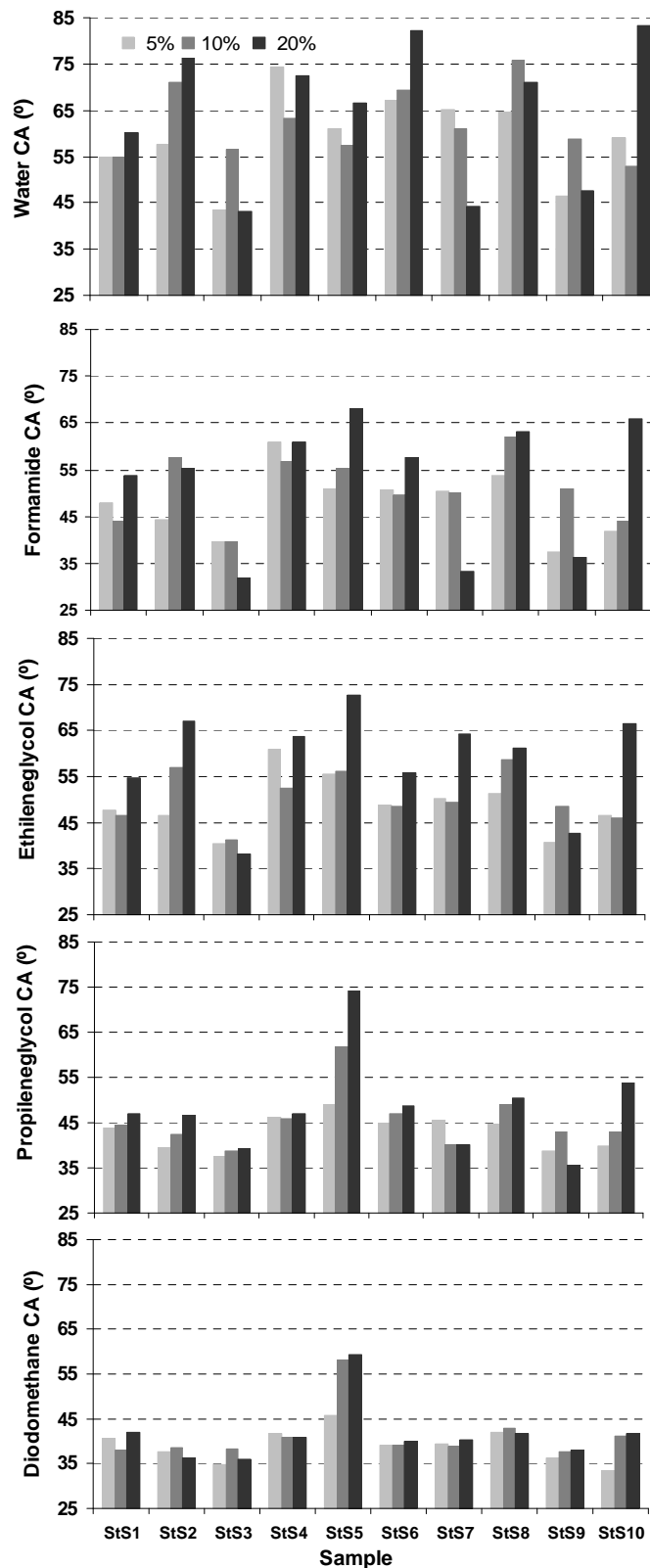


Figure 6.10 – Influence of the amount of the sizing agent on the contact angle values measured with the liquids tested (water, formamide, ethleneglycol, propileneglycol and diodomethane).

This sequence was somehow expected since the polarity of the liquids tested decreases in the same way (water is the most polar whereas diodomethane is non-polar), and the size agents are mainly non-polar compounds.

However, there is one sizing agent, agent S5 (quaternary ditallow methyl epoxypropyl ammonium), that presents a unique behavior: as the polarity of the liquid decreases, the contact angle consistently increases (reaching a remarkably high contact angle value, relatively to the others, for the diodomethane). This indicates that this surface sizing agent has a much larger influence on the surface properties ruling the dispersive interactions than on those ruling the polar interactions.

With regard to the effect of increasing the amount of copolymer (5, 10 and 20 %), all types of tendencies can be observed, as illustrated in Figure 6.10: the contact angle increases with the amount of the sizing agent, the contact angle decreases as the amount of the sizing agent increases or, an inflexion point is detected.

The reason why the increase of the surface sizing concentration originates these distinct types of variation is probably related with the arrangement of the copolymers molecules at the sample surface, i.e., molecule orientation and the availability of their functional groups for interacting with the various liquids. This point will be discussed in the next section, together with the results of the surface energies.

6.2.3 SURFACE ENERGIES

Surface free energy and the corresponding dispersive and polar components were determined, according to OWRK method, as describe in Section 6.1.3. The knowledge of these parameters is essential to assess the impact of the various sizing agents on the sample surface properties. The results obtained are plotted in Figure 6.11, while the numerical values are listed in Appendix E.

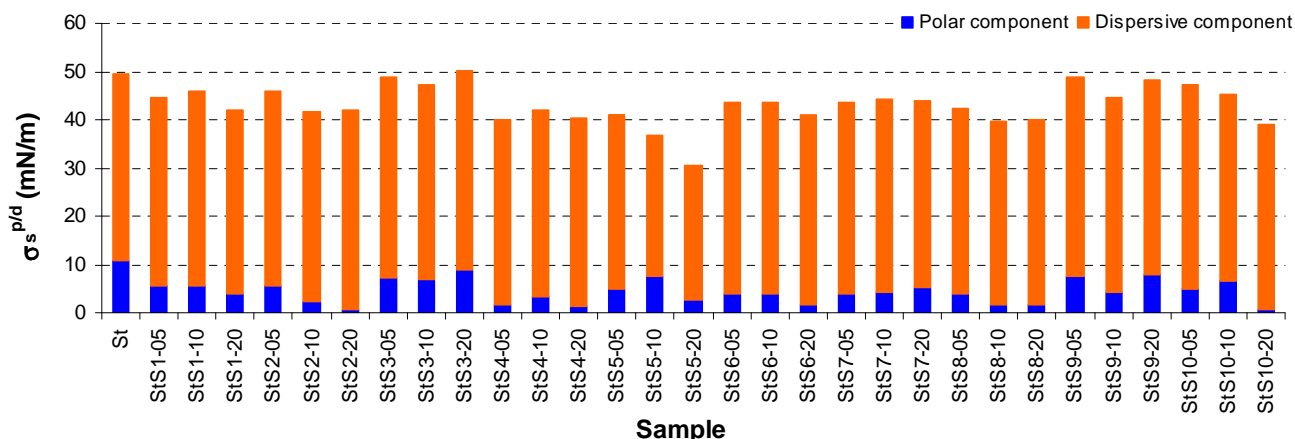


Figure 6.11 - Graphical representation of the polar and dispersive components of the surface energy for the various samples tested.

As it can be seen, the surface free energy of the paper samples is mainly dispersive. Moreover, the addition of the synthetic surface sizing agents to the cationic starch tends to decrease the total surface energy mainly due to the decrease of its polar component rather than the dispersive one, leading to more hydrophobic surfaces, as can be more clearly visible in Figure 6.12 where a star diagram shows the normalized values, relative to the standard sample.

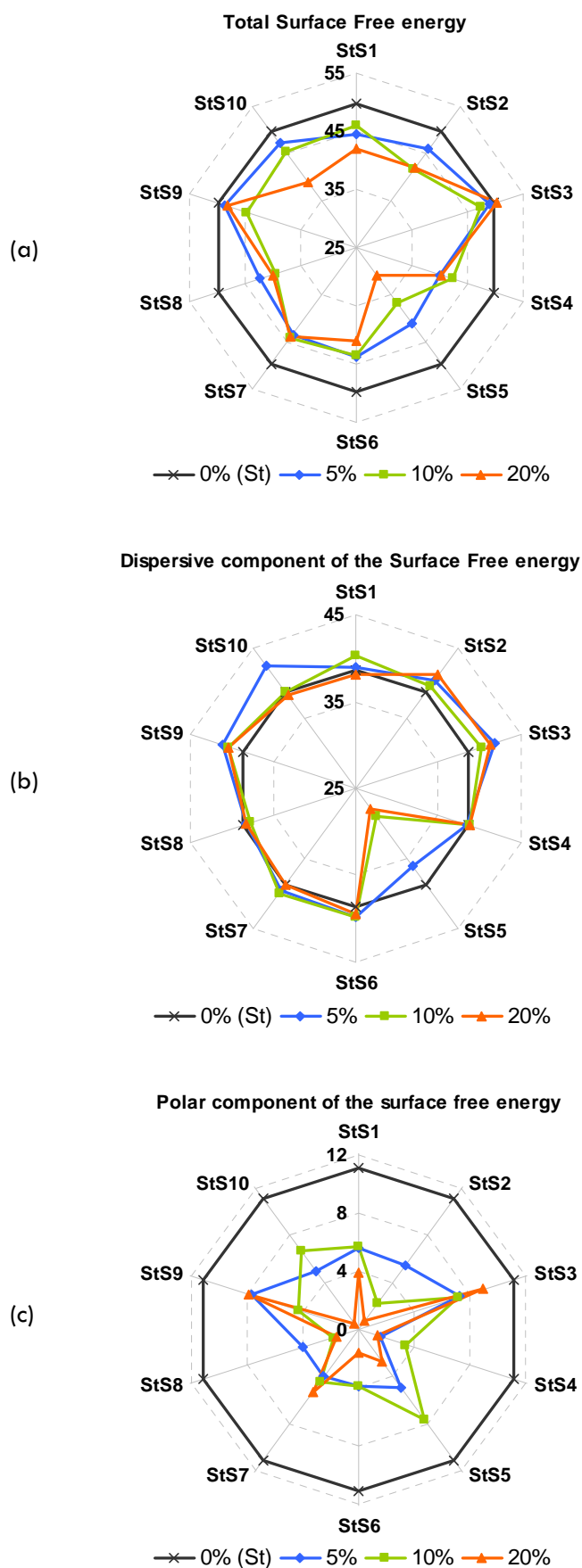


Figure 6.12 – Normalized values (relative to the standard sample) of the total surface free energy (a), dispersive component (b) and polar component (c) of the paper samples.

This effect was expected, since the surface sizing agents added are mainly non-polar compounds. Since the major effect of the addition of the synthetic surface sizing agents is detected in the polar component of the surface energy, the values of this component will be analyzed in more detail in Figure 6.13, regarding the influence of the amount of the sizing agent.

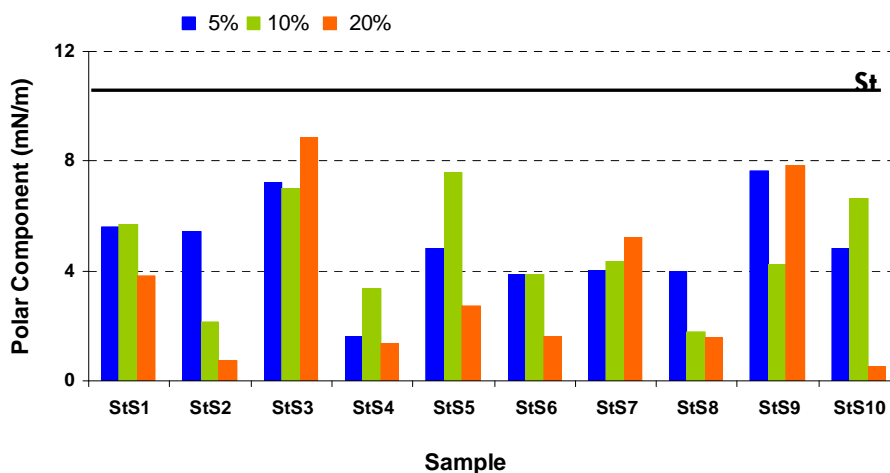


Figure 6.13 – Polar component of the surface free energy for all the samples tested.

As Figure 6.13 shows, the addition of the various synthetic agents significantly reduces the polar component of the surface energy, from 20 to 95 %, depending on the type of compound as well as its amount. Concerning the concentration of the sizing agent, and similarly to Figure 6.10, all types of behaviors are observed, being the most common the existence of an inflection point for the intermediate quantity of the surface sizing agent. As mentioned above, this might be a consequence of the distinct molecular orientations of these agents at the surface of the paper samples.

For instance, samples StS2 and StS8 (that include co-styrene-maleic anhydride and co-styrene-butyl acrylate, respectively) present a consistent decrease in the values of the polar component with the sizing agent concentration, suggesting that the molecules of these copolymers are oriented at the paper surface with the styrene monomer towards the exterior. On the contrary, the oxygen containing monomers are pointing inwards, i.e. towards the fibrous matrix, probably as result of some attraction from the -OH groups of cellulose. However, when the copolymer concentration is increased from 10 to 20 %, the decrease in the polar component is much more attenuated for surface sizing agent S8 (co-styrene-butyl acrylate). This may be because, for the intermediate concentration, their molecules (larger than the ones of co-styrene-maleic anhydride) nearly fill the available sites. Presumably if

the amount of this sizing agent would be further increased, the molecules would re-orient and the polar component would again increase.

This is probably what happened with samples St S3 and StS9 whose polar components exhibit a minimum for 10 % incorporation. Regarding the surface sizing agent S3 (co-acrylonitrile-acrylate), for the lowest concentration (5 %), the less polar nitrile group is most likely oriented outwards. As concentration increases (to 10 %), all the available sites are nearly filled. A further increase in concentration leads not only to the accumulation of the molecules but also to their reorientation. The affinity of their functional groups makes that the acrylate group (more polar) reorient outwards leading to an increase in the polar character of the surface. A similar explanation can be advanced for the sizing agent S9 (co-styrene-acrylate): initially the styrene monomer is the one oriented outwards but the increase of the co-polymer amount after saturation of the available sites originates a re-orientation of the molecule and ultimately a new increase of the polar component. However, in this case, the polar component variations are more pronounced than those found for sample StS3, most certainly because the molecule of compound S9 is larger.

Similar justifications can be produced for the behaviors detected for the remaining surface sizing agents, being the only difference the critical amount needed to change the molecules orientation. This amount is probably related to the particle size of the copolymer, as mentioned above, but might also be related to other factors such as, the penetration of the surface sizing agent or the surface tension of the liquids.

Since, as Figure 6.12 indicates, the major impact of the surface sizing agents on surface energetics seems to be derived from contribution of the polar component, the contact angle was plotted as a function of the surface free energy the (σ_s^p). Figure 6.14 shows the relationship obtained with water while Table 6.6 gathers the results achieved for the remaining liquids tested.

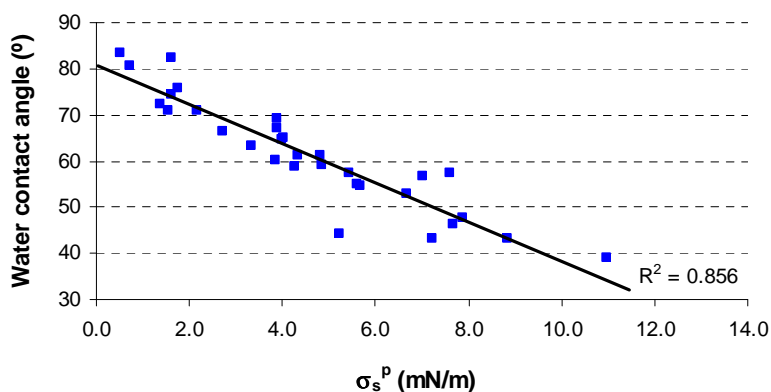


Figure 6.14 - Variation of the water contact angle with the polar component of the surface energy.

Table 6.6 – Correlation between the polar component of the paper surface free energy and the contact angle for the different liquids tested.

Liquid	Liquid Polar Component	Contact angle correlation with σ_s^P
Water	48.05	0.856
Formamide	25.85	0.737
Ethileneglycol	17.35	0.651
Propileneglycol	9.00	0.206
Diodomethane	0.00	0.009

As it can be seen, a good linear correlation is obtained for water, but this correlation deteriorates as the liquid polarity increases. This is an important observation to register, since the inkjet inks are water based, and consequently polar liquids.

6.2.4 DYNAMIC CONTACT ANGLES

In addition to the static contact angle measured immediately after the equilibrium between phases has been reached, the evolution of the contact angle with water throughout time (dynamic contact angle) was investigated. The ultimate purpose of this study is to anticipate the final printing performance. The measurement of the dynamic contact angle corresponds to the analysis of successive pictures captured by the CCD camera approximately every 0.5 sec., during 180 seconds.

As mentioned before, water was the test liquid chosen for this type of study, not only because it is the liquid currently used for most wetting evaluations but also because the printing technology that will be further applied to evaluate print quality is inkjet, which uses water based inks.

From each measurement an output in table form is produced by the equipment software, that includes the drop age value (corresponding to the time interval between the initial equilibrium of the drop with the surface ($t=0$) and the instant of the measurement ($t=t$)), the contact angle measured at time t , the corresponding error of each measurement and the corresponding drop base diameter and drop volume. Table 6.7 presents, as an example, an extract of this type of table.

Table 6.7 - Extract of the dynamic contact angle result table obtained for sample StS4-05, indicating the drop age (Age), contact angle (CA), measurement error, base diameter (BD) and drop volume (Vol).

Measurement n°	Age (sec)	CA(°)	Err (°)	BD (mm)	Vol (µl)
1	0.0	75.0	2.6	3.44	6.85
2	0.4	74.8	2.8	3.46	6.89
3	0.4	74.8	2.7	3.46	6.89
⋮	⋮	⋮	⋮	⋮	⋮
6	1.2	74.1	2.8	3.49	6.94
7	1.2	74.1	2.8	3.49	6.94
8	1.6	73.7	2.6	3.50	6.96
9	1.6	73.6	2.5	3.50	6.96
10	2.0	73.1	2.5	3.52	6.98
⋮	⋮	⋮	⋮	⋮	⋮
168	34.0	61.0	2.2	3.92	7.30
169	34.1	61.1	1.7	3.92	7.30
170	34.4	61.0	2.1	3.92	7.30
171	34.5	61.0	1.9	3.92	7.30
⋮	⋮	⋮	⋮	⋮	⋮
299	66.6	60.9	3.1	4.03	7.65
300	66.6	60.7	2.2	4.03	7.65
301	67.0	60.6	2.5	4.03	7.66
378	82.3	61.3	3.7	4.05	7.77
⋮	⋮	⋮	⋮	⋮	⋮

As can be easily perceived from the example presented above, this type of measurements generates very extensive tables, and the accuracy of the contact angle values measured is verified by the reduced values of the measuring error.

The contact angle values are used to calculate the wetting velocity (defined as the difference between the contact angle measured at 5 and at 60 seconds (Equation 6.23) and to evaluate the variation profiles determined for the contact angle as well as for the drop

spreading (evaluated from the drop base diameter profile) and for the drop absorption (evaluated from the drop volume profile).

It should be stressed that in this text the results presented correspond to the average values obtained for (at least) three independent measurements whereas the results presented in graphical form correspond to an individual measurements representative of the behavior detected for the sample under analysis.

The statistical validity of the wetting velocity results is confirmed by ANOVA, as depicted in Table 6.8.

Table 6.8 – ANOVA results obtained for the wetting velocity values.

Variable	Contribution to total variation (%)		Reproducibility Factor (r)	P	F	F _{critical}
	Among samples	Within samples				
Wetting Velocity	60.53	39.47	0.05	5.85E-44	126.15	1.65

The average wetting velocity (WV) values obtained for each sample are presented in Table 6.9. To facilitate the analysis the results are divided into four groups depending upon the value of the wetting velocity: wetting velocities smaller than 0.1°/sec, wetting velocities between 0.1 and 0.2°/sec, wetting velocities between 0.2 and 0.3°/sec and wetting velocities larger than 0.3°/sec.

Table 6.9 – Values of wetting velocity (WV) (Equation 7.23) obtained for each paper sample using water.

Sample	Wetting Velocity (°/sec)			
	WV ≤ 0.1	0.1 < WV ≤ 0.2	0.2 < WV ≤ 0.3	WV > 0.3
St			0.23 ± 0.02	
StS1-05			0.21 ± 0.00	
StS1-10	0.09 ± 0.01			
StS1-20	0.06 ± 0.02			
StS2-05		0.20 ± 0.00		
StS2-10	0.10 ± 0.02			
StS2-20	0.04 ± 0.02			
StS3-05	0.08 ± 0.02			
StS3-10	0.09 ± 0.01			
StS3-20	0.09 ± 0.02			
StS4-05			0.27 ± 0.02	
StS4-10			0.22 ± 0.01	
StS4-20		0.16 ± 0.03		
StS5-05		0.18 ± 0.01		
StS5-10				0.34 ± 0.03
StS5-20				0.44 ± 0.00
StS6-05			0.29 ± 0.01	
StS6-10			0.30 ± 0.01	
StS6-20				0.36 ± 0.02
StS7-05		0.16 ± 0.01		
StS7-10		0.17 ± 0.00		
StS7-20	0.09 ± 0.00			
StS8-05		0.17 ± 0.00		
StS8-10				0.33 ± 0.01
StS8-20			0.22 ± 0.00	
StS9-05	0.09 ± 0.01			
StS9-10	0.08 ± 0.01			
StS9-20			0.21 ± 0.01	
StS10-05		0.16 ± 0.01		
StS10-10		0.18 ± 0.02		
StS10-20			0.23 ± 0.01	

As this table shows, most of the sizing formulations lead to water wetting velocities smaller than that of the standard sample (St), which is 0.23°/sec. However, it should be stressed that, regarding the wetting velocity, it is not easily obvious which values should be considered “large” or “small”, since the optimum wetting velocity value for a given paper also depends upon absorption and spreading phenomena. Concerning P&W papers it is usually accepted that relatively small wetting velocities are beneficial for inkjet printing performance, if accompanied with a predominance of absorption over spreading. However, small wetting values do not necessarily mean better printing performances. In fact, very small wetting velocities may indicate that the paper has no capacity to absorb the ink solvent, leading to bad printing performance.

Analyzing the performance of the standard sample, in terms of dynamic contact angle (Figure 6.15) it is obvious that the water contact angles decreases abruptly during the first 15 seconds and beyond that, presents a much slower reduction.

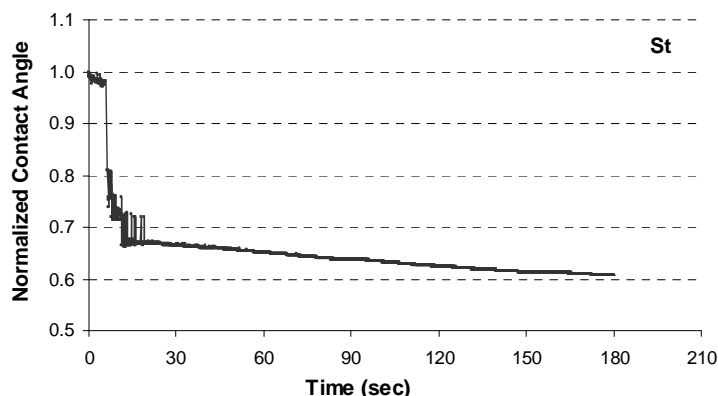


Figure 6.15 – Water contact angle variation for sample St, normalized relatively to the initial value ($t=0$)

This behavior is a consequence of the drop spreading and absorption on the paper surface, respectively illustrated by the variation throughout time of the drop base diameter and of the drop volume, Figure 6.16 (a) and Figure 6.16 (b), respectively.

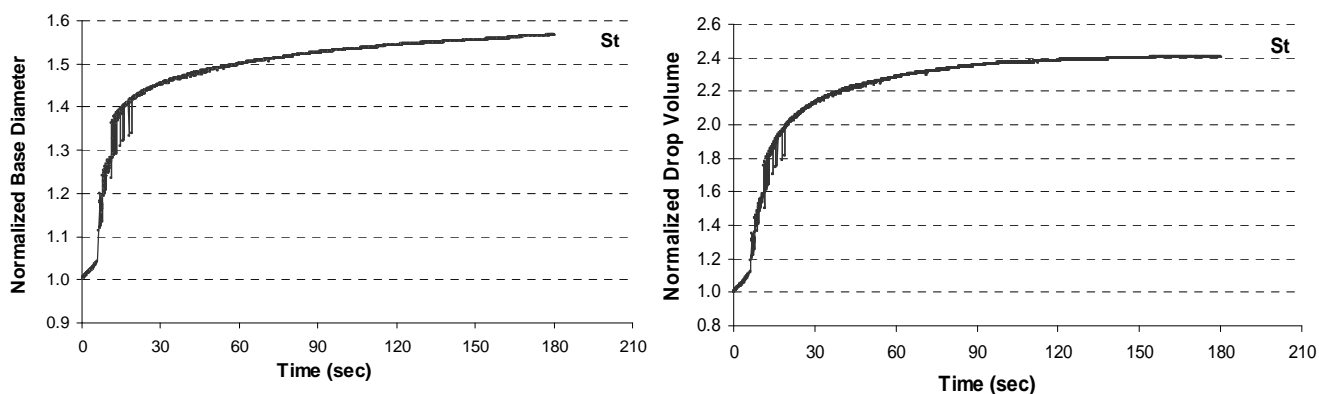


Figure 6.16 – Normalized (relatively to the initial values ($t=0$)) drop base diameters and drop volume values for sample St.

As it is clear from this figure, the variation of these parameters is also very accentuated in the first 15 seconds. Moreover, the evaluation of the drop volume shows an anomalous increase with time. This is unexpected, since the drop is supposed to be gradually absorbed by the paper surface thus leading to a decrease in the drop total volume. This odd fact is probably the result of an excessively high spreading together with a too fast absorption of the drop by the paper fibrous matrix, originating paper swelling. This is (wrongly)

interpreted by the image detecting system as an increase in drop volume. Obviously this behavior is not adequate for printing purposes, indicating, as expected, that the standard sample needs further treatment.

In fact, as Table 6.9 shows, the addition of the synthetic surface sizing agents to the starch suspension usually leads to a decrease in the wetting velocities. However, this decrease can not be analyzed independently of the evaluation of the drop base diameter and volume, as explained before.

The profiles determined for each sample, regarding the normalized contact angle, drop base diameter and drop volume, presented in Appendix E, show that in general the addition of a synthetic surface sizing agent does not originate that unusual increase in drop diameter. Moreover, no significant swelling was observed for any of these samples. This is valid either for wetting velocities larger and smaller than that of the standard sample ($0.23^\circ/\text{sec}$). It can then be concluded that the sizing agents positively influence the wetting process. Figure 6.17 shows a typical result, obtained for sample StS4-05, that exhibits a wetting velocity similar to that of the reference sample ($0.27^\circ/\text{sec}$).

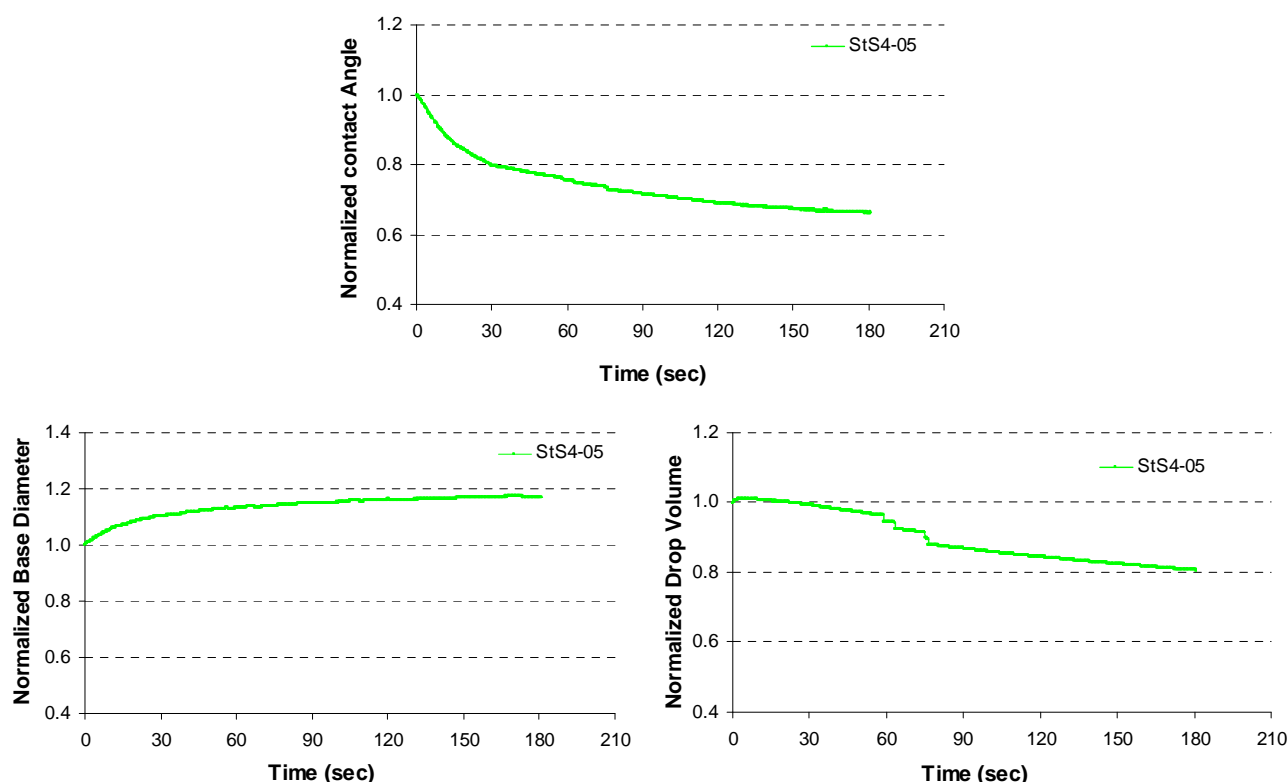


Figure 6.17 – Normalized contact angle and normalized drop volume for sample StS4-05.

In this figure, a gradual decrease of both the normalized contact angle and the drop volume can be noticed. Additionally, no swelling effects were observed at the paper surface. Similar findings were detected for the majority of the samples, confirming that the synthetic surface sizing agents have a controlling action over the dynamics of the wetting phenomenon.

The influence of the concentration of the sizing agent will be studied by analyzing the dynamic contact angle profiles of different samples.

Let us take, for example, the case of the sizing agent S2, co-styrene-maleic anhydride. The graphic of Figure 6.13 indicates that the polar component of the surface free energy decreases as the incorporation percentage of S2 increases. As explained, this is probably because the styrene molecules are always turned outwards, that is, oriented towards the air interface. The results achieved for the dynamic contact angle measurements are also in agreement with this assumption, since an increase in the copolymer amount also results in a progressively lower wetting velocity: 0.20, 0.10 and 0.04°/sec, respectively for 5%, 10% and 20 % of S2.

The normalized contact angle as a function of time is plotted in Figure 6.18. From this plot, it is evident that the higher the percentage of S2 the slower is the profile slope. Nonetheless, for the first few seconds, the distinction between the curves is not so obvious.

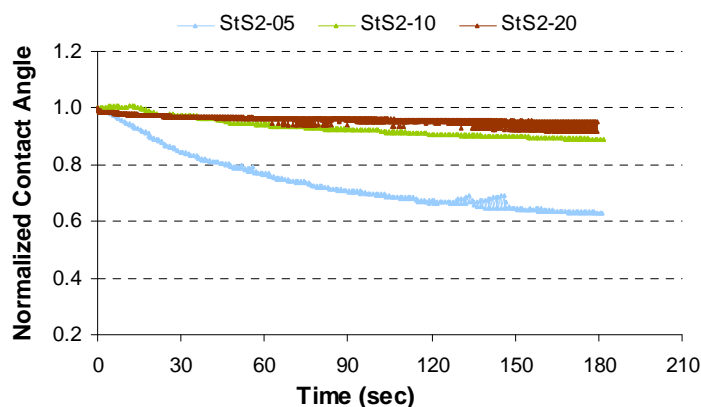


Figure 6.18 – Normalized contact angle for samples sized with the synthetic surface sizing agent S2.

The decrease in the contact angle measured with water when only 5% of S2 is added results from the fact that the hydrophobicity of the styrene is not enough to maintain the value of the initial contact angle. Thus, after the initial wetting, the oxygen atoms of the maleic anhydride monomer are accessible to the water drop, originating the profile of Figure 6.18 for this concentration. When the amount of S2 is increased, the accessibility of the oxygen atoms is

delayed, and the styrene mainly rules the wetting process, and thus no significant decrease in the contact angle occurs. However, and as mentioned before, the analysis of the dynamic contact angle should not be made independently of the drop behavior in terms of drop base diameter (spreading) and drop volume (absorption). These results are presented in Figure 6.19

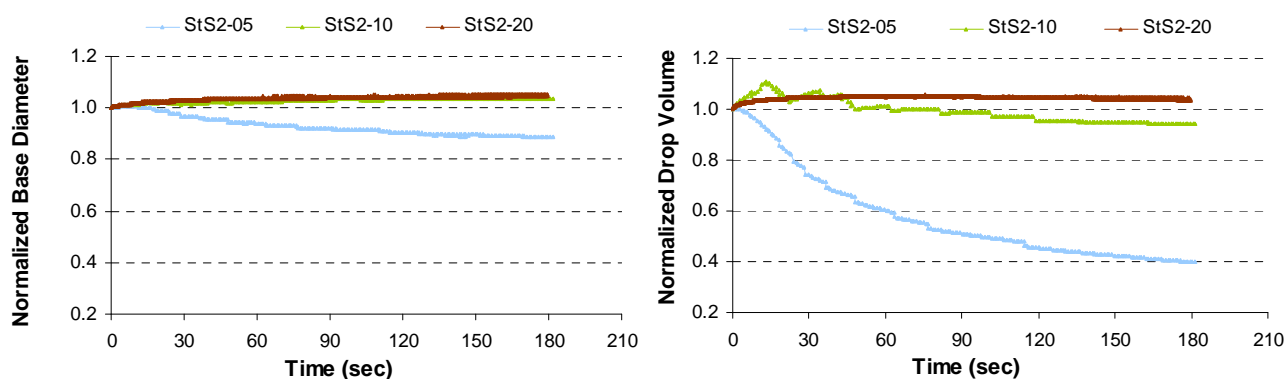


Figure 6.19 – Normalized drop base diameter and drop volume for the samples sized with the synthetic surface sizing agent S2.

As this figure shows, the decrease in the wetting velocity of sample St**S2**-05 is found to be due to high absorption, indicating that the addition of 5% of sizing agent is not sufficient to decrease that absorption. On the contrary, the addition of 20% of S2 seems excessive, since the absorption is negligible and thus almost no contact angle variation is detected. The optimum sizing amount for this surface sizing agent seems to be above 5% and below 20%.

Since the sizing agent S2 is similar in composition to sizing agent S4 (the main difference being the monomers ratio styrene/maleic anhydride that is 3/1 in the case of S2 and 2/1 in the case of S4, (Table 3.2), it was found interesting to compare the dynamic performance of these two copolymers. Figure 6.20 illustrates the variation of contact angle for the three concentrations tested (5, 10 and 20%) of both styrene-maleic anhydride copolymers.

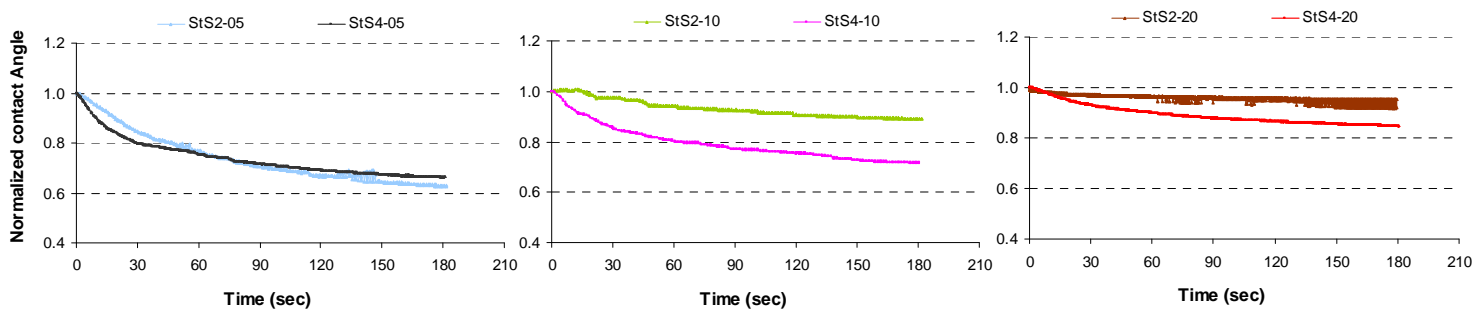


Figure 6.20 – Comparison of the normalized water contact angle values of the sizing agents S2 and S4 for the three different incorporation percentages (5%, 10 % and 20%).

These graphs show that:

- i) for the lower concentration, both co-polymers exhibit practically coincident profiles, corresponding the sample St**S2-05** to a wetting velocity of $0.20^\circ/\text{sec}$ and sample St**S4-05** to $0.27^\circ/\text{sec}$;
- ii) for the intermediate concentration distinct profiles are obtained, corresponding that of S4 to a higher wetting velocity ($0.22^\circ/\text{sec}$ for St**S4-10** and $0.10^\circ/\text{sec}$ for St**S2-10**);
- iii) for the highest concentration, the difference between the dynamic contact angles of both samples is decreased but shows the same trend: wetting velocities of $0.16^\circ/\text{sec}$ and of $0.04^\circ/\text{sec}$ were determined for sample St**S4-20** and St**S2-20**, respectively.

The lower wetting velocities of S2 compared with those of S4 for the same copolymer concentration were expected since the amount of styrene is smaller in the sample StS4.

The spreading and absorption profiles of these samples are compared in Figure 6.21.

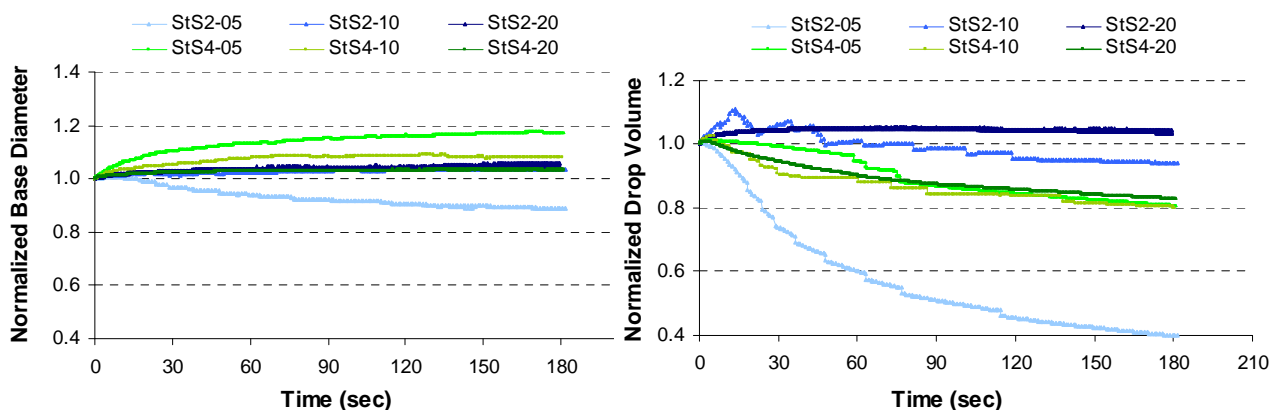


Figure 6.21 – Comparison of the normalized drop base diameter and drop volume for the samples sized with the synthetic surface sizing agents S2 and S4.

Regarding these profiles, the samples sized with the sizing agent S4 are more consistent with the corresponding contact angle profiles, exhibiting a continuous increase in the drop base diameter and a decrease in the drop volume. For 20% of incorporation, the contact angle variation is caused almost only by absorption. This suggests that, most probably, the sample StS4-20 will be the one with better inkjet printing performance among these.

Figure 6.22 and Figure 6.23 illustrate the dynamic behavior of the samples sized with the sizing agent S9 that also contains styrene (co-styrene-acrylate, Table 3.2).

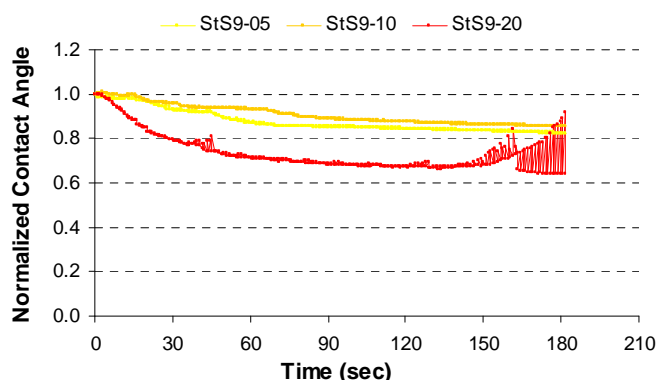


Figure 6.22 - Normalized contact angle for samples sized with the synthetic surface sizing agent S9.

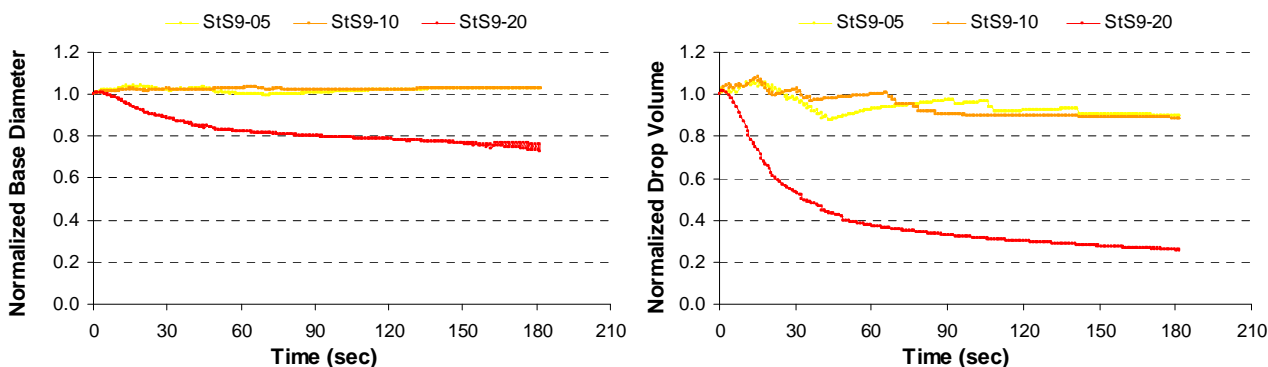


Figure 6.23 - Normalized drop base diameter and drop volume for the samples sized with the synthetic surface sizing agent S9.

The analysis of the surface energy results (Section 6.2.3) suggested that, for 5 and 10% of incorporation of this sizing agent, the styrene groups are the ones oriented outwards. However, at 20% of incorporation, a re-orientation of the molecule takes place and the acrylate groups are the ones facing the air interface. The dynamic behaviors depicted in Figure 6.22 and Figure 6.23 also show similar profiles for the lower concentrations (5 % and 10 %) and a distinctive performance for 20 % of incorporation. The latter corresponds to a

considerable drop absorption that is certainly caused by the OH groups of the acrylate, which are now more accessible for interaction with the water, thus confirming the above assumption.

Since the surface sizing agent S9 is similar to S1 (Table 3.2), the only difference being the molecular configuration (Figure 3.3), it is interesting to compare their dynamic behaviors (Figure 6.24).

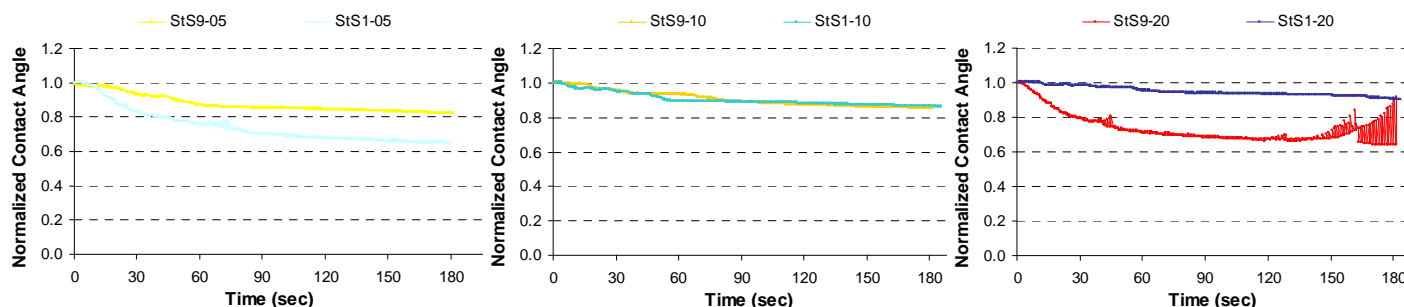


Figure 6.24 - Comparison of the normalized contact angle values at each incorporation percentage for the sizing agents S9 and S1.

As shown in this figure, when the concentration of the sizing agent increases, the dynamic contact angle profiles invert their relative positions: for the lower concentration the decay of the contact angle variation of the sample containing S9 is more attenuated than that containing S1; for the intermediate incorporation, both profiles coincide; and for the highest concentration, sample containing S9 exhibits a more steep variation. Interestingly, as Table 6.9 reports, the highest values of the wetting velocity, $0.21^\circ/\text{sec}$, were achieved for the samples StS1-05 and StS9-20.

This indicates that the accessibility of the OH groups does not change significantly with the increase of the incorporation percentage, and thus the wetting velocity and the contact angle variation decrease with the sizing agent increase.

In the particular case of the 5% incorporation, the difference detected between the profiles of the samples containing S9 and S1 can be associated to the fact that the molecules of styrene, being more close together in the sizing agent S1 Figure 3.3, and its effect is thus less noted when a small amount is used.

Identical analyses can be made for other samples. In general, the sample performance in terms of wetting behavior is in agreement with the results obtained for the surface energy, as expected. However, the accessibility of hydrophilic groups, in particular OH also affects the

dynamic contact angle profile. Additionally, the orientation of the functional groups of the sizing agents at the paper surface is of great importance since it affects the accessibility of the hydrophilic groups.

CHAPTER 7

INVERSE GAS CHROMATOGRAPHY

(IGC)

7 INVERSE GAS CHROMATOGRAPHY (IGC)

IGC derives from the conventional gas chromatography (GC), which is a simple technique used to separate and identify solutes in a mixture, based on the fact that each solute has a particular interaction with the stationary phase and thus will travel through the column at different rates. Inverse gas chromatography (IGC) uses this fact to study of the stationary phase instead of the mobile phase: by using a series of solutes (probes) of well known physicochemical characteristics, it is possible to extract valuable information about the packing material of the column. (Figure 7.1) (Gutierrez et al. 1999; Kunaver et al. 2004; Carvalho et al. 2005; Santos and Guthrie 2005; Wang and Sain 2007).

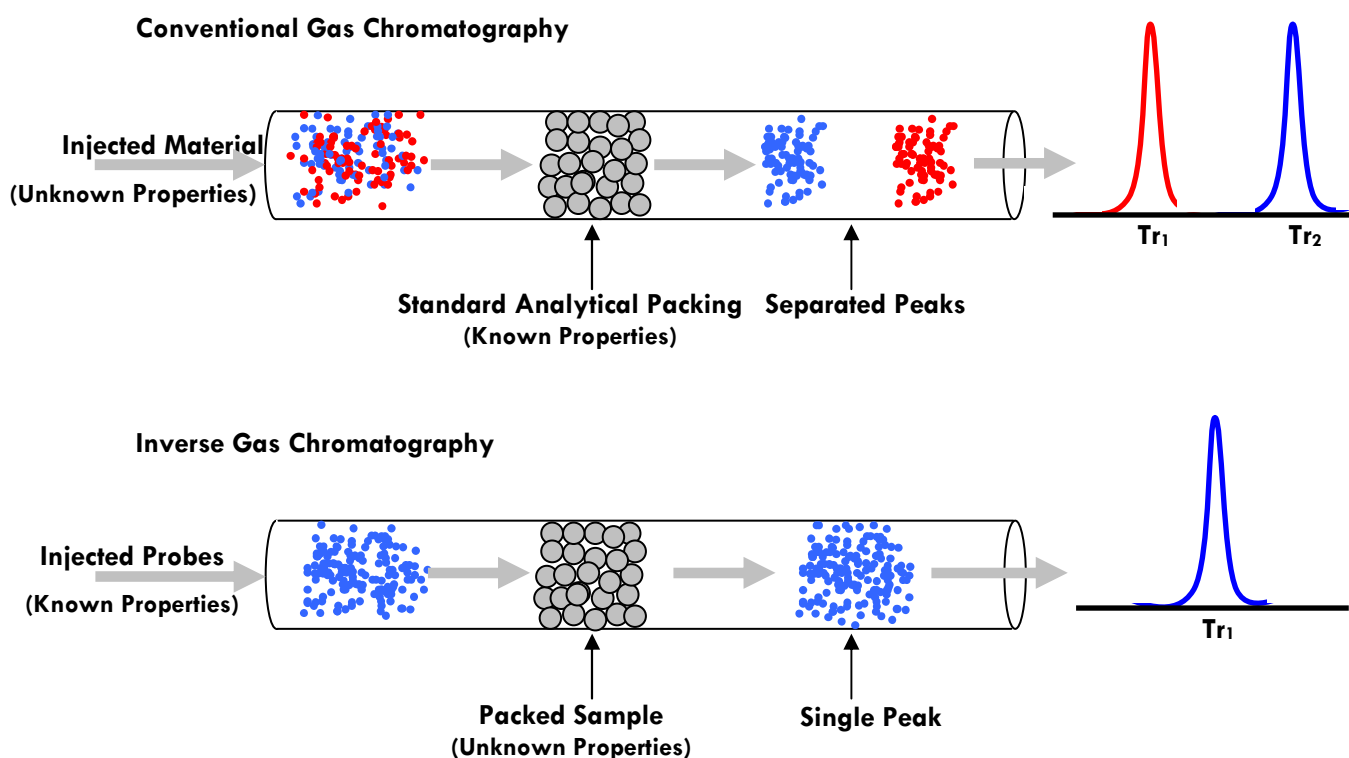


Figure 7.1 – Schematic representation of conventional gas chromatography (GC) and inverse gas chromatography (IGC) analysis.

After the introduction of IGC in 1967, the application of this technique has grown rapidly, being frequently used for the surface characterization of organic and inorganic materials such as polymers, industrial fibers, wood and pulp fibers, composites, coatings, pigments, catalysts as well as particles, glass beads or chemicals. The quantity of related publications has been permanently increasing, covering applications in many fields, like pharmaceutical, ceramics, constructions, pulp and paper or transports (Pyda et al. 1993; Cordeiro et al.

1995; van Asten et al. 2000; Belgacem 2000; Keller and Luner 2000; Wålinder and Gardner 2000; Tze and Gardner 2001; Uhlmann and Schneider 2002; Aquino et al. 2003; Planinšek and Buckton 2003; Kunaver et al. 2004; Baoli et al. 2007; Bardavic et al. 2007; Lindsay et al. 2007; Rjiba et al. 2007; Saxena et al. 2007; Voelkel and Strzemeicka 2007; Wang and Sain 2007).

In the particular case of pulp and paper, the use of IGC to evaluate the properties of fibers and pulps is common, and several studies covering themes such as the surface energetics of cellulose fibers properties, or the effects the cooking and bleaching processes on surface and strength properties can be found in the literature (Felix and Gatenholm 1993; Belgacem et al. 1995; Böras et al. 1997; Liu et al. 1998; Shen et al. 1998; Shen and Parker 1999; van Asten et al. 2000; Belgacem 2000; Aquino et al. 2003; Shakeri and Tabar-Haidar 2004; Carvalho et al. 2005). However, the use of IGC to study paper surface and, in particular, its interaction with ink is more recent and is still matter of development (Shen et al. 2000; Santos et al. 2001; Moutinho et al. 2007a; Moutinho et al. 2008a).

The application of IGC to the surface characterization of paper samples enables the evaluation of the dispersive component of the surface energy arising from London and Van-der-Waals forces as well as its variation with temperature. Moreover, it also enables the analysis of the surface acid-base character according to the Lewis concept (i.e., ability to accept and donate electrons) (Gutierrez et al. 1999; Carvalho et al. 2005; Santos and Guthrie 2005; Wang and Sain 2007; Aquino et al. 2003). It is in this context that IGC will be used in the present work.

The theoretical principles of IGC are a widely discussed matter and many studies can be found in the literature regarding the subject (Belgacem et al. 1995; Cordeiro et al. 1995; Liu et al. 1998; Shen and Parker 1999; van Asten et al. 2000; Belgacem 2000; Wålinder and Gardner 2000; Aquino et al. 2003; Planinšek and Buckton 2003; Kunaver et al. 2004; Shakeri and Tabar-Haidar 2004; Carvalho et al. 2005; Santos and Guthrie 2005; Wang and Sain 2007) thus, only brief considerations, useful to better understand the work, will be presented here.

7.1 THEORY

In an IGC analysis, an inert carrier gas elutes a minute quantity of a probe molecule through a column packed with the material under study. Due to the interactions between the stationary and the mobile phase, the probe molecules are retained for a certain time (t_r), known as the retention time, which is used to calculate the net retention volume (V_n), according to:

$$V_n = (t_r - t_0) \cdot F \cdot J \quad (7.1)$$

where t_0 is the dead retention time of a marker probe, F is the carrier gas flow rate and J is the correction factor for gas compressibility, calculated according to Equation 7.2:

$$J = 1.5 \frac{\left(\frac{P_i}{P_0}\right)^2 - 1}{\left(\frac{P_i}{P_0}\right)^3 - 1} \quad (7.2)$$

P_i and P_0 are the inlet and outlet pressures of the carrier gas, respectively.

Taking into account the fact of the experiments being undertaken at infinite dilution conditions, the free energy of adsorption of the probes on the stationary phase surface per mole (ΔG) can be determined from the retention volume (V_n) according to Equation 7.3:

$$-\Delta G = R \cdot T \cdot \ln(V_n) + C_1 \quad (7.3)$$

where R is the ideal gas constant, T is the absolute column temperature and C_1 is a constant which depends upon the chromatographic column.

Considering that the dispersive and specific components, ΔG^D and ΔG^S , respectively, are additive (Equation 7.4), as suggested by Fowkes in 1987, Equation 7.3 can be rewritten as:

$$\Delta G = \Delta G^D + \Delta G^S \quad (7.4)$$

Considering Equation 7.3, the above equation leads to

$$-(\Delta G^D + \Delta G^S) = R \cdot T \cdot \ln(V_n) + C_1 \quad (7.5)$$

On the other hand, the free energy of adsorption can also be related to the work of adhesion (W_a) according to Equation 7.6:

$$-\Delta G = N \cdot a \cdot W_a \quad (7.6)$$

where N is the Avogadro's number and a is the cross-sectional area of the probe to be tested.

According to Fowkes, The work of adhesion can be considered as the sum of a dispersive (Wa^D) and a specific (Wa^S) component:

$$Wa = W_a^D + W_a^S \quad (7.7)$$

Following this principle, the interactions evaluated by IGC are the dispersive interactions, through the determination of the dispersive component of the surface energy, and the specific interactions, in this case through the determination of the acidic and basic constants, as described in the following Sections (7.1.1 and 7.1.2).

7.1.1 DISPERSIVE COMPONENT OF THE SURFACE FREE ENERGY

When non-polar probes are used (n-alkane series), the interactions are purely of dispersive nature, and Equation 7.7 can be reduced to:

$$Wa = Wa^D \quad (7.8)$$

As presented in Chapter 6, Wa^D can be approximated by the geometric mean of the surface free energy/tension of the phases involved:

$$W_a^D = 2\left(\sqrt{\sigma_s^D \cdot \sigma_L^D}\right) = W_a \quad (7.9)$$

where σ_s^D and σ_L^D are the dispersive components of the solid surface energy and of the liquid surface tension, respectively. Equations 7.3 and 7.6 can then be combined so that:

$$2 \cdot N \cdot a \cdot (\sigma_s^D)^{1/2} \cdot (\sigma_L^D)^{1/2} + C = R \cdot T \cdot \ln(Vn) \quad (7.10)$$

By plotting $R \cdot T \cdot \ln(Vn)$ vs $2 \cdot N \cdot a \cdot (\sigma_L^D)^{1/2}$ for a homologous alkane series (Figure 7.2), a straight line is obtained usually referred to as the reference line. The slope of the reference line leads to the determination of σ_s^D for a given temperature.

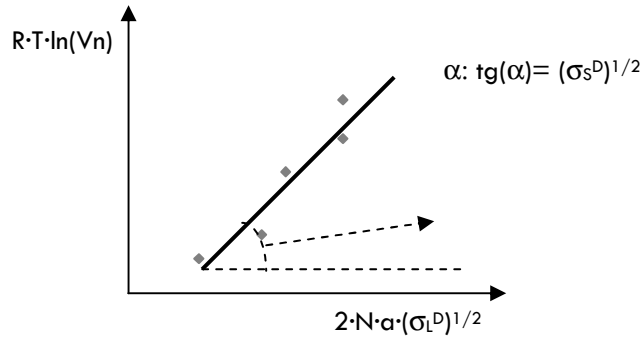


Figure 7.2 – Schematic representation of the method used to calculate σ_s^D at a given temperature using IGC.

7.1.2 ACID-BASE CHARACTER

In the late 70's, it was proposed by Fowkes that the totality of specific interactions may be interpreted as Lewis acid-base forces, and thus that the dispersive forces and acid-base interactions are the primary forces operating across the interface. This approach has been later supported by experimental results.

The acid-base interactions are analyzed through the net retention volume measured using polar probes. In order to obtain the acidic (K_a) and the basic (K_b) parameters of the solid surface, the vertical deviations from the reference line for each polar probe, are quantified, allowing the estimation of the specific component of free energy (ΔG^S) as:

$$-\Delta G^S = R \cdot T \cdot \ln(V_{np}) - R \cdot T \cdot \ln(V_{n_{Ref}}) \quad (7.11)$$

where $V_{n,Ref}$ is the retention volume established by the n-alkanes reference line, and V_{np} is the retention volume of the polar probes. The adhesion work between the polar probes tested and the paper samples (W_a^s) can be obtained from the specific free energy (Eq.7.6) as:

$$W_a^s = \frac{R \cdot T}{N \cdot a} \ln \left(\frac{V_{np}}{V_{n_{Ref}}} \right) \quad (7.12)$$

In order to relate these concepts with the acid-base interactions, which according to Fowkes can be considered as the origin of all specific interactions, it is necessary to make use of the following thermodynamic definitions:

$$\Delta G^{AB} = \Delta H^{AB} - T \cdot \Delta S^{AB} \quad (7.13)$$

$$\Delta H^{AB} = K_a \cdot DN + K_b \cdot AN \quad (7.14)$$

Where the superscript (^{AB}) stands for the acid-base interactions and ΔG is the specific free energy, ΔH the enthalpy of adsorption, ΔS is the entropy of adsorption, K_a is the acidic constant, DN is the Gutmann's donor number, K_b is the basic constant and AN is the Gutmann's acceptor number.

Experiments are undertaken at different temperatures in order to determine the enthalpy (ΔH^S) and the entropy (ΔS^S) of adsorption from the plots of $\Delta G^S/T$ vs $1/T$ for each probe tested, using Equation 7.13 in the following form:

$$\frac{\Delta G^S}{T} = \frac{\Delta H^S}{T} - \Delta S^S \quad (7.15)$$

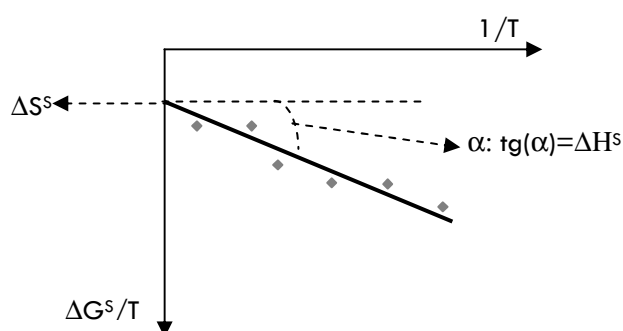


Figure 7.3 - Schematic representation of the calculation method for the ΔH and the ΔS determination at a given temperatures using IGC.

Finally, the acidic (K_a) and basic (K_b) constants are calculated from the linear relation of ΔH^S with DN/AN^* for the series of polar probes characterized by different AN^* and DN numbers (AN^* represents the Gutmann's modified acceptor number), as depicted in Figure 7.4.

$$\frac{(-\Delta H^S)}{AN^*} = K_a \frac{DN}{AN^*} + K_b \quad (7.16)$$

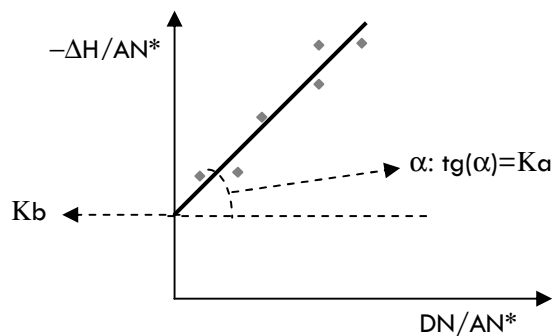


Figure 7.4 - Schematic representation of the calculation method for the K_a and K_b determination using IGC.

7.1.3 EQUIPMENT - DANI GC 1000

In this work, the Chromatograph DANI GC 1000 (Figure 7.5) was used to perform the inverse gas chromatography measurements for all the samples produced (31).



Figure 7.5 – Gas chromatograph DANI GC1000, used in the IGC measurements.

The analysis consists in the determination of retention times followed by an adequate mathematical treatment. The retention times correspond to the time that each gaseous probe is delayed by the solid stationary phase (paper sample) under analysis.

A typical IGC analysis is undertaken in three steps: sample preparation, sample conditioning and analysis.

Sample preparation began by filling the IGC column. For that approximately 2 g of the paper sample was cut into small pieces of approximately $2 \times 2 \text{ mm}^2$ (Figure 7.6 (a)) and subsequently packed into a stainless steel column, 0.5 m long and 0.4 mm ID. To facilitate this

operation and to ensure the quality of the packing, in terms of homogeneity, a vacuum pump was used as illustrated in Figure 7.6 (b). Finally, the column packed with the paper sample as the stationary phase is folded (Figure 7.6 (c)) before being placed and fixed in the equipment. The packed columns were conditioned for approximately 12 h under a helium flow before the beginning of each analysis. Similar experimental procedures have also been adopted by other authors (Cordeiro et al. 1995; Shen et al. 1998; Santos et al. 2001; Carvalho et al. 2005; Santos and Guthrie 2005).

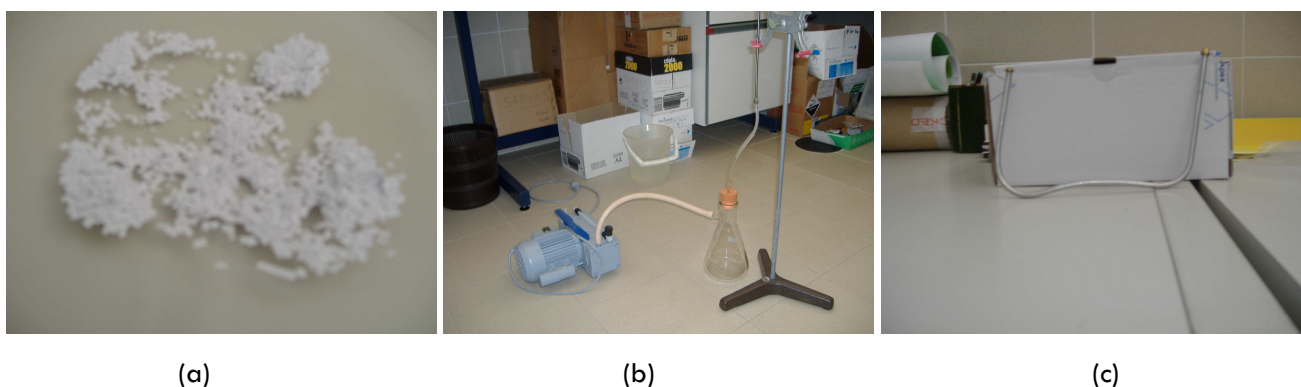


Figure 7.6 –Preparation of samples for IGC measurements: (a) pieces of a paper sample prepared to be packed into the IGC column; (b) Experimental assembly used for packing the columns; (c) IGC column packed and folded, ready to be introduced into the equipment.

The experiments were carried out at temperatures between 35 and 60°C using 5°C steps. This temperature range was selected since it was not possible to operate the equipment below 35°C, and above 60°C, there was the risk of damaging the paper surface by a prolonged exposure to such high temperatures. The injector and detector were set at 180 and 200°C respectively, in order to keep an adequate temperature difference (a minimum difference of 20°C between the injector and detector is desirable) and simultaneously to maintain both temperatures higher than the maximum vaporization temperature of the probes. Helium was used as carrier gas and to each sample tested the flow was selected to ensure that neither absorption nor diffusion of the probes would occur inside the column (preliminary tests were undertaken for this purpose). Small amounts of each probe vapor (<1 µl) were injected into the carrier gas flow to ensure that the experiments were carried out at infinite dilution.

The retention times were determined by measuring the electrical signal with a Flame Ionization Detector (FID) located at the end of the IGC column.

The n-alkane probes used to determine the dispersive component of the surface energy were: n-hexane, n-heptane, n-octane, n-nonane and n-decane. To evaluate the acid/base properties, the polar probes used were: dichloromethane (DCM, CH₂Cl₂, acidic), trichloromethane (TCM, CHCl₃, acidic), acetone (Acet, C₃H₆O, amphoteric), ethyl acetate (ETA, CH₃COOCH₂CH₃, amphoteric) and tetrahydrofuran (THF, C₄H₈O, basic). Natural gas (83.7 % methane) was used to determine the dead retention volume.

The relevant characteristics of the probes used, such as the dispersive component (σ_L^D) of the surface tension, molecular surface area (a), Gutmann's modified acceptor number (AN*), (DN) and Lewis character are gathered in Table 7.1.

Table 7.1 – Properties of the probe molecules used*.

Probe	Nomenclature	Molecular Weight	γ^d (mJ/m ²)	a (Å ²)	AN* (kJ/mol)	DN (kJ/mol)	Lewis Characteristics
C ₆ H ₁₄	C6	86.2	18.4	51.4	-	-	neutral
C ₇ H ₁₆	C7	100.2	20.3	57.0	-	-	neutral
C ₈ H ₁₈	C8	114.2	21.3	62.8	-	-	neutral
C ₉ H ₂₀	C9	128.3	22.7	68.9	-	-	neutral
C ₁₀ H ₂₂	C10	142.3	23.9	75.0	-	-	neutral
CH ₂ Cl ₂	DCM	84.9	27.4	31.5	16.4	0	acidic
CHCl ₃	TCM	119.4	25.0	44.0	22.7	0	acidic
C ₃ H ₆ O	Acet	58.1	16.5	42.5	10.5	71.4	amphoteric
CH ₃ COOCH ₂ CH ₃	ETA	88.1	19.6	48.0	6.3	71.8	amphoteric
C ₄ H ₈ O	THF	72.1	22.5	45.0	2.1	84.4	basic

* Cordeiro et al. 1995; Liu et al. 1998; Shen and Parker 1999; van Asten et al. 2000; Wälinder and Gardner 2000; Shakeri and Tabar-Haidar 2004; Carvalho et al. 2005; Santos 2005

At least three determinations of the retention time were carried out for each of the eleven probes (methane, n-hexane, n-heptane, n-octane, n-nonane and n-decane, trichloromethane, dichloromethane, acetone, ethyl acetate, and tetrahydrofuran), for six different temperatures: 35°C, 40°C, 45°C, 50°C, 55°C and 60°C.

7.2 RESULTS

Figure 7.7 shows peaks obtained from a typical IGC analysis together with the corresponding retention times determined by the Clarity software, coupled to the chromatograph.

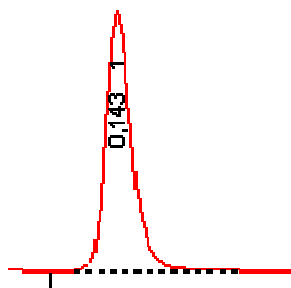


Figure 7.7 – Exemplification of the output undertaken after the injection of a probe into the IGC column: peak obtained for sample St53-10 after the injection of C7 at 45°C.

For the 31 different paper samples tested in this study, a total of at least 200 peaks were obtained, corresponding to six temperatures per sample, eleven probes per temperature and at least three injections per probe. The calculations and subsequent analysis presented in this chapter correspond to average values of the retention time of each pair probe/sample.

First of all, the analysis will be focused on the retention time values, in order to detect generic tendencies and behaviors. Afterwards the dispersive components of the surface free energies and the acid-base character of the paper surface computed from those retention time values will be analyzed.

The effect of the temperature as well as the addition of different synthetic surface sizing agents on the dispersive component of the sample surface energy will also be evaluated. These results will be compared to those obtained by the contact angle measurements. Finally, the acid-base character of the samples will be analyzed by computing the corresponding K_a and K_b values.

As in previous chapters, the statistical validity of the values of the retention time was confirmed by ANOVA. Although the corresponding results are presented in Appendix F (due to the large quantity of data), sorted by probe and temperature, it should be pointed out that the quality of the statistical analysis is ensured by the values of the parameters P , F and $F_{critical}$ (P values between $1.32E-64$ and $1.08E-06$ and F values much higher than the ones of $F_{critical}$ in all cases). For all the probes tested, the variation registered is much more due to inter-samples differences than to intra-samples differences (values between 0.02% and

41.18% for intra samples variation and from 58.82% to 99.98% for inter-samples variation; the large majority of the cases corresponds to inter samples variations above 90%). This indicates that the retention times, and consequently the chemical properties derived from them, clearly allow the differentiation between the samples. The same was found for the contact angle results (Chapter 6), but the opposite was observed for the results of profilometry (Chapter 4) and porosimetry (Chapter 5), leading to the conclusion that the major effect of the addition of the synthetic surface sizing agents is more evident in the chemical, rather than in the physical, properties of the papers surface.

7.2.1 RETENTION TIMES

Tables with the average retention times determined for all the samples can be consulted in Appendix F. Here, the data analysis will be supported by the plots considered more relevant.

Figure 7.8 represents, as an example, the retention times obtained for the n-alkanes tested at 35°C. This plot illustrates the typical behavior of all samples at all the temperature tested and was randomly selected from the remaining plots, which are depicted in Appendix F.

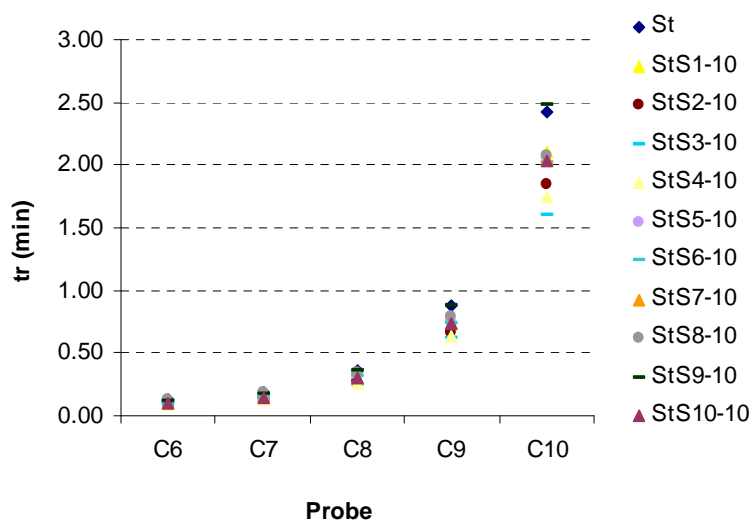


Figure 7.8 – Retention times obtained at 35°C with the n-alkanes for the reference sample and for the samples with 10% of the different surface sizing agents.

This graph shows that the retention times of the non-polar probes increase with the weight and size of the molecules: $tr(C6) < tr(C7) < tr(C8) < tr(C9) < tr(C10)$.

This was expected since both these properties rule the majority of the interactions with the stationary phase when non-polar probes are used.

A similar plot for the polar probes is presented in Figure 7.9. Although less strong, an increasing tendency of t_r with the electron acceptance ability of the probes can still be noticed: $t_r(\text{DCM}) < t_r(\text{TCM}) < t_r(\text{Acet}) < t_r(\text{THF}) < t_r(\text{ETA})$.

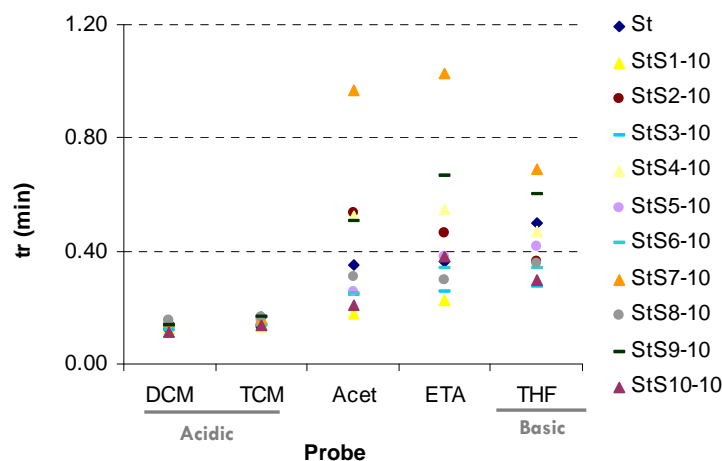


Figure 7.9 - Retention times obtained at 35°C with the polar probes for the reference sample and for the samples with 10% of the different surface sizing agents

In this case, since the probe molecules are not neutral, the retention time values are related, to the modified acceptor number (AN^*) value, generally decreasing with this number, as depicted in Figure 7.10 for samples S1, S3, S5 and S7 at 45°C. The same trend was found for the other synthetic surface sizing agents at all temperatures.

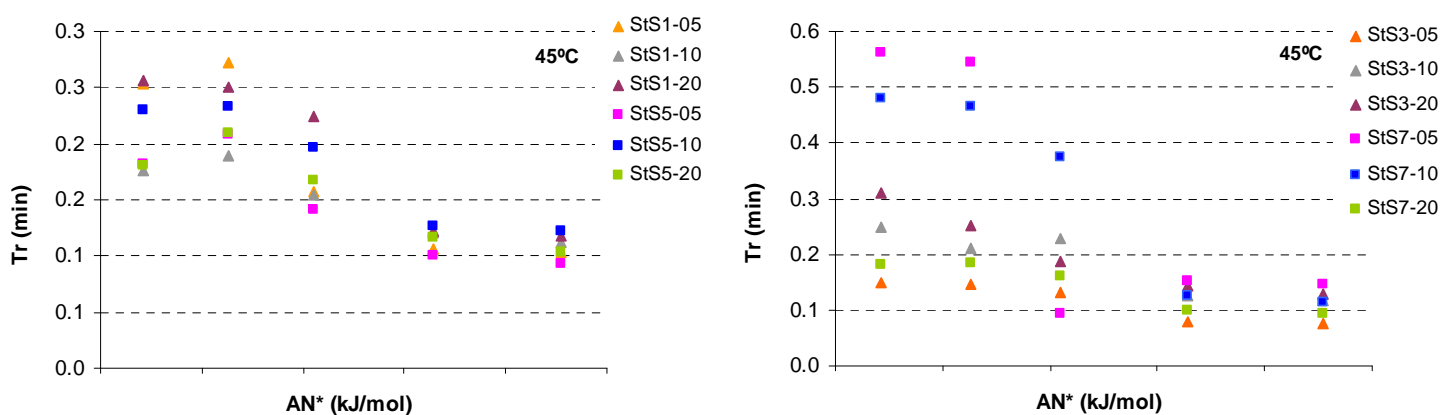


Figure 7.10 –Relation between the retention time of the polar probes and their AN^* values plotted for samples S1, S3, S5 and S7 at 45°C (the information is divided in two plots for easier visualization).

Regarding the influence of the temperature, Figure 7.11 and Figure 7.12 reveal that the increase of the temperature leads, in general, to a decrease in the retention times. Moreover, the higher the temperature the smaller the differences between the retention times of the samples for the same probe. Additionally, the difference between the distinct probes, for the same sample, is also smaller.

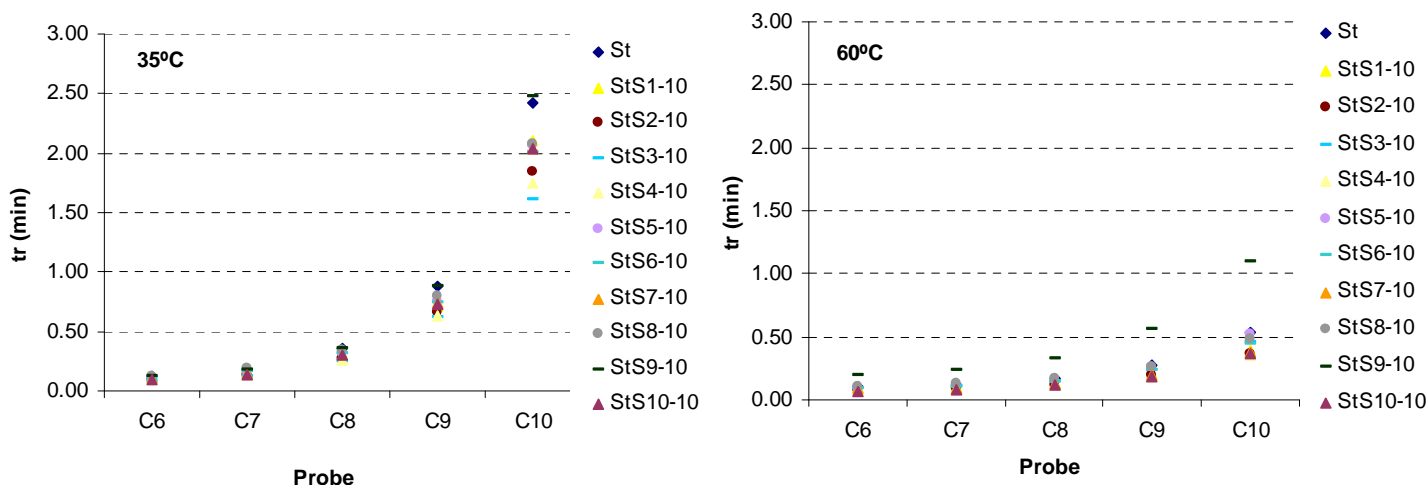


Figure 7.11 – Effect of temperature on the retention times measured with the non-polar probes.

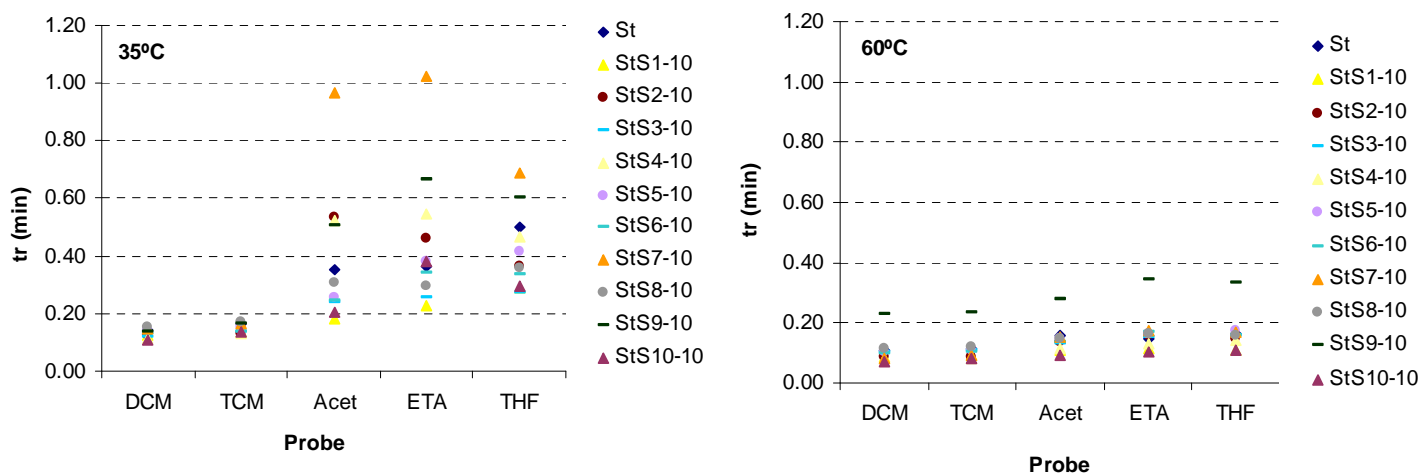


Figure 7.12 - Effect of temperature on the retention times measured with the polar probes.

The reduction in the variation amplitude of the retention times measured for all the samples (31), caused by an increase in temperature, can be better observed in Figure 7.13 for a non-polar probe (C9) and in Figure 7.14 for a polar probe (ETA). Both probes were selected merely to illustrate this fact and are representative of the results obtained for all the probes tested.

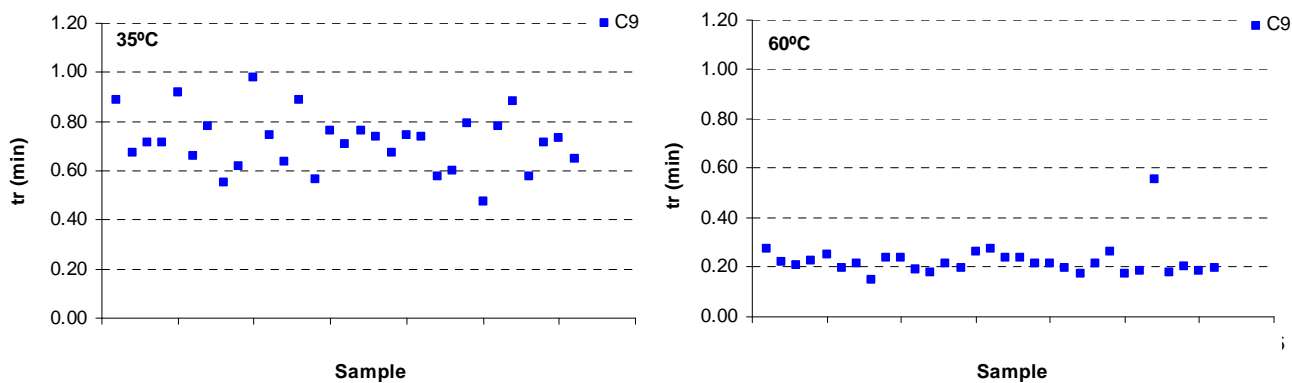


Figure 7.13 - Effect of temperature on the retention times obtained with C9 for all the samples.

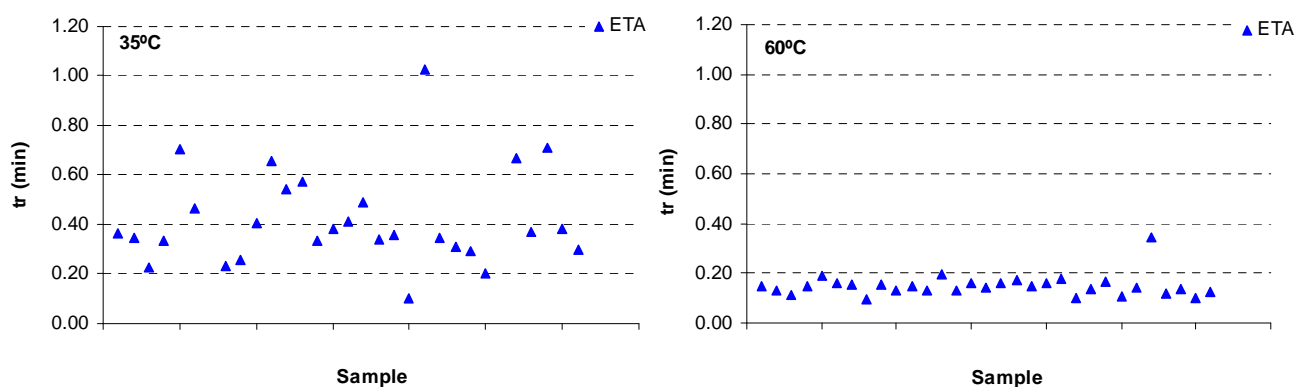


Figure 7.14 - Effect of temperature in the retention times obtained with ETA for all the samples.

7.2.2 DISPERSIVE COMPONENT OF THE SURFACE ENERGY

As mentioned before, from the retention times determined for the n-alkane series at different temperatures, the corresponding value of the dispersive component of the surface free energy (σ_s^D) can be computed.

Figure 7.15 shows the values of σ_s^D obtained for the reference sample and for the samples sized with 5% incorporation of the different synthetic sizing agents as a function of temperature.

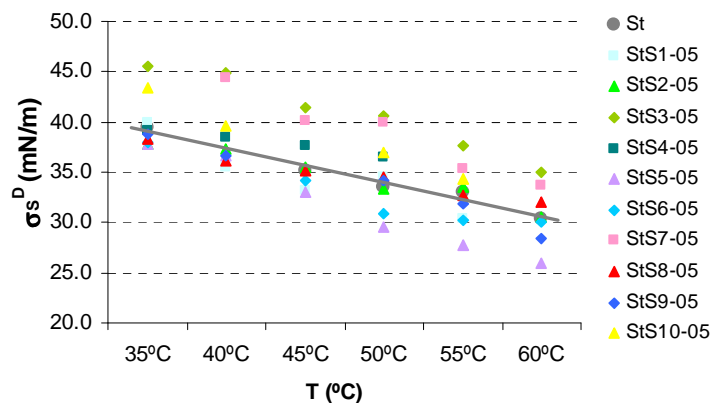


Figure 7.15 – Influence of the temperature on the dispersive component of the surface free energy, for the samples sized with 5% incorporation of synthetic sizing agents (the straight line indicates the behavior of sample St).

This figure shows a tendency for linear decrease of σ_s^D with temperature. Identical trends were found for the remaining the samples, sized with 10% and 20% incorporations (Appendix F). This is in agreement with results previously reported by other authors, regarding pulp and paper studies (Shen et al. 1996; Santos et al. 2001; Carvalho et al. 2005). This decrease with temperature is associated to an entropic contribution of the surface free energy.

Also regarding the magnitude of the σ_s^D values, it should be stressed that similar values can be found in previously published studies, which reported σ_s^D values of 24.6 mN/m at 50°C for an office paper, and 33.4 mN/m at 40°C for handsheets of *Eucalyptus globulus* pulp (Santos et al. 2001; Carvalho et al. 2005).

The quality of the linear correlation between σ_s^D and T is very good for all the samples (with the exception of sample StS1-05), as summarized in Table 7.2. Therefore, these correlations can be used for the calculation of σ_s^D (mN/m) at temperatures that were not tested.

Table 7.2 – Experimental correlations obtained for the variation of σ_s^D with temperature for each of the paper samples tested and corresponding determination coefficient (r^2).

Sample	Equation	r^2
St	$\sigma_s^D = - 0.34 \cdot T(^{\circ}\text{C}) + 50.90$	0.97
StS1-05	$\sigma_s^D = - 0.40 \cdot T(^{\circ}\text{C}) + 52.96$	0.82
StS1-10	$\sigma_s^D = - 0.58 \cdot T(^{\circ}\text{C}) + 62.52$	0.87
StS1-20	$\sigma_s^D = - 0.36 \cdot T(^{\circ}\text{C}) + 51.93$	0.91
StS2-05	$\sigma_s^D = - 0.28 \cdot T(^{\circ}\text{C}) + 48.17$	0.94
StS2-10	$\sigma_s^D = - 0.65 \cdot T(^{\circ}\text{C}) + 65.39$	0.97
StS2-20	$\sigma_s^D = - 0.53 \cdot T(^{\circ}\text{C}) + 58.14$	0.96
StS3-05	$\sigma_s^D = - 0.43 \cdot T(^{\circ}\text{C}) + 61.37$	0.97
StS3-10	$\sigma_s^D = - 0.63 \cdot T(^{\circ}\text{C}) + 67.69$	0.99
StS3-20	$\sigma_s^D = - 0.40 \cdot T(^{\circ}\text{C}) + 57.23$	0.98
StS4-05	$\sigma_s^D = - 0.18 \cdot T(^{\circ}\text{C}) + 45.48$	0.98
StS4-10	$\sigma_s^D = - 0.37 \cdot T(^{\circ}\text{C}) + 52.14$	0.99
StS4-20	$\sigma_s^D = - 0.36 \cdot T(^{\circ}\text{C}) + 51.82$	0.95
StS5-05	$\sigma_s^D = - 0.51 \cdot T(^{\circ}\text{C}) + 56.08$	0.98
StS5-10	$\sigma_s^D = - 0.32 \cdot T(^{\circ}\text{C}) + 52.17$	0.93
StS5-20	$\sigma_s^D = - 0.41 \cdot T(^{\circ}\text{C}) + 54.87$	0.99
StS6-05	$\sigma_s^D = - 0.33 \cdot T(^{\circ}\text{C}) + 49.06$	0.91
StS6-10	$\sigma_s^D = - 0.48 \cdot T(^{\circ}\text{C}) + 57.91$	0.99
StS6-20	$\sigma_s^D = - 0.33 \cdot T(^{\circ}\text{C}) + 49.78$	0.98
StS7-05	$\sigma_s^D = - 0.52 \cdot T(^{\circ}\text{C}) + 64.93$	0.95
StS7-10	$\sigma_s^D = - 0.36 \cdot T(^{\circ}\text{C}) + 53.83$	0.99
StS7-20	$\sigma_s^D = - 0.61 \cdot T(^{\circ}\text{C}) + 61.95$	0.90
StS8-05	$\sigma_s^D = - 0.24 \cdot T(^{\circ}\text{C}) + 46.29$	0.97
StS8-10	$\sigma_s^D = - 0.46 \cdot T(^{\circ}\text{C}) + 57.41$	0.99
StS8-20	$\sigma_s^D = - 0.30 \cdot T(^{\circ}\text{C}) + 49.14$	1.00
StS9-05	$\sigma_s^D = - 0.38 \cdot T(^{\circ}\text{C}) + 52.17$	0.96
StS9-10	$\sigma_s^D = - 0.38 \cdot T(^{\circ}\text{C}) + 52.51$	0.98
StS9-20	$\sigma_s^D = - 0.54 \cdot T(^{\circ}\text{C}) + 60.42$	0.96
StS10-05	$\sigma_s^D = - 0.42 \cdot T(^{\circ}\text{C}) + 57.36$	0.96
StS10-10	$\sigma_s^D = - 0.18 \cdot T(^{\circ}\text{C}) + 47.37$	0.99
StS10-20	$\sigma_s^D = - 0.25 \cdot T(^{\circ}\text{C}) + 50.40$	0.99

It should be mentioned that the values of the temperature coefficients ($d\sigma_s^D/dT$), are also in agreement with those reported in literature for an office paper, of $- 0.35 \text{ mN}/(\text{m}\cdot\text{K})$ in the range $50\text{-}90^{\circ}\text{C}$ and for amorphous cellulose, of $- 0.36 \text{ mN}/(\text{m}\cdot\text{K})$ in the range $50\text{-}100^{\circ}\text{C}$ (Santos et al. 2001).

Concerning the effect of the addition the synthetic surface sizing agents to the cationic starch, it was found that, in general, higher σ_s^D values are obtained for the sizing blends than for

the reference sample (St). The same was detected in the contact angle measurements, as reported in Chapter 6.

This indicates that the sizing agent generally increases the surface ability to establish dispersive interactions, probably due to the higher surface tension of the sizing agents compared to that of the cationic starch (Table 3.3).

However, in addition to the surface tension effect, the size and the spatial orientation of the molecules of sizing agents at the paper surface can also influence its ability to establish dispersive interactions.

Concerning the influence of the type and of the concentration of the sizing agent, different behaviors were detected. Let us examine for instance the results of Figure 7.16 that shows the variation of σ_s^D with the concentration of the sizing agent S2 (co-styrene-maleic anhydride), together with value of the reference sample, for different temperatures. Besides a consistent decrease of σ_s^D with temperature, it is visible that the relative position corresponding to the three incorporation percentages is maintained between 35 °C and 45°C, but above this temperature, quite distinct behaviors can be observed. A dissimilar behavior was detected for the synthetic surface sizing agent S4 (co-styrene-maleic anhydride) which shows a different behavior for each of the temperatures tested. In fact these are just examples of the myriad of patterns found for the various sizing agents.

This is most certainly a consequence of the dispersive interactions being weak by nature, and thus significantly affected by the vibrational movement of the molecules caused by the temperature. In fact the increase in temperature was found to alter the impact of the molecules size and spatial orientation of the molecules on the intensity of the dispersive forces (in particular when the molecules are non linear).

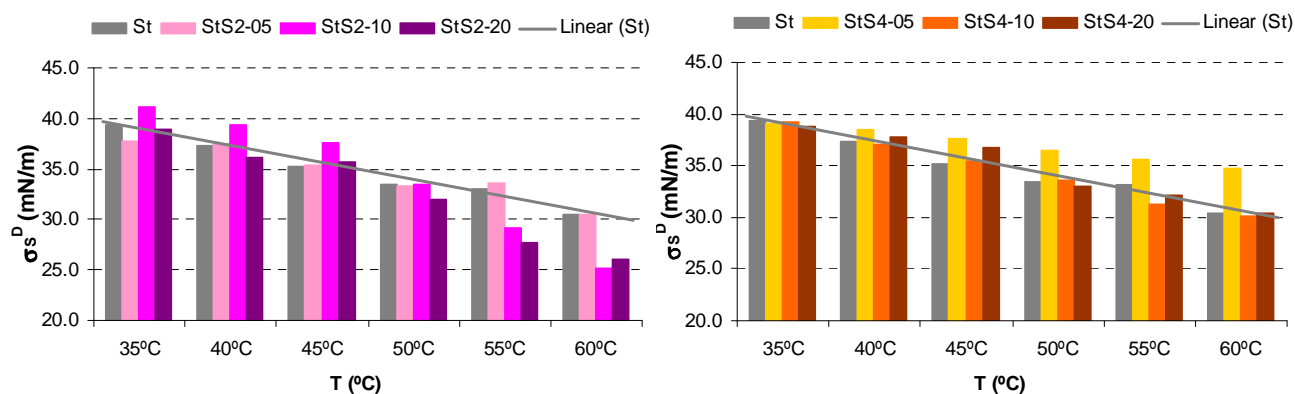


Figure 7.16 - Variation of σ_s^D with concentration and temperature for the samples sized with the surface sizing agents S2 and S4 (St sample is also included, as reference).

This is most pertinent for papers with a reduced polar component (like P&W papers) when subjected to printing devices, such as laser printers, which imply an increase in temperature. In these papers, the dispersive interactions are those ruling the printing process, and thus the results will be extremely dependent on the temperature.

Since σ_s^D was also evaluated from the contact angle measurements, it is interesting to compare the above results with the contact angle data.

7.2.3 IGC VERSUS CONTACT ANGLE IN THE DETERMINATION OF σ_s^D

As already mentioned, below 35°C the IGC equipment can not be operated without substantial experimental problems. Thus to compare the values of σ_s^D determined by IGC with those derived from the contact angle measurements, the former have to be extrapolated to 21°C. The extrapolated values are calculated using the correlations presented in Table 7.2, being the comparison presented in Figure 7.17.

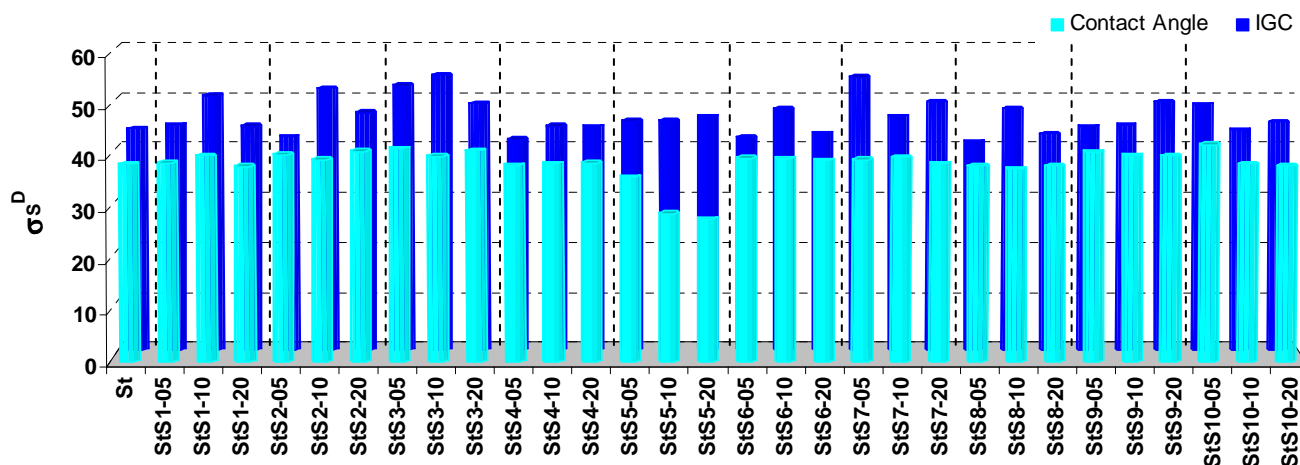


Figure 7.17 – Comparison of the σ_s^D values calculated from the contact angle measurements and from the extrapolation of the IGC data (based on the correlations of Table 7.2).

As this figure clearly shows, the values of the dispersive component of the surface energy derived from IGC are always superior to those derived from the contact angle measurements.

This superiority (mostly between 10 and 20%, but reaching in some cases 40%) is not surprising since the n-alkanes used in the IGC technique to perform the experiments are very stable molecules and are transported in very low concentrations within the inert gas, thus inducing the predominant detection of high energy sites which in turn leads to higher values of σ_s^D . Conversely, the contact angle method detects surface sites of all energy levels, computing an average energy level of the surface (Kwok et al. 1998; Shen et al. 2000). This also leads to higher amplitude of variation of the values determined by IGC, as illustrated in Figure 7.18. In fact, the colored lines of Figure 7.18(b) are more spread than those of Figure 7.18(a), which are mostly coincident.

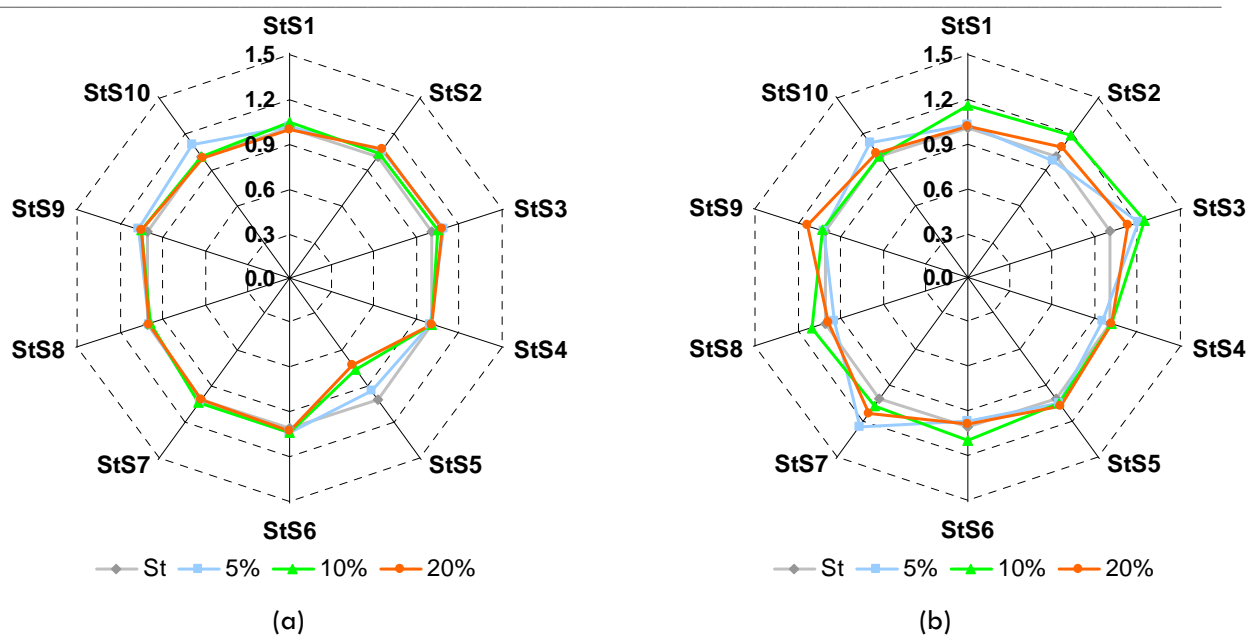


Figure 7.18 – Values σ_s^D (normalized relatively to the reference sample, St) determined for all the samples tested: (a) by contact angle method; (b) by IGC (using the regressions of Table 7.3).

This leads to the conclusion that the IGC seems a more reliable technique when the objective is to differentiate samples in terms of σ_s^D .

7.2.4 ACID-BASE CHARACTER

As mentioned before, besides the dispersive interactions investigated using the n-alkane probes, the acid-base interactions, based on the Lewis concept, can be studied injecting polar probes.

Previous studies published by other authors reported difficulties in evaluating the acid-base character using IGC, due to negative values of $-\Delta H^{AB}$ (Wälinder and Gardner 2000), or to the lack of a clear correlation between the enthalpy of acid-base interaction and the acceptor and donor numbers of the probes (Asten et al. 2000). In the present study, however, the values of $-\Delta H^{AB}$ are positive and good linear relationships were obtained between the enthalpies and the donor and acceptor numbers, thus validating the use of this methodology.

It should be mentioned that the evaluation of the acid-base character of the surface is often performed using the values of the work of adhesion of only one polar and one non-polar probe. However, an accurate determination of K_a and K_b requires that several polar probes

should be tested which is a time consuming process (Shen et al. 1998; Santos et al. 2001; Carvalho et al. 2005). In the present work five polar probes were tested, and subsequently the acid-base character of the surface was evaluated by computing the values of K_a and K_b , according to Figure 7.4. The values obtained for all samples are plotted in Figure 7.19.

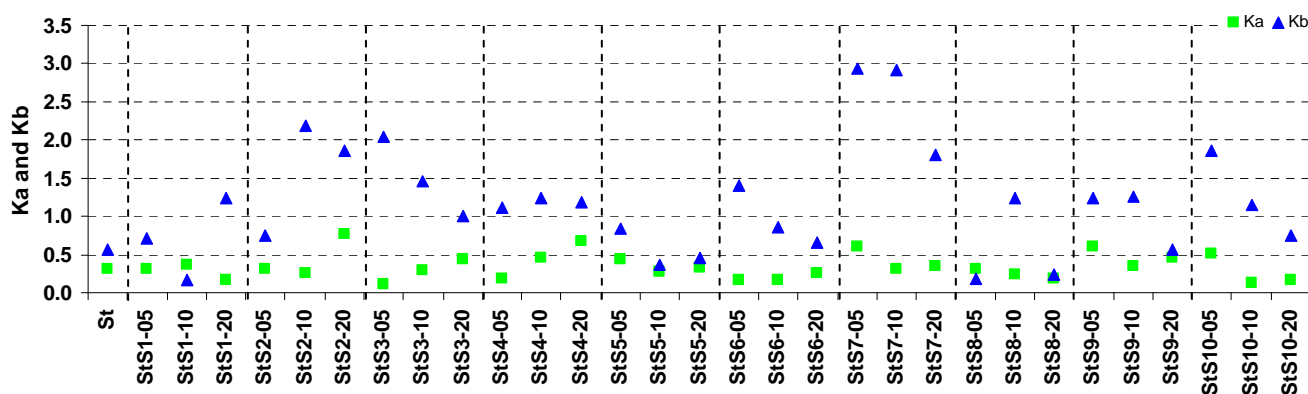


Figure 7.19 – Values of K_a and K_b computed from the IGC measurements for the different sizing agents and different concentrations.

From this plot, it is possible to observe that all the K_a and K_b values determined by IGC have the same order of magnitude, and for most of the samples the K_b values are superior to those of K_a . This indicates that the surface of the papers is predominantly amphoteric with a slight tendency to donate electrons (i.e. with a moderate basic character). In comparison to the sample sized with cationic starch alone (St), it is possible to see that the largest impact of the addition of the synthetic surface sizing agents is specially noticed on the values of K_b .

The surface acid-base character, evaluated by the K_a and K_b values, is ruled by the availability of functional groups at the paper surface. Thus, and similarly to the procedure followed in the last chapter, it is possible to elaborate further about the composition and orientation of the molecules of the sizing agents.

Previously published studies with IGC indicated that surface sizing decreases the paper surface acidity, and stated that the availability of the hydroxyl groups (-OH) at the surface strongly relates to the surface acidity (Tze and Gardner 2001; Shakeri and Tabor-Haidar 2004; Carvalho et al. 2005).

The influence of the percentage of the incorporation of the sizing agent in the blend will be analyzed individually, as in the previous chapter. Furthermore, comparisons with the contact angle results will be made whenever necessary.

Starting with the sample sized with the synthetic sizing agent S1, (co-styrene-acrylate), no relevant differences are found in the K_a values for 5 and 10 % incorporation (StS1-05 and StS1-10). Having in mind that the surface acidic character is related to carboxyl groups (COOH) and the proximity of K_a and K_b values at 5 and 10%, the most likely explanation is that the amounts of the styrene and acrylate functional groups oriented outwards are equivalent. Nonetheless, for the 5% incorporation, a slight predominance of styrene is detected whereas for 10% the opposite occurs (acrylate dominates). For 20% incorporation (StS1-20), a reduction in K_a and an increase in K_b were found, probably due to the electronic cloud of the styrene. This interpretation, based on the molecular orientation, enables to justify the results obtained by the contact angle method for the polar component of the surface free energy (Figure 6.13), which were not explained there.

As for behavior of the sizing agent S9, which has the same composition of S1 (the difference between these two sizing agents lies on arrangement of the monomers), some assumptions regarding the orientation of its molecules at the paper surface were anticipated, in Chapter 6, when analyzing the contact angle results for 5 and 10% of incorporation (Fig. 6.13). As explained then, the styrene monomer was the one oriented outwards, and only for 20% incorporation, the acrylate monomer was the one predominantly turned out. The IGC results confirm this analysis but reveals that at 5% incorporation the amount of styrene and acrylate groups oriented outwards is similar, while at 10% the orientation of the styrene outwards predominates. These results also indicate that the arrangement of the monomers (styrene and acrylate) has a greater influence on the acid-base character of the sample StS9 than in the case of sample StS1 (Figure 3.3).

Although having the same monomers than S1 and S9, the results obtained by IGC for sample StS10 are inconclusive with regard to the orientation of the copolymer molecules at the paper surface.

As for the surface sizing agent S2, composed of styrene and maleic anhydride, the results of the contact angle measurements presented in Section 6.2.3 suggested that its molecules are probably oriented so that the styrene monomer is turned to the exterior and the oxygen of the maleic anhydride monomer point inwards for all concentrations. This hypothesis is in agreement with the IGC results presented in Figure 7.19. In fact, the increase of the K_b values in comparison to the reference sample (St) is certainly due to the presence of the electronic cloud of the styrene monomer. In addition, when the amount of sizing agent is

increased to 20% the electron accepting effect of the oxygen atoms of the maleic anhydride monomer is strongly enhanced, as detected by the increase in K_a .

Analyzing now the concentration of the sizing agent S4, which differs from the sizing agent S2 in the styrene/maleic anhydride ratio (Table 3.2), and considering that styrene causes an increase in K_b (as found for sample StS2), the enhancement of the basic character of samples StS4 in comparison with the St sample was to be expected. However, the increment in K_b is smaller than that found for sample StS2 in agreement with the also smaller styrene amount.

As for the surface sizing agent S3, which is quite distinct from the ones referred to in the previous paragraphs, the analysis relative to the orientation of the acrylonitrile and acrylate monomers at the paper surface derived from the contact angle data (Section 6.2.3) can not be confirmed by the IGC. Nevertheless, the variation of the K_a and K_b values are in perfect agreement with the copolymer composition: for 5% incorporation, a decrease of K_a relatively to the reference sample St is observed, which is a consequence of the smaller acidic character of the copolymer in relation to the cationic starch; increasing the amount of copolymer, the K_a gradually increases due to the augment of the number of electron accepting functional groups.

Regarding the sizing agents S5, S6, S7 and S8, the IGC results are not conclusive in what concerns the influence of the polymer concentration on K_a and K_b values neither on the orientation at their molecules at the surface.

CHAPTER 8

PRINTING QUALITY

8 PRINTING QUALITY

8.1 THEORY

As described in Section 1.5, there are innumerable types of printing processes, however considering its importance in the P&W papers applications, the printing process selected for this work was inkjet printing.

8.1.1 INKJET PRINTING

Inkjet is a non-impact printing process, where the ink is emitted from a jet device, driven by an electronic signal, directly onto the substrate. The principles of inkjet were laid over a century ago, but the practical inkjet devices did not appear until the mid 1960's and in the 1970's significant developmental efforts were made, the ink stream could be controlled and individual droplets could be charged (Svanholm 2004).

However the real breakthrough for inkjet technology came in the early 1980's, associated to the introduction of IBM's personal computer (PC). In the beginning of the 1980's, technological advances such as the thermal printers invented by Canon (UK Patent - GB 2007162A, 1987) and Hewlett Packard (US Patent – US 4490728, 1982) had made inkjet a technology that was more reliable and more affordable, making it a strong potential candidate for desktop printer applications (Svanholm 2004).

In 1984, Hewlett Packard launched their first line of low-cost printers with disposable inkjet print heads, which reduced the cost even further. By the mid-1990's and onwards, the image quality, reliability and cost effectiveness had improved to a point where it was realistic for inkjet to compete with conventional small-scale printing. The resolution was improved from around 100 dots per inch (dpi) in the early 1980's to 2400 dpi in 2004 (Svanholm 2004). In 1982-1984, an inkjet printer cost \$1000-\$6000. Nowadays a desktop inkjet printer can be purchased for as little as \$50.

The principle of inkjet printing consists in directing individual drops to a paper surface in order to create an image. There are two main categories of inkjet printers (Oittinen and Saarelma 1998; Keskitalo 2000; Svanholm 2004):

- ✓ Continuous (Figure 8.1 a)
- ✓ Drop-on-Demand – DoD (Figure 8.1 b)

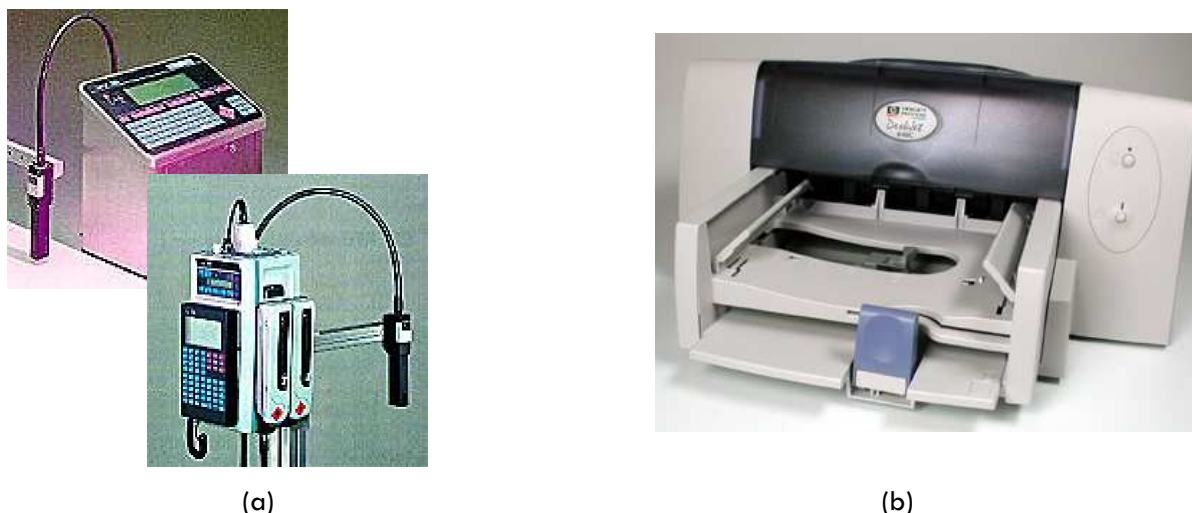


Figure 8.1 – Example of (a) continuous and (b) Drop on Demand inkjet printers.

The continuous printers work by breaking up a continuous liquid stream into single droplets (normally using a piezo driver element). The droplets are subsequently charged individually and passed through a deflection array. The charge decides whether the droplets are to impact onto the substrate or are sent into a gutter and recirculated to the drop generator. The continuous printers are classified by the type of drop deflection method (multiple, binary, Hertz or magnetic deflection) (Svanholm, 2004).

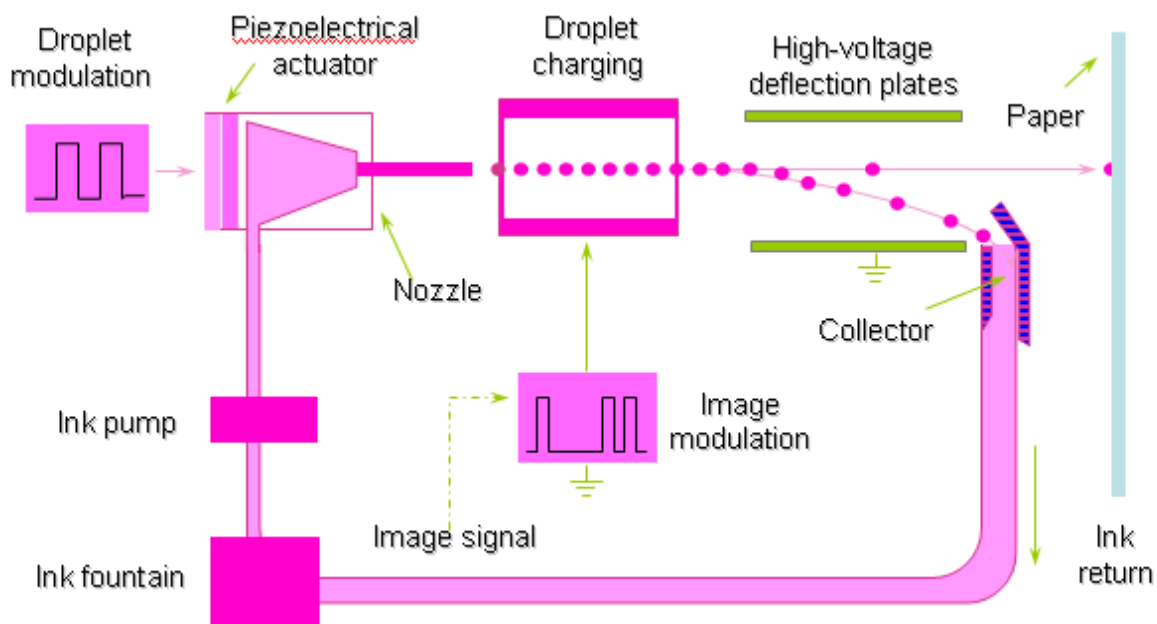


Figure 8.2 – Schematic representation of the continuous inkjet printing system.

The DoD print heads work by ejecting droplets only when they are required for imaging on the substrate. These print heads have a drop-ejection element that is located in an ink channel near the nozzle. When a voltage pulse is applied to the drop ejection element, a droplet is emitted. The DoD printers are organized by the type of drop-ejection element: thermal printers, which emit the droplet by a volume expansion of the heated ink (Figure 8.3), and piezoelectric printers, which work by the high vibration of an electronically charged piezo-ceramic (Figure 8.4). Electrostatic and acoustic DoD printers also exist, but they are far less common than these two (Keskitalo 2000; Svanholm, 2004).

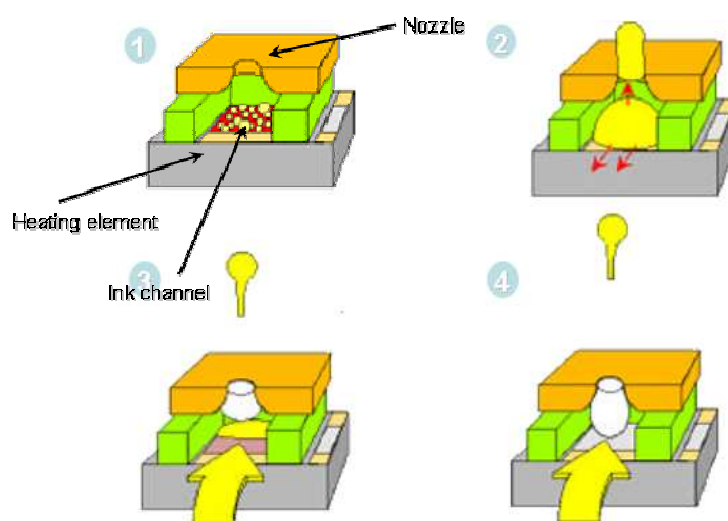


Figure 8.3 - Schematic representation of the thermal inkjet DoD printing system.

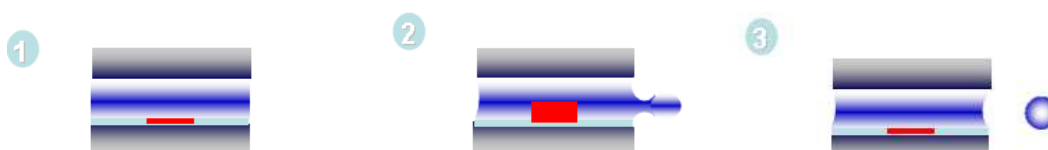


Figure 8.4 - Schematic representation of the piezoelectric inkjet DoD printing system.

Continuous inkjet printers print at higher speeds because the drop generation rate is 10-100 times higher than the one achieved in DoD printers. However, they are also much more complicated and expensive, and this makes them more suitable for industrial applications such as the printing of packages, labels and direct mail (Oittinen and Saarelma 1998; Svanholm, 2004). The use of DoD printers is limited due to the slow speed determined by the systems physics. Consequently, DoD printers are mainly used for office, home and wide format printing applications. Color pictures have an increasingly important role in home and

wide format printing and digital photography is an important driving force behind color printing in homes. In 2002, more than 95% of the color desktop printers in the world were DoD units (Svanholm, 2004).

Inkjet printing is a direct-to-substrate technology, since the ink goes directly from the ink chamber to the paper. It is thus of major importance that the ink to be used is appropriate for the physical process adopted by the print head (Keskitalo 2000; Svanholm 2004).

A characteristic of inkjet inks compared with inks in other printing methods is that they have a low viscosity. This is especially true for the continuous stream inkjet method where rapid drop formation requires viscosity near 1 mPas. In thermal jetting, viscosity is commonly less than 5 mPas, being 10 mPas is the upper limit (Oittinen and Saarelma 1998).

Inkjet inks are composed of mainly four components, with specific functions, as depicted in Table 8.1 (Oittinen and Saarelma 1998; Keskitalo 2000).

Table 8.1 – Inkjet inks components.

Component	Purpose	Usual Proportion (%)
Pigment or Dye	Coloring material	2 - 5
Solvent/vehicle	Carrier phase for the dye or pigment	95 - 98
	Allows the desired low viscosity Prevents ink from drying in the nozzle	
Binder	Binds the pigment on the paper (not always used)	
Additives	Charge generation additives or Preservative additives	2 – 5

Inkjet inks are currently commercially available in two different types: dye and pigment based. In the first the color consists of highly diluted solutions of soluble organic dye molecules, while pigmented inks consist in dispersions of micro-sized ink pigment particles of approximately 0.1 μm (Oittinen and Saarelma 1998; Keskitalo 2000; Glittenberg and Voigt 2004; Svanholm 2004).

The solvents are blends of water and various organic materials, typically high-boiling point alcohols. Solvents are used to enable the ink to penetrate the paper and for jet formation. Ecological aspects, low viscosity and desired drying properties are the main criteria in selecting solvents for the inks (Donigian et al. 1999; Glittenberg and Voigt 2004; Svanholm 2004)

Most aqueous inkjet inks have no binder. Binder-containing inks increase markedly in viscosity when small amounts of solvent are removed. When used, the polymeric binder creates a bridge between the pigment and the substrate. In water based inks the binder consists mainly of water-insoluble styrene- or acrylate-based polymers (Keskitalo 2000; Svanholm 2004)

Additives improve ink properties such as light stability or electrical charge (Oittinen and Saarelma 1998; Donigian et al. 1999; Keskitalo 2000).

Surface tension plays an important role in the runnability of the inkjet printing process. In fact, a high surface tension to form ink drops, but to be able to penetrate the paper, the solvent has to have a low surface tension. In water based inks surface tension is around 30 - 60 dynes/cm, due to the mixing of water with organic compounds. This difference in surface tension suggests that water based inks can not be expected to behave as water (72 dynes/cm), in terms of paper penetration (Donigian et al. 1999; Keskitalo 2000).

Before drying, inkjet ink layers may be 15 μm or more in thickness for each color. For good printed appearance, the dyes should be fixed on the paper's outer surface with only enough lateral spreading from the position of drop impact to merge adjacent drops in solid colors. In fact, proper dye fixation is the key to several components of inkjet print quality and, after drying, the dyes should stay at the surface, even if this is rewetted (Donigian et al. 1999)

Additionally, because inkjet inks are highly fluid, highly surface active and penetrative and also because of the high velocity of impact on the paper, inkjet papers require characteristics that match with the inks and the drop volumes. Inkjet papers must respond to high demands on properties such as surface tension, charge, roughness and porosity (Oittinen and Saarelma 1998; Donigian et al. 1999).

8.1.2 PRINTING QUALITY EVALUATION

As mentioned in Section 1.5.1, there are no absolute definitions and concepts to define print quality and the corresponding paper ideal characteristics. They depend on the final use of the printed product.

An ideal paper for inkjet printing must meet several runnability and printing quality requirements. For runnability the critical operation is feeding, which is influenced by friction coefficient, static electricity and cutting quality. Regarding printing quality, paper-ink

interaction is obviously the key factor, which is ruled by surface roughness, porosity and surface chemistry (Donigian et al. 1999; Levlin and Söderhjelm, 2000; Svanholm 2004).

Printability tests depend on the printing process involved. Certain types of printability test are used for all types of papers regardless the printing method used, while some other test methods are only suitable for papers specific of a certain printing process. For inkjet printing quality some laboratory printing tests are commonly used, such as print density, print through, dot gain, circularity, and sharpness or inter color bleeding (Levlin and Söderhjelm 2000).

The assessment of printing quality either in qualitative or in quantitative terms is the subject of many published studies (Varnell 1998; Chen et al. 2002; Donderi et al. 2003; Mattila et al. 2003; Rosenberger 2003; Danby and Zhou 2004; Lee et al. 2005; Yang et al. 2005; Olsson et al. 2006; Mäkenen et al. 2007; Sreekumar et al. 2007; Ungh et al. 2007; Moutinho et al. 2007b). Some printing quality parameters found relevant for this study are presented in Section 8.1.2.1 (Kowalczyk and Trksak 1998; Oittinen and Saarelma, 1998; Varnell 1998; Lehtinen 2000; Levlin and Söderhjelm 2000; Hladnik 2003; Lee et al. 2005; Moutinho et al. 2007b; Sreekumar et al. 2007).

8.1.2.1 Inkjet Printing Quality Parameters

Printing quality parameters are mainly intended for the evaluation of two different characteristics of the printed image, the intensity or range of the color reproduction and the image contour definition. In this work, the color intensity will be accessed through optical density and gamut area, while for accessing image definition the gain, raggedness and feathering were measured, as described in Section 8.1.2.2.

Optical Density measurement is probably the most commonly used property for printing quality evaluation. It abbreviates as OD, and is given by the relation between the intensity of the light reflected from a paper sheet before printing (I_0) and after printing (I), as described in Figure 8.5. The calculation is performed according to Equation 9.1.



Figure 8.5 - Schematic representation of the light beams involved in the optical density measurement.

$$OD = \log_{10} \frac{I_0}{I} \quad (8.1)$$

A higher value of optical density means less ink penetration. Density measurements do not have standard conditions: usually angles relative to the normal surface of 45° in illumination and zero in detection are used. In terms of printing quality, the higher the optical density values the better.

The evaluation of color reproduction ability is based on the coordinates a^* and b^* , which represent the saturation of the color in the CIELAB color space (Figure 8.6). L^* is a measure of perceived lightness, ranging in the scale 0-100; a^* is a measure of the hue on the red/green axis (a positive value for a^* means red, and a negative value means green); b^* is a measure of hue on the yellow/blue axis (a positive b^* means yellow, and a negative value means blue). Greater values of a^* and b^* correspond to more saturated colors, so that absolute values of a^* and b^* of strongly saturated spectral colors range between 80 and 90 (Levin and Söderhjelm, 2000).

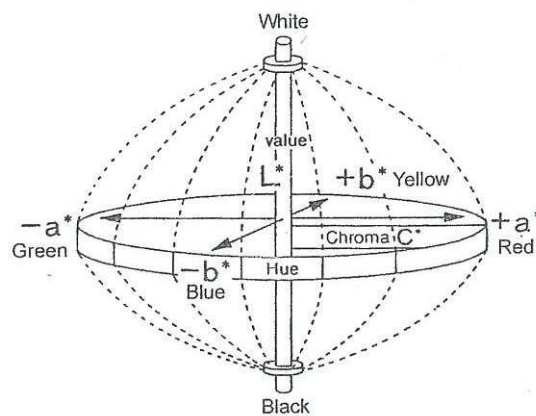


Figure 8.6 – Representation of the CIELAB color space.

Gamut Area is then a color relater parameter, which evaluates the colors that each paper can reproduce. It corresponds to the area of the hexagon whose vertices are the pairs (a^* , b^*) obtained for cyan, yellow, magenta, green, blue and red areas of a specified mask, plotted as depicted in Figure 8.7.

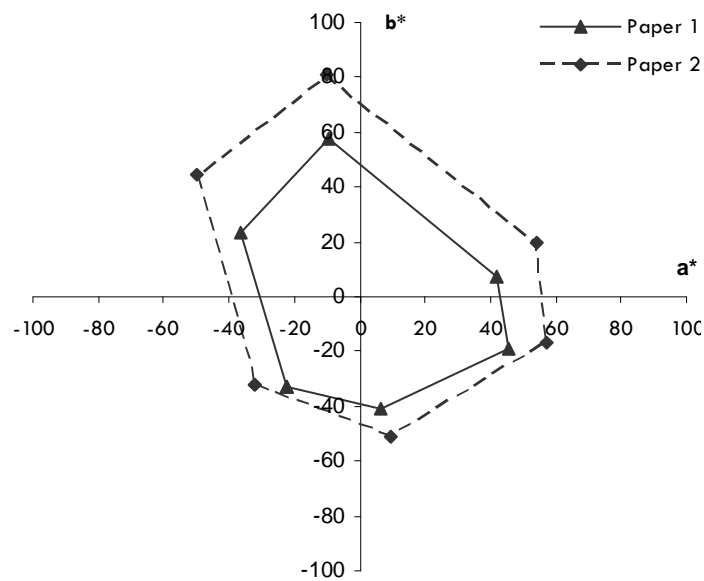


Figure 8.7 - Exemplification of Gamut Area's Graphic representation.

The higher the Gamut Area, the greater is the potential of a paper to reproduce colors. Therefore, paper 2 in Figure 8.7 is better in terms of color range reproduction than paper 1.

As for the image contour definition, several mathematical parameters can be used and sometimes different definitions can be found for the same parameter.

Gain is the difference between the printed area (PA) and the area that should have been printed (target area - TA):

$$Gain = \frac{PA - TA}{TA} \% \quad (8.2)$$

In this case, better printing performance corresponds to smaller gain values.

Feathering corresponds to edge defects caused by ink run along the fibers length (Figure 8.8b). Also in this case, smaller values of feathering correspond to better printing quality.



Figure 8.8 – Exemplification of feathering of a printed area.

Raggedness is the measure of the irregularity of the line contour (the smaller the better). Corresponds to the sum of the differences found between a straight line adjusted to the image line, and the printed line.

When using water based inkjet inks, the extent of spreading and penetration of the ink components in the paper surface and fibrous matrix has a major effect on all these print quality parameters. Poor penetration of the ink vehicle means slow drying of the ink, which results in problems of color bleeding and feathering. On the other hand, too much penetration of the colored dye reduces color saturation, producing an image of inferior quality. For good print quality a compromise must be achieved between ink drying (which requires good penetration) and color saturation (which require poor penetration) (Keskitalo, 2000; Svanholm, 2004).

8.1.2.2 Methodology

For the evaluation of the inkjet printing quality of all the samples produced three main aspects were addressed in this study: color reproduction intensity/range and image definition, as quantitative information, and human perception of printing quality, as subjective qualitative assessment of the papers performance in terms of inkjet printing quality. For that a specific mask was selected were three zones can be isolated (Figure 8.9):

- ✓ **Zone A** – where the color related measurements were performed;
- ✓ **Zone B** – where the line quality was evaluated;
- ✓ **Zone C** – used for the subjective printing quality evaluation.

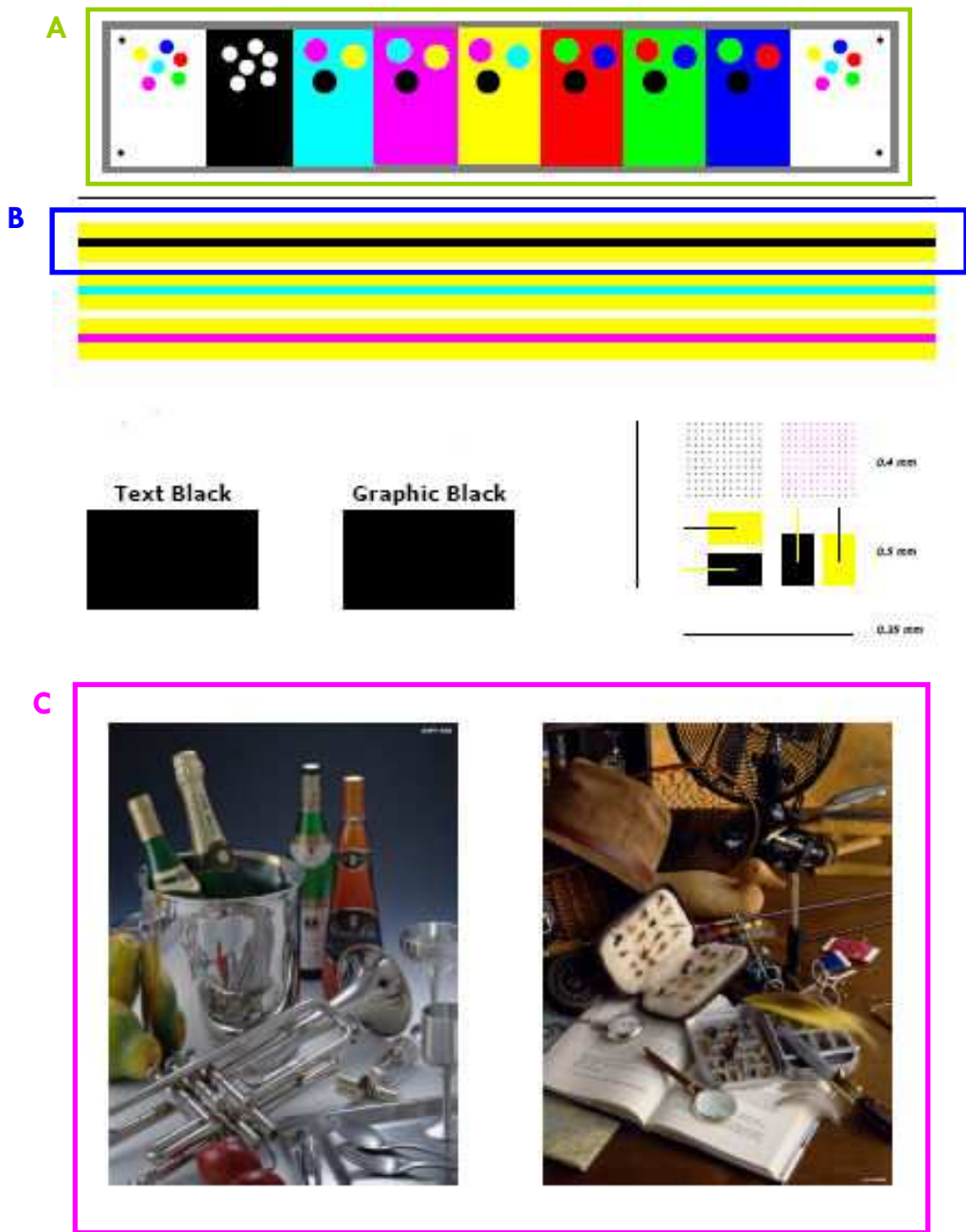


Figure 8.9– Mask printed in the paper samples for the printing quality evaluation.

Several preliminary tests were performed in order to determine the necessary number of prints and the number of measurements to be performed for accessing each parameter. According to those testes, it was decided to print the mask presented in Figure 8.9 in two sheets of each paper sample, using different sides of the sheet.

The paper sheets were printed using an HP5652 inkjet printer, selecting always the same printing mode, indicated in the printer settings as “best”. The printing quality parameters were then assessed for each paper sheet printed.

Optical Density (OD) values were measured in the black, cyan, magenta and yellow areas in the zone indicated as A in Figure 8.9 using the spectrophotometer Gretag D19C. At least three measurements for each color were performed in each printed sample and an average value was computed for the OD values of each color and paper.

The CIE Lab color coordinates (a^* , b^*) used to compute the gamut area values were assessed using the AvaMouse spectrophotometer. For each paper sheet, two separate measurements of a^* and b^* for each of the six colors (A zone of the mask) were performed, and the gamut area was computed using the average values of those measurements. This procedure was repeated for the two sheets printed for each paper type, and the average of the two values was used for further analysis.

Regarding the image definition, accessed in this work by evaluation the line quality a personal image analysis system PIA BASF – 8042319 was used in the black line with yellow background (B zone of the mask). For each type of paper tested, the average of six measurements was considered (three separated measurements for each printed sheet). Each of the three measurements performed by sheet corresponds to a different zone of the printed line and to six measurements of each property. The variables measured by this device are named as plain (mm^2), borderlength (mm) and roughness and are used to access the printing quality parameters gain, feathering and raggedness, respectively.

The subjective evaluation was based on the perception of an independent panel of ten different persons, regarding the images printed (zone C of Figure 8.9). The following procedure was used:

- ✓ The pictures were separated in four groups (corresponding to two pictures in two sheets of each type of paper).
- ✓ Each panel member was asked, for each of the four groups separately, to classify the images according to his personal preference in a 0 to 100 scale, assigning a different classification only when perceiving a relevant difference between the samples.
- ✓ The results were normalized according to the maximum and minimum values used by each person, in order to allow the comparison of the results.
- ✓ The average of the normalized rating achieved for each sample was computed and used for further analysis.

8.2 RESULTS

As presented in Section 8.1.2.2, eight quantitative parameters were accessed for the paper samples under analysis in this work (OD black, OD cyan, OD magenta, OD yellow, Gamut area, gain, feathering and raggedness). To determine which parameters are the most important to describe the samples printability, PCA was used, and a 73% degree of explanation of the results variability (42% 1st component; 31% 2nd component) was obtained (Figure 8.10).

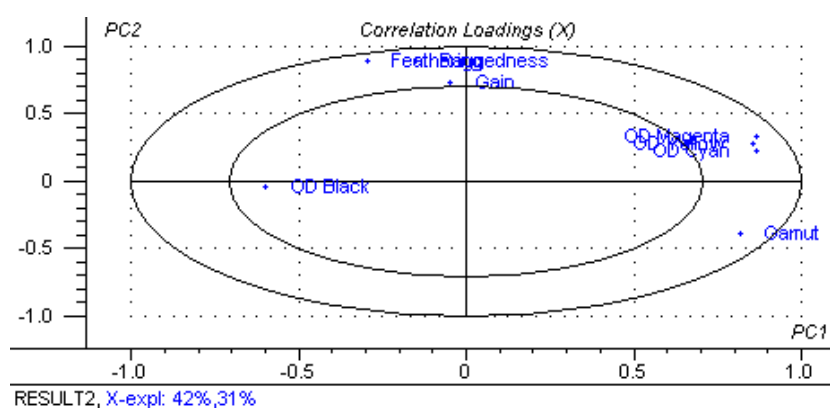


Figure 8.10 – PCA for all the printing quality parameters.

Since the optical densities of the three colors cyan, magenta and yellow are in the same zone of the plot, and yellow is the most critical in terms of achieving a good inkjet printing quality, the OD of cyan and magenta were no further considered. The same overlapping was found for the line quality parameters (feathering, raggedness and gain), after testing several solutions it was decided to consider only the gain. Next, a new PCA was performed using the remaining four variables (OD black, OD yellow, gamut area and gain) and the result is presented in Figure 8.11.

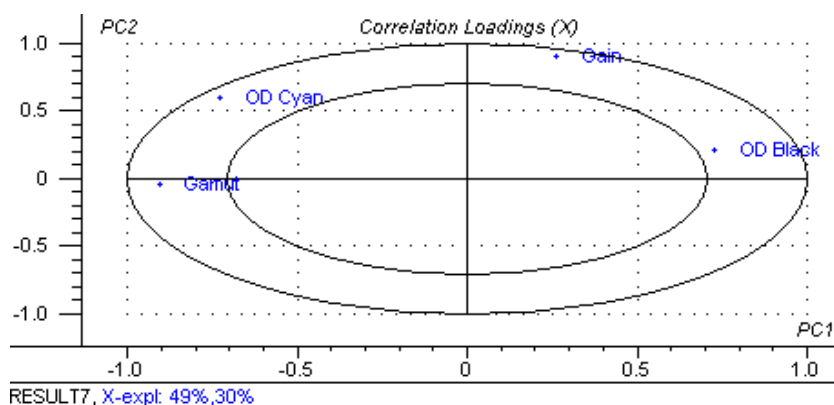


Figure 8.11 – PCA using 4 printing quality parameters.

From Figure 8.11 it is possible to see that the degree of explanation is not largely improved (79% is now reached, 49% corresponding to the 1st component, and 30% to the 2nd component). However the four variables are now quite more disperse, and therefore they will be used for the subsequent analysis. After reducing in 50% the number of variables important to study the printability of the distinct samples, by using PCA, ANOVA was carried out for each of them (Table 8.2).

Table 8.2 – ANOVA of printing quality parameters.

Variable	Contribution for the total variation (%)		Repeatability Factor r	P	F	$F_{critical}$
	Different samples	Inside the samples				
DO Black	67.58	32.42	0.21	4.0E-25	10.84	1.53
DO Yellow	64.90	35.10	0.07	1.7E-22	9.55	1.53
Gamut Area	87.00	13.00	586.04	7.65E-08	7.36	1.81
Gain	84.50	15.50	0.77	2.0E-48	28.18	1.53

The quality of this statistical analysis is ensured by the values of the parameters P, F and $F_{critical}$, and the results reveal that for all variables the larger variation is due to inter-samples differences.

The values achieved for the optical densities are presented in Figure 8.12 for the black color and in Figure 8.13 for the yellow color. The dashed lines limit an interval of 0.2 units of magnitude (in this case relative to the reference sample, St) usually stated and accepted as distinguishable by the human eye in terms of optical density differences (Oittinen and Saarelma, 1998).

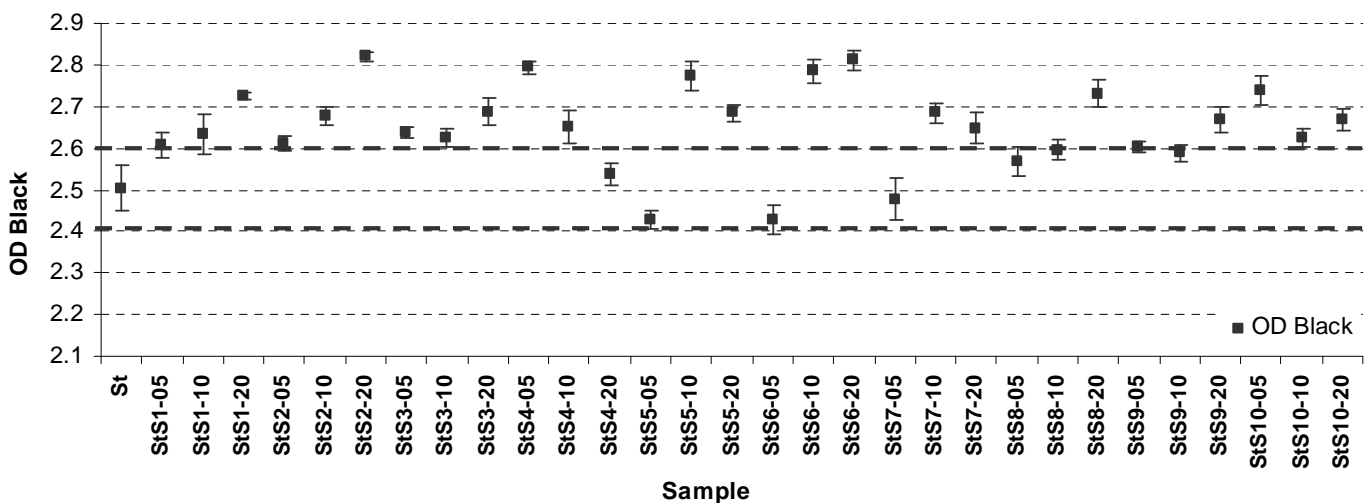


Figure 8.12 – Optical density values achieved for black color. The lines delimit the range in which it is considered that the samples can not be clearly differentiated from the St sample.

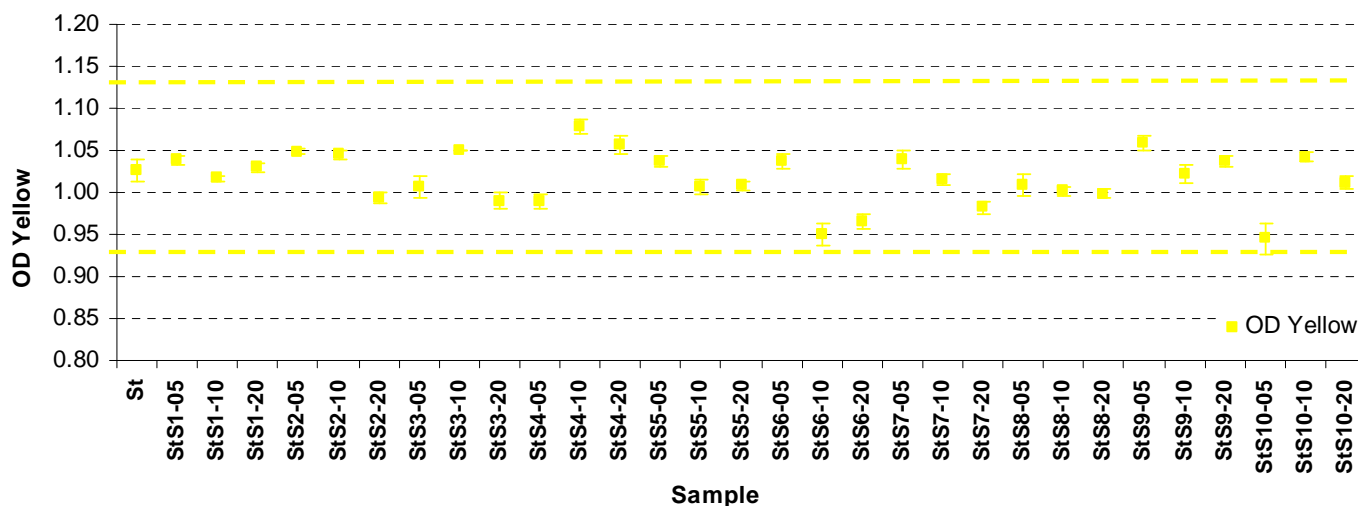


Figure 8.13 - Optical density values achieved for yellow color. The lines delimit the range in which it is considered that the samples can not be clearly differentiated from the St sample.

The black optical density values generally increase with the addition of the synthetic surface sizing agents to the surface sizing formulation (Figure 8.12). As for the yellow optical density a slight increase relative to the reference sample is detected only in some situations (Figure 8.13) and the measurements do not allow to differentiate the samples within the limits considered.

The increase of the OD values is probably influenced by the increase of the surface hydrophobicity of the samples due to the addition of the synthetic surface sizing agent, and it is more visible when using the black ink because it has as surface tension value more close to the one of the water than the one of the yellow ink (Donigian et al. 1999).

It is important to emphasize that, in spite of the small differences, for both black and yellow colors, the optical density values of all samples are acceptable in terms of printing quality (values superior to 2 for black ink and 0.9 for the yellow ink). Nevertheless, and since it is always desirable to reach the highest possible values for this parameters, it is easy to find out that some samples (StS1-05; StS2-05; StS2-10; StS3-10; StS4-10; StS4-20; StS9-05; StS9-20; StS10-10) have a distinguishable positive combined performance, as depicted in Figure 8.14.

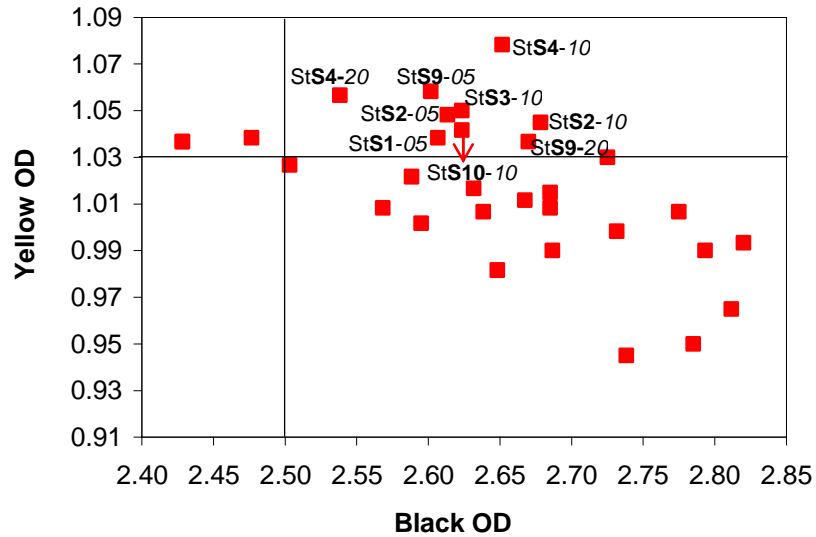


Figure 8.14 – Identification of the samples whose behavior in terms of black and yellow optical densities is improved by the addition of the synthetic surface sizing agents to the sizing formulation.

As mentioned before, while the OD values report the color intensity achieved for specific colors, the gamut area is used to evaluate the paper ability to reproduce a wide range of colors. The results obtained are plotted in Figure 8.15.

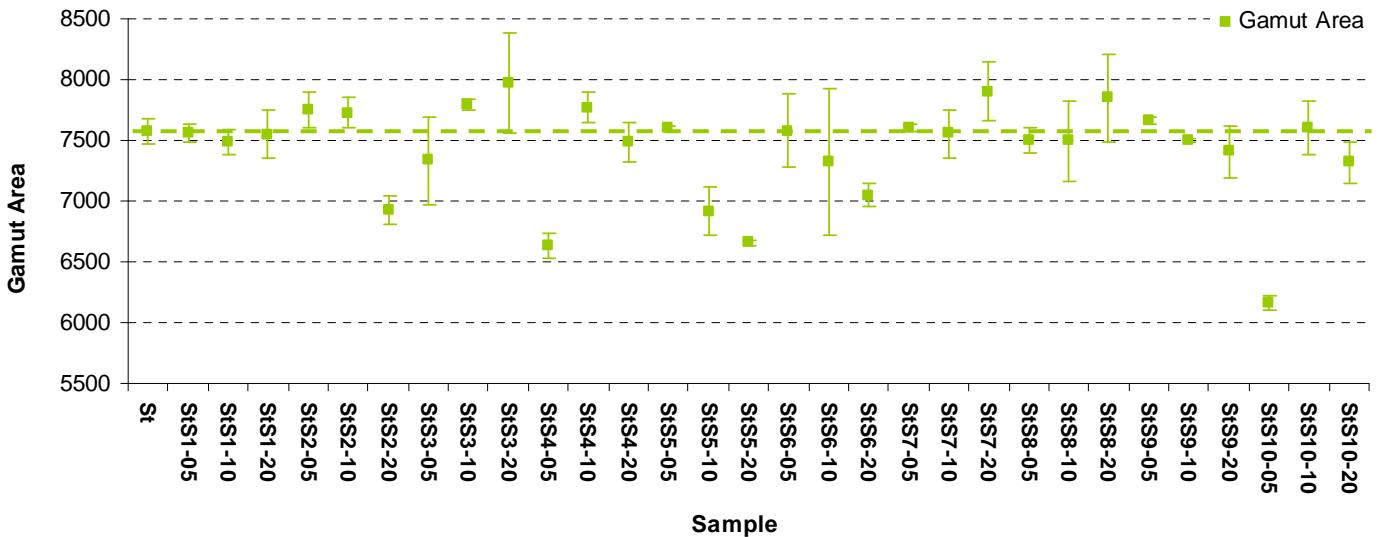


Figure 8.15 – Gamut area values. The dashed line in the figure corresponds to the Gamut area value achieved for sample St.

For most of the samples the gamut area values are satisfactory (values superior to 7000 are usually accepted for this kind of papers and printing process). Using the St sample as reference, also for this variable there is a set of samples with an improved performance

resultant from the addition of the surface sizing agents to the sizing formulation: **StS2-05**; **StS2-10**; **StS3-10**; **StS3-20**; **StS4-10**; **StS7-20**; **StS8-20**; **StS9-05**; **StS10-10**

The results for the gain are presented in Figure 8.16, and it is possible to see that most of the sizing formulations improve the printing performance in terms of image definition.

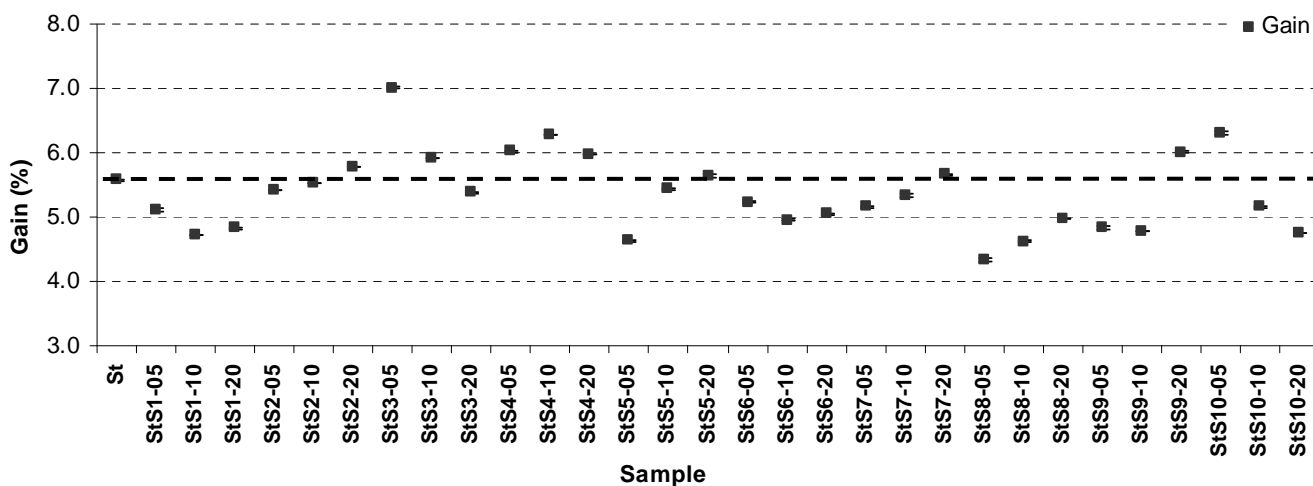


Figure 8.16 – Gain values. The line in the figure refers to the value achieved for the St sample.

As previously mentioned, the printing quality parameters refer to different aspects of the printed image (mainly color saturation or image definition) and thus they must not be analyzed separately. In this context, combining the results obtained for the four parameters (OD black, OD yellow, gamut area and gain), the samples with the best printing performance reported by the quantitative parameters that were analyzed are: **StS2-05**; **StS9-05** and **StS10-10**.

These three samples have styrene in the composition of the sizing agent used in the sizing blend, present values of wetting velocity between 0.09 and 0.2°/sec and polar components of the surface free energy between 6 and 8 mN/m. However, other samples also fitting these characteristics do not exhibit a good printing performance and therefore no definite and unique conclusion can be drawn regarding their combined influence in the printing quality

Besides this quantitative analysis of the inkjet printing performance, and as mentioned before, this work also comprises a subjective evaluation of the printing quality obtained for each sample, from the point of view of the human perception. The results achieved using the methodology presented in Section 8.1.2.2 are plotted in Figure 8.17.

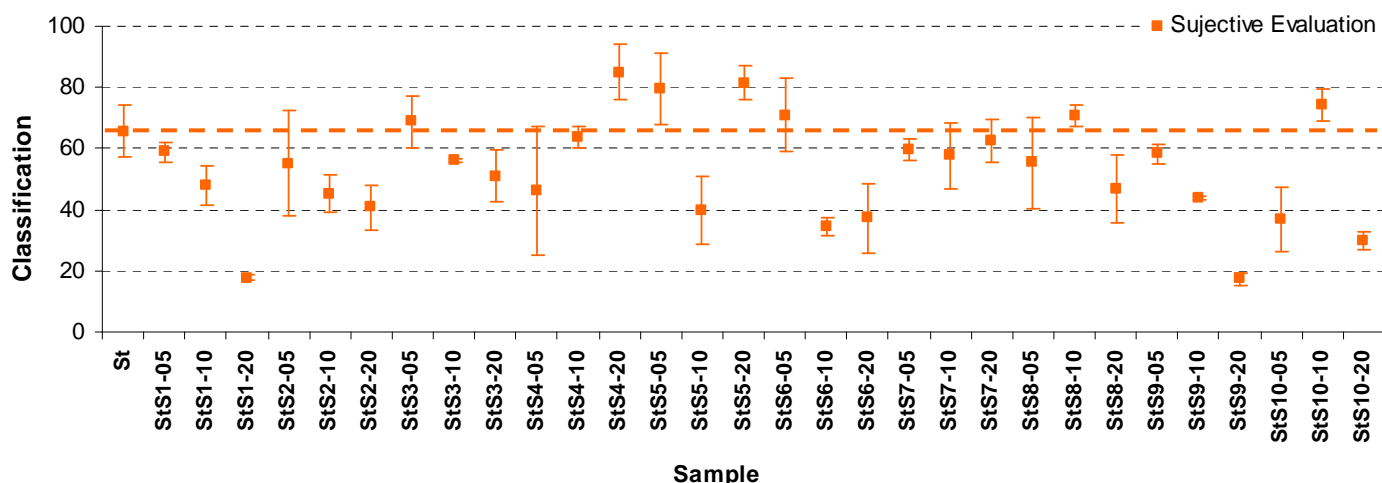


Figure 8.17 – Results achieved from the numerical treatment of the subjective printing quality evaluation (the dashed line indicates the score of sample St).

The deviations presented for the qualitative perception of the printing quality are notoriously higher than those reported along this work, for the quantitative parameters, which is understandable considering the subjective nature of this evaluation. Additionally it is also important to state that the images evaluated are completely different in terms of requirements in color and details (Figure 8.9C).

From Figure 8.17 it is visible that the majority of the samples were classified above 50%, including the reference sample St. This good result for the sample St is not unexpected since, as already mentioned, the reference sample corresponds to the surface sizing treatment usually available in the market for Printing and Writing papers. Most of the samples including synthetic surface sizing agents are identified as having a performance similar or inferior to the one of the reference sample, and among the three samples identified as having the best quantitative printing performance according to the parameters measured only sample StS10-10 is also identified as having good performance in the subjective evaluation.

There is not a clear correlation between the quantitative measurements performed and the subjective evaluation of the inkjet printing quality. In fact, a PLS (Partial Least Squares) model was adjusted and it was verified that the 4 quantitative variables used (OD black, OD yellow, area gamut and gain) can explain the subjective evaluation results in 64% (32 1st components; 32 2nd component), and this explanation is mainly due to the variables

associated to color reproduction and intensity (aprox 60%), less than 4% are explained by the image definition variable (gain).

8.3 CORRELATIONS AND MODELS

From the discussion presented so far and in the previous chapters, it is possible to highlight that the differentiation between samples in terms of printing performance and the detail of the analysis did not reach the same level obtained with the surface characterization techniques, which is a consequence of the differences in the corresponding capacity for the analysis of small and specific differences such as surface properties. Therefore, the use of more precise printing quality evaluation techniques to detect and quantify the differences between the samples is desirable.

Nonetheless the remarks presented, it is possible to state that the addition of synthetic surface sizing agents to the surface sizing formulation improves some printing quality parameters and in some cases an overall improvement of the printing quality in terms of both, quantitative parameters and perceived printing quality was noticed.

In order to relate this printing quality performance with the results of the previous analysis regarding the interactions at the paper surface and the effect of each surface sizing agent into the surface properties of the paper samples, partial least squares (PLS) numerical models were used. Table 8.3 lists the variables used to perform the PLS analysis.

Table 8.3 – Variables considered for PLS models.

Independent Variables (xx)		
	Contact angle with water - CAW	
	Contact angle with water Formamide - CAF	
	Contact angle with Ethileneglycol - CAE	
	Contact angle with Propileneglycol - CAP	
	Contact angle with Diodomethane - CAD	
Surface Characterization	Total surface free energy achieved by contact angle measurements StCA	
	Dispersive component of the surface free energy achieved by contact angle measurements SdCA	
	Polar component of the surface free energy achieved by contact angle measurements SpCA	
	Wetting Velocity WV	
	Dispersive component of the surface free energy achieved by IGC SdIGC	
	Acidic Constant Ka	
	Basic Constant Kb	
	Dependent Variables (yy)	
	Printing Quality	Optical Density for black color ODB
		Optical density for Yellow color ODY
Gamut Area GA		
Gain Gn		
Subjective Evaluation SubEval		

The variables presented in Table 8.3 were also grouped, as an attempt to identify other relevant interactions (Table 8.4).

Table 8.4 – Groups of variables considered for PLS models.

Independent Variables (xx)	
	TotalChar – meaning that all the characterization variables were used
	CAT – referring to all the variables determined by contact angles
	CA – only the values of the contact angles determined for the 5 liquids were used
Dependent Variables (yy)	
	TotalPrint - meaning that all the printing quality variables were used (Quantitative parameters + subjective evaluation)
	Quantitative – refers to all the quantitative printing quality variables measured
	Color – Optical densities and gamut area

Considering the number of variables and the groups that were made, a total of 135 models was considered. Table 8.5 and Table 8.6 summarize the results of those presenting a degree of explanation equal or superior to 10%. For instance, all the characterization variables together explain 14% of the variability of the total printing quality performance, with a coefficient of correlation of 0.02.

Table 8.5 – Results achieved by PLS models using the variables corresponding to the paper surface characterization presented in the previous chapters for the explanation of all the printing quality results, and for the printing quality results divided into two main groups, subjective evaluation and quantitative parameters.

Dependent Variables Set (yy)	Independent Variables Set (xx)	Explanation %*	Correlation Coefficient
TotalPrint	TotalChar	14 (7; 7)	0.02
	CAT	10 (7; 3)	0.09
	CA + WV	12 (3; 9)	0.06
	StCA + SdCA + SpCA+ WV	11 (3; 8)	0.14
	SdIGC+Ka+Kb	10 (8; 2)	0.06
	CAW + Ka + Kb	11 (11; 0)	0.19
SubEval	TotalChar	21 (14; 7)	0.37
	CAT	15 (10; 5)	0.33
	CA + WV	16 (15; 1)	0.38
	StCA + SdCA + SpCA + WV	16 (14; 2)	0.38
Quantitative	TotalChar	16 (8; 8)	0.26
	CAT	12 (8; 4)	0.27
	CA + WV	15 (8; 7)	0.27
	CA	10 (7; 3)	0.26
	StCA + SdCA + SpCA + WV	11 (8; 3)	0.26
	CAW + SpCA + WV	11 (10; 1)	0.32
	CAW + Ka + Kb	11 (9; 2)	0.21
WV + Ka + Kb	12 (7; 5)	0.21	

* Total % (1st component; 2nd component)

Table 8.6 – Results achieved by PLS models using the variables corresponding to the paper surface characterization presented in the previous chapters for the explanation of the quantitative quality results, divided in groups.

Dependent Variables Set (yy)	Independent Variables Set (xx)	Explanation %*	Correlation Coefficient
Color	TotalChar	16 (9; 7)	0.27
	CAT	15 (9; 6)	0.27
	CA + StCA + SdCA + SpCA	10 (8; 2)	0.26
	CA + WV	19 (10; 9)	0.27
	CA	12 (8; 4)	0.26
	StCA + SdCA + SpCA + WV	13 (10; 3)	0.26
	CAW + SpCA + WV	14 (12; 2)	0.32
	WV + Ka + Kb	12 (8; 4)	0.22
Gamut Area	TotalChar	30 (18; 12)	0.42
	CAT	25 (18; 7)	0.42
	CA + StCA + SdCA + SpCA	24 (15; 9)	0.38
	CA + WV	25 (19; 6)	0.43
	CA	23 (15; 8)	0.39
	StCA + SdCA + SpCA + WV	21 (19; 2)	0.44
	StCA + SdCA + SpCA	13 (13; 0)	0.36
	CAW + SpCA + WV	23 (20; 3)	0.44
	CAW + Ka + Kb	12 (12; 0)	0.35
	WV + Ka + Kb	25 (21; 4)	0.43
ODB + ODY	TotalChar	16 (7; 9)	0.30
	CAT	12 (6; 6)	0.29
	CA + WV	16 (6; 10)	0.29
	CA	11 (6; 5)	0.29
ODBlack	TotalChar	13 (8; 5)	0.29
	CAT	11 (8; 3)	0.28
	CA + WV	12 (8; 4)	0.28
	CA	10 (8; 2)	0.28
	StCA + SdCA + SpCA + WV	10 (8; 2)	0.28
	CAW + SpCA + WV	10 (10; 0)	0.31
	CAW + Ka + Kb	10 (10; 0)	0.31
ODYellow	TotalChar	21 (7; 14)	0.27
	CAT	17 (6; 11)	0.23
	CA + WV	21 (6; 15)	0.23
	CA	13 (4; 9)	0.21
	StCA + SdCA + SpCA + WV	10 (6; 4)	0.25
Gain	TotalChar	20 (12; 8)	0.34
	CA + StCA + SdCA + SpCA	10 (5; 5)	0.23
	CA	11 (6; 5)	0.24
	SdIGC + Ka + Kb	16 (16; 0)	0.40
	Ka + Kb	12 (12; 0)	0.25
	SpCA + Ka + Kb	17 (16; 1)	0.40
	CAW + Ka + Kb	18 (18; 0)	0.42
	WV + Ka + Kb	12 (11; 1)	0.34

* Total % (1st component; 2nd component)

From both Table 8.5 and Table 8.6 it is visible that the explanation percentages as well as the correlation coefficients are in general quite small.

The quantitative parameters are more explained by the surface properties determined, and in particular, the gamut area values are quite well explained by the K_a and K_b values achieved by IGC.

The previous analysis shows that the surface characteristics influence the printing quality parameters that were evaluated. However, the techniques and parameters considered in this study do not allow explain and anticipate the impact of the nature, structure or amount of the surface sizing agents on the printing performance.

This means that other paper surface properties and maybe other printing variables than those measured in this study and used in the PLS analysis should also be considered in order to fully understand the paper-ink interactions.

CHAPTER 9

COMPLEMENTARY STUDIES

9 COMPLEMENTARY STUDIES

This chapter reports some relevant studies that were performed using paper samples produced in this work, oriented to specific objectives, and thus subject of isolated papers.

The paper **“Effect of surface sizing on the surface chemistry of paper containing eucalyptus pulp”** aims at verify for this type of papers the suitability of ESCA and ToF-SIMS in obtaining detailed information about the chemical composition of the outermost surface layers of the surface sized papers and at answering the question how those surface layers are affected by the surface sizing formulations.

This specific study allowed to conclude that ESCA complemented with ToF-SIMS is a good way to evaluate the effect of different sizing formulations. The elements present at the samples surfaces were identified and their relative quantity could be evaluated. It was also possible to confirm that the samples surfaces exhibited distinct chemical characteristics. Although both formulations possessed the same percentage of cationic starch, relatively more of this polymer was detected on the sample surfaces, if co-acrylonitrile-acrylate was applied. This result was interpreted in terms of the properties of copolymers particles. It is suggested that the co-acrylonitrile-acrylate particles penetrate deeper to the paper structure than the co-styrene-acrylate particles due to their lower surface tension and therefore leave behind relatively more starch at the paper surface. Additionally, it was found that the increase of the sizing pick-up from 3.5 to 9.0 g m⁻² only slightly changed the surface characteristics. Accordingly, lower amount of size is enough for surface improvement.

The paper **“On the evaluation of the topography of surface sized Eucalyptus based papers”** aims at compare the surface structure of two paper samples with different surface sizing treatments by using Atomic Force Microscopy (AFM). The sizing performance is also evaluated in terms of uniformity, particle size, shape and distribution over the paper surface as well as in terms of surface topography.

This specific study indicated that AFM and SEM can be complementary used to study paper surface sizing. SEM allows a general evaluation of the surface and AFM enables to resolve small details on the paper surface, showing topographic differences not only between the unsized and sized samples but also between samples sized with distinct surface sizing

formulations. In fact, differences both in the copolymer distribution on the paper surface and in the copolymers particle size were clearly visible. Nonetheless, these differences were not reflected in the roughness parameters quantified by AFM. Despite considerable differences between the absolute values of AFM and profilometry, the results of the latter (with much less deviations) confirm that both the unsized and the sized samples exhibited very similar roughness parameter values.

PAPER

EFFECT OF SURFACE SIZING ON THE SURFACE CHEMISTRY OF PAPER CONTAINING EUCALYPTUS PULP

Published in: *Holforschung*; 63; pp: 282-289; 2009

Effect of surface sizing on the surface chemistry of paper containing eucalyptus pulp

Running title: Effect of surface sizing on paper surfaces

Isabel Maria Teixeira Moutinho^{a*},

Anne Marjatta Kleen^b,

Maria Margarida Lopes Figueiredo^a,

Paulo Jorge Tavares Ferreira^a

^a Departamento de Engenharia Química, Universidade de Coimbra

Pólo II – Pinhal de Marrocos, 3030-290 Coimbra, Portugal

^b KCL, Tekniikantie 2, 02150 Espoo, Finland

* Corresponding Author:

Departamento de Engenharia Química, Universidade de Coimbra, Pólo II – Pinhal de Marrocos, 3030-290 Coimbra, Portugal.

Phone: +351.239.798.700.

Fax: +351 239 798 703

E-mail: isamim@gmail.com

KEYWORDS

ESCA, Eucalyptus globulus, Kraft pulp, Surface chemistry, Surface properties, Surface sizing, ToF-SIMS.

Abstract

The effect of different surface sizing formulations on the chemical features of surfaces of the papers produced from Eucalyptus kraft pulp has been studied. The surface analysis techniques electron spectroscopy for chemical analysis (ESCA) and time of flight secondary ion mass spectrometry (ToF-SIMS) has been applied. An uncoated base paper, the reference material, was sized with blends of cationic starch with either co-acrylonitrile-acrylate or co-styrene-acrylate. The results of both techniques are in good agreement and complete each other. It was possible not only to detect the presence of the surface sizing agents on the paper surface but also to distinguish them and evaluate their distribution and

relative concentration. In addition, it was found that application of higher amounts of the sizing formulations, at a constant ratio of 20% copolymer to starch, did not change significantly the chemical properties of the paper surfaces.

Introduction

The papermaking industry has to increase its know-how and to improve the quality of all paper grades (COST E32 2002; Pruszynski 2003) because of the increasing demand of costumers and the competition between information media. For printing and writing papers and other special paper grades, physical and chemical properties of paper surfaces are critical for achieving a good performance of the final products (Lertsutthiwong et al. 2004; Carceller and Juppo 2004; Laleg 2004). The physical structure of the paper surface – its roughness and porosity, for example – plays an outstanding role on the quality of the printed details. The surface is influenced by the structural , and surface characteristics of the fibers, fines, and mineral fillers of the paper matrix, Moreover, the surface chemistry of paper has a great impact on the spreading and absorption rate of coating colors and inks. The surface characteristics of papers depend on the base paper composition and on the surface treatments, such as coating and surface sizing (Rutar and Hladnik 2000; Keskitalo 2000; Oliver et al. 2001; Koskela and Hormi 2003).

Surface sizing influences the porosity, roughness, internal strength of the paper, particles detachment, and the hydrophobic character of surface. The latter is important to prevent excessive absorption of liquids. Starch and synthetic polymers are common sizing chemicals and these also have an influence on the physical and chemical properties of paper bulk (Pruszynski 2003; Koskela and Hormi 2003; Lertsutthiwong et al. 2004; Laleg 2004; Mešic et al. 2004; Moutinho et al. 2007).

The characterization of paper surfaces is of outermost importance for evaluating the effect of sizing and selecting the most appropriate chemicals for a specific base paper (Donigian et al. 1997; Shirazi et al. 2003; Forsström et al. 2003; Hladnik 2003; Lertsutthiwong et al. 2004; Carceller and Juppo 2004; Mešic et al. 204; Ajerschi 2004; Hamers 2005).

From the techniques currently available for chemical characterization of the paper surfaces, the two most capables were selected for this study. These are: 1) electron spectroscopy for chemical analysis (ESCA) and 2) time of flight secondary ion mass spectrometry (ToF-SIMS). Since the fundamentals of these techniques are well described in the literature, only a short description of each one is provided in this text.

ESCA has proved to be a sensitive technique for obtaining information about the chemical composition and structure of a solid surface, within a sampling depth of about 5 nm (Dorris and Gray 1978; Brinen, 1993; Kleen et al. 2003; Kangas and Kleen 2004; Hale et al. 2007). It is based on the energy changes of the emitted electrons to generate a spectrum of peaks corresponding to the elements present on the surface (except hydrogen and helium). The peak areas give measures of the relative amounts of each element (absolute quantitative measurements are seldom feasible), whereas the shape and position of

the peaks reflect the chemical environment of each element, namely their bonding structure (Dorris and Gray 1978; Brinen, 1993; Ström et al. 1993; Kleen et al. 2003; Kangas and Kleen 2004; Hale et al. 2007).

ToF-SIMS analysis provides additional information regarding the identification of not only elements but also molecular species present on the surface. The distribution of molecules at the surface can be deduced from the data, also as a function of depth at a submicron scale. This technique is suited for comparison of samples as it delivers semi-quantitative information of the surface constituents (Kleen 2000a; Kleen 2000b; Kristola 2001; Kangas and Kleen 2004; Kleen 2005; Lee et al. 2006; Parolis et al. 2007). ToF-SIMS is based on ionized particles which are emitted from a solid surface when energetic primary particles bombard that surface. The secondary ions are accelerated into a mass spectrometer, where they are analyzed by measuring their time-of-flight between the sample and the detector. Major compounds in mixtures can be separated. The mass range and resolution of the technique are high. The analyzed area in ToF-SIMS is smaller than that of ESCA, and the surface sensitivity is higher, because ToF-SIMS analyzes the outermost surface layers of 1-2 nm.

There is large body of literature concerning paper analysis by ESCA (Dorris and Gray 1978; Kleen et al. 2002; Shchukarev et al. 2003; Johansson et al. 2005; Freire et al. 2006) or by ToF-SIMS (Brinen and Proverb 1991; Kleen 2000a; Kleen 2000b; Kleen 2005; Fardim and Hombom 2005a; Fardim and Hombom 2005b), or both ESCA and ToF-SIMS (Brinen 1993; Kleen et al. 2003; Kangas and Kleen 2004).

The present work aims at obtaining detailed information about the chemical composition of the outermost surface layers of the surface sized papers and at answering the question how those surface layers are affected by the surface sizing formulations.

Experimental

Paper samples

A calendered uncoated base paper (80 g m⁻²) produced from bleached *Eucalyptus globulus* kraft pulp (ISO Brightness ≈ 90) and without any surface treatment was the reference (denoted as RP). This paper was surface sized with blends of cationic starch with either co-acrylonitrile-acrylate (samples A1 and A2) or co-styrene-acrylate (samples B1 and B2), as described in Table 1.

Table 1 Sample description.

Sample	Surface sizing formulation (% w w ⁻¹)	Sizing Amount (pick-up) (g m ⁻²)	pH of the Sizing Formulation
RP (Reference)	No surface treatment	0.0	xxx
A1	80% of cationic starch	3.5	5.07
A2	20% of co-acrylonitrile-acrylate	9.0	
B1	80% of cationic starch	3.5	6.23
B2	20% of co-styrene-acrylate	9.0	

The copolymers are schematically presented in Figure 1. Elemental analysis (Table 2): EA 1180 CHNS-O from Fisons Instruments (Table 2). Software: ChemSketch software. The cationic starch suspension is a commercial product and supplied by the industry. Particles size measurement: COULTER N4 Plus Submicron Particle Sizer. Surface tension: OCA20 equipment from Dataphysics. Table 2 summarizes the most relevant information regarding the compounds properties with this regard.

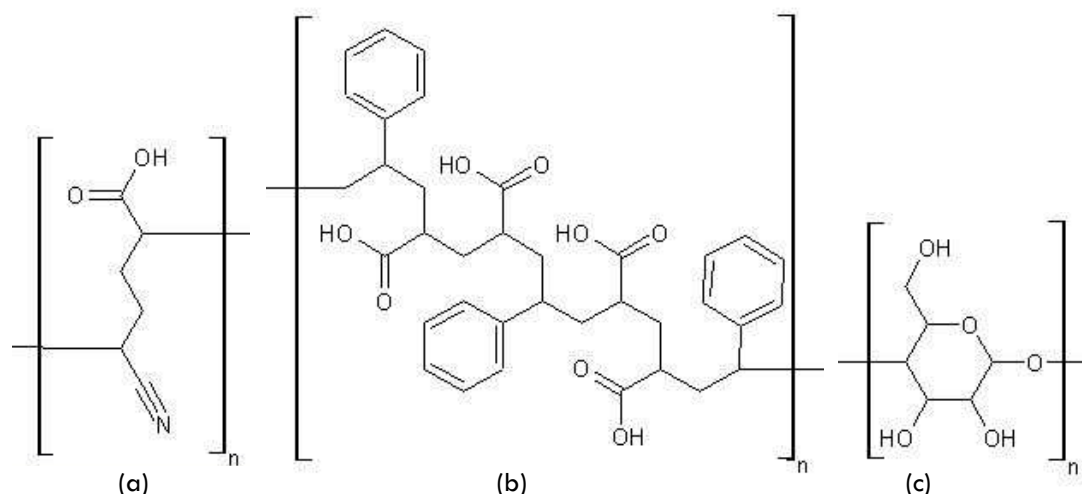


Figure 1 Schematic representation of the molecules used in the surface sizing formulations, computed using the software ChemSketch: (a) co-acrylonitrile-acrylate; (b) co-styrene-acrylate; (c) cationic starch.

Table 2 Properties of the compound in surface sizing formulations.

Compound	Monomers Proportion*	Solids Content (%)	pH	Particles Mean \varnothing (nm)**	Surface Tension (mN m ⁻¹)	Amount (% w w ⁻¹)			
						H	N	C	O
Cationic starch	---	12.8	6.7	299	32.9	6.1	1.2	40.9	42.7
Co-acrylonitrile-	1:1	35.2	3.4	254	47.6	7.6	11.6	61.4	19.5
Co-styrene-acrylate	3:4	13.3	4.3	84	82.2	7.3	0.0	71.9	20.8

* Based on elemental analysis (using the equipment EA 1180 CHNS-O from Fisons Instruments)

** Determined using the COULTER N4 Plus Submicron Particle Sizer

*** Measured with the OCA20 equipment form Dataphysics

The surface sizing formulations were applied by a Mathis laboratory coating device (SVA-IR-B), which operates automatically with different velocities of the applicator roll. A 0.15 mm diameter roll was used at a velocity of 6 m min⁻¹. The total surface sizing pick-up was controlled by the weight applied on top of the applicator roll: in case of no weight, a 3.5 ± 0.3 g m⁻² pick-up was obtained (samples A1 and B1), whereas by placing two weights of 730 g each on the applicator roll a 9.0 ± 0.3 g m⁻² pick-up was obtained (samples A2 and B2). The drying process was performed by an IR drier coupled to the applicator roll (1.0 kW drying intensity), followed by air drying (for at least 10 min). The surface sized samples were no further calendered.

Surface analyses

The ESCA analyses: AXIS 165 high-resolution electron spectrometer; monochromatic Al K α irradiation (12.5 kV, 8 mA). For each sample, survey scans in the range 0-1100 eV (1 eV step, 80 eV analyzer pass energy) and high-resolution spectra of the C 1s region (0.1 eV step, 20 eV pass energy) were recorded at three different locations. The areas of the peaks corresponding to carbon (200-300 eV), calcium (350 eV), nitrogen (400 eV), oxygen (500-600 eV), and sodium (1000-1100 eV) were measured. The analyzed area was approximately 1 mm² and the depth of analysis was 2-10 nm. The sample surfaces were neutralized during the measurements with low-energy electrons.

ToF-SIMS measurements: PHI TRIFT II time-of-flight secondary ion mass spectrometer. High mass resolution spectra and images in positive and negative ion modes were acquired by a ⁶⁹Ga⁺ liquid metal ion gun with 15 keV primary ions in bunched mode for mass spectra and with 25 keV primary ions in unbunched mode for images over the mass range 2-2000 m z⁻¹. The primary ion current was 600 pA and time per channel 0.138 ns. The analysis area was 200 × 200 μm² and the acquisition time 2 min for spectra and 5 min for images. Analytical charge compensation was used for insulating samples. The calculated ion dose was 2.7·10¹¹ cm⁻², which ensured static conditions during data acquisition. Three replicate runs were made for each sample. Selected peak areas were integrated from ToF-SIMS spectra and normalized to the total ion intensity of the spectrum. Images were reconstructed from raw data files with the off-line WinCadence software.

Results and discussion

Electron spectroscopy for chemical analysis (ESCA)

The elements present at the paper surface can be identified from the survey scans obtained by ESCA. Figure 2 includes the results of the reference paper (RP) and of samples A1 and B1. The spectra of samples A2 and B2 corresponding to the largest amount of sizing agents are not shown here because they revealed only minor differences in the intensity of the peaks compared with samples A1 and B1, respectively.

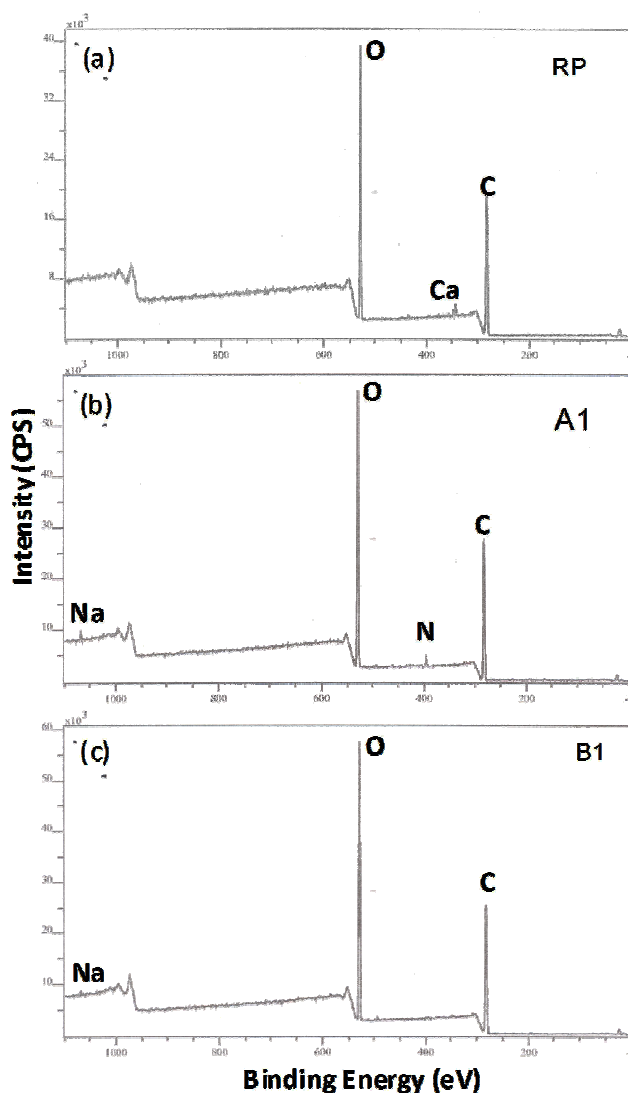


Figure 2 Spectra of the ESCA survey scans: (a) sample RP; (b) sample A1; (c) sample B1.

The peaks corresponding to carbon, oxygen, and sodium can be easily detected in all the samples, whereas calcium is only visible in the reference paper and nitrogen in sample A1 (and A2). As readily visible, the most abundant elements are carbon and oxygen (hydrogen is not detectable by ESCA). For quantification, the amount of each element, relative to all specimens detected in the surface of each sample, was determined by measuring the peak area. The results, based on the analyses of three locations in each paper sample, are summarized in Figure 3 together with the reproducibility of the results. The reproducibility is satisfactory.

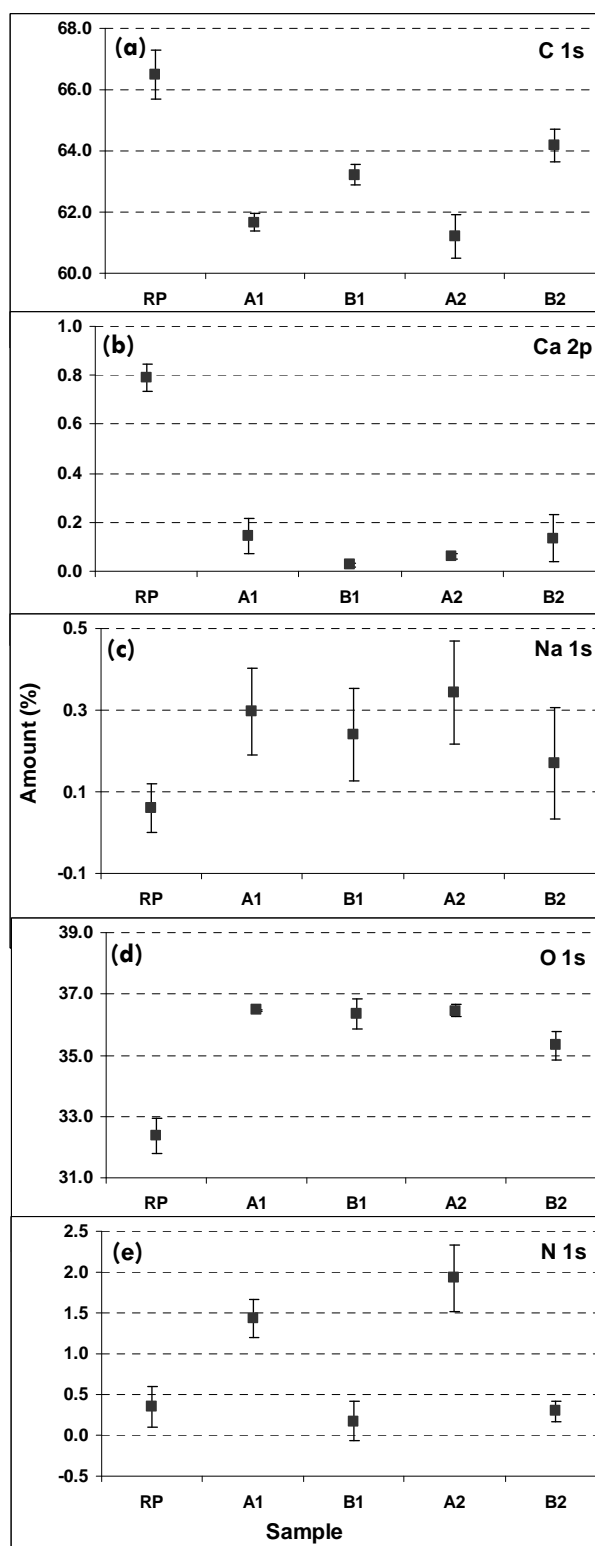


Figure 3 Relative amount of each element, obtained by ESCA for each sample: (a) carbon; (b) calcium; (c) oxygen; (d) sodium; (e) nitrogen.

The amounts of carbon and calcium present at the surface of the reference paper (RP) are higher than those at the surface of the surface sized papers (Figure 3). The opposite is true for oxygen and sodium. The much larger amount of calcium detected in the reference paper is associated with the precipitated

calcium carbonate applied as filler, which is almost completely covered the surface after sizing. The same covering effect may be responsible for the slight decrease of the carbon percentage in the sized samples, while the proportion of oxygen is increased. The presence of NaCl in the cationic starch suspension (supplied by the industry) causes the increase of sodium at the surface of the sized papers, in comparison with the reference paper.

Although the co-styrene-acrylate polymer (B) contained about 1.5% more oxygen than the co-acrylonitrile-acrylate polymer (A), similar amounts of oxygen were found on the surface of A and B sized papers (Figure 3c). This indicates that relatively more of the oxygen-rich starch and less copolymer were found on the A sized papers. Besides, though having a low surface tension, starch has large particles (Table 2) which leads to high surface concentrations. We suggest that copolymer A can easier penetrate into paper than copolymer B, which can be explained by its lower surface tension (Table 2). Finally, and as expected, the quantity of nitrogen increased significantly in samples A1 and A2 due to the presence of acrylonitrile copolymer.

It is obvious that no relevant benefits arise from increasing the surface sizing pick-up from 3.5 to 9.0 g m⁻² since, in general, the differences between the reference paper and samples A1 and A2 are identical. The same is true for samples B1 and B2. Therefore, from a chemical point of view, a pick-up level of 3.5 g m⁻² seems to be enough to promote the key changes intended by surface sizing.

The relative contents of the different “types” of carbon, considering their chemical environment and bonding structure, were determined from their high resolution spectra of carbon (Figure 4).

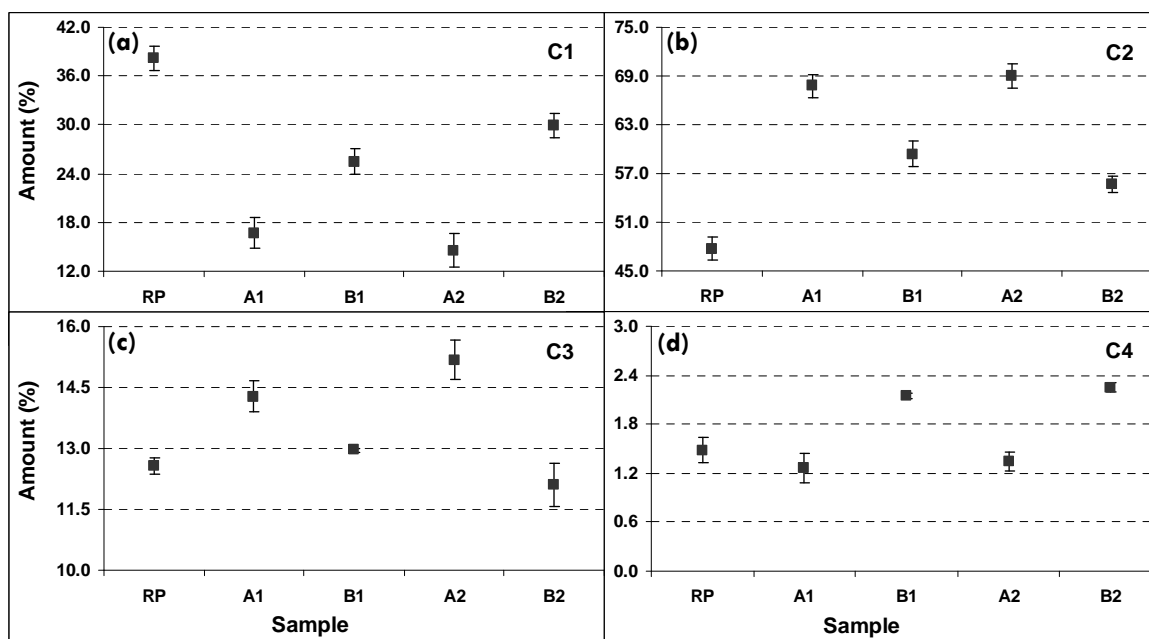


Figure 4 Quantification of the different types of chemical bonds detected by ESCA for the carbon atoms: (a) C1 (C–C, C=C, C–H); (b) C2 (C–O); (c) C3 (C=O, O–C–O); (d) C4 (O–C=O).

These results with a very good reproducibility are in agreement with the molecular structure of the sizing agents depicted in Figure 1. In fact, the relative amount of C1 is considerably higher for RP, especially in comparison with papers A1 and A2, probably mainly because of lower percentage of C=C bonds in the sized papers. Acrylonitrile-acrylate copolymer (A), e.g., do not contain any C=C bonds (Figure 1a). It is also clear that, in terms of the type of different carbon bonds, there is a greater resemblance between samples B1 and B2 and the RP (Figure 4a-c) than between the latter and samples A1 and A2. The exception occurs for the O–C=O bonds (C4, Figure 4d), which are predominant in the styrene-acrylate copolymer (B1 and B2). This result is also supported by the results from elemental analysis demonstrating that the copolymer B contains more oxygen than the copolymer A.

Time of flight secondary ion mass spectrometry (ToF-SIMS)

Both positive and negative ion ToF-SIMS spectra were recorded. In order to identify the most significant peaks corresponding to the sizing agents, subtraction of the reference paper spectrum was performed (Figure 5). The upper parts of each difference spectra show the peaks which are typical for the sized papers, while the peaks in the lower side represent the reference paper. Figure 5a (m/z^{-1} 0 – 70, positive ion difference spectra), Figure 5b (m/z^{-1} 70 – 110, positive ion difference spectra) and Figure 5c (m/z^{-1} 0 – 70, negative ion difference spectra) show the results for paper A1, while the corresponding difference spectra for paper B1 are presented in Figs. 5d-f. The most relevant peaks are listed in Table 3. The difference spectra revealed more typical peaks than presented in Table 3 for both the starch and the acrylates, but the selected peaks are the most intense ones for the compounds and therefore they were evaluated. Sodium, calcium, cationic starch, and acrylate were evaluated from the positive mass spectra, whereas acrylonitrile was analyzed from the negative mass spectra.

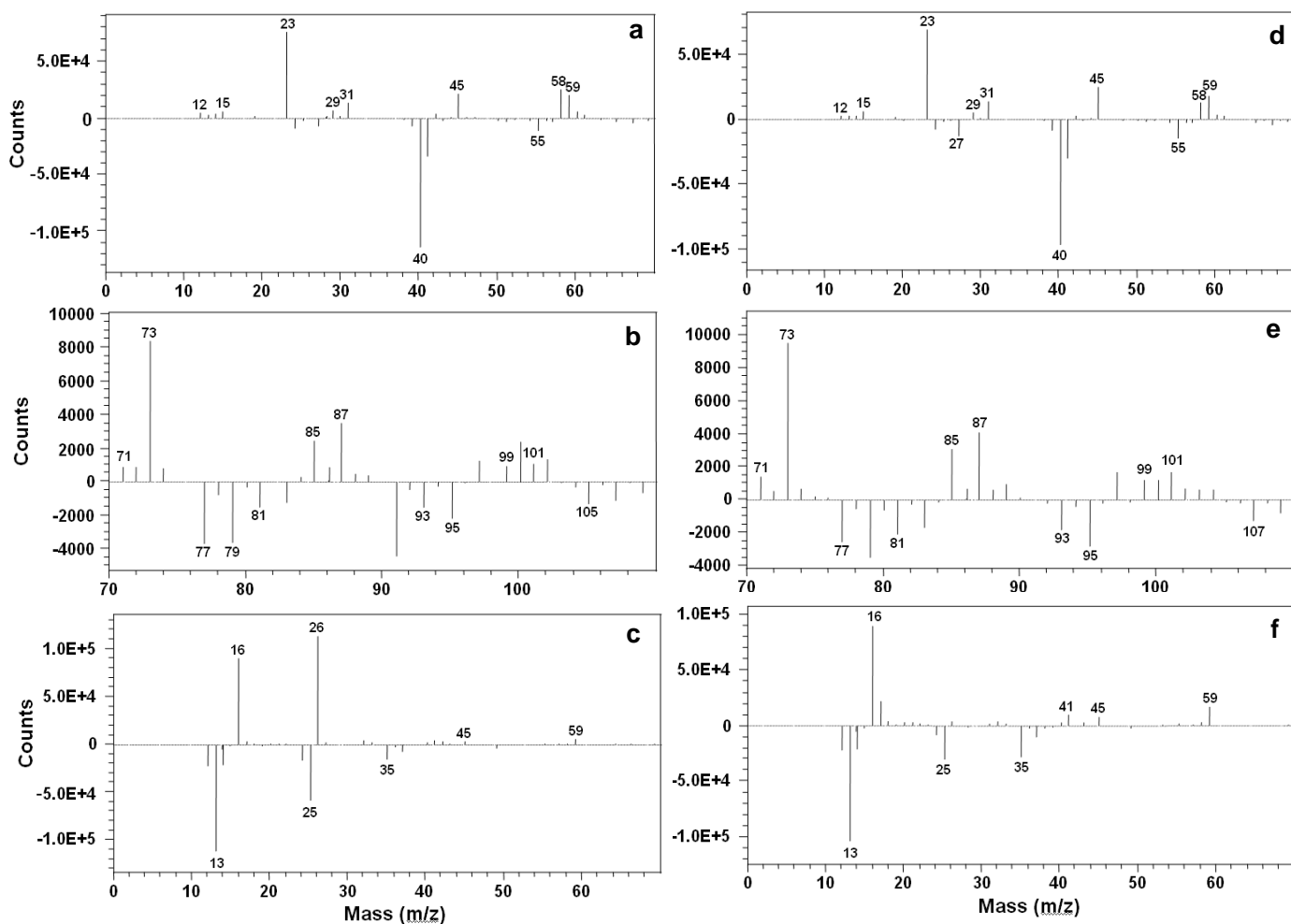


Figure 5 ToF-SIMS difference spectra between the sized paper A1 and the reference paper (a-c) as well as that between the sized paper B1 and the reference paper (d-f).

The difference spectra in Figure 5 confirm that the surfaces of the samples exhibit distinct chemical characteristics. The surface characteristics of the sized papers clearly differ from those of the reference paper. Also, the differently sized papers clearly differ from each other having typical characteristics of their own in addition to their similarities, which originated from cationic starch and acrylate, both present in sized papers. According to Figure 5, the reference paper contains more calcium (peak at m/z^{-1} 40) than the sized papers, whereas the sized papers have more sodium (peak at m/z^{-1} 23), cationic starch (peaks at m/z^{-1} 58 and 59) (Matsushita et al. 2007), and acrylate (peaks at m/z^{-1} 71, 73, 85, 87, 99 and 101) on their surfaces. Since the difference spectra for samples A2 and B2 were quite similar to the ones given for A1 and B1, respectively, they are not presented here. It should be mentioned that, according to some authors, the penetration of the cationic starch may be larger than the depth of analysis achieved by this technique (Lipponen, 2004; Lipponen, 2005).

The difference spectra between the negative ion ToF-SIMS spectra from the sized papers and the RP (Figure 5c,f) indicates the presence of acrylonitrile (peak m/z^{-1} 26) on the surface of A1, but not on the

surface of B1 paper. Corresponding results were also observed for A2 and B2 samples. In addition, the results in Figure 5c,f support the ESCA results (Figure 3c) showing that there is more oxygen (peak $m z^{-1}$ 16) on the surfaces of the sized papers than on the surface of the RP.

As an attempt to determine the relative quantity of each chemical specimen for each paper sample, the areas of the peaks in Table 3 were integrated from the original positive and negative ion ToF-SIMS spectra. The results, after combining the peaks according to their origin, are plotted in Figure 6. Accordingly, the reproducibility of the results is very good.

Table 3 Identification of the most important ion peaks and corresponding compounds detected by the ToF-SIMS analysis on the surface sized samples.

Masses ($m z^{-1}$)	Charge	Possible origin
22.99	+	Na – Salt in both sizing blends
39.96	+	Ca – Base paper
58.07	+	C ₃ H ₈ N – Cationic starch
59.07	+	C ₃ H ₉ N –Cationic starch
71.01	+	C ₃ H ₃ O ₂ – Acrylate (1 double bound)
73.03	+	C ₃ H ₅ O ₂ – Acrylate
85.03	+	C ₄ H ₅ O ₂ – Acrylate (1 double bound)
87.04	+	C ₄ H ₇ O ₂ – Acrylate
99.04	+	C ₅ H ₇ O ₂ – Acrylate (1 double bound)
101.06	+	C ₅ H ₉ O ₂ – Acrylate
26.00	–	CN - Acrylonitrile

Like in ESCA results (Figure 3), the RP exhibits a considerable amount of calcium, while only traces of it were found on all the surface sized samples (Figure 6a). On the other hand, the amount of sodium is much higher in the sized papers (Figure 6b. These results also confirm that NaCl in the starch suspension is detectable at the surface. Only a slight increase in the surface concentration of sodium was observed when the amount of size was almost threefold.

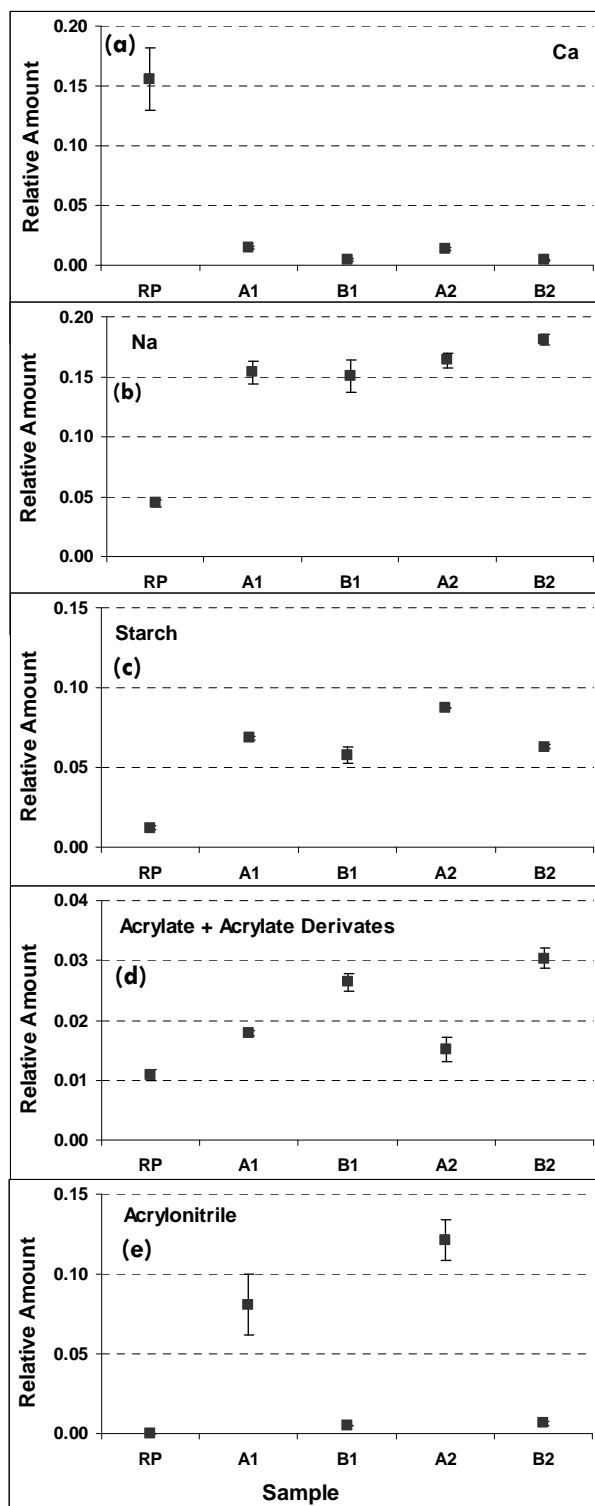


Figure 6 Relative amount of important surface specimens, obtained by ToF-SIMS (a) calcium; (b) sodium; (c) cationic starch; (d) acrylate; (e) acrylonitrile.

As expected, surface sized samples possess more starch at the surface than the reference paper (Figure 6c). Somewhat larger relative amounts of starch are detected on the surfaces of samples A1 and A2 in comparison to B1 and B2. This is in agreement with the results from ESCA. Probably, the co-acrylonitrile-acrylate particles have penetrated more easily the bulk of paper than the co-styrene-acrylate ones. As discussed before, this is probably due to the surface tension values. Some increase in the surface concentration of starch was observed when the amount of size was almost threefold.

The results further confirm the presence of acrylate in all the sizing formulations (Figure 6d). The amount of acrylate on the surfaces of B samples is higher than in the A samples, probably due to its higher concentration in B formulations. Large amount of acrylonitrile was found on the sized A papers, as expected. Paper A2 had clearly higher surface concentration of acrylonitrile than paper A1. Neither the RP nor the sized B papers contain acrylonitrile.

In general, the increase of the surface sizing pick-up from 3.5 to 9.0 g m⁻² in both cases had relatively low impact on the paper surface composition. The surface concentration of sodium and starch increased slightly, while that of acrylonitrile increased somewhat more. These effects were not seen with ESCA. ToF-SIMS is more sensitive with this regard as ESCA.

ToF-SIMS also provides additional information about the spatial distribution of surface compounds. Figure 7 presents the sodium images of the five samples analyzed in this study. Sodium images were chosen since it was already proved that the sodium is from the sizing blends.

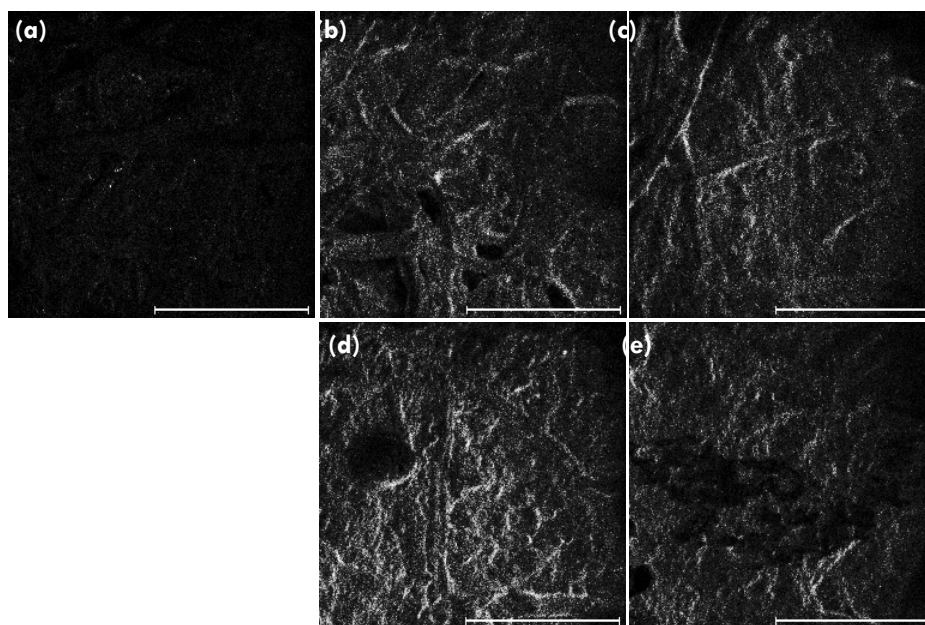


Figure 7 Calcium images of the various samples: a) RP; b) A1; c) B1; d) A2; e) B2.

The larger area of white spots in Figures 7b to 7e confirms the presence of the surface sizing in samples A1, A2, B1 and B2. More sizing was found on A2 and B2 than on A1 and B1, respectively. Although distributed throughout the paper surfaces, the sizing formulation does not form a continuous film.

Conclusions

ESCA complemented with ToF-SIMS proved to be a good way to evaluate the effect of different sizing formulations. The elements present at the samples surfaces were identified and their relative quantity could be evaluated. It was also possible to confirm that the samples surfaces exhibited distinct chemical characteristics. Although both formulations possessed the same percentage of cationic starch, relatively more of this polymer was detected on the sample surfaces, if co-acrylonitrile-acrylate was applied. This result was interpreted in terms of the properties of copolymers particles. It is suggested that the co-acrylonitrile-acrylate particles penetrate deeper to the paper structure than the co-styrene-acrylate particles due to their lower surface tension and therefore leave behind relatively more starch at the paper surface. Additionally, it was found that the increase of the sizing pick-up from 3.5 to 9.0 g m⁻² only slightly changed the surface characteristics. Accordingly, lower amount of size is enough for surface improvement.

Acknowledgements

The authors acknowledge the EU COST E32 Action "Characterization of Paper Surfaces for Improved Printing paper Grades" for the financial support to a STSM at the KCL Pulp and Paper institute, Espoo - Finland and at the Åbo Akademi University, Turku - Finland.

References

- Ajerschi, M., Poirier, N., Pikulik, I. (2004) Colagem superficial sem prensa de colagem – Resultados de máquina de papel piloto. *O Papel/Paprican* pp. 47-58.
- Carceller, R., Juppo, A. (2004) New surface size composition changes paper surface properties for improving ink jet printability of copy paper. *Pap. Puu-Pap. Tim.* 86(3): 161-163.
- COST E32 (2002) Memorandum of Understanding: Characterisation of paper surfaces for improved printing paper grades. European Concerted Research Action COST Action E32, Brussels.
- Brinen, J. S., Proverb, R. J. (1991) SIMS imaging of paper surfaces Part 2. Distribution of organic surfactants. *Nord. Pulp. Pap. Res. J* 6 (4):177-183.
- Brinen, J. S. (1993) The observation and distribution of organic additives on paper surfaces using surface spectroscopic techniques. *Nord. Pulp. Pap. Res. J* 8(1):123-129.
- Donigian, D. W., Ishley, J. N., Wise, K. J. (1997) Coating pore structure and offset printed gloss. *TAPPI J* 80(5):163-172.

- Dorris, G. M., Gray, D. (1978) The surface analysis of paper and wood fibres by ESCA (electron spectroscopy for chemical analysis) Application to cellulose and lignin. *Cell Chem. Technol.* 12:9-23.
- Fardim, P., Hombom, B. (2005a) Origin and surface distribution of anionic groups in different papermaking fibers. *Colloid Surface A* 252: 237-242.
- Fardim, P., Holmbom B. (2005b) ToF-SIMS imaging: a valuable chemical microscopy technique for paper and paper coatings. *Appl. Surf. Sci.* 249:393-407.
- Forsström, U., Fagerholm, K., Saharenen (2003) The role of base paper porosity in MSP coating. *Pap. Puu-Pap. Tim.* 85(8):454-459.
- Freire, C. S. R., Silvestre, A. J. D., Neto, C. P., Gandini, A., Fardim, P., Holmbom, B. (2006) Surface characterization by XPS, contact angle measurements and ToF-SIMS of cellulose fibers partially esterified with fatty acids. *J Colloid Interf. Sci.* 301:205-209.
- Hale, P. S., Kappen, P., Prissanaroon, W., Brack, N., Pigram, P. J., Liesegang, J. (2007) Minimizing silicone transfer during micro-contact printing. *Appl. Surf. Sci.* 253:3746-3750.
- Hamers, C., others (2005) Curtain coating for graphic. *Pulp & Paper Intern.* 47:36-37.
- Hladnik, A. (2003) Ink-jet printing and image analysis. Presentation at Universidade da Beira Interior, Covilhã, Portugal.
- Johansson, L. S., Campbell, J. M., Fardim, P., Hultén, A. H., Boisvert, J. P., Ernstsson, M. (2005) An XPS round robin investigation on analysis of wood pulp fibers and filter paper. *Surf. Sci.* 584:126-132
- Kangas, H., Kleen, M. (2004) Surface chemical and morphological properties of mechanical pulp fines. *Nord. Pulp. Pap. Res. J* 19(2):191-199.
- Keskitalo, I. The penetration of water-based inks into laboratory sheets made from bleached eucalypt kraft pulp. Master's Thesis, Luleå Tekniska Universitet, Sweden, 2000.
- Kleen, M. (2000a) Surface chemistry of kraft pulp fibers during TCF bleaching studied by ToF-SIMS. 6th European Workshop on Lignocellulosics and Pulp (EWLP), September 3–6, 2000, Bordeaux, France, pp. 41–44.
- Kleen, M. (2000b) ToF-SIMS as a new analytical tool for studies of pulp fiber surface chemistry. International Symposium on cellulose and lignocellulosics chemistry 2000 (ISCLC), Dec. 16-18, 2000, Kunming, China, pp. 290-294.
- Kleen, M., Sjöberg, J., Dahlman, O., Johansson, L.-S., Koljonen, K., Stenius, P. (20002) The effect of ECF and TCF bleaching on the chemical composition of soda-anthraquinone and kraft pulp surfaces. *Nord. Pulp. Pap. Res. J* 17(3):357-363.
- Kleen, M., Kangas, H., Laine, C. (2003) Chemical characterization of mechanical pulp fines and fiber surface layers. *Nord. Pulp. Pap. Res. J* 18(4):61-368.

- Kleen, M. (2005) Surface lignin and extractives on hardwood RDH kraft pulp chemically characterized by ToF-SIMS. *Holzforschung* 59(5):481-487.
- Koskela, J P., Hormi, O. E. O. (2003) Improving the printability of paper with long-chain quaternaries. *APITTA J* 56(4):296-300.
- Kristola, J. Spatial distribution of wood extractives and lignin on the surface of mechanical pulp, fibers and fines. Master of science thesis, Laboratory of Forest Products Chemistry, Faculty of chemical Engineering, Åbo Akademi University, Finland, 2001.
- Laleg, M. (2004) Colagem superficial com quitosana e com misturas de quitosana e amidos. *O Papel/Paprican* 33-45.
- Lee, T. G., Kim, J., Shon, H. K., Jung, D., Moon, D. W. (2006) Chemical derivatization technique in ToF-SIMS for quantification analysis of surface amine groups. *Appl. Surf. Sci.* 252:6632-6635.
- Lertsutthiwong, P., Nazhad, M. M., Chandkrachang, S., Stevens, W. F. (2004) Chitosan as a surface sizing agent for offset printing paper. *APITTA J* 57(4): 274-280.
- Lipponen, J., Lappalainen, T., Astola, J., Grön, J. (2004) Novel method for quantitative starch penetration analysis through iodine staining and image analysis of cross-sections of uncoated fine paper. *Nord. Pulp. Pap. Res. J* 19(3): 300-308.
- Lipponen, J. Surface sizing with starch solutions at high solids contents. Doctor's Thesis, Laboratory of Paper Technology, Helsinki University of Technology, Espoo, Finland, 2005.
- Matsushita, Y., Sekiguchi, T., Saito, K., Kato, T., Imai, T., Fukushima, K. (2007) The characteristic fragment ions and visualization of cationic starches on pulp fiber using ToF-SIMS. *Surf. Interface Anal.* 39 (2007):501-505.
- Mešic, B., Järnström, L., Hjärthag, C., Lestelius, M. (2004) Effects of application temperature in paper surface sizing with temperature-responsive starch on water repellency and flexographic printability. *APITTA J* 57(4):281-285 & 298.
- Moutinho, I. M. T., Ferreira, P. J. T., Figueiredo, M. M. L. (2007) Impact of surface sizing on inkjet printing quality. *Ind. Eng. Chem. Res.* 46:6183-6188.
- Oliver, J., Chen, J., Tosto, F. (2001) Impact of paper surface structure on print quality. COST European E11 Meeting, 4-5 October, 2001, Espoo, Finland, pp.1-9.
- Parolis, L. A. S., van der Merwe, R., van Leerdam, G. C., Prins, F. E., Smeink, R. G. (2007) The use of ToF-SIMS and microflotation to assess the reversibility of binding of CMC onto talc. *Minerals Eng.* 20:970-978.
- Pruszynski, P. (2003) Recent developments in papermaking chemicals. WWP Keynote lectures pp. 82-90.
- Rutar, V., Hladnik, A. (2000) Penetration tests and influence of paper sheet structure on its sorption ability. Presented at the COST Action E11 Workshop, Grenoble, France.

Shchukarev, A. V., Mattsson, R., Ödberg, L. (2003) XPS imaging of surface diffusion of alkylketene dimmer on paper surfaces. *Colloid Surface A* 219:35-43.

Shirazi, M., Esmail, N., Garnier, G., van de Ven, T. G. M. (2003) Starch penetration into paper in a size press. *Proc. 5th International Paper and Coating Symposium, Montreal, Canada.*

Ström, G., Carlsson, G., Schulz, A. (1993) Chemical composition of coated paper surfaces determined by means of ESCA. *Nord. Pulp. Pap. Res. J* 1:105-112.

PAPER

ON THE EVALUATION OF THE TOPOGRAPHY OF SURFACE SIZED EUCALYPTUS BASED PAPERS

Submitted to: Industrial & Engineering Chemistry Research (I&ECR); 2009.

(Under adjustment after Reviewers comments, for publication)

On the evaluation of the topography of surface sized Eucalyptus based papers

Isabel Moutinho^{a}, Petri Ihalainen^b, Margarida Figueiredo^a, Jouko Peltonen^b, Paulo Ferreira^a*

^a Chemical Engineering Department, Coimbra University, Pólo II – Pinhal de Marrocos, 3030-290
Coimbra, Portugal

^b Department of Physical Chemistry, Åbo Akademi University, Domkyrkotorget 3, FI-20500 Åbo, Finland

* To whom correspondence should be addressed. Phone +351.239.798.700. Fax +351.239.798.703.

E-mail: isamim@gmail.com

ABSTRACT

The surface properties of paper depend not only on the fibrous matrix but also on the final treatment of the paper surface. The present work compares paper samples with two different surface sizing treatments by using AFM and profilometry to assess topography and roughness parameters as well as to evaluate the spreading of the sizing formulation and to estimate sizing agent particle sizes. The results were confronted with dynamic light scattering measurements regarding particle size. This work shows that AFM is a valuable technique to visualize the effects of sizing onto the paper surface. However, due to the small pick up applied no differences could be detected in terms of the surface roughness parameters.

KEYWORDS

AFM, Optical profilometry, Light scattering, Surface sizing, Surface roughness.

INTRODUCTION

Printing quality is strongly influenced by the structural and chemical properties of paper surface, which depend not only on the fibrous matrix but also on the final treatment of the surface. This treatment may be of physical nature, like calendering, and/or of chemical nature, like surface sizing or coating. A common practice in industry regarding surface sizing, which was also followed in this work, is to use a blend of cationic starch and a synthetic surface sizing agent¹⁻³.

Many studies pertaining paper coating can be found in the open literature, concerning in particular the characterization of paper surface in terms of physical and chemical properties⁴⁻⁷. However, not many of these are related to the surface sizing of fine papers. The present work aims at comparing the surface structure of two paper samples with different surface sizing treatments by using Atomic Force Microscopy

(AFM). The sizing performance will be evaluated in terms of uniformity, particle size, shape and distribution over the paper surface as well as in terms of surface topography.

Although Scanning Electron Microscopy (SEM) has been traditionally used for surface analysis, it requires a laborious sample preparation (that can eventually change surface topography), needs vacuum and does not provide high contrast images on flat surfaces⁸. To overcome these drawbacks, AFM has been alternatively used, since it provides direct three-dimensional images of almost any type of surface in ambient air conditions, requires no sample preparation and can resolve extremely small surface features both at the micro- and nanoscale. Additionally, AFM images can be used to quantify surface roughness parameters. Other surface properties as hardness and adhesion can also be assessed. The technique seems therefore especially suited for the present study and has been previously applied by other authors for pulp & paper characterization⁹⁻¹². The principles of AFM are well described in the literature¹³⁻¹⁵ and therefore will not be detailed here.

In the present work, the results obtained by AFM will be confronted with those of SEM in what concerns the homogeneity of the surface treatment. The topographic parameters obtained by AFM will also be compared with those provided by Optical Profilometry, a non-contact technique increasingly used for studies of the paper surface^{3, 16}. The equivalent mean diameter of the sizing particles estimated by AFM will be further compared with measurements carried out in the sizing suspensions by Dynamic Light Scattering (DLS).

EXPERIMENTAL METHODS

Two distinct surface sizing treatments applied on a calendered uncoated base paper produced with a Eucalyptus globulus Kraft pulp were analyzed. Two different blends of cationic starch and acrylate copolymers, described in Table 1, were used for surface sizing. A sample of the base paper without any surface treatment was taken as reference (RP).

Table 1. Sample identification.

Sample	Surface sizing formulation (% w/w)
RP (Reference Paper)	No surface treatment
A1	80% of cationic starch* 20% of co-acrilonitrile-acrylate
B1	80% of cationic starch* 20% of co-styrene-acrylate

The surface sizing formulations were applied using a Mathis laboratory device, SVA-IR-B, which operates automatically with different velocities of the applicator roll. A 0.15 mm roll was used and its velocity adjusted to 6m/min, so that a total surface sizing pick-up of 3.5 ± 0.3 g/m² (on both sides of the sheet) was obtained. The drying process was performed in two steps: firstly

using an IR drier coupled to the applicator roll (1.0 kW) followed by air drying for at least 10 min. The surface sized samples were no further calendered.

The chemicals used for the preparation of the sizing formulations were provided by a paper mill instead of being prepared in laboratory. Because of this, information about their properties was limited and/or confidential and thus the most relevant had to be experimentally determined (Table 2). The calculation of the ratio of monomers of each copolymer was based on elemental analysis. These results together with the software ChemSketch enabled to derive the schematic representation of the chemical composition of the co-polymers, depicted in Figure 2.

Table 2. Properties of the compounds used to prepare the surface sizing formulations.

Compound	Properties		
	Ratio of Monomers**	Solids Content (%)	pH
Cationic starch*	---	12.8	6.7
Co-acrilonitrile-acrylate (A)	1:1	35.2	3.4
Co-styrene-acrylate (B)	3:4	13.3	4.3

* The cationic starch suspension was collected at the paper mill, and includes other process additives used in industry, such as optical brightener (OBA) and salt.

** Based on elemental analysis (using the equipment EA 1180 CHNS-O from Fisons Instruments)

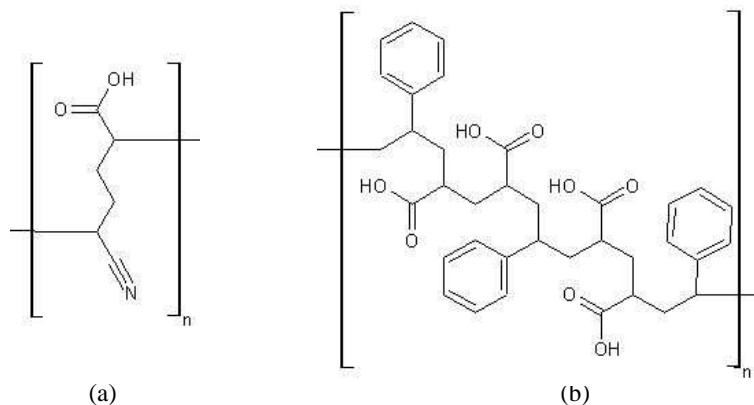


Figure 1. Schematic representation of the surface sizing agents: (a) co-acrilonitrile-acrylate. (b) co-styrene-acrylate.

AFM experiments were performed with a Nanoscope IIIa microscope from Digital Instruments Inc equipped with the Extender Electronics Module, which enables phase imaging in the tapping mode. High and low tapping images were acquired. Silicon cantilevers with a resonance frequency of 250-319 kHz were used. The damping ratio set point amplitude/free amplitude was varied between 0.5 and 0.8, and scanning rates from 0.7 to 2.0 Hz were used. The free amplitude varied between 100 and 150 nm. Images of the surface topography and phase

contrast, corresponding to 512×512 pixels in size were acquired by measuring the three samples (RP, A1, B1) in air. For that, areas of $5 \times 5 \mu\text{m}^2$ were analyzed. Filtering was not used during scanning.

From AFM data, the following roughness parameters were computed, using at least eight images per sample^{17, 18}: average roughness (S_a , μm); root mean square roughness (S_q , μm); maximum peak height (S_p , μm) maximum valley depth (S_v , μm); skewness (S_{sk}); and the ratio of the developed surface area to the nominal surface area (S_{dr}).

The JSM-5310 Scanning Electron Microscope (SEM) from Jeol was used with a 20 kV electronic beam intensity and images with magnifications from $200\times$ to $3500\times$ were acquired (the images obtained with higher magnifications were not good enough for further analysis).

The profilometry measurements were carried out using a monochromatic laser profilometer Altisurf 500 from AltiMet coupled with the PaperMap software. For each sample at least six images of $4 \times 4 \text{ mm}^2$ in size were scanned with a scanning resolution of $2 \mu\text{m}$. From the 2000 profiles obtained for each piece, the aforementioned roughness parameters were computed.

Mean particle size and size distributions were measured for the sizing formulations by dynamic light scattering (DLS) using the Coulter N4 Plus^{19, 20}. Samples were previously sonicated. At least three independent measurements were performed for each sample²⁰.

RESULTS AND DISCUSSION

Scanning Electron Microscopy (SEM) was first applied in order to evaluate qualitatively the uniformity of the surface treatment. The resulting images are presented in Figure 2.

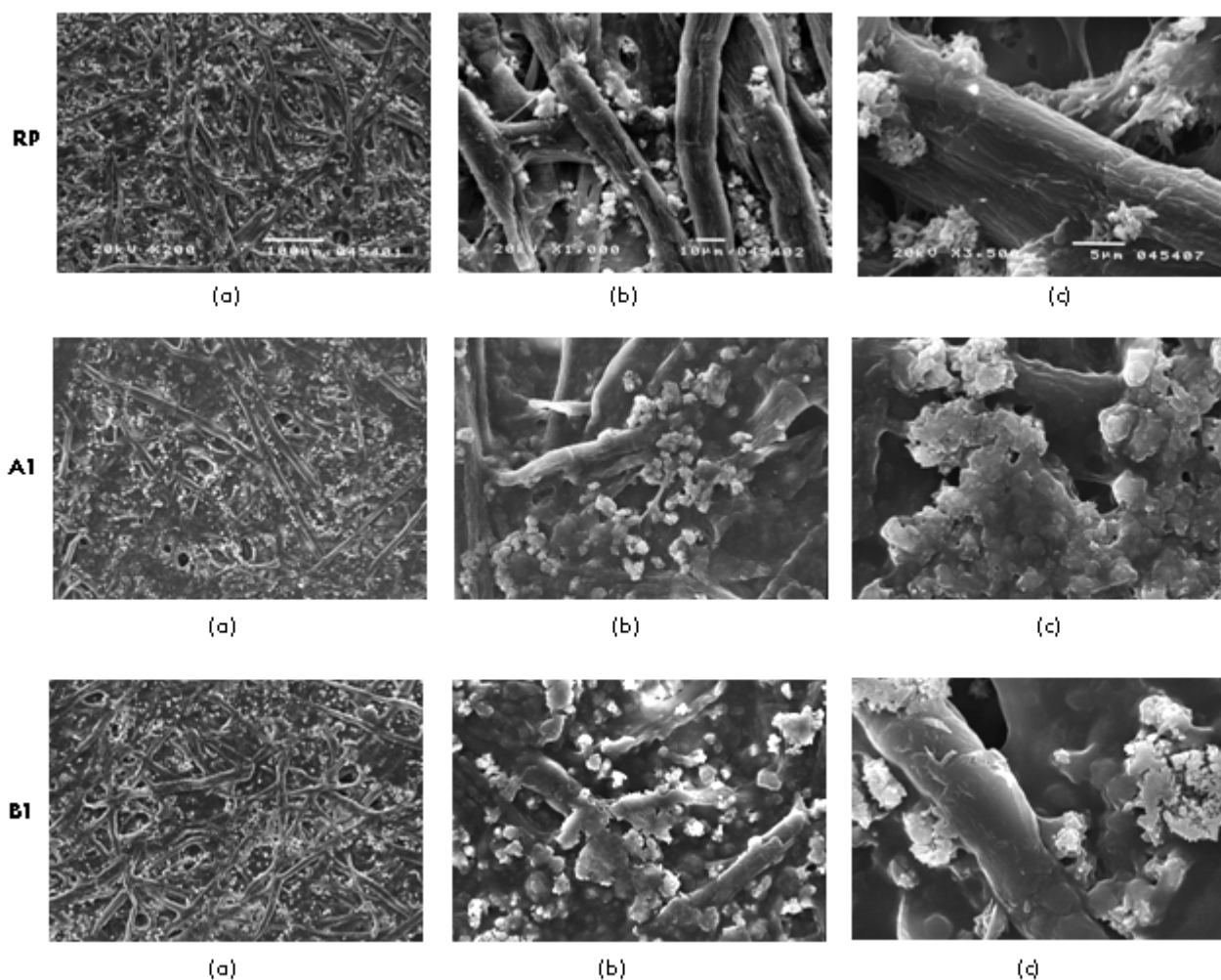


Figure 2. SEM images of the reference paper (RP) and of the surface sized samples A1 and B1 for different amplifications (a) 200 \times , (b) 1000 \times and (c) 3500 \times , obtained using a 20 kV electronic beam.

The SEM images in Figure 2 reveal that surface sizing has changed the surface to a more closed structure with less porosity between the cellulose fibres. However, no fine structure can be resolved on the studied paper surfaces.

On the contrary, a more detailed structure is seen in Figure 3 which shows AFM topographic (a), phase contrast (b) and 3D simulation (c) images obtained in the high tapping mode for the samples RP, A1 and B1.

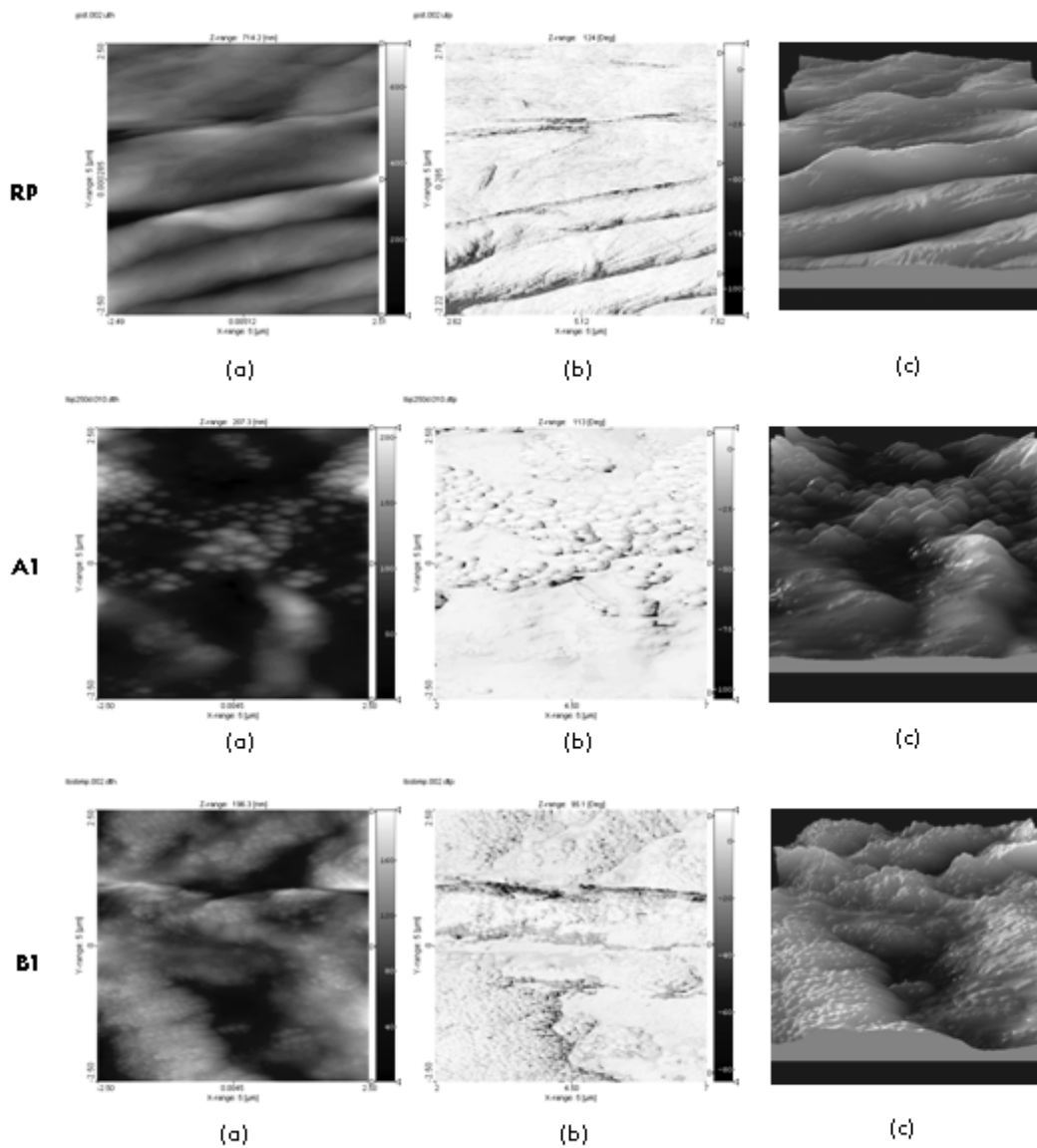


Figure 3. Topographic (a), phase contrast (b) and 3D simulation (c) images of the samples RP, A1 and B1 obtained by AFM using high tapping mode. The images size is $5 \times 5 \mu\text{m}^2$.

For the reference sample the fine structure of the cellulose fibre is resolved, consisting of bundles of microfibrils. In the sized samples these bundles are not visible, instead, a smoother surface is apparent with a granular fine structure. The differences between the sized samples appear in terms of spreading of sizing formulation as well as the size of the grains (particles). The co-styrene-acrylate appears to be more evenly spread over the paper surface than the co-acrylonitrile-acrylate. Besides, the particles of the former appear to be smaller and more spherical than those of the latter.

The average values obtained for the topographical parameters, together with the corresponding deviation values are listed in Table 3. Besides the roughness parameters, also the diameter of

the particles was estimated based on the projected areas of the particles by using a dedicated image analysis software (SPIP®).

Table 3. Topographic parameters obtained by AFM for the reference paper (RP) and for the surface sized samples A1 and B1.

Parameter	RP	A1	B1
Sa (µm)	0.06 ± 0.02	0.07 ± 0.05	0.06 ± 0.05
Sq (µm)	0.09 ± 0.03	0.09 ± 0.07	0.08 ± 0.06
Sp (µm)	0.11 ± 0.05	0.11 ± 0.10	0.09 ± 0.09
Sv (µm)	0.10 ± 0.04	0.11 ± 0.08	0.07 ± 0.05
Ssk	-0.38 ± 0.81	-0.14 ± 0.33	-0.04 ± 0.23
Sdr (%)	19.2 ± 14.1	25.7 ± 37.1	14.5 ± 21.0
Mean Particle Diameter AFM (nm)	-----	≈ 350	≈ 150

All the topographic parameters exhibited a large standard deviation. This may refer to the low homogeneity of the surfaces at the nanoscale. However, the most probable explanation is the analyzed image area ($5 \times 5 \mu\text{m}^2$) in contrast to the size of the imaged objects, which may result in a data set in which part of the images represent a fibre surface, part of the images represent edges of the fibres, and some of the images may even represent the sizing material appearing between cellulose fibres.

Higher values were expected for the roughness parameters Sa, Sq, Sp and Sv of the reference paper, when comparing to those of the surface sized samples, due to the distinct topographic features clearly visible in the 3D simulations of Figure 3. In spite of the aforementioned limitations, the visual inspection of the AFM images revealed two important differences between the surface sized samples A1 and B1, not detected by the SEM analysis: the particles corresponding to the sizing formulation of sample B1 are smaller (as confirmed by the values of Table 3) and more uniformly distributed on the paper surface.

As mentioned before, the results of AFM were confronted with those obtained by dynamic light scattering (regarding particle size) and profilometry (regarding topographic parameters). Table 4 presents the comparison of the diameter of the particles computed from AFM data and directly measured in the sizing suspensions by DLS.

Table 4. Comparison of the mean particle diameters computed from AFM data and measured by DLS.

Compound	AFM	DLS
	Particle diameter (nm)	Hydrodynamic diameter (nm)
Co-acrylonitrile-acrylate (A)	≈ 350	255
Co-styrene-acrylate (B)	≈ 150	83.6
Mean Diameter _B /Mean Diameter _A (D _B /D _A)	0.43	0.33

This table shows that the values derived from AFM are larger than those obtained by DLS but the relative size (D_B /D_A) only differs by 10%. It should be pointed out that discrepancies between the results of the two techniques were expected since, in AFM, particles are analyzed in the solid state being most probably aggregated, whereas by DLS they are analyzed in the liquid suspension adequately dispersed. Furthermore, the tip-sample convolution results in distorted (too large) lateral dimensions of the imaged objects. The low values obtained for the polydispersity index guarantee the reliability of the DLS analysis (0.38 and 0.21 for A and B, respectively). The results of the optical profilometry analysis are listed in Table 5.

Table 5. Topographic parameters obtained by Profilometry for the reference paper (RP) and for the surface sized samples A1 and B1.

Parameter	RP	A1	B1
S _a (μm)	2.87 ± 0.11	2.97 ± 0.04	2.96 ± 0.09
S _q (μm)	3.60 ± 0.14	3.74 ± 0.04	3.69 ± 0.08
S _p (μm)	2.57 ± 0.19	2.28 ± 0.07	2.88 ± 0.01
S _v (μm)	4.04 ± 0.17	4.57 ± 0.18	3.54 ± 0.11
S _{sk}	-0.31 ± 0.04	-0.49 ± 0.04	-0.14 ± 0.03
S _{dr} (%)	10.27 ± 0.33	10.35 ± 0.07	8.67 ± 0.02

The absolute values of the parameters S_a, S_q, S_p and S_v in Table 5 are larger than those obtained by AFM (at least by two orders of magnitude), demonstrating the strong scale-dependence of the analyzed parameter, typical for a non-stationary surface. This apparent discrepancy obtained with different techniques is also found in the results reported by other authors (Xu et al. 2005). The standard deviations for each measurement are much smaller, indicating that roughness at the macro-scale was less heterogeneous than roughness at the micro-scale (assessed by AFM). The much larger areas scanned by profilometry may certainly contribute to this remarkable reduction in the variability of the results. From Table 5, it is also clear that, once again, no significant differences exist between the three samples, in agreement

with the results of AFM, and that the surface of the paper samples is mainly composed of valleys rather than peaks since S_v is consistently larger than S_p and, simultaneously, S_{sk} is negative.

In general, the results of AFM and optical profilometry show that the three samples tested appeared visually different, but the data was too heterogeneous to be able to demonstrate quantitative differences in the roughness parameter values. Two facts may contribute to this result: i) the pick-up used in each surface size treatment (approximately 1,7 g/m², similar to the values used in industry) was probably not enough to introduce significant changes in the surface roughness of the reference paper; and, ii) the two sizing formulations being too identical to cause distinct impacts on topographic parameters (in fact, they contain both 80% of starch and only 20% of different copolymers (co-acrilonitrile-acrylate or co-styrene-acrylate) with different particle sizes). Nonetheless, it should be mentioned that these formulations originate important differences in terms of surface chemistry, as described by the authors in another publication²¹.

CONCLUSIONS

The above results confirm that AFM and SEM can be complementary used to study paper surface sizing, SEM allows a general evaluation of the surface and AFM enables to resolve small details on the paper surface, showing topographic differences not only between the unsized and sized samples but also between samples sized with distinct surface sizing formulations. In fact, differences both in the copolymer distribution on the paper surface and in the copolymers particle size were clearly visible. Nonetheless, these differences were not reflected in the roughness parameters quantified by AFM

Despite considerable differences between the absolute values of AFM and profilometry, the results of the latter (with much less deviations) confirm that both the unsized and the sized samples exhibited very similar roughness parameter values.

ACKNOWLEDGEMENTS

The authors acknowledge the EU COST E32 Action "Characterization of Paper Surfaces for Improved Printing paper Grades" for the financial support to a STSM at the KCL Pulp and Paper institute, Espoo - Finland and at the Åbo Akademi University, Turku - Finland.

REFERENCES

- (1) Koskela, J. P., Hormi, O. E. O.; Improving the printability of paper with long-chain quaternaries; *Appita Journal*; **2003**; 56(4); 296-300.
- (2) Pruszyński, P.; Recent developments in papermaking chemicals; *WWP Keynote lectures*; **2003**; 82-90.
- (3) Moutinho, I. M. T., Ferreira, P. J. T., Figueiredo, M. M. L.; Impact of surface sizing on inkjet printing quality; *Ind. Eng. Chem. Res.*; 46(19); **2007**; 6183-6188.
- (4) Donigian, D. W., Ishley, J. N., Wise K. J.; Coating pore structure and offset printed gloss; *Tappi J*; 80(5); **1997**; 163-172
- (5) Hladnik, A.; *Ink-jet printing and image analysis*; Technical Seminar, Beira Interior University, Covilhã (Portugal); 2003.
- (6) Forsström, U., Fagerholm, K., Saharenen; The role of base paper porosity in MSP coating; *Paperi ja Puu – Paper and Timber*; **2003**; 85(8); 454-459.
- (7) Hamers, C., others; Curtain coating for graphics better coverage, printability and runnability are among the advantages cited; *Pulp and Paper Industry*; **July 2005**; 36-37.
- (8) Chinga, G., Helle, T.; Structure characterisation of pigment layer on paper by scanning electron microscopy and image analysis; *Nord. Pulp Pap. Res. J.*; 17(3); **2002**; 307-312.
- (9) Koljonen, K., Österberg, M., Johansson, L.-S., Stenius, P.; Surface chemistry and morphology of different mechanical pulps determined by ESCA and AFM; *Colloids Surf.: Physicichem Eng. Aspects*; 228; **2003**; 143-158.
- (10) Gustafsson, J.; *Surface characterization of chemical and mechanical pulp fibres by AFM and XPS*; Academic Dissertation; Department of Physical Chemistry; Åbo Akademi University (Finland); 2004.
- (11) Irvine, J. A., Aston, D. E., Berg, J. C.; The use of atomic force microscopy to measure the adhesive properties of sized and unsized papers; *Tappi J.*; 82(5); **1999**; 172-174.
- (12) Xu, R., Fleming, P.D., Pekarovicova, A.; The effect of ink jet paper roughness on print gloss; *J Imag Sci Tech*; 49(6); **2005**; 660-666.
- (13) Garcia, R., Perez, R.; Dynamic atomic force microscopy methods; *Surface Science Reports*; 47 (6-8); **2002**; 197-301.

- (14) Drelich, J., Tormoen, G. W., Beach, E. R.; Determination of solid surface tension from particle-substrate pull-off forces measured with the atomic force microscope; *J Colloid Interface Sci*; 280; **2004**; 484-497.
- (15) Das, S., Sreeram, P. A., Raychaudhuri, A. K., Sai, T. P., Brar L. K.; Non-contact dynamic mode atomic force microscope: effects of nonlinear atomic forces; *IEEE Conference*; **2006**; 458-462.
- (16) Ashori, A., Raverty, W. D., Vanderhoek, N., Ward, J. V. (); Surface topography of kenaf (*hibiscus cannabinus*) sized papers; *Bioresource Technology*; 99(2); **2008**; 404-410.
- (17) Cohen, D. K.; Glossary of Surface Texture Parameters; Michigan Metrology ; <http://www.michmet.com/Download.htm>; 2006.
- (18) Stout, K.J., Sullivan, P.J., Dong, W.P., Mainsah, E., Luo, N., Mathia, T., Zahouani, H.,; *Publication no. EUR 15178 EN of the Commission of the European Communities*; Luxembourg; 1994.
- (19) Alince, B., Porubská, J., Van de Ven, T. G. M.; Light scattering and microporosity in paper; *JPPS*; 28(3); **2002**; 93-98.
- (20) Elizalde, O., Leal, G., Leiza, J.; Particle Size Distribution Measurements of Polymeric Dispersions: A Comparative Study; *Part Part Syst Char*; 17(5-6); **2001**; 236 – 243.
- (21) Moutinho, I. , Kleen, A. M., Figueiredo, M. M., Ferreira, P. J.; Effect of surface sizing on the surface chemistry of paper containing eucalyptus pulp; *Holzforschung*; 63(3); **2009**; 282-289.

CHAPTER 10

CONCLUSIONS

10 CONCLUSIONS

Having already outlined the relevant aspects of each of the covered topics within the respective chapters, the main conclusions to be drawn relate essentially to the integration and summary of these aspects. The major objective of this study was to analyze the alterations in physical and chemical properties of the paper surface caused by the application of different surface sizing formulations (constituted by mixtures of cationic starch and minor quantities of distinct synthetic copolymers) and the impact of these physical and chemical alterations on the inkjet printing quality of uncoated fine papers. The use of these surface sizing blends raised additional difficulties due to the lack of information about the chemical composition and structure of the copolymers, since these were industrial products and the only information available was basically about the monomers that constituted each copolymer. A trial and error procedure was then implemented to determine the monomers proportion. This was based on the comparison between the elements ratios calculated from a previous estimation and those measured by elemental analysis. Knowing the chemical composition, a schematic representation of the molecules structure was then proposed and validated by additional measurements of the compounds properties, such as particle size and surface tension.

The different surface sizing formulations were applied to the paper sheets ($\approx 3.5 \text{ g/m}^2$) and some surface properties of the treated papers were determined using distinct techniques (some of them not routinely used for paper surfaces). The differences between the results were explained in terms of composition of the corresponding copolymers used and their quantities. Having in mind that the surface sizing is only a small percentage of a printing and writing paper composition, that the variation of the applied sizing formulations was only in the amount of copolymer added (20% at most, in order to be not far from the industrial practice) and also that some of the copolymers had identical composition, the initial expectation was for relatively small magnitude effects. Thus, and in order to guarantee that the differences between the samples were statistically valid, an analysis of variance was consistently applied to all the results of the various surface characterization techniques.

The results obtained can be divided in two major groups: those related to the physical properties of the paper sheets (surface roughness and porosity) and those related to their chemical characteristics (surface free energy, dispersive and polar components, and acid-base character).

Regarding the 3D topographical parameters measured by laser profilometry, it was shown that the surfaces are moderately rough with a predominance of valleys over peaks. With respect to porosity, mercury porosimetry has shown that a value around 56% was found for practically all samples. Additionally, the pore sizes exhibited a bimodal distribution with one peak around 3 μm and another around 20 μm . The increase in the quantity of copolymer incorporated in the blend led to a slight decrease in both porosity and pore size. In general, it can be concluded that no significant changes were induced by the distinct sizing blends in terms of surface roughness and paper porosity. As mentioned above, this is a logical consequence of the surface sizing treatment, since only small amounts of sizing were applied which in turn differed only in even smaller quantities of incorporated copolymers. Nonetheless, complementary studies carried out with AFM for some of the samples enabled to resolve small details on the paper surface allowing to detect differences in the size, shape and spatial distribution of the surface sizing agents' molecules at the paper surface.

Contrary to the results obtained in terms of surface topography, the differences in the composition of the surface sizing blends had a relevant impact on the chemical properties of the paper surface, as measured by contact angle and inverse gas chromatography. With respect to the contact angle, both static and dynamic measurements were undertaken. A preliminary study of paper topography's influence revealed that surface roughness does not significantly affect the contact angle values of the tested samples. As expected, the addition of the copolymers to the cationic starch increased paper surface hydrophobicity in different degrees according to the respective composition and concentration. As for the derived surface energetics results, it was shown that the P&W papers' surface is predominantly dispersive, meaning that the polar and acid-base interactions have a smaller influence on paper behavior. However, these secondary interactions allow detailing the influence of the surface modifications, since they are more specific than the dispersive ones. In fact, the values of the polar component of the surface free energy obtained for different copolymer concentrations enabled to present solid hypotheses concerning the orientation of the molecules at the paper surface, namely regarding the different functional groups.

Additionally, the dynamic contact angle measurements carried out with water to analyze the wetting behavior have confirmed some of these hypotheses and revealed that the addition of the synthetic surface sizing agents has an effect of controlling the wetting phenomena, both in terms of spreading and absorption.

The IGC analysis of the dispersive interactions has not only confirmed but in some cases also complemented the hypotheses raised for the molecules' orientation based on the contact angle measurements. Furthermore, it was verified that the paper's dispersive component of the surface free energy decreases as the temperature increases and that the values derived from IGC are always above the ones determined from contact angle measurements, due to the specificities of the techniques. As for the acid-base character it was found that the paper surface is amphoteric with a slightly basic character (K_b values always higher than those of K_a) and that the addition of the synthetic surface sizing agents to the traditional sizing formulation increases the surface ability to establish acid-base interactions due to a general increase of K_a and K_b values (more relevant for K_b).

From the results of both contact angle and IGC measurements, it was possible to find out that, in general, styrene based surface sizing agents induce more consistent and logical variations, associated to the chemical properties of the compounds. As for the distribution of the surface sizing agents on the surface, it was verified that they stay at the paper surface in layers, and the amount necessary to complete each layer depends on the size of the copolymer molecules. Moreover, the functional groups of the sizing agent turned towards the air interface are those that mostly influence the paper surface properties.

Complementary studies using ESCA and ToF-SIMS undertaken for some of the paper samples enabled not only to confirm the above findings but also to detect differences in the penetration of the copolymer particles into the paper structure, explained as a result of distinct copolymer surface tensions. Furthermore, the use of these techniques has shown that the increase of the sizing pick-up (up to 9.0 g/m²) does not significantly change the chemical properties of the paper surfaces.

The final inkjet printing performance, evaluated through the determination of several parameters related to color reproduction and image definition (as measured by optical densities, gamut area and gain), has shown that the surface sizing agents including styrene proved to be, in general, more successful than the remaining sizing agents tested.

Regarding the surface sizing agents' molecules orientation, it was confirmed that for better inkjet printing performances the predominance of non-polar rather than polar groups turned outwards is desirable. However the predominance of these polar groups can not be excessive since they must also be accessible for paper-ink interactions in order to allow the ink to dry fast.

As for the subjective evaluation of the inkjet printing quality performed by a panel of end-users, it was verified that the human perception of quality in a printed image is more associated to parameters related with color reproduction quality (optical densities and gamut area) than parameters reporting image definition (gain).

From all the available results, it can be concluded that the techniques used to analyze the paper surface seem to be more sensitive to differences in the sizing blend formulations than those specifically used to evaluate inkjet printing quality. This leads to the conclusion that the final printing performance is clearly under-evaluated with the existing techniques.

Nonetheless, the results point to some recommended windows for the values of key variables that potentiate a good printing quality:

$75^{\circ} < \text{water contact angle} < 85^{\circ}$;

$0.09^{\circ}/\text{sec} < \text{wetting velocity} < 0.19^{\circ}/\text{sec}$

$6 \text{ mN/m} < \text{polar component of the surface free energy} < 12 \text{ mN/m}$

Finally, in the total set of samples, those with an overall better performance are samples **StS9-05** and **StS10-10**, which include co-styrene-acrylate copolymers in the sizing blend.

Additionally, the work developed throughout these years and the results that were obtained suggest some further studies in order to better understand the interactions ruling the printing process and the sizing agents' influence on inkjet printability of uncoated fine papers.

A deeper chemical characterization of the industrial compounds used in papermaking, taking advantage of polymer chemistry, computational analysis and reversing engineering, would be of utmost interest and usefulness.

In spite of the fact that the methodology used for the surface sizing operation in the laboratory was quite reliable and sufficient to fulfil the objectives of the study, the knowledge of other variables involved in the process such as the temperature and rheological properties of the sizing formulations as well as the room temperature would be helpful to better characterize the sizing process.

The delamination of the treated paper samples and the subsequent analysis of the distinct layers both by SEM and FT-IR would contribute to a deeper insight on the effect of the surface sizing process and of the absorption and spreading of inks.

Based on the results that were obtained with some of the copolymers, the use of tailor-made sizing agents containing styrene would also provide a deeper insight on the interactions occurring at paper surface. A larger variability in the composition of the surface sizing formulations in terms of the percentage of surface sizing agent is also recommended, to better understand the influence of each compound.

Finally, and in order to obtain printing quality results with a detail close to that provided by the techniques used for the surface characterization, further developments in specific techniques to evaluate printing parameters are mandatory. This would most certainly help to achieve more comprehensive and reliable correlations between the surface properties and the final inkjet printing quality as well as to establish more consistent mathematical models.

CHAPTER 11

REFERENCES

11 REFERENCES

A

- Adamson A. W., Gast A. P. (1997); **Physical chemistry of surfaces**; 5th edition; John Wiley & Sons Inc.; New York; 291-363 and 379-420.
- Ahlroos J., Grön J. (2001); **Coating-paper interactions for metered size press coated mechanical grades based on TMP and SGW pulps**; *Tappi Journal*; 84(5); 68.
- Alinec B., Porubská J., Van de Ven T. G. M. (2002); **Light scattering and microporosity in paper**; *Journal of Pulp and Paper Science*; 28(3); 93-98.
- Ajerschi M., Poirier N., Pikulik I. (2004.); **Colagem superficial sem prensa de colagem – Resultados de máquina de papel piloto**; *O Papel/Paprican*; 47-58.
- Andersson C., Järnström L., Mesic B. (2006); **Controlled penetration of starch and hydrophobic sizing agent in surface sizing of porous materials**; *Appita Journal*; 59(3); 207-212.
- Aquino A. I., Martins A. A., Figueiredo M. M., Carvalho M. G. (2003); **Effect of beating and sizing on the surface properties of Eucalyptus globulus fibres**; Proc. 28th Eucepa conference – Sustainable Development for the pulp and paper industry; Lisbon.
- Ashori A., Raverty W. D., Vanderhoek N., Ward J. V. (2008); **Surface topography of kenaf (*hibiscus cannabinus*) sized papers**; *Bioresource technology*; 99(2); 404-410.
- Aspler J. S., Davis S., Lyne M. B. (1987); **The surface chemistry of paper in relation to dynamic wetting and sorption of water and lithographic fountain solutions**; *Journal of Pulp and Paper Science*; 13(2); J55-J60.
- Aspler J. S. (1993); **Interactions of ink and water with the paper surface in printing**; *Nordic Pulp and Paper Research Journal*; 8(1); 68-74.
- van Asten A., van Veenendaal N., Koster S. (2000); **Surface characterization of industrial fibers with inverse gas chromatography**; *Journal of Chromatography A*; 888; 175-196.

B

- Baoli S., Qianru Z., Lina J., Yang L., Bin L. (2007); **Surface Lewis acid base properties of polymers measured by inverse gas chromatography**; *Journal of Chromatography A*; 1149; 390-393.

- Bardavid S. M., Schulz P. C., Arancibia E. L. (2007); **IGC studies of binary cationic surfactants mixtures**; *Journal of Colloid and Interface Science*; 316; 114-119.
- Barros G. G. (2004); **Optical topographical characterization for flexographic printability assessment** ; *Licentiate Thesis*; Karlstad University; Sweden.
- Brandão E. (1999); **Colagem superficial: Experiência e reflexões sobre sua aplicação**; *Proc. 16º Encontro Tecnicelpa*; Covilhã; 165-176.
- Branton P., Baker R. R. (2002); **Methods for the structural characterisation of cigarette paper**; *Oral presentation - 56th Tobacco Science Research Conference*; Lexington; Kentucky; USA; September 29 to October 2.
- Brinen J. S. (1993); **The observation and distribution of organic additives on paper surfaces using surface spectroscopic techniques**; *Nordic Pulp and Paper Research Journal*; (1); 123-129.
- Bastos F. S. (2004); **Avaliação da textura superficial e comportamento ao desgaste do esmalte dentário**; *Tese de Mestrado*; Universidade Federal de Minas Gerais; Brasil.
- Bauer D., Bergh N. O., von Flaven A., Palm C., Lüttgen W., Baurneister M. (1999); **Starch – Characterization and use in the paper industry**; *Proc. APV annual conference*; Damsldt.
- Belgacem M. N., Czeremuskin G., Sapiuha S. (1995); **Surface characterization of cellulose fibers by XPS and inverse gas chromatography**; *Cellulose*; 2; 145-157.
- Belgacem M. N. (2000); **Characterization of polysaccharides, lignin and other woody components by inverse gas chromatography: A review**; *Cellulose Chemistry and Technology*; 34; 357-383.
- Bico J., Thiele U., Quéré D. (2002); **Wetting of textured surfaces**; *Colloids and Surfaces A: Physicochemical and Engineering Aspects*; 206; 41-46.
- Börsas L., Sjöström J., Gatenholm P. (1997); **Characterization of surfaces of CTMP fibers using inverse gas chromatography combined with multivariate data analysis**; *Nordic Pulp and Paper Research Journal*; 12(4); 220-224.
- Borch J. (1982); **Sizing additives affect polymer-paper adhesion**; *Tappi Journal*; 65(2); 72-73.

Bordurtha P. A., Matthews G. P., Kettle J. P., Roy I. M. (2005); **Influence of anisotropy on the dynamic wetting and permeation of paper coatings**; *Journal of Colloid and Interface Science*; 283; 171-189.

Breda J. P. M. D. (2001); **Estudo do efeito da composição da mistura fibrosa na qualidade da impressão com jacto de tinta**; Tese de Mestrado; Universidade da Beira Interior.

Briggs D., Rance D.G., Briscoe B.J. (1989); **Surface properties**; In: Booth C., Price C. (book eds.); **Polymer characterization**; In: Allen G, Bevington J.C. (series eds.); **Comprehensive Polymer Science - The Synthesis, Characterization, Reactions & Applications of Polymers**; Pergamon Press; Oxford; 707-732.

Browning B. L., (1977); **Analysis of paper**; 2nd edition; Marcel Dekker Inc.; New York.

C

Carvalho M. G. (2005); **Surface characterization by using inverse gas chromatography: application to fibres (pulp) and paper**; *Seminário*; Universidad de Misiones; Argentina; Setembro.

Carvalho M. G., Santos J. M. R. C. A., Martins A. A., Figueiredo M. M. (2005); **The effects of beating, web forming and sizing on the surface energy of Eucalyptus globules kraft fibres evaluated by inverse gas chromatography**; *Cellulose*; 12; 371-383.

Carceller R., Juppo A. (2004); **New surface size composition changes paper surface properties for improving ink jet printability of copy paper**; *Paperi ja Puu – Paper and Timber*; 86(3); 161-163.

Cassei A. B. D., Baxter S. (1944); **Wettability of porous surfaces**; *Transactions of Faraday Society*; 40; 546-551.

Cassei A. B. D. (1948); **Contact Angles**; 11-15.

Chen J., Oliver J., Smith G., Haun J. (2002); **A print quality monitoring program for roto-grade newsprint, Part I: Preliminary design of printing quality evaluation**; *Pulp and Paper Canada*; 130 (3); 32-35.

Chhabra I., Spelt J. K., Yip C. M., Kortschot M. T. (2005); **An Investigation of pulp fibre surface by atomic force microscopy**; *Journal of Pulp and Paper Science*; 31819; 52-56.

Chinga G., Helle T. (2002a); **Quantification of structure details of LWC paper coating layers**; *Nordic Pulp and Paper Research Journal*; 17(3); 313-318.

Chinga G., Helle T. (2002b); **Structure characterisation of pigment layer on paper by scanning electron microscopy and image analysis**; *Nordic Pulp and Paper Research Journal*; 17(3); 307-312.

Connors T. E., Banerjee S. (1995); **Surface analysis of paper**; CRC Press; New York.

Cohen D. K. (2006); **Glossary of Surface Texture Parameters**; Michigan Metrology; <http://www.michmet.com/Download.htm>.

Conceição S., Santos N., Velho J., Ferreira J. M. (2003); **Influence of rheology on paper coated properties**; *WWP Pulp and Paper Science and Technology: Papermaking Science and Technology*; 199-204.

Cordeiro N., Neto C. P., Gandini A., Belgacem M. N. (1995); **Characterization of the cork surface by inverse gas chromatography**; *Journal of colloid and interface science*; 174; 246-249.

D

Danby R., Zhou H. (2004); **Numerical evaluation of the printability of paper surfaces**; *Pulp & Paper Canada*; 105(9); 38-42.

Das S., Sreeram P. A., Raychaudhuri A. K., Sai T. P., Brar L. K. (2006); **Non-contact dynamic mode atomic force microscope: effects of nonlinear atomic forces**; *IEEE conference*; 10-13 Jan; 458-462.

Dataphysics (n.d.); **Surface chemistry – The Fundamentals of contact angle measurements**; Manual de instruções do equipamento OCA 20.

Donderi D. C., Jordan B., Aspler J., O'Neill M. (2003); **The subjective print quality of commercial heatset offset prints on lightweight coated paper**; *Pulp & Paper Canada*; 104(9); 35-37.

Dong W. P., Sullivan P. J., Stout K. J. (1994a); **Comprehensive study of parameters for characterizing three-dimensional surface topography III: Parameters for characterizing amplitude and some functional properties**; *Wear*; 178; 29-43.

Dong W. P., Sullivan P. J., Stout K. J. (1994b); **Comprehensive study of parameters for characterizing three-dimensional surface topography IV: Parameters for characterizing spatial and hybrid properties**; *Wear*; 178; 45-60.

Donigian D. W., Ishley J. N., Wise K. J. (1997); **Coating pore structure and offset printed gloss**; *Tappi Journal*; 80(5); 163-172.

Donigian D. W., Wernett P. C., McFadden M. G., McKay J. (1999); **Ink.jet dye fixation and coating pigments**; *Tappi Journal*; 82(8); 175-182.

E

Engström G. (2005); **Interactions between coating colour and base sheet in pigment coating**; *Proc. 13th Fundamental Research Symposium*; Cambridge; 1011 – 1073.

Ernstsson M. (2005); **Surface chemistry of paper – surface composition and spectroscopic characterization techniques**; *FPIRC Course n° 14*; Estocolmo; Setembro 2005.

Exner R. (2001); **Synthesis & application of polymer sizing agents**; *Proc. Pira International Conference - Scientific & Technical Advances In The Internal & Surface Sizing Of Paper & Board*; Prague.

F

Fardim P. (2002); **Papel e química de superfície parte II – Revestimento e printabilidade**; *O papel*; Maio 2002; 75-83.

Fardim P., Durán N. (2005); **Effects of kraft pulping on the interfacial properties of Eucalyptus pulp fibers**; *J. Braz. Chem. Soc.*; 16(5); 915-921.

Felix J. M., Gatenholm P. (1993); **Characterization of cellulose fibers using inverse gas chromatography**; *Nordic Pulp and Paper Research journal*; 1; 200-203.

Forsström U., Fagerholm K., Saharenen (2003); **The role of base paper porosity in MSP coating**; *Paperi ja Puu – Paper and Timber*; 85(8); 454-459.

Fowkes F. M. (1987); **Role of acid-base interfacial bonding in adhesion**; *Journal of Adhesion Science and Technology*; 1(1); 7-27.

G

Gadelmawla E. S., Koura M. M., Maksoud T. M. A., Elewa I. M., Soliman H. H. (2002); **Roughness parameters**; *Journal of Materials Processing Technology*; 123; 133-145.

Garcia M. F. (2004); **Revestimento: a evolução do papel**; *O Papel*; (3); 41-46.

Garret P. D., Lee K. I. (1998); **Characterization of polymers for paper surface sizings using contact angle methods**; *Tappi Journal*; 81(4); 198-203.

Genes P. G. (1985); **Wetting: statics and dynamics**; *Reviews of Modern Physics*; 57(3); 827-863.

Glittenberg D., Voigt A. (2004); **How to improve ink-jet papers Its possible to build in desired properties without breaking the bank**; *Pulp and Paper International*; 19-21.

Glittenberg D., Leonhardt P. (2007); **High-dosable wet-end starch for strength improvement allows new, more economic papermaking concepts**; *Science and Technology – Das Papier*; 9; 32-38.

Gu W., Bousfield W., Tripp C. P. (2007); **The role of surface hydrophobicity in offset ink setting**; *Nordic Pulp and Paper Research Journal*; 22(1); 57-60.

Gurau V., Bluemle M. J., De Castro E. S., Tsou Y., Mann Jr^a J. A., Zawodzinski Jr^a T. A. (2006); **Characerization of transport properties in gás diffusion layers for proton Exchange membrane fuel cells 1. wettability (internal contact angle to water and surface energy of GDL fibers)**; *Journal of Powder Sciences*; 160; 1156-1162.

Gutierrez M. C., Rubio J., Rubio F., Oteo J. L. (1999); **Inverse gas Chromatography: a new approach to the estimation of specific interaction**; *Journal of Chromatography A*; 845; 53-66.

H

Hladnik A. (2003); **Ink-jet printing and image analysis**; Seminário; Universidade da Beira Interior; Covilhã.

Hoang V., Ly H. H., Shen W., Parker I. H. (s.d.); **The interaction of ink-jet inks and uncoated papers**; 269-276.

J

Johnson R. W., Abrams L., Maynard B., Amick T. J. (1999); **Use of mercury porosimetry to characterize pore structure and model end-use properties of coated papers – part I: Optical and strength properties**; *Tappi Journal*; 82(1); 239-251.

K

Kangas H., Kleen M. (2004); **Surface chemical and morphological properties of mechanical pulp fines**; *Nordic Pulp and Paper Research Journal*; 19(2); 191-199.

Kannangara D., Zhang H., Shen W. (2006); **Liquid-paper interactions during liquid drop impact and recoil on paper surfaces**; *Colloids and Surfaces A: Physicochem. Eng. Aspects*; 280; 203-215.

Keller D. S., Lune, P. (2009); **Surface energetics of calcium carbonates using inverse gas chromatography**; *colloids and surfaces A: Physicochemical and Engineering Aspects*; 161; 401-415.

Keskitalo I. (2000); **The penetration of water-based inks into laboratory sheets made from bleached eucalypt Kraft pulp**; *Master's Thesis*; Luleå Tekniska Universitet; Sweden.

Kleen M., Kangas H., Laine C. (2003); **Chemical characterization of mechanical pulp fines and fiber surface layers**; *Nordic Pulp and Paper Reseach Journa*; 18(4); 361-368.

Knauf G. H., Doshi M. R. (1986); **Calculayions of aerodynamic porosity, specific surface área, and specific volume from Gurley seconds measurements**; *Institute of Paper Chemistry Technical Paper Series*; 183; 1-7.

Koljonen K. (2004); **Effect of surface properties of fibers on some paper properties of mechanical and chemical pulp**; *Master of science thesis*; Laboratory of Forest Products Chemistry, Department of Forest Products Technology, Helsinki University of Technology; Espoo; Finland.

Koljonen K., Stenius P. (2005), **Surface characterization of single fibers from mechanical pulps by contact angle measurements**; *Nordic Pulp and Paper Research Journal*; 20(1), 107-113.

Kowalczyk G. E., Trksak R. M. (1998); **Image analysis of ink-jet quality for multi use office paper**; *Tappi Journal*; 81(110); 181-190.

Kunaver M., Zadnik J., Planinsek O., Srcic S. (2004); **Inverse gas chromatography – A different approach to characterization of solids and liquids**; *Acta Chim. Slov.*; 51; 373-394.

Kwok D. Y., Lam C. N. C., Li A., Leung A., Wu R., Mok E., Neuman A. W. (1998); **Measuring and interpreting contact angles: a complex issue**; *Colloids and Surfaces A. Physicochemical and Engineering Aspects*; 142; 219-235.

L

Lai S. C. S. (2003); **Mimichink nature: Physical basis and artificial synthesis of the Lótus-effect**; *Tese*; Universidade de Leiden.

Laleg M. (2004); **Colagem superficial com quitosana e com misturas de quitosana e amidos**; *O Papel/Paprican*, 33-45.

Lee H. L., Shin J. Y., Koh C., Ryu H., Lee D., Sohn C. (2002); **Surface sizing with cationic starch: its effect on paper quality and papermaking process**; *Tappi Journal*; 1(1); 34-40.

Lee H., Joyce M. K., Fleming P. D., Cawthorne J. E. (2005); **Influence of silica and alumina oxide on coating structure and print quality of ink-jet papers**; *Tappi Journal*; 4(1); 11-16.

Lee T. G., Kim J., Shon H. K., Jung D., Moon D. W. (2006); **Chemical derivatization technique in ToF-SIMS for quantification analysis of surface amine groups**; *Applied Surface Science*; 252; 6632-6635.

Lehtinen E. (2000); **Pigment coating and surface sizing of paper**; Papermaking Science and Technology encyclopedia vol. 11; Fapet Oy; Helsinki; 2000

Lertsutthiwong P., Nazhad M. M., Chandkrachang S., Stevens W. F. (2004); **Chitosan as a surface sizing agent for offset printing paper**; *Appita Journal*; 57(4); 274-280.

Levlin J., Söderhjelm L. (2000); **Pulp and paper testing**; Papermaking Science and technology encyclopedia vol 17; Fapet Oy; Helsinki; 2000.

Lindsay J. D. (1990); **The Anisotropic Permeability of Paper**; *Tappi J.*; 73(5): 223.

Lindsay J. D. (1998); **The Anisotropic Permeability of Paper: Theory, Measurements, and Analytical Tools**; *IPC Technical Paper Series #289*; The Institute of Paper Chemistry; Appleton; Wisconsin.

Lindsay B., Abel M. L., Watts J. F. (2007); **A study of electrochemically treated PAN based carbon fibers by IGC and XPS**; *Carbon*; 45; 2433-2444.

Liu, F. P., Rials, T. G.; Simonsen, J. (1998); **Relationship of wood surface energy to surface composition**; *Langmuir*; 14(2); 536-541.

Lohmander S., Rigdahl M. (2000); **Influence of a shape factor of pigment particles on the rheological properties of coating colours**; *Nordic Pulp and Paper Research Journal*; 15(3); 231-236.

M

Marmur A. (2006); **Soft contact: measurement and interpretation of contact angles**; *Soft Matter*; 2; 12-17.

Mangin P. J. (1993); **A structural approach to paper surface characterization**; Proc. Process and product Quality Conference; Tappi; Atlanta; 17-23.

Martin A. H. (2008); **Porosity Guide**; at www.paperonewb.com.

Mäkinen M. O. A., Jääskeläinen T., Parkkinen J., (2007); **Improving optical properties of printing papers with dyes: A theoretical study**; *Nordic Pulp and Paper Research Journal*; 22(2), 236-243.

Mattila U., Tahkola K., Nieminen S., Kleen M. (2003); **Penetration and separation of coldset ink resin and oils in uncoated paper studied by chromatographic methods**; *Nordic Pulp and Paper Research Journal*; 18(4); 413-420.

Mešič B., Järnström L., Hjärthag C., Lestelius M. (2004); **Effects of application temperature in paper surface sizing with temperature-responsive starch on water repellency and flexographic printability**; *Appita Journal*; 57(4); 281-285 & 298.

Micromeritics (2000); **Autopore IV 9500 Operator's manual**.

Moura M. J., Ferreira P. J., Figueiredo M. M. (2005); **Mercury intrusion porosimetry in pulp and paper technology**; *Powder Technology*; 160; 61-66.

Moutinho I., Figueiredo M. M., Ferreira P. J. (2004); **Influência dos agentes de colagem superficial na estrutura do papel – uma análise química**; *Relatório de Seminário*; Universidade de Coimbra.

Moutinho I., Oliveira P., Figueiredo M., Ferreira P. (2007a); **Evaluating the surface energy of surface sized printing and writing papers**; *Proc. XX Encontro Nacional Tecnicelpa*; 10-12 Outubro 2007; Tomar; Portugal.

Moutinho I. M. T., Ferreira P. J. T., Figueiredo M. M. L. (2007b); **Impact of surface sizing on inkjet printing quality**; *Ind. Eng. Chem. Res.*; 46 / (19); 6183-6188.

Moutinho I., Figueiredo M. M., Ferreira P. J. (2008a); **“Caracterización de la Superficie de Papeles de Impresión y Escritura con Encolado Superficial”**; *Celulosa y Papel*; Vol 24 (nº 2); 6:15.

Murakami K., Imamura R. (1980); **Porosity and gas permeability**; *Handbook of Physical and Mechanical Testing of Paper and Paperboard*; vol. 2; Marcel Dekker Inc.; New York; pp 57-80.

N

Nissi M. V. H., Savolainen A., Talja M., Raija M., R. (1999); **Polymer dispersion coated HD papers**; *Tappi Journal*; 82(1); 252-256.

O

Oittinen P., Saarelma H. (1998); **Printing**; Papermaking Science and Technology encyclopedia vol. 13; Fapet Oy; Helsinki; 1998.

Olkkonen T., Lipponen J. (2007); **Starch penetration in surface sizing at various parameters – pilot and production machine experience**; *Science & Technology – Das Papier*;

Olsson R., Yang L., van Stam J., Lestelius M. (2006), **Effects on ink setting in flexographic printing: Coating polarity and dot gain**; *Nordic Pulp and Paper Research Journal*; 21(59); 569-574.

P

Paulapuro H. (2000); **Papermaking Part 1, Stock Preparation and Wet End**; Papermaking Science and Technology encyclopedia vol. 11; Fapet Oy; Helsinki; 2000.

Planinšek O., Buckton G. (2003); **Inverse gas chromatography: Considerations about appropriate use for amorphous and crystalline powders**; *Journal of Pharmaceutical Sciences*; 92(6); 1286-1294.

Prinz M., Schultz W.-S. (2007); **Sizing agents for surface and wet end application**; *Professional Papermaking*; 1; 44-49.

Putkisto K., Maijala J., Grön J., Rigdahl M. (2004); **Polymer coating of paper using dry surface treatment: Coating structure and performance**; *TAPPI JOURNAL*; 3(11), 16-23.

Pyda M., Sidqi M., Keller D. S., Luner P. (1993); **An inverse gas chromatographic study of calcium carbonate with alkylketene dimmer**; *Tappi Journal*; 76(4); 79-85.

R

Ridgway C. J., Gane P. A. C. (2003); **Bulk density measurement and coating porosity calculation for coated paper samples**; *Nordic Pulp and Paper Research Journal*; 18(1); 24-31.

Rjiba N., Nardin M., Dréan J. Y., Frydrych R. (2007); **A study of the surface properties of corron fibers by inverse gas chromatography**; *Journal of colloids and Interface Science*; 314; 373-380.

Roe R., Baccheta V. L., Wong P. M. G. (1967); **Refinement of pendant drop method for the measurement of surface tension of viscous liquids**; *The Journal of Physical Chemistry*; 71(13); 4190-4193.

Rosenberger R. R. (2003); **Quantitatively relating ink jet print quality to human perception**; *Pulp and Paper Canada*; 104(3); 35-38.

S

Santos J. M. R. C. A., Gil M. H., Portugal A., Guthrie J. T. (2001); **Characterisation of the surface of a multi-purpose office paper by inverse gas chromatography**; *Cellulose*; 8; 217-224.

Santos J. M. R. C. A., Guthrie J. T. (2005); **Analysis of interactions in multicomponent polymeric systems: The key-role of inverse gas chromatography**; *Materials Science and Engineering*; 50; 79-107.

Saxena A., Kendrick J., Grisey I., Mackin L. (2007); **Application of molecular modeling to determine the surface energy of mannitol**; *International journal of Pharmaceutics*; 343; 173-180.

Seppänen R., von Bahr M., Tiberg F., Zhmud B. (2004); **Surface energy characterization of AKD sized papers**; *Journal of Pulp and Paper Science*; 30(3); 70-73.

Sequera J. (1999); **Encolado superficial para hacer papeles más competitivos**; *El Papel*; Noviembre, 50-52.

Shakeri A., Tabar-Haidar K. (2004); **Surface characterization of pulp paper fibers using inverse gas chromatography**; *Iranian Polymer Journal*; 13(69); 471-478.

Shen W., Yao W., Li M., Parker I. (1998); **Characterization of eucalypt fibre surface using inverse gas chromatography and X-ray photoelectron spectroscopy**; *Appita Journal*; 51(29); 147-151.

Shen W., Parker I. H. (1999); **Surface composition and surface energetics of various eucalypt pulps**; *CELLULOSE*; 41-55.

Shen W., Filonanko Y., Truong Y., Parker I. H., Brack N., Pigram P., Liesegang J. (2000); **Contact angle measurement and surface energetics of sized and unsized paper**; *Colloids and Surfaces A: Physicochemical and Engineering Aspects*; 173; 117-126.

Sreekumar J., Sain M., Farnood R., Dougherty W. (2007); **Influence of styrene maleic anhydride imide on ink-jet print quality and coating structure**; *Nordic Pulp and Paper research Journal*; 22(3); 307-313.

Stout K.J., Sullivan P.J., Dong W.P., Mainsah E., Luo N., Mathia T., Zahouani H. (1993); **The development of methods for the characterization of roughness on three dimension**; Publication no. EUR 15178 EN of the Commission of the European Communities; Luxembourg.

Ström G. (2005); **Techniques to characterize surface energy - surface energy of papers**; *FPIRC Course n° 14*; Estocolmo; Setembro.

Svanholm E. (2004); **An experimental study of inkjet receptive coatings**; *Graduation Thesis*; Karlstad University.

Swain P., Lipowsky R. (1998); **Contact angles on heterogeneous surfaces: a new look at Cassie's and Wenzel's laws**; *Cornell university library* (<http://arxiv.org>);1-10.

T

Thomas T. R. (1998); **Rough Surfaces**; Imperial College Press; London.

TrueGage Surface Metrology (2008); **TrueMap v4 Help System**; URL: <http://www.truegage.com/help/TrueMap>.

Tze W. T., Gardner, D. J. (2001); **Contact angle and IGC measurements for probing surface-chemical changes in the recycling of wood pulp fibers**; *J. Adhesion Sci. Technology*; 15(2); 223-241.

U

Uhlmann P., Schneider S. (2002); **Acid-base and energy characterization of grafted polyethylene using inverse gas chromatography**; *Journal of Chromatography A*; 969; 73-80.

Ungh J., Nilson C-M., Verikas A. (2007); **Analysis of paper, print and press interaction from online measurements in a press room**; *Nordic Pulp and Paper Research Journal*; 22(3); 383-387.

URL 1: <http://www.pharmainfo.net/> (22.12.2008)

URL 2: <http://www.taylor-hobson.com/en/news-tutorials-publications/25/> (06.03.2009)

URL 3: <http://www.surfoptic.com/sirs%20measurement%20parameters.htm>

URL 4: <http://www.paperonweb.com/grade11.htm> (20.04.2009)

V

Varnell D. F. (1998); **Paper properties that influence ink-jet printing**; *Pulp & Paper Canada*; 99(4); 37-42.

Voelkel A., Strzemiecka B. (2007); **Characterization of fillers used in abrasive articles by means of inverse gas chromatography and principal component analysis**; *International Journal of Adhesion & Adhesives*; 27; 188-194.

Vyörykkä J (2005); **Confocal Raman Microscopy**; *FPIRC Course n° 14*; Estocolmo; Setembro 2005.

W

Wågberg L., Westerlind C. (2000); **Spreading of droplets of different liquids on specially structured papers**; *Nordic Pulp and Paper Research Journal*; 15(5); 598-606.

Wågberg L., Johansson P. (2002); **Characterization of paper surfaces using optical profilometry**; In: Borch J., Lyne M. B., Mark R. E., Habeger Jr. C. C. (book eds.); **Handbook of physical testing of paper**; Marcel Dekker Inc.; New York; 429-435.

Wålinder M. E. P., Gardner D. J. (2000); **Surface energy of extracted and non-extracted Norway spruce wood particles studied by inverse gas chromatography (IGC)**; *Wood and Fiber Science*; 32(4); 478-488.

Wang B., Sain M. (2007); **The effect of chemically coated nanofiber reinforcement on biopolymer based nanocomposites**; *BioResources*; 2(3); 371-388.

Wenzel R. N. (1936); **Resistance of solid surfaces to wetting by water**; *Industrial and Engineering Chemistry*; 28(8); 988-994.

Wenzel R. N. (1949); **Surface roughness and contact angle**; 1466-1467; DOI: 10.1021/j1547a015.

Y

Yang L., Fogden A., Pauler N., Sävborg Ö., Kruse B. (2005), **Anovel method for studying ink penetration of a print**; *Nordic Pulp and Paper Research Journal*; 20(4), 423-429.

FIGURES INDEX

Figure 1.1 - Trends in maximum operating speeds of paper machines (Paulapuro 2000).....	5
Figure 1.2 – Schematic representation of the production process for printing and writing papers.....	6
Figure 1.3 - Structure of starch and cellulose.	9
Figure 1.4 - Starch during cooking.	10
Figure 1.5 - Polymer-starch film formation on paper surface.....	11
Figure 1.6 – Schematic representation of a pond size press.....	11
Figure 1.7 – Schematic representation of a film size press.	12
Figure 1.8 - Schematic representation of flexography printing principle.....	15
Figure 1.9 – Schematic representation of rotogravure printing principle.....	15
Figure 1.10 - Schematic representation of offset printing principle.	16
Figure 2.1 – Schematic representation of the methodology used in this work.....	23
Figure 2.2 – Equipment used in the surface sizing process (a) picture; (b) schematic representation. The paper sheet is placed in the support table and secured with the sample holder, after, using a syringe, a straight line of sizing blend is manually spread in front of the applicator roll, with it in the start position (right in front of the sample holder) by pressing the start bottom on the control panel, the applicator roll spreads the sizing blend at the paper surface and the IR dryer dries it partially immediately after the application.....	25
Figure 2.3 – Mask used to evaluate inkjet printing quality.	30
Figure 3.1 – Example of the information available in a product datasheet.....	33
Figure 3.2 – Algorithm used for the determination of the monomers' proportion of each of the copolymers used.	35
Figure 3.3 – Schematic representation of the molecules' structure of the compound used in the surface sizing: (a) cationic starch; (b) Co-styrene-acrylate; (c) Co-styrene-maleic anhydride; (d) Co-acrylonitrile-acrylate; (e) Co-styrene-maleic anhydride; (f) Quaternary ditallow methyl epoxypropyl ammonium; (g) Methylated Melamine; (h) Co-styrene-	

dimethylaminopropylamine maleimide; (i) Co-styrene-butyl acrylate; (j) Co-styrene-acrylate; (k) Co-styrene-acrylate.....	37
Figure 4.1 – Different surface texture components (URL 2; URL 3).....	43
Figure 4.2 – Exemplification of the deviations from the reference plane for a given profile line (Gadelmawla et al. 2002).....	45
Figure 4.3 – Representation of the surface height deviations for a given profile line: (a) real values; (b) absolute values (Cohen 2006).....	46
Figure 4.4 – Typical surface structure, demonstrating peaks and valleys (Cohen 2006).....	47
Figure 4.5 - Exemplification of the peaks height and valleys depth measurement for a given profile line (Gadelmawla et al. 2002).....	48
Figure 4.6 – Example of a surface with an Sds value of 2600 peacks/mm ² (Cohen 2006).....	49
Figure 4.7 – Exemplification of the summits identification (Cohen 2006).....	49
Figure 4.8 – Exemplification of the differentiation between two samples with similar Sa using the Sdq values (Cohen 2006).....	50
Figure 4.9 - Principle of a contacting stylus instrument profilometer: A cantilever (1) is holding a small tip (2) that is sliding along the horizontal direction (3) over the object's surface (5). Following the profile the cantilever is moving vertically (4). The vertical position is recorded as the measured profile (6) shown in light green.....	52
Figure 4.10 – Schematic representation of the different types for reflection of the incident radiation.	53
Figure 4.11– Schematic representation of the optical profilometer used in this work (Ashori et al. 2008).....	54
Figure 4.12 – Exemplification of the 3D surface profile (topographic map) obtained from the profilometry measurements for one of the samples tested: (a) profile without any mathematical treatment; (b) profile after the leveling operation; (c) profile after form removal; (d) profile after filtering waviness and roughness; (e) final topographic profile, after thresholding.....	56
Figure 4.13 – Exemplification, for one of the samples tested, of all the parameters obtained from the profilometry measurements performed with Altisurf® 500.....	57
Figure 4.14 - Output obtained from each of the profilometry measurements. In this case, for sample St as an example.....	58
Figure 4.15 - PCA using the descriptive variables obtained by profilometry.....	59

Figure 4.16 - PCA using 7 of the descriptive variables.....	59
Figure 4.17 – Sa and values obtained for all the paper samples, divided according to the amount of surface sizing agent added; (a) Sa values for samples with 5% of surface sizing agent; (b) Sa values of the samples with 10% of surface sizing agent, (c) Sa values of the samples with 20% of surface sizing agent. Lines delimit the interval (based on ANOVA) in which the samples are not distinguishable from the St sample.....	61
Figure 4.18 – Influence of the surface sizing agent concentration in the Sa values; (a) surface sizing agent S1; (b) surface sizing agent S4, (c) surface sizing agent S5, (d) surface sizing agent S7.....	62
Figure 4.19 – Str values obtained for all the samples.	64
Figure 5.1 – Schematic representation of a penetrometer used in mercury intrusion porosimetry (URL1 2008). It is constituted by a small reservoir where the sample is placed and a long stem. All this is full of mercury at the lowest pressure. As pressure is increased, mercury penetrates into the sample pores (intrusion) and the length of penetrometer stem that is filled with mercury decreases. The difference in mercury level corresponds to the volume intruded in the sample.	69
Figure 5.2 – Mercury porosimeter AutoPore IV 9500.	70
Figure 5.3 - Differential (a) and cumulative (b) pore size distribution diagrams for sample St.....	72
Figure 5.4 – Differential (a) and cumulative (b) pore size distribution diagrams for samples St, StS6-05, StS6-10 and StS6-20.....	72
Figure 5.5 – Total porosity values obtained for all paper samples.	74
Figure 5.6 – Total porosity values, compared with sample St, of the samples (a) with 5% of surface sizing agent; (b) with 10% of Surface sizing agent; (c) with 20% of surface sizing agent. The dashed lines delimit the interval (based on ANOVA) in which the samples are not distinguishable from the St sample.....	74
Figure 6.1 – Schematic representation of paper-ink interaction.	79
Figure 6.2 – Contact angle formation on a solid surface according to the Young equation.....	80
Figure 6.3 – Representation of the possible wetting situations: (a) non wetting, (b) partial wetting and (c) complete wetting.....	80
Figure 6.4 – Equipment used for the contact angle measurement - OCA 20 from Dataphysics.	87

Figure 6.5 – Schematic representation of the surface roughness influence in contact angle values. .. 89

Figure 6.6 – Schematic representation of a drop on a rough surface according to Cassee model..... 90

Figure 6.7 - Schematic representation of a drop on a rough surface according to Wenzel. 90

Figure 6.8 - Comparison of the contact angle values before and after the application of the Wenzel correction for water (a) and diodomethane (b). 94

Figure 6.9 - Contact angle values with water, measured for the reference samples and the samples sized with the addition of 5% of synthetic surface sizing agent..... 95

Figure 6.10 – Influence of the amount of the sizing agent on the contact angle values measured with the liquids tested (water, formamide, ethilene glycol, propilene glycol and diodomethane). 96

Figure 6.11 - Graphical representation of the polar and dispersive components of the surface energy for the various samples tested. 98

Figure 6.12 – Normalized values (relative to the standard sample) of the total surface free energy (a), dispersive component (b) and polar component (c) of the paper samples..... 99

Figure 6.13 – Polar component of the surface free energy for all the samples tested. 100

Figure 6.14 - Variation of the water contact angle with the polar component of the surface energy. 102

Figure 6.15 – Water contact angle variation for sample St, normalized relatively to the initial value (t=0)..... 106

Figure 6.16 – Normalized (relatively to the initial values (t=0)) drop base diameters and drop volume values for sample St..... 106

Figure 6.17 – Normalized contact angle and normalized drop volume for sample StS4-05..... 107

Figure 6.18 – Normalized contact angle for samples sized with the synthetic surface sizing agent S2. 108

Figure 6.19 – Normalized drop base diameter and drop volume for the samples sized with the synthetic surface sizing agent S2..... 109

Figure 6.20 – Comparison of the normalized water contact angle values of the sizing agents S2 and S4 for the three different incorporation percentages (5%, 10% and 20%). 110

Figure 6.21 – Comparison of the normalized drop base diameter and drop volume for the samples sized with the synthetic surface sizing agents S2 and S4..... 110

Figure 6.22 - Normalized contact angle for samples sized with the synthetic surface sizing agent S9.	111
Figure 6.23 - Normalized drop base diameter and drop volume for the samples sized with the synthetic surface sizing agent S9.....	111
Figure 6.24 - Comparison of the normalized contact angle values at each incorporation percentage for the sizing agents S9 and S1.	112
Figure 7.1 – Schematic representation of conventional gas chromatography (GC) and inverse gas chromatography (IGC) analysis.....	117
Figure 7.2 – Schematic representation of the method used to calculate σ_s^D at a given temperature using IGC.....	121
Figure 7.3 - Schematic representation of the calculation method for the ΔH and the ΔS determination at a given temperatures using IGC.....	122
Figure 7.4 - Schematic representation of the calculation method for the K_a and K_b determination using IGC.....	123
Figure 7.5 – Gas chromatograph DANI GC1000, used in the IGC measurements.....	123
Figure 7.6 –Preparation of samples for IGC measurements: (a) pieces of a paper sample prepared to be packed into the IGC column; (b) Experimental assembly used for packing the columns; (c) IGC column packed and folded, ready to be introduced into the equipment.	124
Figure 7.7 – Exemplification of the output undertaken after the injection of a probe into the IGC column: peak obtained for sample St S3-10 after the injection of C7 at 45°C.....	126
Figure 7.8 – Retention times obtained at 35°C with the n-alkanes for the reference sample and for the samples with 10% of the different surface sizing agents.....	127
Figure 7.9 - Retention times obtained at 35°C with the polar probes for the reference sample and for the samples with 10% of the different surface sizing agents	128
Figure 7.10 –Relation between the retention time of the polar probes and their AN* values plotted for samples S1, S3, S5 and S7 at 45°C (the information is divided in two plots for easier visualization).....	128
Figure 7.11 – Effect of temperature on the retention times measured with the non-polar probes...	129
Figure 7.12 - Effect of temperature on the retention times measured with the polar probes.	129

Figure 7.13 - Effect of temperature on the retention times obtained with C9 for all the samples...130

Figure 7.14 - Effect of temperature in the retention times obtained with ETA for all the samples...130

Figure 7.15 – Influence of the temperature on the dispersive component of the surface free energy, for the samples sized with 5% incorporation of synthetic sizing agents (the straight line indicates the behavior of sample St).131

Figure 7.16 - Variation of σ_s^D with concentration and temperature for he samples sized with the surface sizing agents S2 and S4 (St sample is also included, as reference).....134

Figure 7.17 – Comparison of the σ_s^D values calculated from the contact angle measurements and from the extrapolation of the IGC data (based on the correlations of Table 7.2).....135

Figure 7.18 – Values σ_s^D (normalized relatively to the reference sample, St) determined for all the samples tested: (a) by contact angle method; (b) by IGC (using the regressions of Table 7.3).....136

Figure 7.19 – Values of Ka and Kb computed from the IGC measurements for the different sizing agents and different concentrations.137

Figure 8.1 – Example of (a) continuous and (b) Drop on Demand inkjet printers.....144

Figure 8.2 – Schematic representation of the continuous inkjet printing system.....144

Figure 8.3 - Schematic representation of the thermal inkjet DoD printing system.....145

Figure 8.4 - Schematic representation of the piezoelectric inkjet DoD printing system.....145

Figure 8.5 - Schematic representation of the light beams involved in the optical density measurement.148

Figure 8.6 – Representation of the CIELAB color space.149

Figure 8.7 - Exemplification of Gamut Area’s Graphic representation.150

Figure 8.8 – Exemplification of feathering of a printed area.150

Figure 8.9– Mask printed in the paper samples for the printing quality evaluation.....152

Figure 8.10 – PCA for all the printing quality parameters.....154

Figure 8.11 – PCA using 4 printing quality parameters.....154

Figure 8.12 – Optical density values achieved for black color. The lines delimit the range in which it is considered that the samples can not be clearly differentiated from the St sample.155

Figure 8.13 - Optical density values achieved for yellow color. The lines delimit the range in which it is considered that the samples can not be clearly differentiated from the St sample. 156

Figure 8.14 – Identification of the samples whose behavior in terms of black and yellow optical densities is improved by the addition of the synthetic surface sizing agents to the sizing formulation..... 157

Figure 8.15 – Gamut area values. The dashed line in the figure corresponds to the Gamut area value achieved for sample St. 157

Figure 8.16 – Gain values. The line in the figure refers to the value achieved for the St sample.... 158

Figure 8.17 – Results achieved from the numerical treatment of the subjective printing quality evaluation (the dashed line indicates the score of sample St)..... 159

TABLES INDEX

Table 1.1 – Classification of papers according to different criteria.....	5
Table 1.2 - Development of printing and other visualization methods.....	14
Table 2.1 – Compounds used in the surface sizing formulations.....	26
Table 2.2 – Characterization techniques used to characterize paper surface.	29
Table 3.1 – Elemental analysis results.....	36
Table 3.2 – Composition of the surface sizing agents.	36
Table 3.3 – Compounds Properties.	38
Table 4.1 – ANOVA results for the profilometry variables selected by PCA.....	60
Table 4.2 – Values of the roughness parameters S_p , S_v and S_{sk} obtained for the different paper samples.	63
Table 5.1 – Exemplification of the mercury porosimetry output, using samples St and StS4-20.....	71
Table 5.2 - ANOVA results for porosity.....	73
Table 6.1 – Summary of the theories presented for surface energy calculations based on contact angle measurements.....	85
Table 6.2 – Properties of the test liquids used in this work.	86
Table 6.3 – Drop volumes used for different liquids.	87
Table 6.4 – ANOVA of the contact angle results.	92
Table 6.5 – Values of the Sdr parameter (Appendix C) and of the corresponding correction factors, R , calculated for each sample using Equation 6.22.	93
Table 6.6 – Correlation between the polar component of the paper surface free energy and the contact angle for the different liquids tested.....	102

Table 6.7 - Extract of the dynamic contact angle result table obtained for sample StS4-05, indicating the drop age (Age), contact angle (CA), measurement error, base diameter (BD) and drop volume (Vol).	103
Table 6.8 – ANOVA results obtained for the wetting velocity values.....	104
Table 6.9 – Values of wetting velocity (WV) (Equation 7.23) obtained for each paper sample using water.	105
Table 7.1 – Properties of the probe molecules used*.	125
Table 7.2 – Experimental correlations obtained for the variation of σ_s^D with temperature for each of the paper samples tested and corresponding determination coefficient (r^2).....	132
Table 8.1 – Inkjet inks components.	146
Table 8.2 – ANOVA of printing quality parameters.	155
Table 8.3 – Variables considered for PLS models.	162
Table 8.4 – Groups of variables considered for PLS models.....	162
Table 8.5 – Results achieved by PLS models using the variables corresponding to the paper surface characterization presented in the previous chapters for the explanation of all the printing quality results, and for the printing quality results divided into two main groups, subjective evaluation and quantitative parameters.....	163
Table 8.6 – Results achieved by PLS models using the variables corresponding to the paper surface characterization presented in the previous chapters for the explanation of the quantitative quality results, divided in groups.	164

APPENDIX

APPENDIX A

DATASHEETS OF THE SYNTHETIC SURFACE SIZING AGENTS

Datasheet of S1 – Co-styrene-acrylate

Chemical Description	Chemische Basis	Styrene acrylate copolymer Styrol-Acrylat-Copolymer	
Ionicity	Ladungscharakter	Weakly anionic Schwach anionisch	
Solids	Feststoffgehalt	%	23,5–25,5
Form supplied	Lieferform	Aqueous polymer dispersion Wäßrige Polymerdispersion	
Density	Dichte	g/cm ³ (20 °C)	1,02–1,06
pH value (as supplied)	pH-Wert Lieferform)		4,0–6,0
Viscosity	Viskosität	mPa · s (Brookfield RV; spindle 1; 100 rpm; 20 °C (Brookfield RV; Spindel 1; 100 min ⁻¹ ; 20 °C)	< 30
Storage stability	Lagerbeständigkeit	12 months ex. works The product must be protected from freezing. 12 Monate ab Lieferung Werk Das Produkt muß frostfrei gelagert werden	
Recommended for	Haupteinsatzgebiete	Surface sizing agent for paper and board. Application in the size press with fluorescent whiteners. Surface coloring with anionic direct and acid dyestuffs as well as anionic color pigments. Oberflächenleimungsmittel für Papier und Karton. Leimpressenauftrag gemeinsam mit optischen Aufhellern. Oberflächenfärbung in Kombination mit anionisch-substantiven und sauren Farbstoffen sowie anionischen Farbpigmenten.	
Remarks	Bemerkungen	Notes on safety: see safety data sheet. Hinweise zur Sicherheit: siehe Sicherheitsdatenblatt.	

 Technical application

Surface sizing in the size press, film press or similar units.

Advantages of [redacted]

1. No need to adjust pH of the size press solution.
2. Effective on acid and neutral base papers; [redacted] does not require alum for sizing development.
3. Can be combined with anionic and nonionic auxiliaries.
4. Sizing is stable to alkaline liquids.
5. Low viscosity, easy to handle.
6. No unpleasant odour.
7. [redacted] does not impart wet strength to the paper allowing broke to be repulped without problem.

Surface sizing with [redacted] offers the following advantages over internal sizing:

1. Produces stronger paper, e.g. higher bursting strength and tensile strength.
2. Reduces dusting and picking.
3. Improvement in inkjet printability.
4. [redacted] does not effect the fluorescent properties of internally added fluorescent whitening agents. By reducing the amount of internal added rosin size (UV-absorber) in an acid sheet, the effectiveness of a FWA can be enhanced.
5. Improves the ageing resistance of papers.
6. Level of sizing can be corrected faster.
7. No deposits on paper machine felts, screens and white water.

 Technical notes on application

Mode of action

Application of [redacted] in the size press reduces the water absorption of the paper. The presence of aluminium ions in the base paper is not necessary for obtaining optimum results.

[redacted] is anionic and compatible with fluorescent whiteners, anionic direct and acid dyes. [redacted] can be applied together with these products in the size press.

The normal drying temperatures on the paper machine are sufficient to develop full sizing. No additional curing period is required.

 Technische Anwendungen

Oberflächenleimung in der Leimpresse, Filmpresse und ähnlichen Auftragsaggregaten.

[redacted] bietet folgende Vorteile:

1. Keine pH-Einstellung erforderlich.
2. Wirksam auf sauer und neutral gefahrenen Rohpapieren, ein Zusatz von Aluminiumsulfat ist nicht erforderlich.
3. Kombinierbar mit anionischen und nichtionogenen Hilfsmitteln.
4. Gegen alkalische Flüssigkeiten stabile Leimung.
5. Niedrige Viskosität, daher leichte Handhabung.
6. Keine Geruchsbelästigung.
7. [redacted] verleiht dem Papier keine Naßfestigkeit, daher problemlose Aufarbeitung des Ausschusses.

Im Vergleich zur Leimung in der Papiermasse bietet eine Oberflächenleimung mit [redacted] folgende Vorteile:

1. Höhere Papierfestigkeiten, z.B. Berst- und Reißfestigkeit.
2. Geringes Stauben und Rupfen.
3. Verbesserung der Inkjet-Druckbarkeit.
4. Einsparung von optischen Aufhellern durch Wegfall der UV-Absorption des Harzleims.
5. Bessere Alterungsbeständigkeit der Papiere.
6. Schnellere Korrektur des Leimungsgrades.
7. Keine Verschmutzung der Papiermaschinensiebe und -filze sowie der Abwässer.

 Technische Hinweise

Wirkungsweise

[redacted] – in der Leimpresse aufgetragen – setzt die Wasseraufnahme des Papiers herab. Zur Erzielung von optimalen Werten ist die Anwesenheit von Aluminiumionen im Rohpapier nicht notwendig.

Da [redacted] einen anionischen Charakter besitzt, ist es mit optischen Aufhellern, anionisch-substantiven und sauren Farbstoffen verträglich und kann mit diesen in der Leimpresse kombiniert werden.

Zur vollen Ausbildung der Leimung genügt die in der Papiermaschine übliche Trockentemperatur. Eine Nachreifung des Papiers ist nicht erforderlich.

Product description

Pre-sizing of base paper

Normally, the more absorbent the paper in the size press, the better the results achieved with [REDACTED]. Excessive pre-sizing in the stock can impair the performance of [REDACTED] by inhibiting penetration into the sheet.

If pick-up of the size press solution is too high, it can cause problems drying the sheet. This can normally be avoided by optimizing the level of internal sizing. Eg. additions of as low as 0.05–0.2 % rosin size to the stock reduce the wet pick-up in the size press allowing the paper to be dried after the size press without problems.

The normal fillers can be added to the base paper. Very good results are obtained with calcium carbonate fillers.

Amount required

The amount of [REDACTED] required depends on a number of factors such as the composition of the furnish, absorbency of the base paper and the degree of sizing required. Experience has shown that 0.2–0.8 % commercial product on dry weight of paper is generally sufficient.

Other additives

Since [REDACTED] is anionic, it can be precipitated by strongly cationic substances. However, adding cationic products internally to the stock does not impair [REDACTED] efficiency.

Temperature

[REDACTED] remains stable in the size press solution up to approx. 70 °C (160 °F). The size press solution should be cooled to below 70 °C (160 °F) before adding [REDACTED].

Produktbeschreibung

Vorleimung des Rohpapiers

Normalerweise wird man mit [REDACTED] einen um so besseren Effekt erzielen, je aufnahmefähiger das Papier ist, wenn es in die Leimpresse gelangt. Eine zu starke Vorleimung in der Papiermasse kann die Wirkung von [REDACTED] deutlich herabsetzen.

Eine zu hohe Flottenaufnahme in der Leimpresse, welche u.U. zu Schwierigkeiten mit der Kapazität der Nach Trockengruppe hinter der Leimpresse führen kann, läßt sich in den meisten Fällen durch eine geringe Masseleimung sehr gut verhindern. Schon Zusätze von z.B. 0,05–0,2 % Harzleim zur Papiermasse erniedrigen in den meisten Fällen die Naßaufnahme in der Leimpresse so weit, daß eine problemlose Trocknung möglich ist.

Im Rohpapier können die üblichen Füllstoffe eingesetzt werden. Mit Calciumcarbonat als Füllstoff erzielt man sehr gute Ergebnisse.

Zusatzmenge

Die benötigte Menge an [REDACTED] ist von verschiedenen Faktoren wie Rohstoffzusammensetzung, Aufnahmefähigkeit des Rohpapiers sowie dem geforderten Leimungsgrad abhängig. Wie die Erfahrung gezeigt hat, kommt man in den meisten Fällen mit 0,2–0,8 % Handelsware aus, bezogen auf das Gewicht des trockenen Papiers.

Andere Hilfsmittel

Da [REDACTED] ein anionisches Produkt ist, wird es durch kationische Substanzen ausgefällt. Zusätze kationischer Produkte zur Papiermasse stören den Leimungseffekt jedoch nicht.

Temperatur

[REDACTED] behält seine Stabilität in der Leimungsflotte bis ca. 70 °C. Vor Zusatz des Produktes sollte die Leimpresenflotte unter 70 °C abgekühlt werden.

Product description

Addition point

BAYSIZE S AGP can be added batch-wise at the starch solution storage tank as well as continuously in the operating tank or the feeding pipe to the size press.

is low-foaming, so defoamers are not normally required.

Guide formulation for application in the size press:



Guide formulation for gate-roll application:



Use in food packaging papers

is approved for use in food packaging papers and board under Recommendation XXXVI of the German Federal Institute for Consumer Health Protection and Veterinary Medicine (BgVV).

BAYSIZE S AGP is generally applied at the size press with a starch solution. A medium to low-viscosity nonionic or anionic starch is normally used. Since the type of starch can affect sizing to some extent, the efficiency of in combination with the size should be tested before use. Such tests can be performed in our technical service laboratories at any time. can also be applied without starch, i.e. simply diluted with water.

Produktbeschreibung

Zusatzstelle

kann sowohl diskontinuierlich in den Leimflottenvorratsbehälter als auch kontinuierlich in den Arbeitsbehälter oder die Leitung zur Leimpresse dosiert werden. ist schaumarm, so daß Entschäumer normalerweise nicht benötigt werden.

Beispiel für den Einsatz in der Leimpresse



Beispiel für den Einsatz am Gate-Roll:



Verwendung für Papiere zur Lebensmittelverpackung

ist nach Empfehlung XXXVI des Bundesamtes für gesundheitlichen Verbraucherschutz und Veterinärmedizin (BgVV) für Lebensmittelverpackungspapiere und -kartons zugelassen.

In der Regel wird zusammen mit einer Stärkelösung in der Leimpresse eingesetzt. Man verwendet gewöhnlich mittel- bis niedrigviskose, nichtionogene bzw. anionische Stärken. Da die Stärkeart in gewissem Umfang den Leimungseffekt beeinflussen kann, sollte die Wirksamkeit von in Kombination mit der Stärke vorher überprüft werden. Dies kann jederzeit in unserem anwendungstechnische Papierlabor durchgeführt werden. Der Einsatz von auch ohne Stärkeinsatz, d. h. nur mit Wasser verdünnt, ist ebenso möglich.

Datasheet of S2 – Co-styrene-maleic anhydride**1 - IDENTIFICACION DEL PRODUCTO Y DE LA SOCIEDAD**NOMBRE DEL PRODUCTO : 

PROVEEDOR O NOMBRE DE LA SOCIEDAD :

- NOMBRE :

- DIRECCION :

- TELEFONO :

- FAX :

- INTERNET :



APLICACIONES :
Tintas, pinturas y barnices, revestimientos.
Tratamiento de superficies (Papel).
Tratamiento del cuero

URGENCE / EMERGENCY / EMERGENCIA / NOTRUFNUMMER / N° 24/24 :

Pays / Countries / Países / Länder	Tel.
DK, FI, FR, DE, IE, IT, LU, NL, NO, PT, ES, SE, BE, GB	+800 76767600
AT, TR, CH, RO, BG, AL, BA, HR, HU, SI, YU, MK	+49 89 45560 321
BY, CZ, SK, EE, LV, LT, MD, RU, PL, UA	+420 2 2186 0618
GR	+30 2 10 42 96 678

2 - COMPOSICION/INFORMACION SOBRE LOS COMPONENTES

PREPARACION :

- NOMBRE QUIMICO O NOMBRE GENERICO :

STYRENE-MALEIMIDE COPOLYMER, ACETATE - AQUEOUS
SOLUTION

- COMPONENTES O IMPUREZAS QUE CONTRIBUYEN A LOS PELIGROS :

STYRENE-MALEIMIDE COPOLYMER, ACETATE

Símbolo	Oración R	Oración S	N° Index	N° CAS
Xi	R 38	S 26		
	R 41	S 28		
		S37/39		

% de concentración: ~ 25 %

Acetic acid

Simbolo	Oración R	Oración S	N° Index	N° CAS
C	R 10	S 23	607-002-00-6	64-19-7
	R 35	S 26		
		S 45		

% de concentración: < 5 %

3 - IDENTIFICACION DE LOS PELIGROS

EFFECTOS SOBRE LA SALUD : Irita la piel (R38).
Riesgo de lesiones oculares graves (R41).

PELIGROS FISICOS Y QUIMICOS : Productos de descomposición térmica tóxicos.

4 - PRIMEROS AUXILIOS

INHALACION : Retirar al sujeto de la zona contaminada. Hacerle respirar aire fresco.

CONTACTO CON LA PIEL : Retirar las ropas ensuciadas.
Lavar con agua jabonosa y enjuagar con agua.

CONTACTO CON LOS OJOS : En caso de contacto con los ojos, lávense inmediata y abundantemente con agua y acúdase a un médico.

INGESTION : No inducir al vómito, llamar inmediatamente a un médico.

5 - MEDIDAS DE LUCHA CONTRA INCENDIOS

MEDIOS DE EXTINCION :

- RECOMENDADOS : Polvo, espuma, agua pulverizada, nieve carbónica.

- CONTRAINDICADOS : Chorro de agua.

PELIGROS ESPECIFICOS : En caso de incendio y/o explosión no respire los humos.
Riesgo de formación de productos tóxicos en caso de incendio.
Suprimir los puntos calientes.
Alejar los contenedores.

PROTECCION DE LOS PARTICIPANTES : Llevar aparato respiratorio autónomo.
Usar indumentaria adecuada, guantes y aparato de protección para los ojos/la cara.

6 - MEDIDAS A TOMAR EN CASO DE DISPERSION ACCIDENTAL

PRECAUCIONES INDIVIDUALES : Usar equipos de protección (sección 8).

PRECAUCIONES PARA LA PROTECCION DEL MEDIO AMBIENTE : Evitar verter en las alcantarillas.
No dejar que el producto se incorpore al medio ambiente.

METODOS DE LIMPIEZA :

-
- RECUPERACION : Contener el derrame.
Recuperar el producto mediante fijación con absorbente (arena, tierra, vermiculita).
Recuperar el producto en un recipiente para destrucción posterior.
- ELIMINACION : Incineración en instalación autorizada.
-

7 - MANIPULACION Y ALMACENAMIENTO

MANIPULACION :

- PREVENCIÓN DE LA EXPOSICIÓN DE LOS TRABAJADORES :
- Utilizar únicamente en lugares bien ventilados.
 - En caso de ventilación insuficiente, utilizar un equipo respiratorio adecuado.
 - Evitese el contacto con la piel y los ojos.
 - No comer, ni beber, ni fumar durante su utilización.
- PREVENCIÓN DE INCENDIOS Y EXPLOSIONES :
- Evitar almacenar durante largos periodos.

ALMACENAMIENTO :

- CONDICIONES DE ALMACENAMIENTO :

- RECOMENDADOS :
- Conservar únicamente en el recipiente de origen.
 - Almacenar al abrigo del hielo.
 - Almacenar al abrigo del sol.
 - Conservar alejado del calor.

- MATERIAS INCOMPATIBLES :
- Bases.
 - Oxidantes fuertes.

- MATERIALES DE EMBALAJE :

- RECOMENDADOS :
- Toneles de acero pintados y revestidos en el interior con resina fenólica.
 - Toneles de acero doblados de polietileno.
 - Polietileno.

- NO ACONSEJADOS :
- Hierro.
 - Cobre.
-

8 - CONTROLES DE LA EXPOSICIÓN/PROTECCIÓN INDIVIDUAL

VALORES LIMITES (VLE, VME, ETC.):

- Nombre del producto : Acetic acid

8 horas (VME)	8 horas (VME)	Periodo corto (VLE)	Periodo corto (VLE)	De conformidad a
ppm	mg/m ³	ppm	mg/m ³	
		10	25	FR (INRS 1989)

EQUIPAMIENTO DE PROTECCIÓN INDIVIDUAL :

- PROTECCIÓN RESPIRATORIA : En caso de ventilación insuficiente, utilizar un equipo respiratorio adecuado.

- PROTECCIÓN DE LAS MANOS :	No usar guantes de latex natural. Productos sin solventes añadidos : usar guantes de nitrilo. Productos combinados con solventes : usar guantes gruesos (>0.5 mm) de nitrilo. Reemplazar inmediatamente los guantes en caso de rotura o de cambio de aspecto (dimensiones, color, flexibilidad, etc).
- PROTECCION DE LOS OJOS :	Llevar una máscara facial o gafas. Evitar lentes de contacto.
OTROS :	Buena ventilación. Tomar una ducha al final del trabajo. Instalación de fuentes oculares.

9 - PROPIEDADES FISICAS Y QUIMICAS

ASPECTO :

- ESTADO FISICO :	Líquido.
- COLOR :	Amarillo
- OLOR :	Con un olor característico.
- pH :	4-6

TEMPERATURAS ESPECIFICAS :

- PUNTO O RANGO DE EBULLICION :	90°C
---------------------------------	------

RIESGO DE INCENDIO O EXPLOSION :

- PUNTO DE INFLAMACION :	> 90°C
- TEMPERATURA DE AUTOINFLAMACION :	Acetic acid : 427°C

- LIMITES DE EXPLOSIVIDAD O DE INFLAMABILIDAD EN EL AIRE :

Baja	Alta
5.4 %	16 % @ 100°C (Acetic acid)

PRESION DE VAPOR : Acetic acid : 2.7 kPa (30°C)

DENSIDAD :

-

SOLUBILIDAD :

- EN EL AGUA : Soluble en el agua.

- EN LOS SOLVENTES ORGANICOS :

-

VISCOSIDAD : < 500 mPa.s (30 °C)

10 - ESTABILIDAD Y REACTIVIDAD

ESTABILIDAD : Estable en condiciones normales de almacenamiento (sección 7).

PRODUCTOS DE DESCOMPOSICION PELIGROSOS :

Por descomposicion térmica, riesgo de formación de :
Vapores ácidos, monóxido de carbono y dióxido de carbono.
Sustancias tóxicas.

REACCIONES PELIGROSAS CON : Oxidantes fuertes.
Bases concentradas.

11 - INFORMACIONES TOXICOLOGICAS

IRRITACION CUTANEA : Irrita la piel (R36).
IRRITACION OCULAR : Riesgo de lesiones oculares graves (R41).
INHALACION : Puede causar una irritación de las vías respiratorias.

12 - INFORMACIONES ECOLOGICAS

IMPACTO POSIBLE SOBRE EL MEDIO AMBIENTE / ECOTOXICIDAD :
No verter en alcantarillas o en el medio ambiente. Se debe eliminar
en un punto autorizado de recogida de residuos.

13 - CONSIDERACIONES RELATIVAS A LA ELIMINACION

MEDIDAS DE DESTRUCCION : Incineración en instalación autorizada.
PROCEDIMIENTO DE DESTRUCCION DEL EMBALAJE CONTAMINADO :
El embalaje limpio puede ser reciclado.

14 - INFORMACIONES RELATIVAS AL TRANSPORTE

REGLAMENTACION INTERNACIONAL :
Este producto no ha sido reglamentado.

15 - INFORMACIONES REGLAMENTARIAS

REGLAMENTACIONES COMUNITARIAS (CE) :
Directiva 91/155/CEE modificada por la Directiva 93/112/CEE y por
Directiva 2001/58/CE : Fichas de datos de seguridad.

- ETIQUETADO CE : Dir. 2001/59/CE : 28a adaptación de la Directiva 67/548/CE, JOCE
del 21/08/2001, n° L 225.
Directiva 1999/45/EC - OJEC L200 - 30/07/99.
Preparados peligrosos : Directiva 99/45 modificada por Directiva
2001/60/CE - OJEC L228 - 22/08/2001.

Frasas R : R 38 - Irrita la piel.
R 41 - Riesgo de lesiones oculares graves.

Frasas S : S 26 - En caso de contacto con los ojos, lávense inmediata y
abundantemente con agua y acúdase a un médico.
S 28
En caso de contacto con la piel, lávase inmediata y
abundantemente con agua jabonosa.
S37/39 : Usen guantes adecuados y protección para los ojos/la
cara.

Símbolos : XI - Irritante

16 - OTRAS INFORMACIONES

OTROS :

APLICACIONES :
Ver sección 1.
De conformidad con lo dispuesto en la Directiva 2001/58/CE, el texto integral de las frases de riesgo (frases R) a las que se refiere el apartado 2 se indica a continuación:
Inflamable (R10).
Provoca quemaduras graves (R35).
Irrita la piel (R38).
Riesgo de lesiones oculares graves (R41).

Esta ficha completa la información técnica de utilización, pero no la reemplaza. Las informaciones que contiene se basan en el estado de nuestros conocimientos relativos al producto concernido con fecha del : 03 09 2003 .

Datasheet of S3 – Co-styrene-acrylate

2. Composition/information on ingredients

C.A.S. Number	Content (W/W)	Chemical name
7732-18-5	>= 64.0 - <= 66.0 %	Water
64-19-7	<= 1.5 %	acetic acid
	7.0 %	Trade Secret
	27.0 %	Trade Secret
50-00-0	0.1 %	Formaldehyde

3. Hazard identification

Emergency overview

WARNING: MAY CAUSE EYE, SKIN AND RESPIRATORY TRACT IRRITATION.
 INGESTION MAY CAUSE GASTRIC DISTURBANCES.
 MAY CAUSE PULMONARY EDEMA.

Potential health effects

Primary routes of exposure

Routes of entry for solids and liquids include eye and skin contact, ingestion and inhalation. Routes of entry for gases include inhalation and eye contact. Skin contact may be a route of entry for liquified gases.

Irritation:

Contact may result in eye irritation. Contact may result in skin irritation. Ingestion may cause irritation of the gastrointestinal tract. Irritating to respiratory system.

4. First-aid measures

General advice:

Remove contaminated clothing.

If inhaled:

Remove the affected individual into fresh air and keep the person calm. Assist in breathing if necessary. Immediate medical attention required.

If on skin:

Wash affected areas thoroughly with soap and water. If irritation develops, seek medical attention.

If in eyes:

Flush with copious amounts of water for at least 15 minutes. If irritation develops, seek medical attention.

5. Fire-fighting measures

Flash point: approx. > 100 °C (DIN 51758)

Suitable extinguishing media:
water fog, foam, dry extinguishing media

Protective equipment for fire-fighting:
Firefighters should be equipped with self-contained breathing apparatus and turn-out gear.

6. Accidental release measures

Environmental precautions:
This product is regulated by CERCLA ("Superfund").

Cleanup:
Spills should be contained, solidified, and placed in suitable containers for disposal.

7. Handling and storage

Handling

General advice:
Ensure thorough ventilation of stores and work areas.

Storage

General advice:
Keep container tightly closed and dry; store in a cool place.
Store protected against freezing.

Storage stability:
Storage temperature: 5 - 30 °C

Temperature tolerance
Protect from temperatures below: 5 °C
Protect from temperatures above: 30 °C

8. Exposure controls and personal protection

Components with workplace control parameters

acetic acid	OSHA	PEL 10 ppm 25 mg/m ³ ;
	ACGIH	TWA value 10 ppm ; STEL value 15 ppm ;
Formaldehyde	OSHA	TWA value 0.75 ppm ; STEL value 2 ppm ; OSHA_ACT
		0.5 ppm ;
	ACGIH	CLV 0.3 ppm ;

Respiratory protection:

Wear a N10 SH-certified (or equivalent) organic vapour/particulate respirator as needed.

Hand protection:

Chemical resistant protective gloves

Eye protection:

Tightly fitting safety goggles (chemical goggles). Wear face shield if splashing hazard exists.

General safety and hygiene measures:

Do not inhale gases/vapours/aerosols. Handle in accordance with good industrial hygiene and safety practice. Hands and/or face should be washed before breaks and at the end of the shift. Avoid contact with skin and eyes.

9. Physical and chemical properties

Form:	liquid	
Odour:	product specific	
Colour:	milky white	
pH value:	3.5	(20 °C) (DIN/ISO 976)
<i>Information on: water</i> solidification temperature:	0 °C	
.....		
:	100 °C	
<i>Information on: water</i> boiling temperature:	100 °C	(1,000 h Pa)
.....		
<i>Information on: water</i> Vapour pressure:	23 mbar	(20 °C)
.....		
Density:	1.0 g/cm ³	(20 °C)
Viscosity, dynamic:	40 mPa.s	(20 °C) (ISO 2555)
Miscibility with water:		miscible

10. Stability and reactivity

Conditions to avoid:

No conditions known that should be avoided.

Substances to avoid:

No substances known that should be avoided.

Hazardous reactions:

The product is chemically stable.

Decomposition products:

Hazardous decomposition products: carbon monoxide, Carbon dioxide, hydrocarbons

Corrosion to metals:

No corrosive effect on metal.

Oral:

LD50/rat: > 2,000 - 10,000 mg/kg

The product has not been tested. The statement has been derived from products of a similar structure and composition.

Skin irritation:

rabbit: non-irritant (OECD Guideline 404)

Eye irritation:

rabbit: non-irritant (OECD Guideline 405)

Chronic toxicity

Other information:

Based on our experience and the information available, no adverse health effects are expected if handled as recommended with suitable precautions for designated uses.

12. Ecological information

Environmental fate and transport

Biodegradation:

Test method: OECD 302B; ISO 9888; 88/302/EEC, part C

Method of analysis: DOC reduction

Degree of elimination: > 70 %

Evaluation: Easily eliminated from water.

The product can be virtually eliminated from water by abiotic processes

e.g. adsorption onto activated sludge.

The product has not been tested. The statement has been derived from products of a similar structure and composition.

Bioaccumulation:

Based on its structural properties, the polymer is not biologically available. Accumulation in organisms is not to be expected.

Environmental toxicity

Acute and prolonged toxicity to fish:

OECD Guide-line 203 static

zebra fish/LC50 (96 h): > 100 mg/l

Acute toxicity to aquatic invertebrates:

OECD Guideline 202, part 1 static

Daphnia magna/EC50 (48 h): > 100 mg/l

The product has not been tested. The statement has been derived from products of a similar structure and composition.

Toxicity to aquatic plants:

0 EC Directive 201 green algae/EC50 (72 h): > 100 mg/l

Nominal concentration. The product has not been tested. The statement has been derived from products of a similar structure and composition.

Toxicity to microorganisms:

DIN/EN/ISO 8192-0/EC Directive 209-88/302/EEC, P. C activated sludge, domestic/EC20 (0.5 h): > 100 mg/l

The product has not been tested. The statement has been derived from products of a similar structure and composition.

:

The inhibition of the degradation activity of activated sludge is not anticipated when introduced to biological treatment plants in appropriate low concentrations.

Other ecotoxicological advice:

Do not release untreated into natural waters. At the present state of knowledge, no negative ecological effects are expected.

13. Disposal considerations**Waste disposal of substance:**

Incinerate or dispose of in a licensed facility.

Do not discharge into drains/surface waters/groundwater.

Contaminated packaging:

Dispose of in a licensed facility. Recommend crushing, puncturing or other means to prevent unauthorized use of used containers.

14. Transport information

Reference Bill of Lading

15. Regulatory informationFederal Regulations

Registration status:

TSCA, US released / listed

State regulations

State RTK

<u>CAS Number</u>	<u>Chemical name</u>	<u>State RTK</u>
7732-18-5	Water	NJ, PA, MA
64-19-7	acetic acid	MA, NJ, PA
	Trade Secret	NJ, PA, MA
	Trade Secret	NJ, PA, MA
50-00-0	Formaldehyde	MA, NJ, PA

CA Prop. 65:

THIS PRODUCT CONTAINS A CHEMICAL(S) KNOWN TO THE STATE OF CALIFORNIA TO CAUSE CANCER.

Datasheet of S4 – Co-styrene-maleic anhydride**1 - IDENTIFICACION DEL PRODUCTO Y DE LA SOCIEDAD**NOMBRE DEL PRODUCTO : 

PROVEEDOR O NOMBRE DE LA SOCIEDAD :

- NOMBRE :

- DIRECCION :

- TELEFONO :

- FAX :

- INTERNET :

APLICACIONES :

Tratamiento de superficies (Papel).

Tratamiento del cuero

Tintas, pinturas y barnices, revestimientos, ceras para suelos, detergentes.

URGENCE / EMERGENCY / EMERGENCIA / NOTRUFNUMMER / N° 24/24 :

Pays / Countries / Países / Länder	Tel.
DK, FI, FR, DE, IE, IT, LU, NL, NO, PT, ES, SE, BE, GB	+800 76767600
AT, TR, CH, RO, BG, AL, BA, HR, HU, SI, YU, MK	+49 89 45560 321
BY, CZ, SK, EE, LV, LT, MD, RU, PL, UA	+420 2 2186 0618
GR	+30 2 10 42 96 678

2 - COMPOSICION/INFORMACION SOBRE LOS COMPONENTES

PREPARACION :

- NOMBRE QUIMICO O NOMBRE GENERICO :

ESTERIFIED STYRENE-MALEIC ANHYDRIDE COPOLYMER,
AMMONIUM SALT - AQUEOUS SOLUTION

- OTROS :

Polímero : ~ 15 % en masa

3 - IDENTIFICACION DE LOS PELIGROSPELIGROS FISICOS Y QUIMICOS : Productos de descomposición térmica tóxicos.
No fácilmente biodegradable**4 - PRIMEROS AUXILIOS**

INHALACION :

Retirar al sujeto de la zona contaminada. Hacerle respirar aire fresco.

CONTACTO CON LA PIEL :

Retirar las ropas ensuciadas.
Lavar con agua jabonosa y enjuagar con agua.

INGESTION : No inducir al vómito, llamar inmediatamente a un médico.

5 - MEDIDAS DE LUCHA CONTRA INCENDIOS

MEDIOS DE EXTINCION :

- RECOMENDADOS : Polvo, espuma, agua pulverizada, nieve carbónica.

- CONTRAINDICADOS : Chorro de agua.

PELIGROS ESPECIFICOS : En caso de incendio y/o explosión no respire los humos.
Riesgo de formación de productos tóxicos en caso de incendio.
Suprimir los puntos calientes.
Enfriar el recipiente con agua pulverizada.

PROTECCION DE LOS PARTICIPANTES :

Llevar aparato respiratorio autónomo.
Usar indumentaria adecuada, guantes y aparato de protección para los ojos/la cara.

6 - MEDIDAS A TOMAR EN CASO DE DISPERSION ACCIDENTAL

PRECAUCIONES INDIVIDUALES : Usar equipos de protección (sección 8).

PRECAUCIONES PARA LA PROTECCION DEL MEDIO AMBIENTE : Evitar verter en las alcantarillas.
No dejar que el producto se incorpore al medio ambiente.

METODOS DE LIMPIEZA :

- RECUPERACION : Contener el derrame.
Recuperar el producto mediante fijación con absorbente (arena, tierra, vermiculita).
Recuperar el producto en un recipiente para destrucción posterior.

- ELIMINACION : Incineración en instalación autorizada.

7 - MANIPULACION Y ALMACENAMIENTO

MANIPULACION :

- PREVENCION DE LA EXPOSICION DE LOS TRABAJADORES : Utilizar únicamente en lugares bien ventilados.
En caso de ventilación insuficiente, utilizar un equipo respiratorio adecuado.
Evitese el contacto con la piel y los ojos.
No comer, ni beber, ni fumar durante su utilización.

ALMACENAMIENTO : Evitar almacenar durante largos periodos.

- CONDICIONES DE ALMACENAMIENTO :

RECOMENDADOS : Conservar el recipiente en lugar fresco y bien ventilado.
Almacenar al abrigo del sol o de cualquier fuente de ignición.
Conservar alejado del calor.
Almacenar al abrigo del hielo.

- MATERIAS INCOMPATIBLES :	Acidos Oxidantes fuertes.
- MATERIALES DE EMBALAJE :	
RECOMENDADOS :	Toneles de plástico. Vidrio.
NO ACONSEJADOS :	Hierro, acero, aluminio.

8 - CONTROLES DE LA EXPOSICION/PROTECCION INDIVIDUAL

EQUIPAMIENTO DE PROTECCION INDIVIDUAL :

- PROTECCION RESPIRATORIA :	En caso de ventilación insuficiente, utilizar un equipo respiratorio adecuado.
- PROTECCION DE LAS MANOS :	No usar guantes de latex natural. Productos sin solventes añadidos : usar guantes de nitrilo. Productos combinados con solventes : usar guantes gruesos (>0.5 mm) de nitrilo. Reemplazar inmediatamente los guantes en caso de rotura o de cambio de aspecto (dimensiones, color, flexibilidad, etc).
- PROTECCION DE LOS OJOS :	Llevar una máscara facial o gafas. Evitar lentes de contacto.
OTROS :	Buena ventilación. Tomar una ducha al final del trabajo. Instalación de fuentes oculares.

9 - PROPIEDADES FISICAS Y QUIMICAS

ASPECTO :

- ESTADO FISICO :	Líquido.
- COLOR :	Amarillo
- OLOR :	Ammoniaco
- pH :	8.5 - 9.5
DENSIDAD :	1050 kg/m ³
SOLUBILIDAD :	
- EN EL AGUA :	Soluble en el agua.
VISCOSIDAD :	< 500 mPa.s (30°C)

10 - ESTABILIDAD Y REACTIVIDAD

ESTABILIDAD : Estable en condiciones normales de almacenamiento (sección 7).

PRODUCTOS DE DESCOMPOSICION PELIGROSOS :

Por descomposición térmica, riesgo de formación de :
Vapores ácidos, monóxido de carbono y dióxido de carbono.
Sustancias tóxicas.
Amoniaco.

Datasheet of S6 – Methylated Melamine**Product Specifications**

<i>Property</i>	<i>Value</i>
Solids, %	78.0 ± 2.0
Viscosity (25°C), mPa.s	600-900
Appearance	Clear liquid
pH (50% with water)	8.5-9.6

Technical Data

	<i>Typical value</i>
Specific gravity (20°C) g/ml	1.24-1.28
Shelf life (20-25°C)	about 6 months
Dilutability with water	in any proportion

Note

The information and statements herein are believed to be reliable, but are not to be construed as a warranty or representation for which we assume legal responsibility. Users should undertake sufficient verification and testing to determine the suitability for their particular purpose of any information on products referred to herein.

Datasheet of S7 – Co-styrene-dimethylaminopropylamine maleimide**1 - IDENTIFICACION DEL PRODUCTO Y DE LA SOCIEDAD**NOMBRE DEL PRODUCTO : 

PROVEEDOR O NOMBRE DE LA SOCIEDAD :

- NOMBRE :

- DIRECCION :

- TELEFONO :

- FAX :

- INTERNET :

APLICACIONES :

Tintas, pinturas y barnices, revestimientos.

Tratamiento de superficies (Papel).

Tratamiento del cuero

URGENGE / EMERGENCY / EMERGENCIA / NOTRUFNUMMER / N° 24/24 :

Pays / Countries / Países / Länder	Tel.
DK, FI, FR, DE, IE, IT, LU, NL, NO, PT, ES, SE, BE, GB	+800 76767600
AT, TR, CH, RO, BG, AL, BA, HR, HU, SI, YU, MK	+49 89 45580 321
BY, CZ, SK, EE, LV, LT, MD, RU, PL, UA	+420 2 2186 0618
GR	+30 2 10 42 96 678

2 - COMPOSICION/INFORMACION SOBRE LOS COMPONENTES

SUBSTANCIA :

- NOMBRE QUIMICO O NOMBRE GENERICO :

STYRENE-MALEIMIDE COPOLYMER

3 - IDENTIFICACION DE LOS PELIGROS

EFECTOS SOBRE LA SALUD : Riesgo de lesiones oculares graves (R41).

PELIGROS FISICOS Y QUIMICOS : La mezcla de polvos y de aire puede ser explosiva.
Productos de descomposición térmica tóxicos.**4 - PRIMEROS AUXILIOS**

INHALACION : Retirar al sujeto de la zona contaminada. Hacerle respirar aire fresco.

CONTACTO CON LA PIEL : Retirar las ropas ensuciadas.
Lavar con agua jabonosa y enjuagar con agua.

CONTACTO CON LOS OJOS :	En caso de contacto con los ojos, lavar inmediata y abundantemente con agua y acudir a un médico.
INGESTION :	No inducir al vómito, llamar inmediatamente a un médico.

5 - MEDIDAS DE LUCHA CONTRA INCENDIOS

MEDIOS DE EXTINCION :

- RECOMENDADOS : Polvo, espuma, agua pulverizada, nieve carbónica.

- CONTRAINDICADOS : Chorro de agua.

PELIGROS ESPECIFICOS : En caso de incendio y/o explosión no respire los humos.
Riesgo de formación de productos tóxicos en caso de incendio.
Suprimir los puntos calientes.
Alejar los contenedores.

PROTECCION DE LOS PARTICIPANTES :

Llevar aparato respiratorio autónomo.
Usar indumentaria adecuada, guantes y aparato de protección para los ojos/la cara.

6 - MEDIDAS A TOMAR EN CASO DE DISPERSION ACCIDENTAL

PRECAUCIONES INDIVIDUALES : Usar equipos de protección (sección 8).

PRECAUCIONES PARA LA PROTECCION DEL MEDIO AMBIENTE :
Evitar verter en las alcantarillas.
No dejar que el producto se incorpore al medio ambiente.

METODOS DE LIMPIEZA :

- RECUPERACION : Contener el derrame.
Recuperar el producto mediante aspiración.
Recuperar el producto en un recipiente para destrucción posterior.

- ELIMINACION : Incineración en instalación autorizada.

7 - MANIPULACION Y ALMACENAMIENTO

MANIPULACION : Manipular evitando las liberaciones de polvo.
Trasvasar bajo presión de nitrógeno.

- PREVENCION DE LA EXPOSICION DE LOS TRABAJADORES :
Utilizar únicamente en lugares bien ventilados.
En caso de ventilación insuficiente, utilizar un equipo respiratorio adecuado.
Evítese el contacto con la piel y los ojos.
No comer, ni beber, ni fumar durante su utilización.

ALMACENAMIENTO : Evitar almacenar durante largos períodos.
Puesta a tierra de las instalaciones.

- CONDICIONES DE ALMACENAMIENTO :

RECOMENDADOS : Mantener el recipiente bien cerrado y en lugar seco.
Almacenar al abrigo del sol o de cualquier fuente de ignición.
Conservar alejado del calor.

A EVITAR :	Evitar la acumulación de cargas electrostáticas.
- MATERIAS INCOMPATIBLES :	Bases. Oxidantes fuertes.
- MATERIALES DE EMBALAJE :	
RECOMENDADOS :	Sacos de papel. Barriles de cartón.
NO ACONSEJADOS :	Hierro.

8 - CONTROLES DE LA EXPOSICION/PROTECCION INDIVIDUAL

Control de la atmósfera (polvo inhalable : 10 mg/m³).

EQUIPAMIENTO DE PROTECCION INDIVIDUAL :

- PROTECCION RESPIRATORIA :	Llevar máscara contra polvo.
- PROTECCION DE LAS MANOS :	No usar guantes de latex natural. Productos sin solventes añadidos : usar guantes de nitrilo. Productos combinados con solventes : usar guantes gruesos (>0.5 mm) de nitrilo. Reemplazar inmediatamente los guantes en caso de rotura o de cambio de aspecto (dimensiones, color, flexibilidad, etc).
- PROTECCION DE LOS OJOS :	Llevar una máscara facial o gafas. Evitar lentes de contacto.
OTROS :	Buena ventilación. Tomar una ducha al final del trabajo. Instalación de fuentes oculares.

9 - PROPIEDADES FISICAS Y QUIMICAS

ASPECTO :

- ESTADO FISICO :	Escamas
- COLOR :	Amarillo
- OLOR :	Aminas
- pH :	-
RIESGO DE INCENDIO O EXPLOSION :	
- PUNTO DE INFLAMACION :	
DENSIDAD :	1300 kg/m ³
SOLUBILIDAD :	
- EN EL AGUA :	Insoluble en el agua.
- EN LOS SOLVENTES ORGANICOS :	Soluble en : Cetonas (Acetona, Metilacetona, Metilisobutilcetona) : > 50 g/100 ml (30°C) Eter (Tetrahidrofurano, Dioxano) : > 50 g/100 ml (30°C)
VISCOSIDAD :	No aplicable.

Datasheet of S8 – Co-styrene-butyl acrylate

*1. Identificação da substância/preparação e da sociedade/empresa

[REDACTED]

Uso:
Auxiliar para papel

[REDACTED]

2. Composição/informação sobre os componentes

Copolimerizado de ésteres acrílicos/acrilato de butilo/estireno, preparação aquosa, contém

ácido acético
% em peso: 3-9
N° CAS: 64-19-7
símbolo de perigo: C
frases R: 10-35

[REDACTED]

3. Identificação de perigos

See indicação de perigo.

4. Primeiros socorros

Após inalação de aerossol/vapor/poeiras: Levar o sinistrado para o ar livre; é necessário assistência médica no caso de dificuldades de respiração.

Contacto da pele: lavar com água abundante, sabão ou outros produtos apropriados.

Contacto com os olhos: Em caso de contacto com os olhos, lavá-los com as pálpebras abertas com água abundante. Em seguida, consultar eventualmente um médico (oftalmologista).

Após ingestão: Enxaguar a buca com muita água. NÃO fazer vomitar, é necessário assistência médica.

5. Medidas de combate a incêndios

Produto extintor: névoa de água, espuma, extintor seco, CO₂

No combate ao incêndio, usar aparelho respiratório com admissão de ar independente do ambiente.

6. Medidas a tomar em caso de fugas acidentais

Recolher com material absorvente e deitar em recipientes que possam ser fechados.

***7. Manuseamento e armazenagem**

Mantém o recipiente bem fechado em local bem ventilado.
Evitar aquecimento superior a 40 °C e arrefecimento inferior a 0 °C.

- sensível a congelamento -

Classe de armazenagem VCI: 12

Tempo de armazenagem 6 meses.

***8. Controlo da exposição/protecção individual**

Com respeito ao controlo da exposição ver Capítulo 15.

Protecção dos olhos: Óculos de protecção herméticos.
Protecção das mãos: utilizar luvas de protecção apropriadas (p.ex. Policlórepreno - CR). Após contaminação pelo produto, mudar imediatamente as luvas e eliminá-las correctamente.

Evitar o contacto com a pele e a inalação de vapores. Cuidar de uma boa aspiração durante a aplicação e de uma ventilação suficiente dos recintos de trabalho.

Mantém afastado de bebidas e produtos alimentares.

Não comer, beber ou fumar durante o trabalho.

Retirar imediatamente todo o vestuário contaminado.

Antes dos intervalos e no fim do trabalho lavar as mãos e utilizar um creme de protecção

9. Propriedades físicas e químicas		método de ensaio
Forma:	líquido	
Cor:	branco até cor-de-rosa	
Cheiro:	cheiro fraco	
Temperatura de ebulição:	a partir de 100 °C	
Densidade:	1,0-1,05 g/cm ³	
Pressão do vapor:	23 mbar a 20 °C	
	123 mbar a 50 °C	
Viscosidade:	< 50 mPa·s a 23 °C	
Solubilidade em água:	miscível	
pH:	3,0-4,0	
Ponto de inflamação:	não inferior a 100 °C	DIN 51758

10. Estabilidade e reactividade

Decomposição-térmica: Não se verifica decomposição térmica no caso de armazenagem e manipulação adequadas.

11. Informação toxicológica



Ainda não se dispõe de dados toxicológicos.

12. Informação ecológica

Ainda não se dispõe de dados ecológicos.

Classe de perigo para a água (WGK): 1 - pouco perigoso para a água
WGK = Classificação de acordo com a lei alemã das águas
(segundo o Apêndice 4 VwVwS)

Datasheet of S9 – Co-styrene-acrylate

Chemical Description	Chemische Basis	Styrene acrylate copolymer Styrol-Acrylat-Copolymer	
Ionicity	Ladungscharakter	Amphoteric Amphoter	
Solids	Feststoffgehalt	%	24,0-26,0
Form supplied	Lieferform	Aqueous polymer dispersion Wäßrige Polymerdispersion	
Density	Dichte	g/cm ³ (20 °C)	1,02-1,06
pH value (as supplied)	pH-Wert (Lieferform)		4,0-6,0
Viscosity	Viskosität	mPa · s (Brookfield RV; spindle 1; 100 rpm; 20 °C (Brookfield RV; Spindel 1; 100 min ⁻¹ ; 20 °C)	<50
Storage stability	Lagerbeständigkeit	12 months ex  works The product must be stored free from freezing. 12 Monate ab Lieferung Werk  Das Produkt muß frostfrei gelagert werden.	
Recommended for	Haupt Einsatzgebiete	Surface sizing agent for paper and board. Oberflächenleimungsmittel für Papier und Karton.	
Remarks	Bemerkungen	Notes on safety: see safety data sheet. Hinweise zur Sicherheit: siehe Sicherheitsdatenblatt.	

Advantages of BAYSIZ S BMP:

1. No need to adjust pH of the size press solution.
2. Effective on acid and neutral base papers; [redacted] does not require alum for sizing development.
3. Can be combined with anionic, weakly cationic and nonionic auxiliaries.
4. Sizing is stable to alkaline liquids.
5. Low viscosity, easy to handle.
6. No unpleasant odour.
7. [redacted] does not impart wet strength to the paper allowing broke to be repulped without problem.
8. No foaming of the size press solution.

Surface sizing with [redacted] offers the following advantages over internal sizing:

1. Improves the toner adhesion.
2. Improvement in inkjet printability.
3. Reduces dusting and picking.
4. Produces stronger paper, e.g. higher bursting strength and tensile strength.
5. Level of sizing can be corrected faster.
6. No deposits on paper machine felts, screens and white water.

Technical notes on application

Mode of action

Application of [redacted] in the size press changes the wettability of the paper and reduces its water absorption. The presence of aluminium ions in the base paper is not necessary for obtaining optimum results.

Since BAYSIZ S BMP is amphoteric, it can be applied in the size press with fluorescent whiteners, direct dyes or basic dyes.

The normal drying temperatures on the paper machine are sufficient to develop full sizing. No additional curing period is required.

[redacted] has good stability in the presence of large quantities of electrolytes.

[redacted] bietet folgende Vorteile:

1. Keine pH-Einstellung erforderlich.
2. Wirksam auf sauer und neutral gefahrenen Rohpapieren, ein Zusatz von Aluminiumsulfat ist nicht erforderlich.
3. Kombinierbar mit anionischen, schwach kationischen und nichtionogenen Hilfsmitteln.
4. Gegen alkalische Flüssigkeiten stabile Leimung.
5. Niedrige Viskosität, daher leichte Handhabung.
6. Keine Geruchsbelastigung.
7. [redacted] verleiht dem Papier keine Nassfestigkeit, daher problemlose Aufarbeitung des Ausschusses.
8. Kein Schäumen der Leimpresenflotte.

Im Vergleich zur Leimung in der Papiermasse bietet eine Oberflächenleimung mit [redacted] folgende Vorteile:

1. Verbesserung der Tonerhaftung.
2. Verbesserung der Inkjet-Druckbarkeit.
3. Geringes Stauben und Rupfen.
4. Höhere Papierfestigkeiten, z.B. Berst- und Reißfestigkeit.
5. Schnellere Korrektur des Leimungsgrades.
6. Keine Verschmutzung der Papiermaschinensiebe und -filze sowie der Abwässer.

Technische Hinweise

Wirkungsweise

[redacted] – in der Leimpresse aufgetragen – verändert die Benetzbarkeit des Papiers und setzt die Wasseraufnahme des Papiers herab. Zur Erzielung von optimalen Werten ist die Anwesenheit von Aluminiumionen im Rohpapier nicht notwendig.

Da [redacted] einen amphoteren Charakter besitzt, kann es mit optischen Aufhellern, substantiven oder basischen Farbstoffen in der Leimpresse kombiniert werden.

Zur vollen Ausbildung der Leimung genügt die in der Papiermaschine übliche Trockentemperatur. Eine Nachreifung des Papiers ist nicht erforderlich.

[redacted] zeigt eine gute Stabilität gegen über höheren Elektrolytgehalten.

Product description**Pre-sizing of base paper**

Normally, the more absorbent the paper in the size press, the better the results achieved with [REDACTED]

Excessive pre-sizing in the stock can impair the performance of [REDACTED] by inhibiting penetration into the sheet.

If pick-up of the size press solution is too high, it can cause problems drying the sheet. This can normally be avoided by optimizing the level of internal sizing.

E.g. additions of as low as 0.05–0.2 % internal sizing agent to the stock reduce the wet pick-up in the size press allowing the paper to be dried after the size press without problems.

The normal fillers can be added to the base paper. Very good results are obtained with calcium carbonate fillers.

Amount required

The amount of [REDACTED] required depends on a number of factors such as the composition of the furnish, absorbency of the base paper and the degree of sizing required. Experience has shown that 0.2–0.8 % commercial product on dry weight of paper is generally sufficient.

Other additives

Since [REDACTED] is amphoteric can be used in combination with weakly cationic auxiliaries.

Temperature

[REDACTED] remains stable in the size press solution up to approx. 70 °C (160 °F). The size press solution should be cooled to below 70 °C (160 °F) before adding [REDACTED].

Produktbeschreibung**Vorleimung des Rohpapiers**

Normalerweise wird man mit [REDACTED] einen um so besseren Effekt erzielen, je aufnahmefähiger das Papier ist, wenn es in die Leimpresse gelangt. Eine zu starke Vorleimung in der Papiermasse kann die Wirkung von [REDACTED] deutlich herabsetzen.

Eine zu hohe Flottenaufnahme in der Leimpresse, welche u.U. zu Schwierigkeiten mit der Kapazität der Nach Trockengruppe hinter der Leimpresse führen kann, lässt sich in den meisten Fällen durch eine geringe Masseleimung sehr gut verhindern. Schon Zusätze von z.B. 0,05–0,2 % Masseleimungsmittel zur Papiermasse erniedrigen in den meisten Fällen die Nassaufnahme in der Leimpresse so weit, dass eine problemlose Trocknung möglich ist.

Im Rohpapier können die üblichen Füllstoffe eingesetzt werden. Mit Calciumcarbonat als Füllstoff erzielt man sehr gute Ergebnisse.

Zusatzmenge

Die benötigte Menge an [REDACTED] ist von verschiedenen Faktoren wie Rohstoffzusammensetzung, Aufnahmefähigkeit des Rohpapiers sowie dem geforderten Leimungsgrad abhängig. Wie die Erfahrung gezeigt hat, kommt man in den meisten Fällen mit 0,2–0,8 % Handelsware aus, bezogen auf das Gewicht des trockenen Papiers.

Andere Hilfsmittel

Da [REDACTED] ein amphoterer Produkt ist, kann es auch in Kombination mit schwach kationischen Hilfsmitteln eingesetzt werden.

Temperatur

[REDACTED] behält seine Stabilität in der Leimungsflotte bis ca. 70 °C. Vor Zusatz des Produktes sollte die Leimpressenflotte unter 70 °C abgekühlt werden.

Product description

Types of starch

██████████ is generally applied at the size press with a starch solution. A medium to low-viscosity nonionic, anionic or cationic starch is normally used. Since the type of starch can affect sizing to some extent, the efficiency of ██████████ in combination with the size should be tested before use. Such tests can be performed in our technical service laboratories at any time.

██████████ can also be applied without starch, i.e. simply diluted with water.

Addition point

██████████ can be added batch-wise at the starch solution storage tank as well as continuously in the operating tank or the feeding pipe to the size press.

██████████ is low-foaming, so defoamers are not normally required.

Use in food packaging papers

██████████ is approved for use in food packing papers and board under Recommendation XXXVI of the German Federal Institute for Consumer Health Protection and Veterinary Medicine (BgVV).

Produktbeschreibung

Stärkesorten

In der Regel wird ██████████ zusammen mit einer Stärkelösung in der Leimpresse eingesetzt. Man verwendet gewöhnlich mittel- bis niedrigviskose, nicht-ionogene, anionische oder kationische Stärken. Da die Stärkesorte in gewissem Umfang den Leimungseffekt beeinflussen kann, sollte die Wirksamkeit von ██████████ in Kombination mit der Stärke vorher überprüft werden. Dies kann jederzeit in unserem anwendungstechnischen Papierlabor durchgeführt werden. Der Einsatz von ██████████ auch ohne Stärkezusatz, d.h. nur mit Wasser verdünnt, ist ebenso möglich.

Zusatzstelle

██████████ kann sowohl diskontinuierlich in den Leimflottenvorratsbehälter als auch kontinuierlich in den Arbeitsbehälter oder die Leitung zur Leimpresse dosiert werden.

██████████ ist schaumarm, so daß Entschäumer normalerweise nicht benötigt werden.

Verwendung für Papiere zur Lebensmittelverpackung

██████████ ist nach Empfehlung XXXVI des Bundesamtes für gesundheitlichen Verbraucherschutz und Veterinärmedizin (BgVV) für Lebensmittelverpackungspapiere und -kartons zugelassen.

Datasheet of S10 – Co-styrene-acrylate

Chemical family: Polymer, dispersion
 Synonyms: STYRENE ACRYLATE COPOLYMER DISPERSION

2. Composition/information on ingredients

<u>C.A.S Number</u>	<u>Content (W/W)</u>	<u>Chemical name</u>
	7.0 %	Trade Secret
	>= 15.0 - <= 16.0 %	Trade Secret
127-09-3	>= 1.0 - <= 2.0 %	Sodium acetate
7732-18-5	>= 74.0 - <= 76.0 %	Water

3. Hazard identificationEmergency overview

CAUTION: MAY CAUSE EYE, SKIN AND RESPIRATORY TRACT IRRITATION.
 INGESTION MAY CAUSE GASTRIC DISTURBANCES.
 Eye wash fountains must be easily accessible.
 Wear full face shield if splashing hazard exists.
 Use with local exhaust ventilation.
 Wear protective clothing.

Potential health effectsPrimary routes of exposure

Routes of entry for solids and liquids include eye and skin contact, ingestion and inhalation. Routes of entry for gases include inhalation and eye contact. Skin contact may be a route of entry for liquified gases.

Acute toxicity:

Ingestion may cause gastrointestinal disturbances.

Irritation:

Irritation is possible when the product comes in contact with the skin, respiratory tract or the eyes.

Repeated dose toxicity:

No other known chronic effects.

4. First-aid measures

General advice:

Remove contaminated clothing.

If inhaled:

Remove the affected individual into fresh air and keep the person calm. Assist in breathing if necessary. Immediate medical attention required.

If on skin:

Wash affected areas thoroughly with soap and water. If irritation develops, seek medical attention.

If in eyes:

In case of contact with the eyes, rinse immediately for at least 15 minutes with plenty of water. If irritation develops, seek medical attention.

If swallowed:

Rinse mouth and then drink plenty of water. Do not induce vomiting. Never induce vomiting or give anything by mouth if the victim is unconscious or having convulsions. Immediate medical attention required.

5. Fire-fighting measures

Flash point: > 212 °F (DIN 51758)

Suitable extinguishing media:

water, dry extinguishing media, carbon dioxide, foam

Hazards during fire-fighting:

No particular hazards known.

Protective equipment for fire-fighting:

Firefighters should be equipped with self-contained breathing apparatus and turn-out gear.

6. Accidental release measures

Personal precautions:

No special precautions necessary.

Cleanup:

Spills should be contained and placed in suitable containers for disposal.

7. Handling and storage

Handling

Protection against fire and explosion:

No explosion proofing necessary.

8. Exposure controls and personal protection

Advice on system design:
Provide local exhaust ventilation to control vapours/mists.

Personal protective equipment

Respiratory protection:
Do not exceed the maximum use concentration for the respirator facepiece/cartridge combination. For emergency or non-routine, high exposure situations, use a NIOSH-certified full facepiece pressure demand self-contained breathing apparatus (SCBA) or a full facepiece pressure demand supplied-air respirator (SAR) with escape provisions. Wear a NIOSH-certified (or equivalent) organic vapour/particulate respirator as needed.

Hand protection:
Chemical resistant protective gloves

Eye protection:
Tightly fitting safety goggles (chemical goggles).

General safety and hygiene measures:
No special measures necessary if stored and handled correctly. Wear protective clothing as necessary to prevent contact. Avoid inhalation of vapours/mists. Wash soiled clothing immediately.

9. Physical and chemical properties

Form:	dispersion	
Odour:	ester-like, mild	
Colour:	grey	
pH value:	5.5 - 7	
Freezing point:	approx. 32 °F	(760 mmHg)
Boiling point:	approx. 212 °F	(760 mmHg)
Viscosity, dynamic:	22 - 32 mPa.s	
Miscibility with water:		miscible

10. Stability and reactivity

Conditions to avoid:
Avoid extreme heat.

Substances to avoid:
No substances known that should be avoided.

Hazardous reactions:
The product is chemically stable.

11. Toxicological information

12. Ecological information

13. Disposal considerations

Waste disposal of substance:
Incinerate in a licensed facility.
Dispose of in a licensed facility.
Do not discharge substance/product into sewer system.

Container disposal:
Dispose of in a licensed facility. Recommend crushing, puncturing or other means to prevent unauthorized use of used containers.

RCRA: None

14. Transport information

Reference Bill of Lading

15. Regulatory information

Federal Regulations

Registration status:
TSCA, US released / listed

SARA hazard categories (EPCRA 311.812): Not hazardous

State regulations

State RTK

<u>CAS Number</u>	<u>Chemical name</u>	<u>State RTK</u>
	Trade Secret	NJ, PA, MA
	Trade Secret	NJ, PA, MA

APPENDIX B

SURFACE SIZING FORMULATIONS

Table B.1 – Samples obtained after the surface sizing application.

Sample	Surface sizing Formulation (% w/w)	Sample	Surface sizing Formulation (% w/w)
St	100% Cationic Starch	StS6-05	95% Cationic Starch 5% S6
StS1-05	95% Cationic Starch 5% S1	StS6-10	90% Cationic Starch 10% S6
StS1-10	90% Cationic Starch 10% S1	StS6-20	80% Cationic Starch 20% S6
StS1-20	80% Cationic Starch 20% S1	StS7-05	95% Cationic Starch 5% S7
StS2-05	95% Cationic Starch 5% S2	StS7-10	90% Cationic Starch 10% S7
StS2-10	90% Cationic Starch 10% S2	StS7-20	80% Cationic Starch 20% S7
StS2-20	80% Cationic Starch 20% S2	StS8-05	95% Cationic Starch 5% S8
StS3-05	95% Cationic Starch 5% S3	StS8-10	90% Cationic Starch 10% S8
StS3-10	90% Cationic Starch 10% S3	StS8-20	80% Cationic Starch 20% S8
StS3-20	80% Cationic Starch 20% S3	StS9-05	95% Cationic Starch 5% S9
StS4-05	95% Cationic Starch 5% S4	StS9-10	90% Cationic Starch 10% S9
StS4-10	90% Cationic Starch 10% S4	StS9-20	80% Cationic Starch 20% S9
StS4-20	80% Cationic Starch 20% S4	StS10-05	95% Cationic Starch 5% S10
StS5-05	95% Cationic Starch 5% S5	StS10-10	90% Cationic Starch 10% S10
StS5-10	90% Cationic Starch 10% S5	StS10-20	80% Cationic Starch 20% S10
StS5-20	80% Cationic Starch 20% S5	-----	-----

APPENDIX C

PROFILOMETRY RESULTS

Table C.1 - Amplitude parameters obtained from profilometry experiments.

Sample	Amplitude Parameters					
	Sa (μm)	Sq (μm)	Sp (μm)	Sv (μm)	St (μm)	Ssk
St	2.92 ± 0.10	3.67 ± 0.11	8.83 ± 0.31	10.88 ± 0.33	19.70 ± 0.64	-0.27 ± 0.03
StS1-05	2.97 ± 0.07	3.70 ± 0.07	8.93 ± 0.55	11.17 ± 0.48	20.07 ± 0.60	-0.25 ± 0.07
StS1-10	3.08 ± 0.22	3.88 ± 0.26	9.07 ± 0.90	11.72 ± 0.88	20.78 ± 1.17	-0.37 ± 0.18
StS1-20	2.78 ± 0.08	3.45 ± 0.06	8.44 ± 0.15	9.81 ± 0.41	18.36 ± 0.70	-0.16 ± 0.01
StS2-05	2.94 ± 0.10	3.70 ± 0.12	8.82 ± 0.48	11.45 ± 0.69	20.08 ± 0.76	-0.41 ± 0.10
StS2-10	3.11 ± 0.16	3.92 ± 0.18	9.00 ± 1.00	12.05 ± 0.59	21.07 ± 0.63	-0.50 ± 0.14
StS2-20	2.72 ± 0.07	3.40 ± 0.03	8.14 ± 0.21	10.50 ± 0.21	18.66 ± 0.17	-0.32 ± 0.06
StS3-05	2.90 ± 0.05	3.69 ± 0.03	8.15 ± 0.04	11.67 ± 0.27	19.90 ± 0.30	-0.45 ± 0.04
StS3-10	2.97 ± 0.10	3.71 ± 0.13	9.35 ± 0.30	10.16 ± 0.41	19.50 ± 0.83	-0.14 ± 0.05
StS3-20	2.97 ± 0.04	3.74 ± 0.04	8.36 ± 0.08	11.95 ± 0.21	20.30 ± 0.14	-0.49 ± 0.04
StS4-05	2.94 ± 0.17	3.74 ± 0.18	9.16 ± 0.27	10.90 ± 0.67	19.82 ± 1.05	-0.27 ± 0.04
StS4-10	2.89 ± 0.10	3.63 ± 0.13	8.48 ± 0.11	11.12 ± 0.86	19.53 ± 0.94	-0.39 ± 0.09
StS4-20	2.81 ± 0.15	3.52 ± 0.19	8.31 ± 0.19	10.09 ± 0.47	18.72 ± 0.92	-0.24 ± 0.03
StS5-05	3.37 ± 0.17	4.31 ± 0.15	9.29 ± 0.21	13.38 ± 0.67	22.93 ± 0.71	-0.46 ± 0.08
StS5-10	3.00 ± 0.07	3.78 ± 0.07	9.21 ± 0.27	10.48 ± 0.43	19.78 ± 0.65	-0.19 ± 0.02
StS5-20	3.15 ± 0.29	3.97 ± 0.37	9.10 ± 0.37	12.22 ± 1.77	21.48 ± 2.23	-0.28 ± 0.11
StS6-05	2.91 ± 0.10	3.70 ± 0.07	8.89 ± 0.11	10.87 ± 0.60	19.72 ± 0.50	-0.25 ± 0.04
StS6-10	3.02 ± 0.07	3.77 ± 0.07	9.17 ± 0.28	11.00 ± 0.28	20.18 ± 0.49	-0.25 ± 0.04
StS6-20	2.84 ± 0.14	3.61 ± 0.12	8.92 ± 0.18	10.14 ± 0.32	18.95 ± 0.68	-0.19 ± 0.04
StS7-05	2.93 ± 0.05	3.67 ± 0.04	8.23 ± 0.19	11.77 ± 0.21	20.13 ± 0.37	-0.43 ± 0.07
StS7-10	3.00 ± 0.14	3.70 ± 0.10	8.59 ± 0.16	10.93 ± 0.41	19.93 ± 0.85	-0.22 ± 0.07
StS7-20	3.02 ± 0.22	3.87 ± 0.22	9.44 ± 0.83	10.94 ± 0.75	20.40 ± 1.43	-0.22 ± 0.04
StS8-05	3.04 ± 0.13	3.82 ± 0.16	8.95 ± 0.13	11.28 ± 0.44	20.47 ± 0.77	-0.27 ± 0.03
StS8-10	2.89 ± 0.16	3.65 ± 0.18	8.66 ± 0.82	11.38 ± 0.54	20.07 ± 0.74	-0.37 ± 0.16
StS8-20	3.45 ± 0.10	4.28 ± 0.07	10.85 ± 0.26	12.42 ± 0.67	22.88 ± 0.78	-0.25 ± 0.08
StS9-05	2.96 ± 0.11	3.73 ± 0.06	8.80 ± 0.36	11.63 ± 0.86	20.35 ± 1.01	-0.38 ± 0.11
StS9-10	3.01 ± 0.19	3.70 ± 0.18	8.93 ± 0.43	10.87 ± 0.91	20.05 ± 1.56	-0.21 ± 0.04
StS9-20	2.96 ± 0.09	3.69 ± 0.08	9.03 ± 0.05	10.15 ± 0.07	19.20 ± 0.00	-0.14 ± 0.03
StS10-05	2.95 ± 0.07	3.66 ± 0.05	8.90 ± 0.17	10.71 ± 0.83	19.60 ± 0.59	-0.32 ± 0.06
StS10-10	2.87 ± 0.23	3.61 ± 0.28	8.58 ± 0.91	10.85 ± 0.52	19.42 ± 1.41	-0.32 ± 0.09
StS10-20	2.85 ± 0.20	3.51 ± 0.18	8.69 ± 0.58	11.03 ± 0.83	19.48 ± 1.34	-0.29 ± 0.07

Table C.2 – Spatial and Hybrid parameters obtained from profilometry experiments.

Sample	Spatial Parameters		Hybrid Parameters	
	Str	Sdq ($\mu\text{m}/\mu\text{m}$)	Ssc ($1/\mu\text{m}$)	Sdr (%)
St	0.49 ± 0.04	0.50 ± 0.01	0.19 ± 0.00	11.33 ± 0.28
StS1-05	0.58 ± 0.11	0.48 ± 0.03	0.17 ± 0.01	10.75 ± 1.19
StS1-10	0.38 ± 0.06	0.46 ± 0.00	0.17 ± 0.01	9.95 ± 0.19
StS1-20	0.43 ± 0.07	0.45 ± 0.01	0.18 ± 0.00	9.43 ± 0.29
StS2-05	0.55 ± 0.04	0.48 ± 0.01	0.17 ± 0.00	10.83 ± 0.43
StS2-10	0.56 ± 0.14	0.50 ± 0.01	0.17 ± 0.01	11.24 ± 0.45
StS2-20	0.46 ± 0.04	0.45 ± 0.01	0.16 ± 0.00	9.23 ± 0.22
StS3-05	0.62 ± 0.06	0.48 ± 0.02	0.17 ± 0.00	10.46 ± 1.03
StS3-10	0.47 ± 0.03	0.47 ± 0.01	0.17 ± 0.00	10.30 ± 0.28
StS3-20	0.52 ± 0.02	0.47 ± 0.00	0.17 ± 0.00	10.35 ± 0.07
StS4-05	0.53 ± 0.05	0.49 ± 0.02	0.18 ± 0.01	10.96 ± 0.81
StS4-10	0.47 ± 0.00	0.50 ± 0.01	0.18 ± 0.00	11.25 ± 0.21
StS4-20	0.49 ± 0.04	0.46 ± 0.02	0.16 ± 0.01	9.73 ± 0.63
StS5-05	0.45 ± 0.03	0.52 ± 0.01	0.18 ± 0.00	12.20 ± 0.36
StS5-10	0.48 ± 0.05	0.50 ± 0.03	0.19 ± 0.01	11.62 ± 1.21
StS5-20	0.45 ± 0.09	0.47 ± 0.02	0.17 ± 0.01	10.28 ± 0.88
StS6-05	0.49 ± 0.11	0.48 ± 0.01	0.19 ± 0.00	10.85 ± 0.21
StS6-10	0.42 ± 0.04	0.48 ± 0.01	0.18 ± 0.00	10.80 ± 0.41
StS6-20	0.49 ± 0.04	0.49 ± 0.01	0.18 ± 0.00	10.92 ± 0.33
StS7-05	0.68 ± 0.02	0.48 ± 0.01	0.17 ± 0.00	10.63 ± 0.33
StS7-10	0.54 ± 0.10	0.47 ± 0.02	0.18 ± 0.01	10.28 ± 0.73
StS7-20	0.42 ± xxx	0.50 ± xxx	0.18 ± xxx	11.40 ± xxx
StS8-05	0.41 ± 0.07	0.50 ± 0.01	0.18 ± 0.00	11.37 ± 0.47
StS8-10	0.59 ± 0.17	0.50 ± 0.01	0.18 ± 0.01	11.30 ± 0.52
StS8-20	0.40 ± 0.06	0.49 ± 0.02	0.18 ± 0.01	10.93 ± 0.93
StS9-05	0.55 ± 0.09	0.49 ± 0.01	0.18 ± 0.00	11.27 ± 0.38
StS9-10	0.45 ± 0.05	0.47 ± 0.01	0.18 ± 0.00	10.29 ± 0.41
StS9-20	0.37 ± 0.10	0.43 ± 0.00	0.17 ± 0.00	8.67 ± 0.02
StS10-05	0.42 ± 0.11	0.48 ± 0.01	0.19 ± 0.00	10.80 ± 0.43
StS10-10	0.54 ± 0.09	0.47 ± 0.02	0.18 ± 0.00	10.10 ± 0.76
StS10-20	0.70 ± 0.07	0.48 ± 0.01	0.17 ± 0.01	10.43 ± 0.54

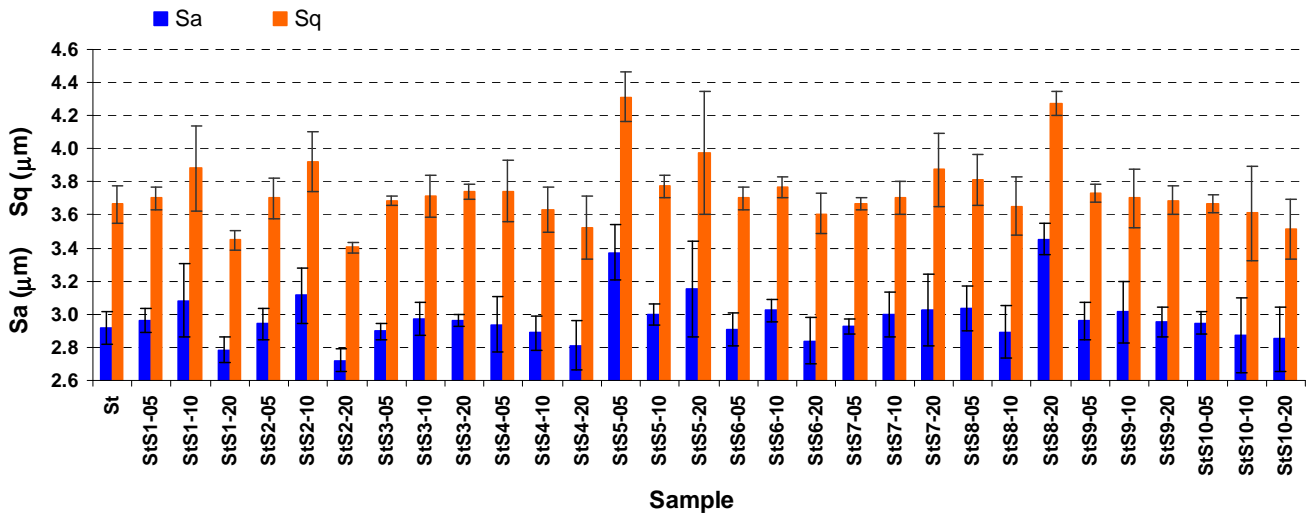


Figure C.1 - Sa and Sq values obtained for all the 31 paper samples.

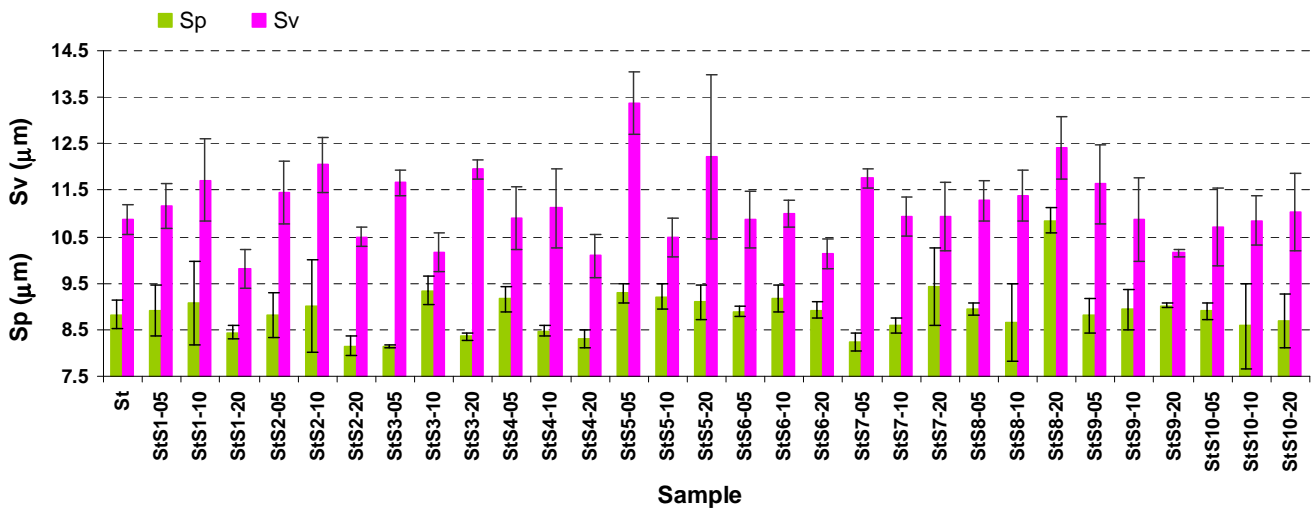


Figure C.2 – Sp and Sv values obtained for all the 31 paper samples.

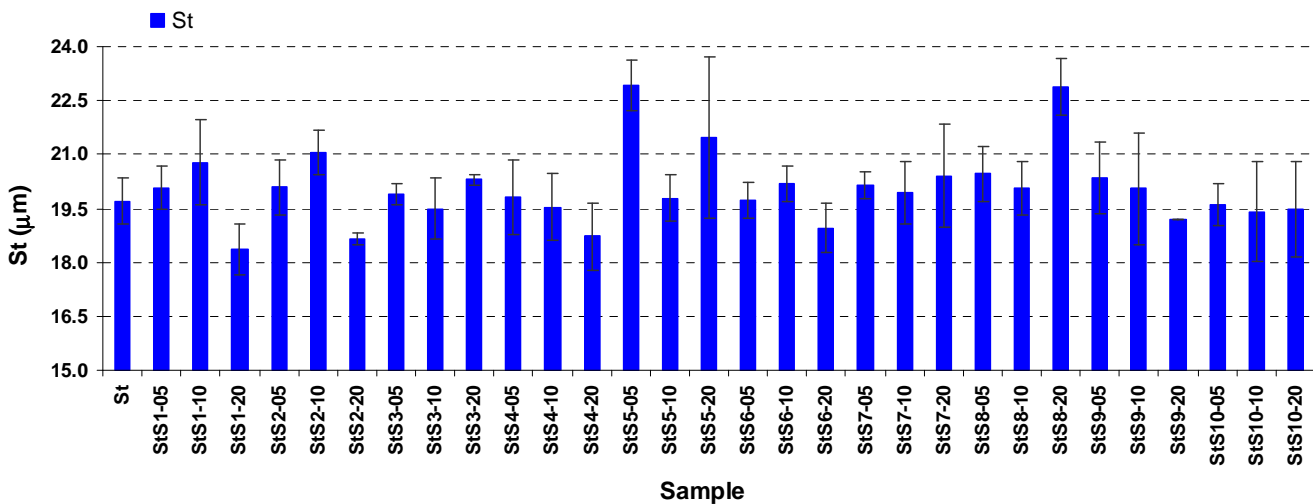


Figure C.3 - St values obtained for all the 31 paper samples

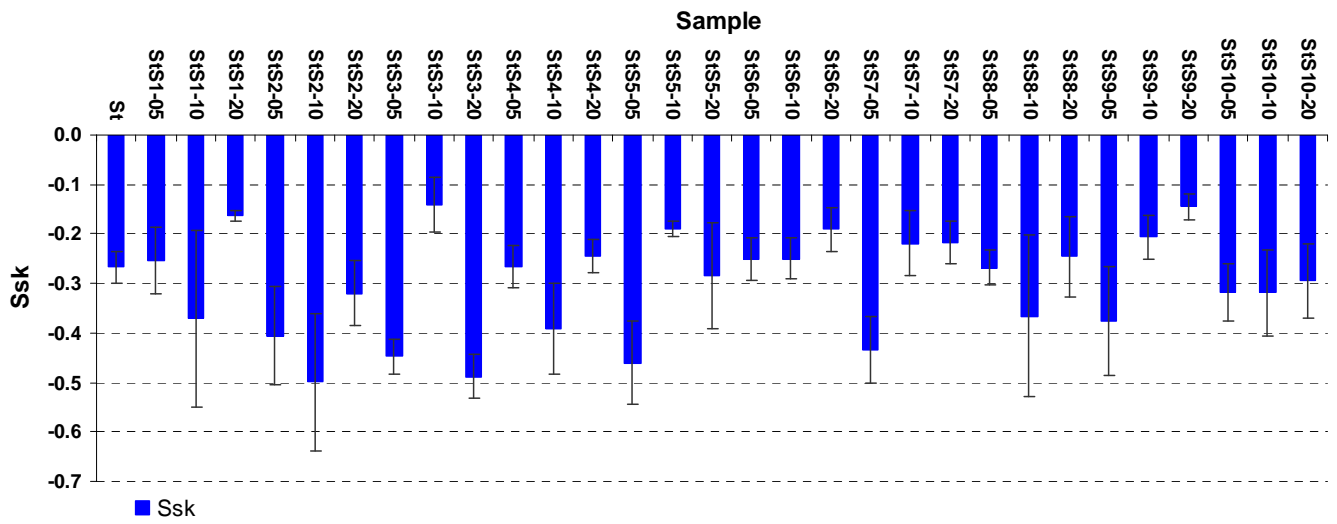


Figure C.4 – Ssk values obtained for all the 31 paper samples.

APPENDIX D

11.1 MERCURY POROSIMETRY RESULTS

Table D.1a – Information achieved by mercury porosimetry for the reference samples and the samples sized with the synthetic surface sizing agents S1, S2 and S4 at the three different amounts.

Sample	Total intrusion volume (ml/g)	Bulk Density at 0.52 psia (g/ml)	Apparent Skeletal Density (g/ml)	Porosity (%)
St	0.762	0.745	1.715	56.800
	0.794	0.724	1.701	57.447
	0.711	0.787	1.785	55.940
	0.788	0.729	1.710	57.391
StS1-05	0.770	0.732	1.683	56.467
	0.751	0.739	1.662	55.536
	0.764	0.731	1.658	55.888
StS1-10	0.714	0.762	1.671	54.406
	0.756	0.751	1.743	56.884
	0.729	0.764	1.723	55.683
StS1-20	0.748	0.745	1.684	55.754
	0.810	0.724	1.752	58.689
	0.769	0.737	1.699	56.654
StS2-05	0.789	0.743	1.799	58.682
	0.777	0.727	1.672	56.522
	0.810	0.709	1.666	57.452
StS2-10	0.745	0.761	1.761	56.775
	0.726	0.764	1.716	55.486
	0.757	0.751	1.742	56.897
StS2-20	0.730	0.756	1.687	55.172
	0.824	0.710	1.715	58.567
	0.753	0.750	1.728	56.551
StS3-05	0.755	0.739	1.674	55.837
	0.710	0.752	1.616	53.443
	0.823	0.709	1.702	58.336
	0.790	0.720	1.73	58.010
StS3-10	0.768	0.733	1.676	56.272
	0.808	0.713	1.681	57.596
	0.772	0.728	1.665	56.256
	0.829	0.707	1.707	58.581
StS3-20	0.839	0.691	1.646	58.007
	0.789	0.726	1.701	57.338
	0.809	0.722	1.736	58.411
	0.712	0.766	1.689	54.615
	0.730	0.759	1.702	55.417

Table D.1b – Information achieved by mercury porosimetry for samples sized with the synthetic surface sizing agents S4, S5, S6, S7 and S8 at the three different amounts.

Sample	Total intrusion volume (ml/g)	Bulk Density at 0.52 psia (g/ml)	Apparent Skeletal Density (g/ml)	Porosity (%)
StS4-05	0.730	0.750	1.710	55.860
	0.726	0.759	1.691	55.126
	0.782	0.729	1.696	57.023
StS4-10	0.830	0.691	1.622	57.396
	0.786	0.725	1.687	57.020
	0.780	0.723	1.659	56.411
StS4-20	0.785	0.718	1.646	56.383
	0.739	0.748	1.674	55.306
	0.758	0.732	1.649	55.570
StS5-05	0.778	0.708	1.577	55.099
	0.728	0.756	1.685	55.119
	0.747	0.703	1.483	52.561
StS5-10	0.753	0.740	1.673	55.756
	0.850	0.677	1.598	57.611
	0.774	0.710	1.574	54.914
StS5-20	0.784	0.729	1.706	57.229
	0.776	0.704	1.557	54.743
	0.853	0.664	1.531	56.637
StS6-05	0.817	0.711	1.698	58.117
	0.732	0.748	1.652	54.731
	0.731	0.739	1.608	54.036
StS6-10	0.766	0.741	1.717	56.816
	0.742	0.754	1.714	56.001
	0.742	0.727	1.577	53.913
StS6-20	0.783	0.718	1.640	56.233
	0.754	0.714	1.550	53.910
	0.824	0.681	1.554	56.146
StS7-05	0.817	0.695	1.610	56.826
	0.765	0.686	1.448	52.588
	0.793	0.683	1.495	54.285
StS7-10	0.707	0.772	1.700	54.588
	0.759	0.735	1.666	55.857
	0.757	0.706	1.518	53.489
StS7-20	0.810	0.710	1.710	58.430
	0.774	0.722	1.641	55.975
	0.728	0.724	1.534	52.766
StS8-05	0.767	0.732	1.670	56.139
	0.711	0.746	1.592	53.108
	0.759	0.709	1.536	53.845
StS8-10	0.825	0.705	1.686	58.190
	0.777	0.713	1.600	55.440
	0.718	0.730	1.533	52.390
StS8-20	0.821	0.701	1.653	57.595
	0.733	0.706	1.462	51.726
	0.735	0.731	1.581	53.735

Table D.1c – Information achieved by mercury porosimetry for samples sized with the synthetic surface sizing agents S9 and S10 at the three different amounts.

Sample	Total intrusion volume (ml/g)	Bulk Density at 0.52 psia (g/ml)	Apparent Skeletal Density (g/ml)	Porosity (%)
StS9-05	0.767	0.724	1.629	55.529
	0.678	0.739	1.485	52.204
	0.733	0.728	1.561	53.363
StS9-10	0.825	0.704	1.686	58.190
	0.777	0.713	1.600	55.440
	0.718	0.730	1.533	52.390
StS9-20	0.821	0.701	1.653	57.595
	0.733	0.706	1.462	51.726
	0.735	0.731	1.581	53.735
StS10-05	0.763	0.749	1.748	57.150
	0.776	0.734	1.706	56.953
	0.764	0.724	1.618	55.277
StS10-10	0.828	0.701	1.673	58.088
	0.791	0.720	1.672	56.946
	0.757	0.716	1.564	54.226
StS10-20	0.798	0.716	1.678	57.276
	0.771	0.723	1.638	55.831
	0.704	0.738	1.539	52.021

Table D.2 – Total porosity values obtained for all the paper samples

Sample	Total Porosity (%)	Sample	Total Porosity (%)
St	56.80 ± 0.76	StS6-05	58.12 ± 2.18
StS1-05	56.47 ± 0.47	StS6-10	56.82 ± 1.50
StS1-10	54.41 ± 1.24	StS6-20	56.23 ± 1.32
StS1-20	55.75 ± 1.50	StS7-05	56.83 ± 2.13
StS2-05	58.68 ± 1.08	StS7-10	54.59 ± 1.18
StS2-10	56.78 ± 0.78	StS7-20	58.43 ± 2.84
StS2-20	55.17 ± 1.71	StS8-05	56.14 ± 1.58
StS3-05	56.27 ± 1.11	StS8-10	58.19 ± 2.90
StS3-10	57.60 ± 1.17	StS8-20	57.60 ± 2.98
StS3-20	57.34 ± 1.96	StS9-05	55.53 ± 2.68
StS4-05	55.86 ± 0.96	StS9-10	55.08 ± 1.39
StS4-10	57.40 ± 0.50	StS9-20	55.05 ± 0.33
StS4-20	56.38 ± 0.56	StS10-05	57.15 ± 1.03
StS5-05	55.10 ± 1.47	StS10-10	58.09 ± 1.98
StS5-10	55.76 ± 1.38	StS10-20	57.28 ± 2.71
StS5-20	57.23 ± 1.30	-----	-----

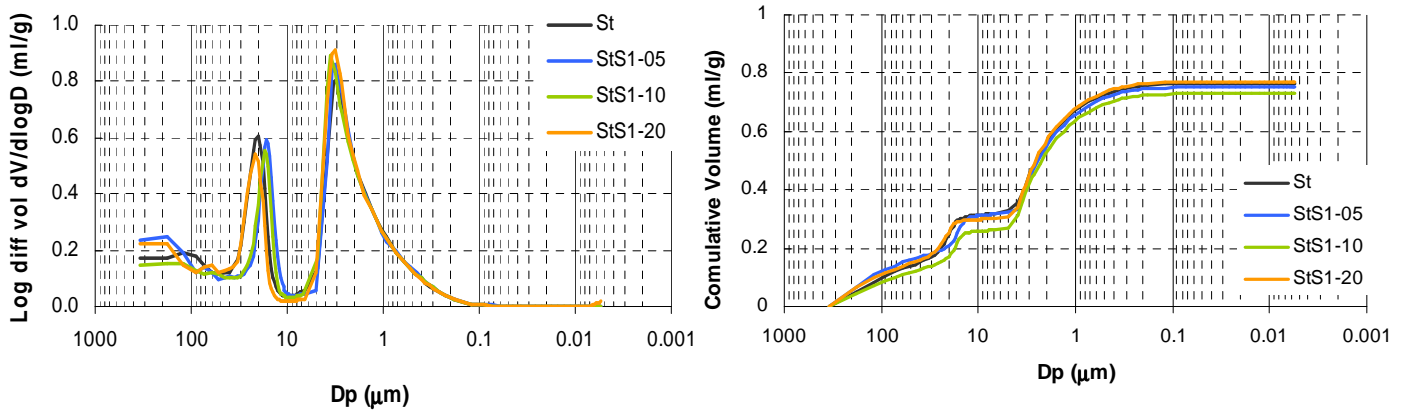


Figure D.1 - Differential (a) and cumulative (b) pore size distribution diagrams for samples sized with surface sizing agent S1

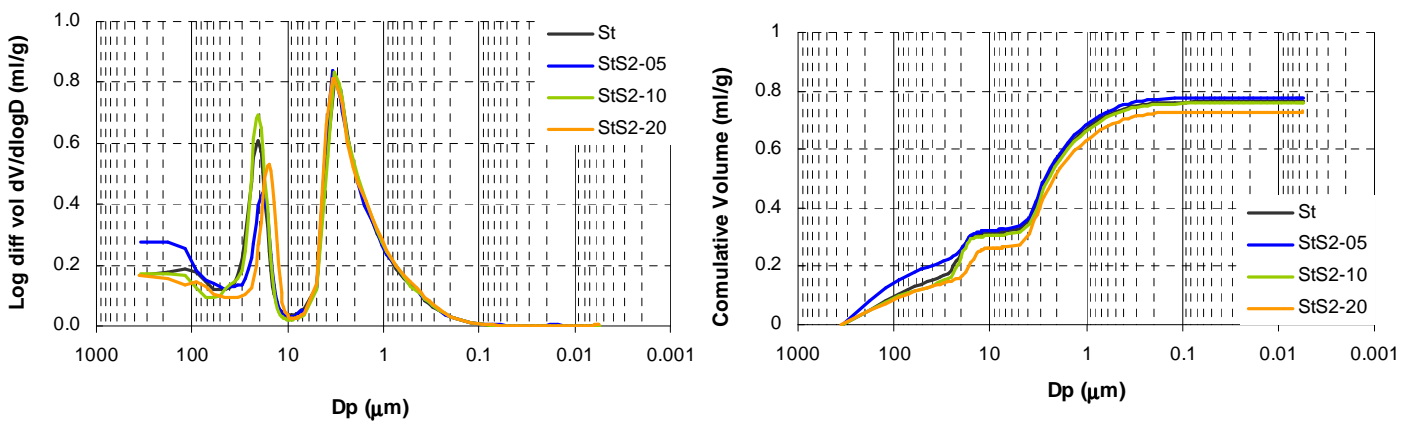


Figure D.2 - Differential (a) and cumulative (b) pore size distribution diagrams for samples sized with surface sizing agent S2

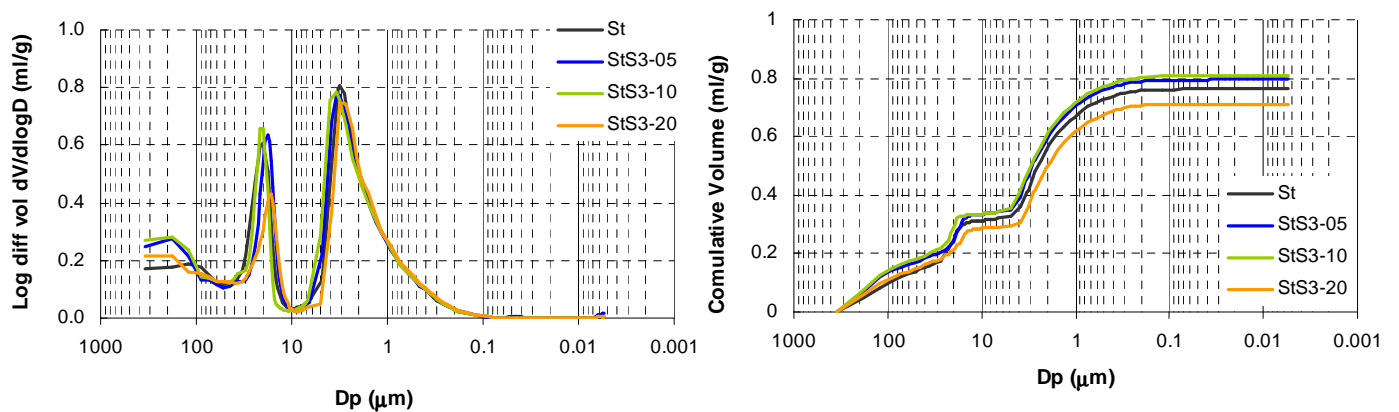


Figure D.3 - Differential (a) and cumulative (b) pore size distribution diagrams for samples sized with surface sizing agent S3

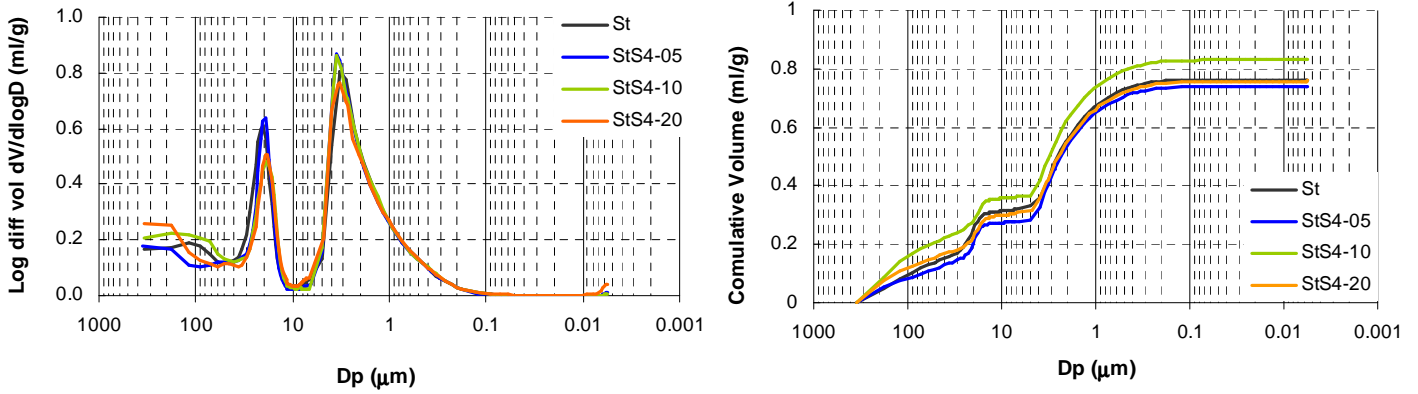


Figure D.4 - Differential (a) and cumulative (b) pore size distribution diagrams for samples sized with surface sizing agent S4

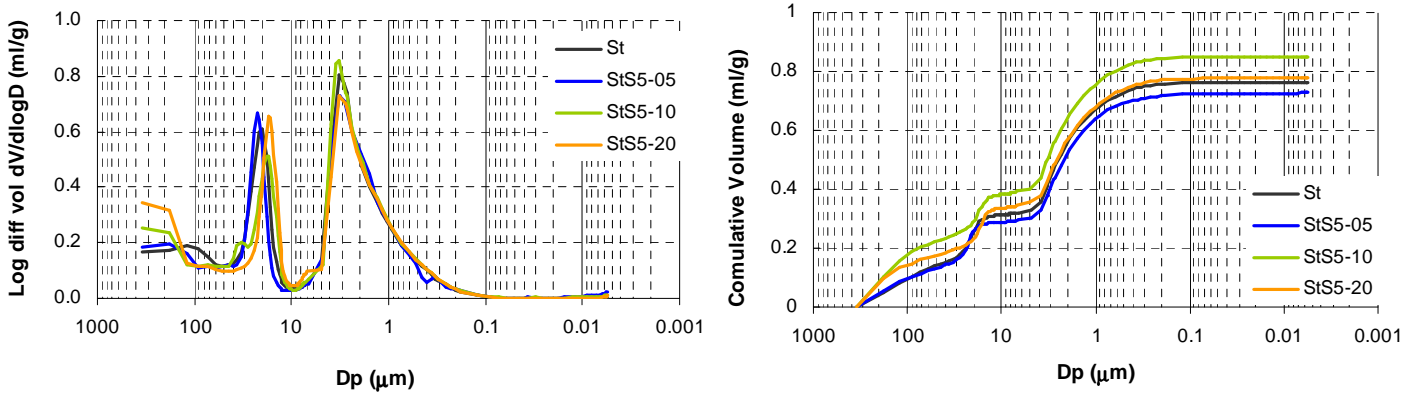


Figure D.5 - Differential (a) and cumulative (b) pore size distribution diagrams for samples sized with surface sizing agent S5

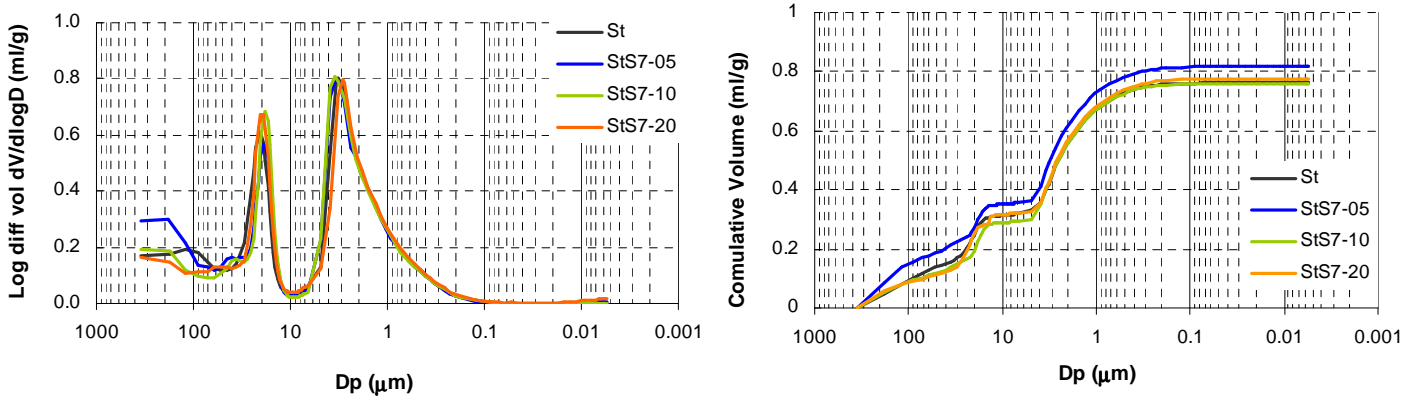


Figure D.6 - Differential (a) and cumulative (b) pore size distribution diagrams for samples sized with surface sizing agent S7

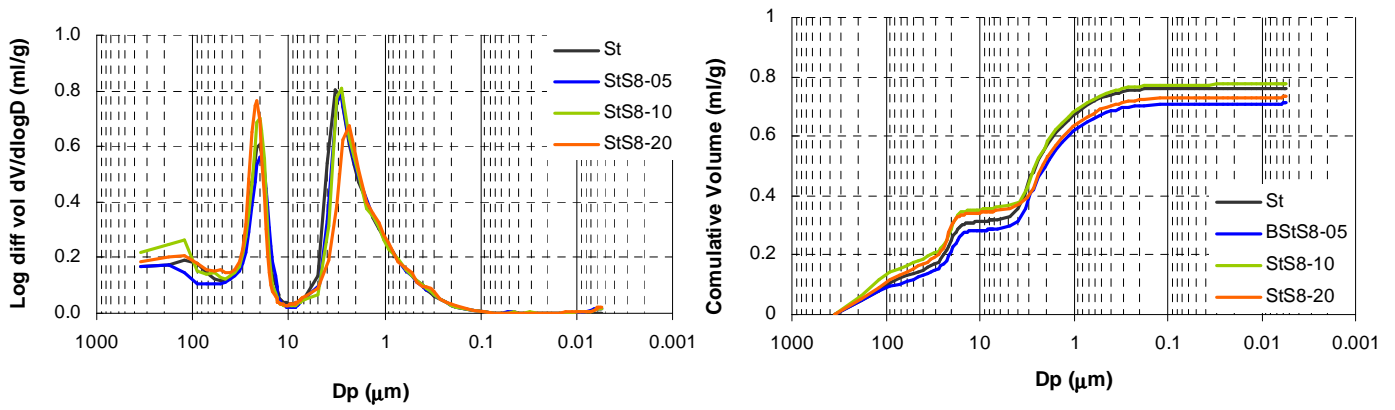


Figure D.7 - Differential (a) and cumulative (b) pore size distribution diagrams for samples sized with surface sizing agent S8

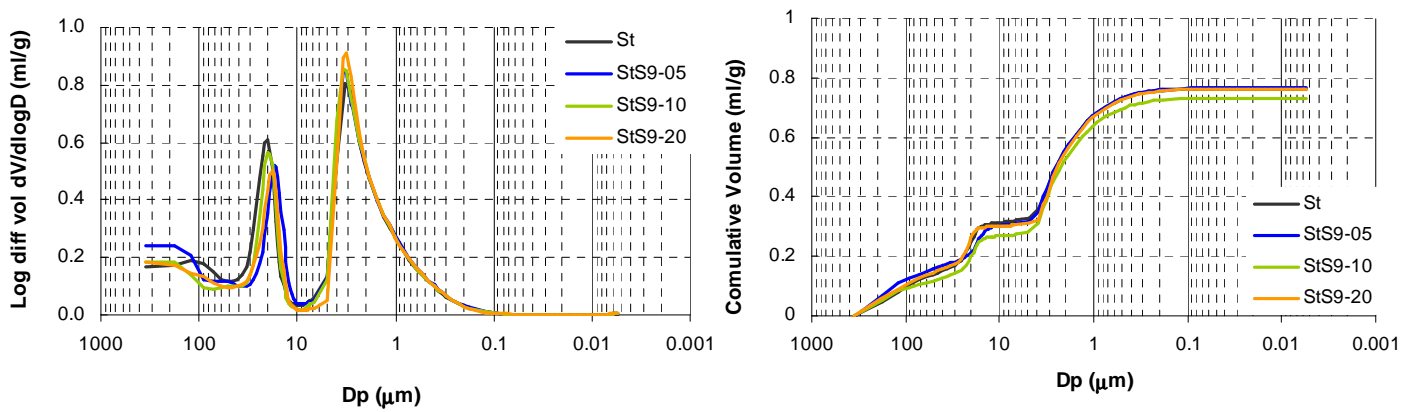


Figure D.8 - Differential (a) and cumulative (b) pore size distribution diagrams for samples sized with surface sizing agent S9

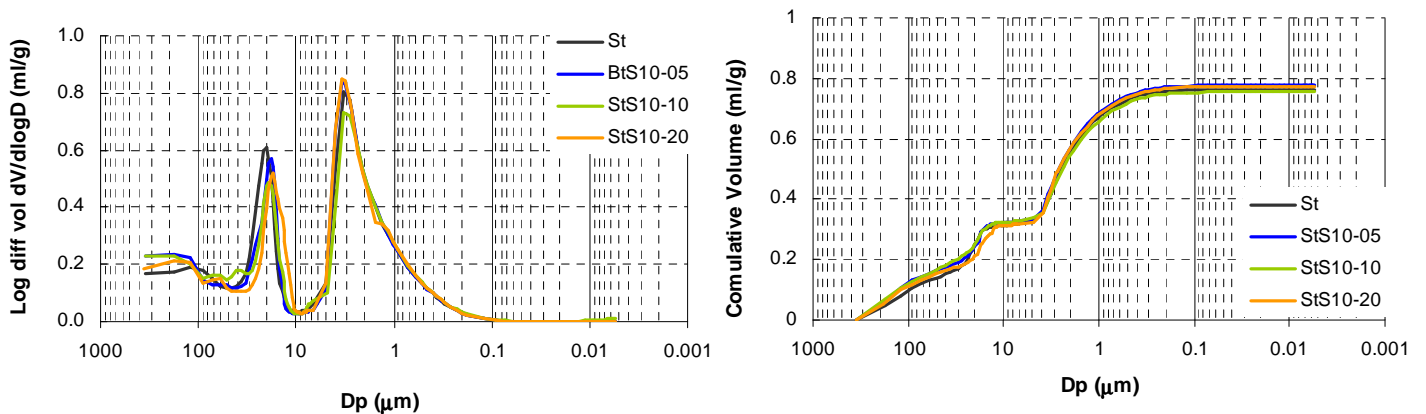


Figure D.9 - Differential (a) and cumulative (b) pore size distribution diagrams for samples sized with surface sizing agent S10

APPENDIX E

CONTACT ANGLE MEASUREMENTS

Table E.1 – Contact angle values measured with each of the five liquids tested for all samples (before correction).

Sample	Diodomethane (°)	Propileneglycol (°)	Ethylenglycol (°)	Formamide (°)	Water (°)
St	33.0 ± 1.4	26.9 ± 1.1	27.3 ± 1.0	17.0 ± 0.8	30.3 ± 1.5
StS1-05	32.9 ± 1.4	37.0 ± 1.7	41.8 ± 1.6	42.2 ± 1.5	50.4 ± 1.9
StS1-10	29.8 ± 1.2	38.1 ± 1.6	40.8 ± 1.5	37.9 ± 1.6	50.6 ± 1.5
StS1-20	35.6 ± 1.1	41.8 ± 1.8	50.7 ± 1.0	49.7 ± 1.1	57.0 ± 1.3
StS2-05	28.6 ± 1.0	31.2 ± 1.5	40.3 ± 1.8	37.6 ± 1.7	53.5 ± 1.6
StS2-10	29.5 ± 1.0	34.7 ± 1.5	52.8 ± 1.3	53.6 ± 1.5	68.7 ± 1.6
StS2-20	28.2 ± 1.4	41.4 ± 1.4	64.7 ± 0.9	51.7 ± 1.5	79.6 ± 2.6
StS3-05	25.1 ± 0.9	28.9 ± 0.8	32.9 ± 1.5	31.8 ± 0.8	36.5 ± 0.9
StS3-10	30.2 ± 1.4	30.6 ± 1.0	33.9 ± 1.5	31.7 ± 1.0	52.6 ± 1.6
StS3-20	26.6 ± 1.0	31.3 ± 1.2	29.8 ± 0.9	20.7 ± 0.9	36.5 ± 0.9
StS4-05	34.1 ± 1.4	39.6 ± 1.5	57.4 ± 0.9	57.3 ± 1.1	72.6 ± 1.4
StS4-10	32.8 ± 1.2	39.2 ± 1.8	47.2 ± 1.5	52.6 ± 1.3	60.0 ± 2.4
StS4-20	33.8 ± 1.5	41.6 ± 1.5	60.9 ± 1.6	57.7 ± 1.4	70.7 ± 1.7
StS5-05	38.5 ± 1.8	42.6 ± 0.9	50.5 ± 1.5	45.2 ± 1.0	57.2 ± 1.2
StS5-10	53.8 ± 1.0	58.1 ± 1.4	51.5 ± 1.2	50.7 ± 1.0	52.9 ± 1.5
StS5-20	55.9 ± 1.3	72.6 ± 1.7	70.8 ± 1.1	65.9 ± 1.7	64.0 ± 0.8
StS6-05	30.6 ± 0.6	38.5 ± 1.7	43.2 ± 1.3	45.3 ± 0.7	64.6 ± 1.4
StS6-10	30.9 ± 1.1	40.8 ± 1.6	42.9 ± 1.2	44.2 ± 0.8	67.0 ± 1.4
StS6-20	32.0 ± 1.6	42.8 ± 1.7	51.4 ± 1.1	53.5 ± 1.3	81.4 ± 1.5
StS7-05	31.4 ± 1.4	39.2 ± 1.8	44.8 ± 1.0	45.3 ± 1.7	62.2 ± 1.4
StS7-10	30.7 ± 1.4	32.6 ± 1.0	44.0 ± 1.6	45.0 ± 1.7	57.8 ± 1.2
StS7-20	31.8 ± 1.3	31.6 ± 1.4	60.9 ± 1.6	21.3 ± 1.0	37.2 ± 1.0
StS8-05	34.1 ± 1.1	37.5 ± 1.6	45.8 ± 1.2	48.7 ± 1.4	61.4 ± 1.4
StS8-10	35.4 ± 1.5	43.1 ± 1.6	54.7 ± 1.8	58.6 ± 1.8	74.1 ± 1.3
StS8-20	34.1 ± 0.9	45.1 ± 1.4	57.5 ± 1.8	59.8 ± 1.4	68.9 ± 1.8
StS9-05	26.3 ± 0.6	29.6 ± 0.9	32.4 ± 0.9	28.0 ± 1.3	39.9 ± 0.9
StS9-10	29.4 ± 0.8	36.4 ± 1.8	43.1 ± 1.2	45.9 ± 1.6	55.2 ± 0.8
StS9-20	31.1 ± 1.3	28.0 ± 0.8	37.0 ± 1.5	29.0 ± 0.8	42.8 ± 1.9
StS10-05	22.3 ± 1.1	31.9 ± 1.4	40.3 ± 1.8	34.4 ± 1.4	55.3 ± 1.0
StS10-10	34.1 ± 1.2	36.2 ± 1.7	40.1 ± 1.3	37.8 ± 1.5	48.3 ± 0.8
StS10-20	34.6 ± 1.2	49.5 ± 1.4	63.8 ± 1.3	63.3 ± 1.5	82.6 ± 1.5

Table E.2 – Contact angle values with each of the five liquids tested for all samples, after the application of the Wenzel correction (corrected values).

Sample	Contact angles (°)				
	Diodomethane	Propileneglycol	Ethylenglycol	Formamide	Water
St	41.12	36.77	37.04	30.80	39.15
StS1-05	40.70	43.85	47.69	48.02	54.86
StS1-10	37.89	44.30	46.49	44.14	54.74
StS1-20	42.01	47.06	54.63	53.77	60.15
StS2-05	37.61	39.49	46.52	44.37	57.54
StS2-10	38.52	42.35	57.08	57.76	70.94
StS2-20	36.21	46.63	66.97	55.43	80.49
StS3-05	34.93	37.57	40.53	39.70	43.30
StS3-10	38.41	38.71	41.19	39.52	56.59
StS3-20	35.88	39.26	38.15	32.04	43.24
StS4-05	41.73	46.02	60.95	60.86	74.37
StS4-10	40.93	45.85	52.36	56.91	63.29
StS4-20	40.77	47.04	63.69	60.86	72.47
StS5-05	45.77	49.00	55.46	51.10	61.13
StS5-10	58.05	61.74	56.10	55.43	57.29
StS5-20	59.44	74.27	72.65	68.27	66.58
StS6-05	39.06	45.09	48.88	50.61	67.24
StS6-10	39.25	46.91	48.61	49.68	69.35
StS6-20	40.13	48.59	55.77	57.57	82.25
StS7-05	39.51	45.53	50.10	50.52	65.07
StS7-10	38.77	40.19	49.29	50.12	61.11
StS7-20	40.28	40.13	64.11	33.24	44.36
StS8-05	41.97	44.57	51.25	53.66	64.54
StS8-10	42.91	49.00	58.72	62.09	75.75
StS8-20	41.71	50.48	61.03	63.03	71.06
StS9-05	36.32	38.61	40.64	37.48	46.41
StS9-10	37.82	43.13	48.54	50.88	58.84
StS9-20	38.01	35.66	42.70	36.41	47.53
StS10-05	33.38	39.98	46.50	41.87	59.08
StS10-10	41.23	42.87	45.99	44.14	52.83
StS10-20	41.81	53.98	66.43	65.99	83.30

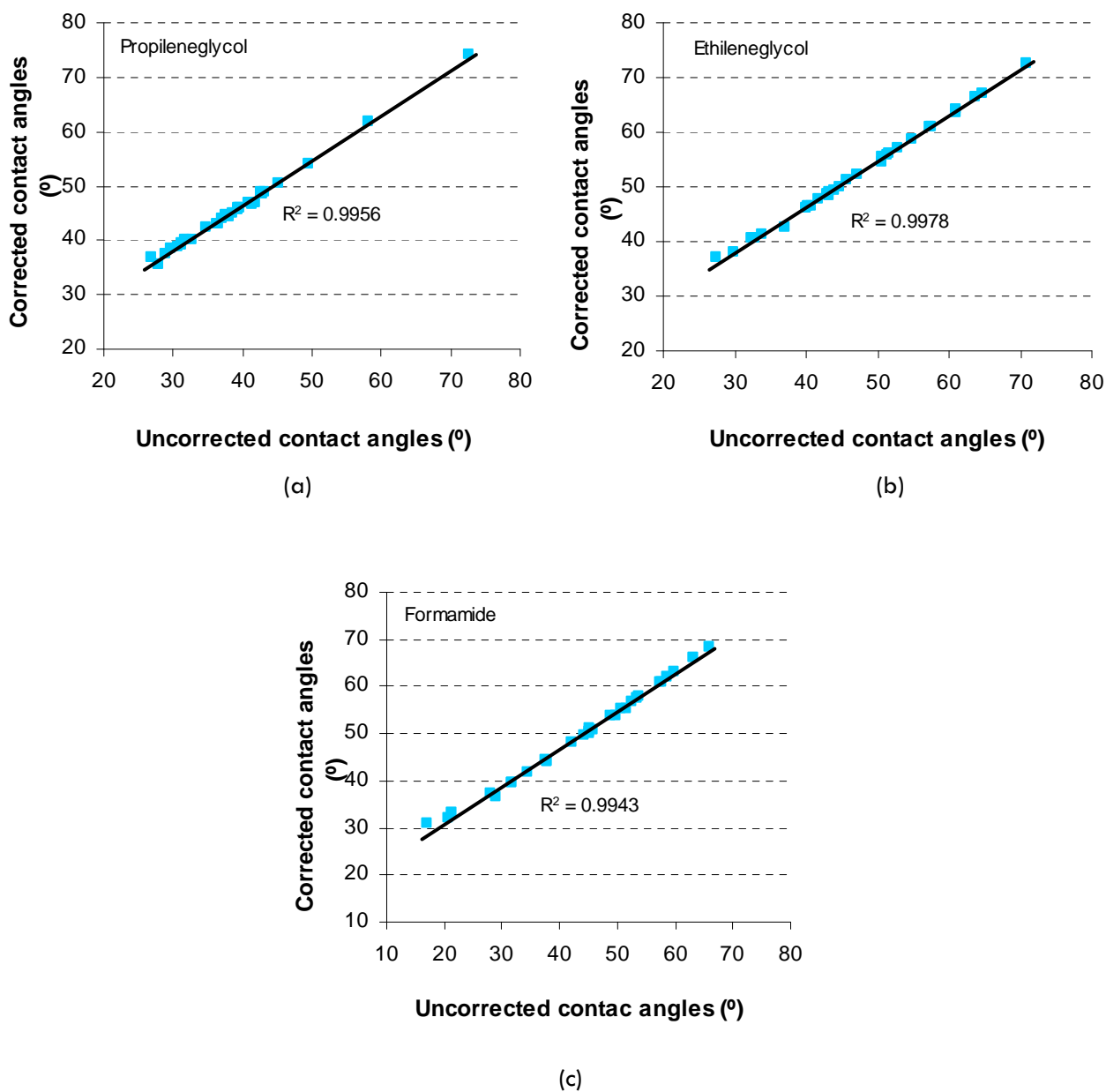


Figure E.1 - Comparison between the contact angle values before and after the application of the Wenzell correction for propilenglycol (a), ethilenglycol (b) and formamide (c).

Table E.3 – Surface free energy, corresponding dispersive and polar components of the surface energy and polar character computed before the correction of the contact angle values.

Sample	Surface Energy (mN/m)			σ_s^p/σ_s (%)
	σ_s	σ_s^d	σ_s^p	
St	51.83 ± 0.69	32.20 ± 0.5	19.63 ± 0.48	37.87
StS1-05	44.52 ± 0.69	39.35 ± 0.58	5.17 ± 0.37	11.61
StS1-10	46.24 ± 0.56	41.06 ± 0.46	5.18 ± 0.32	11.20
StS1-20	42.39 ± 0.55	38.52 ± 0.48	3.87 ± 0.26	9.13
StS2-05	46.68 ± 0.47	42.79 ± 0.39	3.89 ± 0.27	8.33
StS2-10	43.95 ± 0.42	43.13 ± 0.39	0.83 ± 0.13	1.89
StS2-20	43.34 ± 0.54	43.33 ± 0.54	0.00 ± 0.01	0.00
StS3-05	52.45 ± 0.39	42.34 ± 0.30	10.12 ± 0.24	19.29
StS3-10	46.77 ± 0.65	38.26 ± 0.51	8.51 ± 0.39	18.20
StS3-20	52.81 ± 0.45	40.39 ± 0.34	12.42 ± 0.29	23.52
StS4-05	40.34 ± 0.61	39.24 ± 0.59	1.10 ± 0.16	2.73
StS4-10	43.06 ± 0.56	41.22 ± 0.51	1.84 ± 0.22	4.27
StS4-20	40.37 ± 0.66	39.46 ± 0.63	0.91 ± 0.17	2.25
StS5-05	38.47 ± 0.84	28.8 ± 0.64	9.67 ± 0.54	25.14
StS5-10	36.58 ± 0.68	27.58 ± 0.50	9.00 ± 0.46	24.60
StS5-20	30.88 ± 0.75	21.92 ± 0.57	8.95 ± 0.48	28.98
StS6-05	46.99 ± 0.31	43.30 ± 0.25	3.68 ± 0.18	7.83
StS6-10	45.58 ± 0.50	41.64 ± 0.45	3.94 ± 0.23	8.64
StS6-20	41.93 ± 0.67	40.89 ± 0.65	1.04 ± 0.17	2.48
StS7-05	43.35 ± 0.62	40.32 ± 0.56	3.03 ± 0.26	6.99
StS7-10	42.88 ± 0.61	38.72 ± 0.53	4.16 ± 0.31	9.70
StS7-20	51.6 ± 0.64	35.28 ± 0.47	16.31 ± 0.43	31.61
StS8-05	43.01 ± 0.64	39.9 ± 0.48	3.11 ± 0.25	7.23
StS8-10	39.90 ± 0.67	38.52 ± 0.64	1.38 ± 0.22	3.46
StS8-20	41.69 ± 0.42	41.18 ± 0.40	0.51 ± 0.11	1.22
StS9-05	51.49 ± 0.30	43.74 ± 0.21	7.75 ± 0.21	15.05
StS9-10	48.01 ± 0.40	42.51 ± 0.31	5.50 ± 0.25	11.46
StS9-20	48.35 ± 0.62	37.19 ± 0.47	11.16 ± 0.40	23.08
StS10-05	58.03 ± 0.47	45.88 ± 0.35	12.16 ± 0.32	20.95
StS10-10	47.5 ± 0.61	36.54 ± 0.47	10.95 ± 0.39	23.05
StS10-20	40.42 ± 0.53	40.36 ± 0.53	0.06 ± 0.04	0.15

Table E.4 – Surface free energy, dispersive and polar components of the surface energy and polar character computed after the correction of the contact angle values..

Sample	Surface Energy (mN/m)			σ_s^p/σ_s (%)
	σ_s	σ_s^d	σ_s^p	
St	49.65 ± 0.10	38.68 ± 0.05	10.97 ± 0.09	22.09
StS1-05	44.49 ± 0.09	38.89 ± 0.05	5.60 ± 0.07	12.59
StS1-10	46.01 ± 0.09	40.32 ± 0.05	5.69 ± 0.07	12.37
StS1-20	42.02 ± 0.07	38.17 ± 0.05	3.85 ± 0.05	9.16
StS2-05	45.93 ± 0.08	40.49 ± 0.05	5.44 ± 0.06	11.84
StS2-10	41.71 ± 0.06	39.54 ± 0.05	2.16 ± 0.04	5.18
StS2-20	41.88 ± 0.05	41.15 ± 0.05	0.73 ± 0.02	1.74
StS3-05	48.99 ± 0.09	41.75 ± 0.05	7.24 ± 0.07	14.78
StS3-10	47.15 ± 0.09	40.13 ± 0.05	7.02 ± 0.08	14.89
StS3-20	50.16 ± 0.10	41.30 ± 0.05	8.85 ± 0.09	17.64
StS4-05	40.02 ± 0.06	38.38 ± 0.05	1.63 ± 0.03	4.07
StS4-10	42.13 ± 0.07	38.79 ± 0.05	3.33 ± 0.04	7.90
StS4-20	40.20 ± 0.06	38.82 ± 0.05	1.38 ± 0.03	3.43
StS5-05	40.94 ± 0.08	36.14 ± 0.05	4.81 ± 0.06	11.75
StS5-10	36.67 ± 0.10	29.08 ± 0.06	7.59 ± 0.08	20.70
StS5-20	30.63 ± 0.07	27.92 ± 0.06	2.72 ± 0.04	8.88
StS6-05	43.71 ± 0.07	39.82 ± 0.05	3.89 ± 0.05	8.90
StS6-10	43.61 ± 0.07	39.74 ± 0.05	3.88 ± 0.05	8.90
StS6-20	40.99 ± 0.06	39.38 ± 0.05	1.61 ± 0.03	3.93
StS7-05	43.56 ± 0.07	39.56 ± 0.05	4.01 ± 0.05	9.21
StS7-10	44.25 ± 0.08	39.92 ± 0.05	4.33 ± 0.06	9.79
StS7-20	44.01 ± 0.08	38.78 ± 0.05	5.23 ± 0.07	11.88
StS8-05	42.26 ± 0.08	38.28 ± 0.05	3.99 ± 0.05	9.44
StS8-10	39.56 ± 0.06	37.8 ± 0.05	1.76 ± 0.03	4.45
StS8-20	39.90 ± 0.06	38.34 ± 0.05	1.56 ± 0.03	3.91
StS9-05	48.76 ± 0.10	41.10 ± 0.05	7.66 ± 0.09	15.71
StS9-10	44.64 ± 0.08	40.37 ± 0.05	4.27 ± 0.06	9.57
StS9-20	48.15 ± 0.09	40.26 ± 0.05	7.88 ± 0.08	16.37
StS10-05	47.35 ± 0.08	42.51 ± 0.04	4.84 ± 0.06	10.22
StS10-10	45.29 ± 0.09	38.62 ± 0.05	6.67 ± 0.07	14.73
StS10-20	38.89 ± 0.05	38.35 ± 0.05	0.53 ± 0.02	1.36

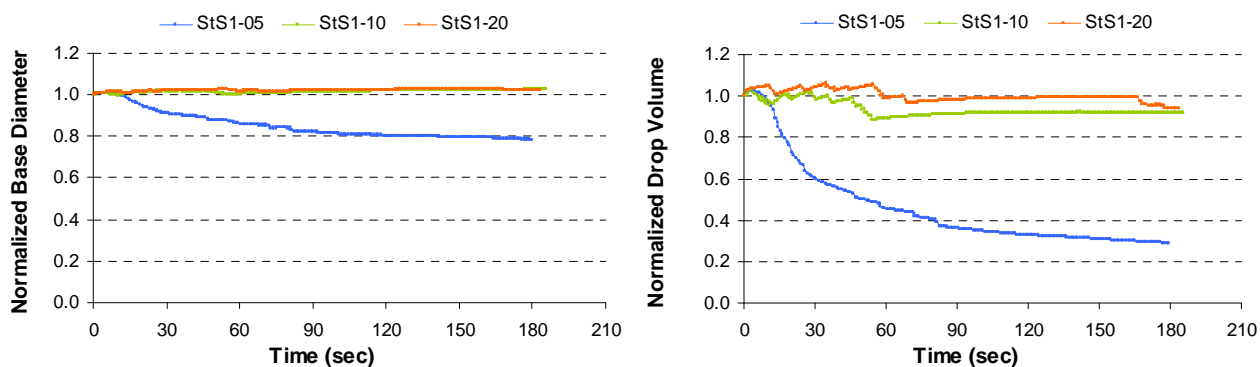


Figure E.2 - Normalized (relatively to the initial values ($t=0$)) drop base diameters and drop volume values for samples sized using the synthetic surface sizing agent S1.

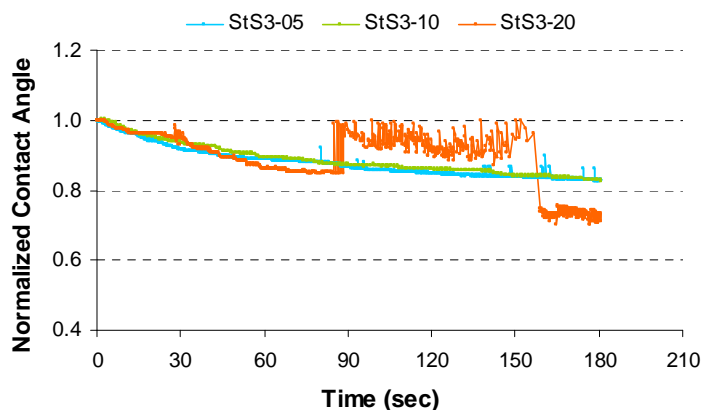


Figure E.3 - Water contact angle variation for samples sized using the synthetic surface sizing agent S3, normalized relatively to the initial value ($t=0$)

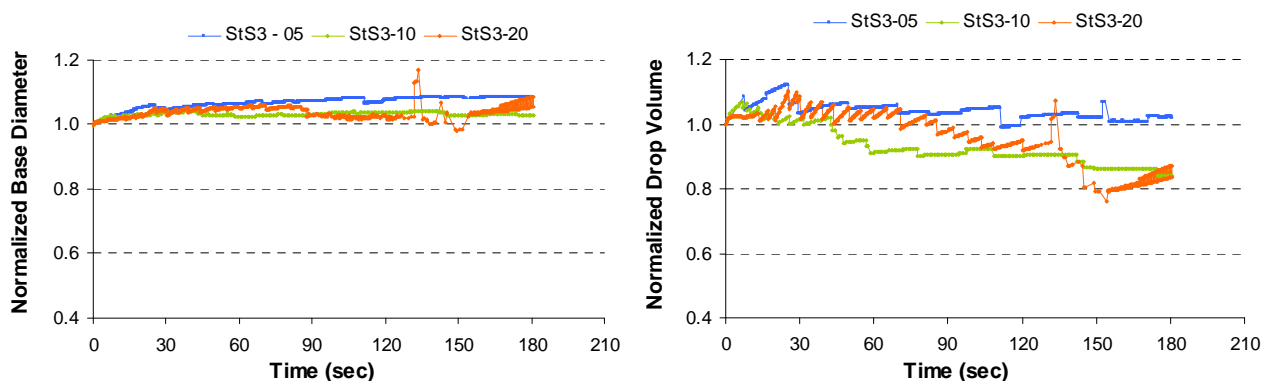


Figure E.4 - Normalized (relatively to the initial values ($t=0$)) drop base diameters and drop volume values for samples sized using the synthetic surface sizing agent S3.

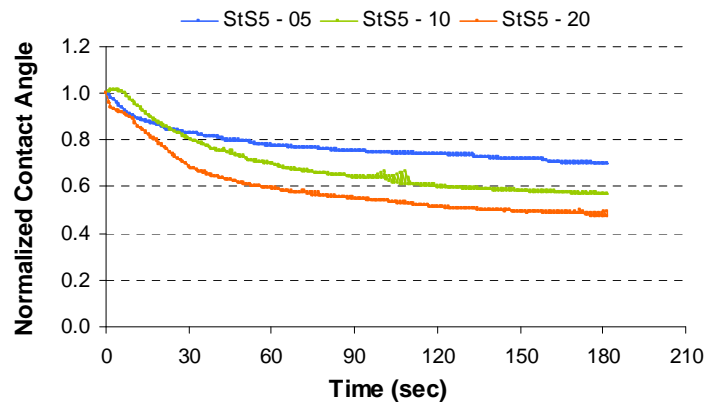


Figure E.5 - Water contact angle variation for samples sized using the synthetic surface sizing agent S5, normalized relatively to the initial value ($t=0$)

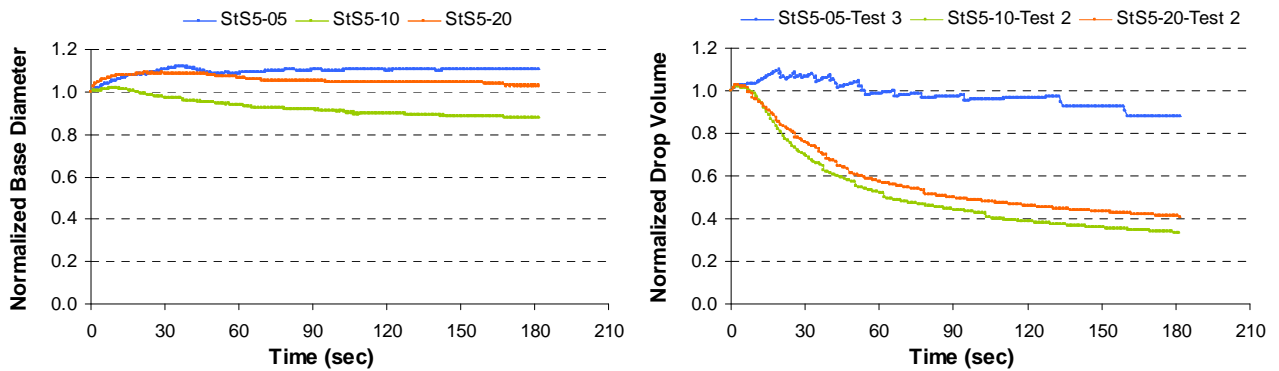


Figure E.6 - Normalized (relatively to the initial values ($t=0$)) drop base diameters and drop volume values for samples sized using the synthetic surface sizing agent S5.

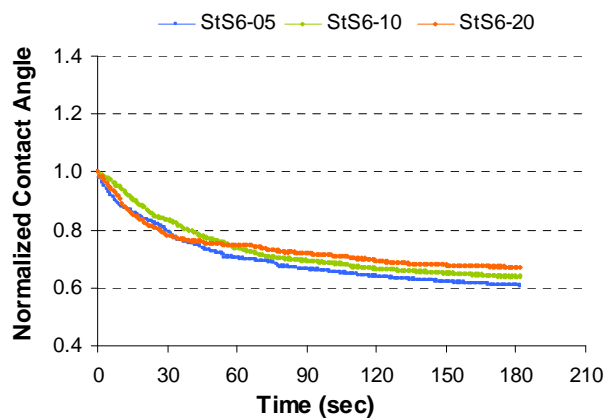


Figure E.7 - Water contact angle variation for samples sized using the synthetic surface sizing agent S6, normalized relatively to the initial value ($t=0$)

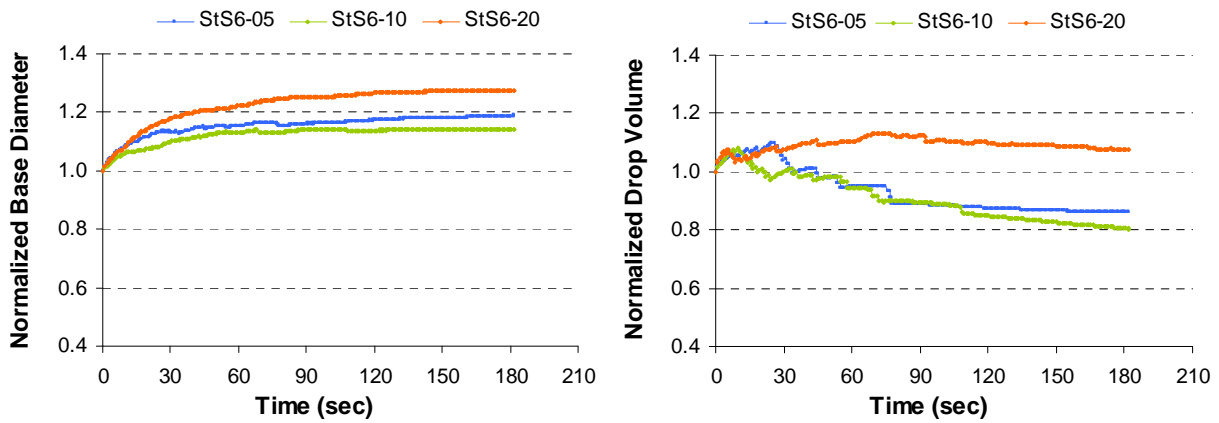


Figure E.8 - Normalized (relatively to the initial values ($t=0$)) drop base diameters and drop volume values for samples sized using the synthetic surface sizing agent S6.

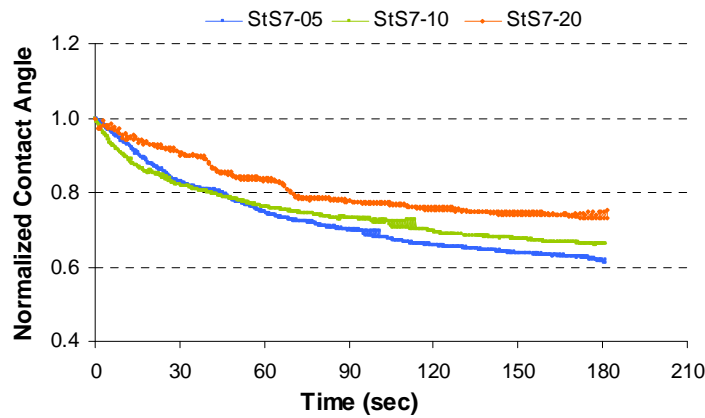


Figure E.9 - Water contact angle variation for samples sized using the synthetic surface sizing agent S7, normalized relatively to the initial value ($t=0$)

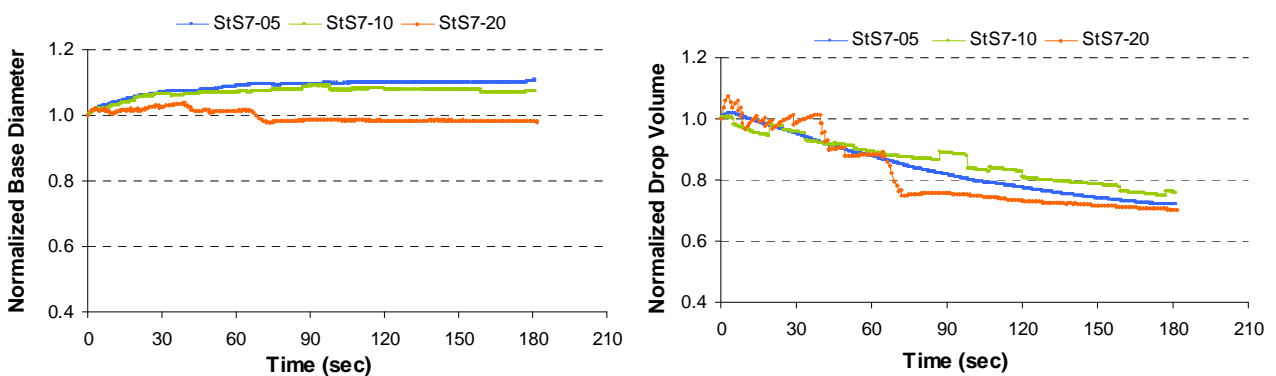


Figure E.10 - Normalized (relatively to the initial values ($t=0$)) drop base diameters and drop volume values for samples sized using the synthetic surface sizing agent S7.

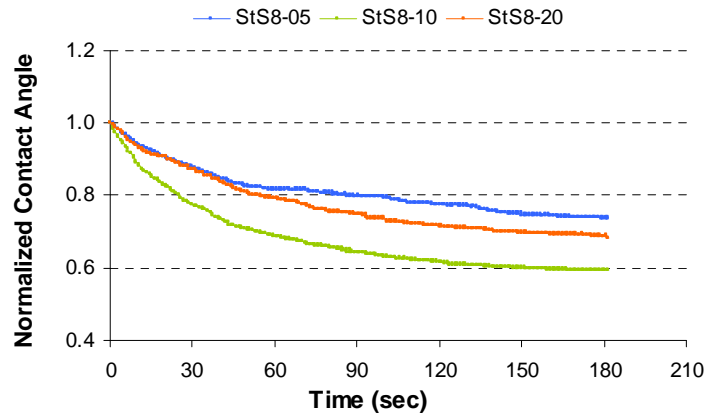


Figure E.11 - Water contact angle variation for samples sized using the synthetic surface sizing agent S8, normalized relatively to the initial value ($t=0$)

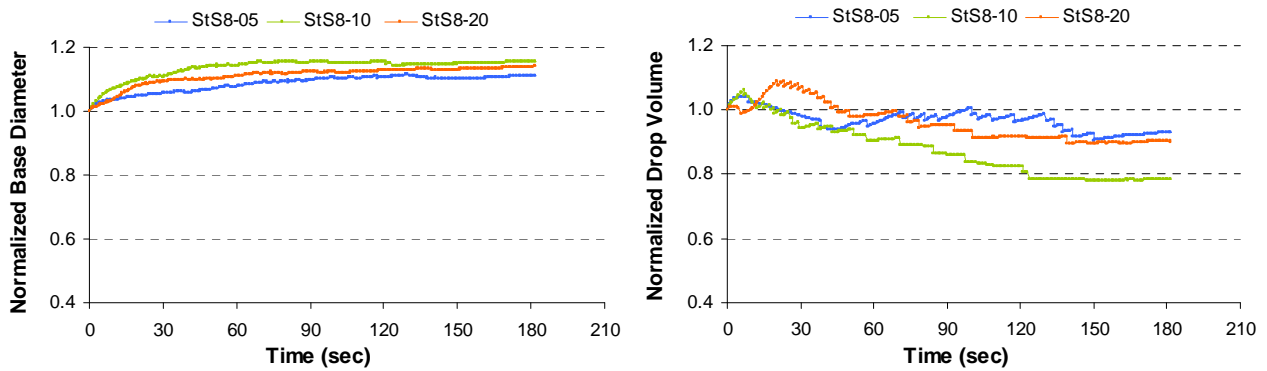


Figure E.12 - Normalized (relatively to the initial values ($t=0$)) drop base diameters and drop volume values for samples sized using the synthetic surface sizing agent S8.

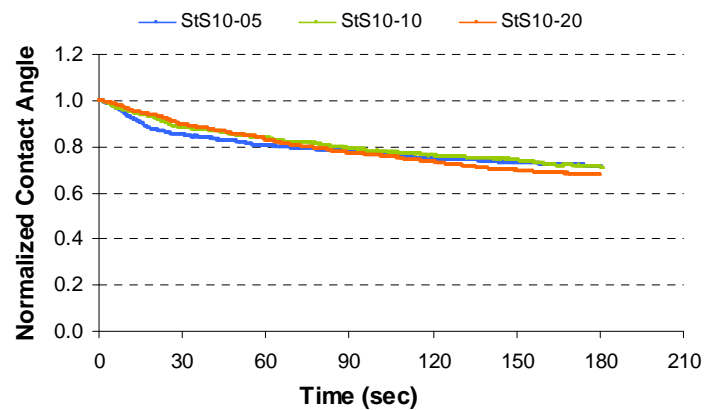


Figure E.13 - Water contact angle variation for samples sized using the synthetic surface sizing agent S10, normalized relatively to the initial value ($t=0$)

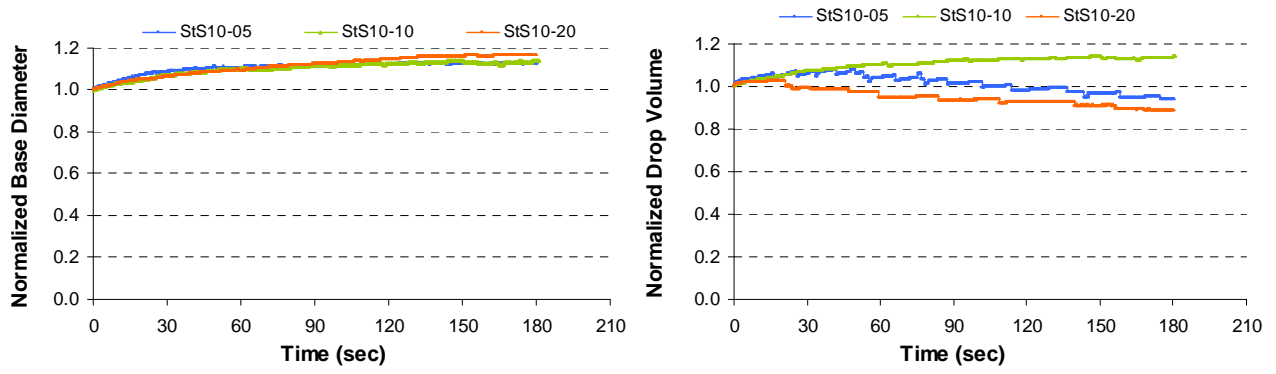


Figure E.14 - Normalized (relatively to the initial values ($t=0$)) drop base diameters and drop volume values for samples sized using the synthetic surface sizing agent S10.

APPENDIX F

INVERSE GAS CHROMATOGRAPHY

Tabel F.1 - ANOVA of the retention times determined by IGC.

Variable (Probe)	T (°C)	Contribution for the total variation (%)		Reproducibility Factor (r)	P	F	F _{critical}
		Inter-Samples	Intra-Samples				
Methane	35	99.19	0.81	0.004	5.47E-27	134.70	1.81
	40	99.24	0.76	0.004	5.04E-21	113.32	1.90
	45	99.19	0.81	0.005	3.12E-24	122.00	1.84
	50	99.09	0.91	0.004	1.74E-23	108.60	1.84
	55	99.38	0.62	0.005	6.80E-29	176.34	1.81
	60	99.88	0.12	0.003	5.87E-34	768.72	1.87
C6	35	99.63	0.37	0.003	1.96E-31	284.75	1.82
	40	99.33	0.67	0.005	2.95E-29	167.07	1.80
	45	99.84	0.16	0.003	3.67E-32	571.62	1.87
	50	99.32	0.68	0.004	1.67E-23	136.26	1.87
	55	99.90	0.10	0.003	1.54E-25	666.50	2.01
	60	99.82	0.18	0.004	1.71E-31	511.92	1.87
C7	35	99.59	0.41	0.005	9.42E-31	257.95	1.82
	40	99.88	0.12	0.003	9.45E-37	844.57	1.84
	45	99.88	0.12	0.003	1.70E-35	825.30	1.85
	50	99.72	0.28	0.003	1.11E-26	311.61	1.90
	55	99.85	0.15	0.004	1.74E-31	607.72	1.88
	60	99.96	0.04	0.002	3.47E-36	2132.78	1.92
C8	35	99.91	0.09	0.005	1.72E-46	1267.17	1.78
	40	99.87	0.13	0.006	1.66E-41	886.44	1.80
	45	99.90	0.10	0.006	1.89E-43	1154.17	1.80
	50	99.88	0.12	0.003	5.31E-29	692.37	1.94
	55	99.36	0.64	0.013	6.35E-23	139.70	1.88
	60	99.93	0.07	0.004	2.62E-38	1290.75	1.85
C9	35	99.86	0.14	0.016	3.53E-50	996.47	1.74
	40	99.90	0.10	0.015	4.77E-47	1173.64	1.77
	45	99.95	0.05	0.009	1.68E-46	2078.99	1.81
	50	99.79	0.21	0.008	2.89E-34	494.63	1.83
	55	99.93	0.07	0.007	1.09E-37	1421.23	1.87
	60	99.92	0.08	0.008	3.86E-36	1101.41	1.87
C10	35	99.84	0.16	0.049	4.76E-54	944.58	1.71
	40	99.81	0.19	0.060	5.00E-46	701.13	1.74
	45	99.91	0.09	0.030	1.59E-48	1410.92	1.77
	50	99.90	0.10	0.016	5.59E-42	1105.34	1.81
	55	97.19	2.81	0.111	5.32E-15	32.27	1.87
	60	99.96	0.04	0.011	4.29E-48	2597.47	1.81
DCM	35	91.80	8.20	0.021	4.23E-15	16.04	1.72
	40	95.97	4.03	0.017	4.43E-22	34.97	1.72
	45	99.19	0.81	0.008	9.37E-30	147.09	1.78
	50	97.97	2.03	0.007	2.23E-23	59.66	1.77
	55	99.58	0.42	0.006	2.14E-26	220.36	1.87
	60	99.73	0.27	0.006	4.74E-29	341.97	1.87
TCM	35	94.83	5.17	0.017	1.28E-17	24.45	1.74

	40	99.98	0.02	0.016	1.32E-64	7123.91	1.75
	45	99.31	0.69	0.008	7.34E-33	181.10	1.76
	50	98.85	1.15	0.005	8.30E-23	88.60	1.83
	55	99.87	0.13	0.004	3.60E-31	692.29	1.90
	60	99.89	0.11	0.004	9.86E-32	765.03	1.90
Acet	35	69.01	30.99	0.619	7.09E-09	5.19	1.62
	40	87.10	12.90	0.147	2.72E-14	11.71	1.68
	45	73.34	26.66	0.208	1.08E-06	4.59	1.69
	50	73.26	26.74	0.114	7.32E-07	4.66	1.68
	55	91.82	8.18	0.053	1.48E-15	16.46	1.72
	60	91.46	8.54	0.038	1.80E-16	16.78	1.70
ETA	35	95.22	4.78	0.321	7.67E-24	33.18	1.69
	40	58.82	41.18	0.534	3.24E-03	2.38	1.69
	45	94.75	5.25	0.150	2.54E-22	29.50	1.69
	50	85.37	14.63	0.087	9.74E-11	8.75	1.71
	55	94.70	5.30	0.043	3.92E-21	27.98	1.70
	60	94.72	5.28	0.041	4.90E-19	25.73	1.72
THF	35	92.03	7.97	0.426	1.02E-21	21.95	1.66
	40	79.94	20.06	0.252	2.56E-10	7.17	1.67
	45	90.76	9.24	0.119	5.73E-17	16.37	1.69
	50	94.20	5.80	0.043	9.95E-20	24.90	1.71
	55	93.93	6.07	0.046	2.84E-17	21.65	1.73
	60	94.25	5.75	0.037	2.49E-20	25.67	1.70

Tabel F.2 – Retention times obtained at 35°C with each of the probes tested, for all the 31 samples produced.

35°C		Compound									
Sample	Methane	C6	C7	C8	C9	C10	DCM	TCM	Acet	ETA	THF
St	0.091	0.123	0.183	0.362	0.885	2.425	0.140	0.165	0.350	0.365	0.502
StS1-05	0.077	0.100	0.150	0.293	0.673	1.867	0.117	0.127	0.280	0.347	0.320
StS1-10	0.090	0.110	0.159	0.302	0.715	2.107	0.127	0.137	0.180	0.225	0.291
StS1-20	0.083	0.108	0.157	0.307	0.711	1.917	0.132	0.152	0.221	0.333	0.361
StS2-05	0.080	0.117	0.184	0.368	0.921	2.555	0.155	0.160	0.525	0.707	0.847
StS2-10	0.077	0.099	0.143	0.277	0.657	1.847	0.127	0.129	0.534	0.464	0.365
StS2-20	0.067	0.097	0.150	0.309	0.778	2.186	0.132	0.153	0.987	1.767	1.724
StS3-05	0.067	0.080	0.120	0.229	0.550	1.477	0.102	0.107	0.265	0.234	0.220
StS3-10	0.077	0.083	0.123	0.247	0.618	1.606	0.121	0.134	0.242	0.255	0.272
StS3-20	0.100	0.129	0.197	0.397	0.978	2.686	0.143	0.169	0.394	0.404	0.517
StS4-05	0.083	0.110	0.162	0.313	0.746	2.029	0.153	0.163	0.440	0.654	0.479
StS4-10	0.067	0.090	0.136	0.263	0.637	1.751	0.116	0.133	0.521	0.545	0.469
StS4-20	0.067	0.101	0.167	0.350	0.888	2.487	0.135	0.174	1.239	0.574	1.582
StS5-05	0.073	0.079	0.133	0.250	0.567	1.556	0.108	0.126	0.238	0.333	0.296
StS5-10	0.087	0.110	0.167	0.323	0.760	2.064	0.140	0.153	0.255	0.382	0.417
StS5-20	0.077	0.100	0.150	0.297	0.710	1.883	0.117	0.130	0.279	0.410	0.322
StS6-05	0.090	0.120	0.167	0.323	0.760	2.047	0.137	0.167	0.327	0.490	0.430
StS6-10	0.080	0.107	0.160	0.313	0.740	2.013	0.130	0.137	0.247	0.340	0.337
StS6-20	0.080	0.107	0.153	0.290	0.670	1.810	0.135	0.137	0.257	0.357	0.377
StS7-05	0.090	0.100	0.153	0.305	0.747	2.044	0.162	0.170	0.097	0.102	0.932
StS7-10	0.083	0.107	0.157	0.307	0.740	2.043	0.147	0.163	0.967	1.026	0.688
StS7-20	0.077	0.093	0.136	0.247	0.578	1.548	0.105	0.123	0.286	0.345	0.293
StS8-05	0.077	0.101	0.143	0.267	0.600	1.604	0.120	0.129	0.312	0.310	0.417
StS8-10	0.100	0.128	0.187	0.344	0.793	2.081	0.153	0.168	0.309	0.295	0.358
StS8-20	0.067	0.083	0.120	0.213	0.475	1.239	0.091	0.103	0.135	0.202	0.212
StS9-05	0.070	0.100	0.152	0.311	0.777	2.143	0.125	0.153	0.787	1.643	1.457
StS9-10	0.083	0.117	0.180	0.363	0.882	2.479	0.139	0.164	0.506	0.667	0.603
StS9-20	0.054	0.077	0.120	0.240	0.575	1.619	0.093	0.113	0.280	0.368	0.516
StS10-05	0.083	0.103	0.153	0.297	0.713	1.948	0.132	0.143	0.359	0.709	0.415
StS10-10	0.070	0.094	0.143	0.297	0.731	2.037	0.110	0.138	0.207	0.382	0.295
StS10-20	0.073	0.093	0.140	0.272	0.647	1.760	0.113	0.132	0.294	0.300	0.263

Tabel F.3 – Retention times obtained at 40°C with each of the probes tested, for all the 31 samples produced.

40°C	Compound										
Sample	Methane	C6	C7	C8	C9	C10	DCM	TCM	Acet	ETA	THF
St	0.093	0.120	0.170	0.307	0.689	1.777	0.131	0.153	0.289	0.350	0.291
StS1-05	0.070	0.093	0.133	0.247	0.530	1.347	0.113	0.120	0.253	0.233	0.393
StS1-10	0.088	0.109	0.149	0.257	0.562	1.529	0.120	0.129	0.168	0.195	0.211
StS1-20	0.083	0.105	0.143	0.255	0.545	1.382	0.120	0.140	0.238	0.264	0.278
StS2-05	0.070	0.096	0.143	0.270	0.632	1.646	0.121	0.129	0.371	0.499	0.495
StS2-10	0.070	0.082	0.113	0.199	0.440	1.141	0.107	0.109	0.338	0.287	0.268
StS2-20	0.061	0.084	0.123	0.230	0.530	1.386	0.103	0.113	0.306	0.433	0.407
StS3-05	0.066	0.076	0.103	0.182	0.395	1.011	0.083	0.093	0.213	0.171	0.213
StS3-10	0.075	0.089	0.127	0.223	0.502	1.293	0.118	0.130	0.261	0.225	0.259
StS3-20	0.097	0.127	0.186	0.337	0.761	1.974	0.146	0.170	0.255	0.471	0.411
StS4-05	0.075	0.093	0.130	0.227	0.500	1.263	0.111	0.117	0.241	0.339	0.341
StS4-10	0.067	0.087	0.123	0.220	0.494	1.274	0.113	0.117	0.467	0.425	0.463
StS4-20	0.070	0.097	0.141	0.276	0.649	1.721	0.128	0.131	0.350	0.517	0.424
StS5-05	0.070	0.087	0.120	0.207	0.437	1.087	0.096	0.110	0.170	0.224	0.242
StS5-10	0.087	0.107	0.150	0.263	0.587	1.510	0.127	0.130	0.203	0.333	0.283
StS5-20	0.077	0.097	0.137	0.253	0.550	1.403	0.107	0.120	0.207	0.273	0.200
StS6-05	0.083	0.113	0.153	0.273	0.593	1.533	0.123	0.150	0.230	0.373	0.380
StS6-10	0.080	0.100	0.143	0.257	0.560	1.483	0.123	0.127	0.230	0.280	0.283
StS6-20	0.083	0.103	0.140	0.250	0.543	1.360	0.120	0.123	0.250	0.343	0.320
StS7-05	0.083	0.100	0.147	0.273	0.632	1.657	0.157	1.698	0.087	0.787	0.687
StS7-10	0.083	0.100	0.137	0.243	0.542	1.391	0.120	0.133	0.596	0.740	0.476
StS7-20	0.072	0.089	0.122	0.211	0.454	1.153	0.102	0.110	0.179	0.268	0.301
StS8-05	0.077	0.097	0.133	0.229	0.490	1.224	0.113	0.121	0.254	0.273	0.271
StS8-10	0.097	0.120	0.162	0.280	0.594	1.485	0.139	0.145	0.275	0.289	0.253
StS8-20	0.067	0.080	0.107	0.173	0.360	0.867	0.087	0.096	0.125	0.187	0.164
StS9-05	0.067	0.090	0.130	0.238	0.543	1.413	0.111	0.126	0.488	0.645	0.826
StS9-10	0.096	0.138	0.212	0.403	0.986	2.820	0.197	0.224	0.400	0.632	0.472
StS9-20	0.057	0.073	0.107	0.199	0.442	1.147	0.087	0.099	0.248	0.250	0.334
StS10-05	0.083	0.097	0.133	0.237	0.523	1.347	0.120	0.130	0.309	0.659	0.362
StS10-10	0.073	0.092	0.133	0.239	0.559	1.445	0.101	0.121	0.155	0.213	0.212
StS10-20	0.080	0.097	0.130	0.233	0.513	1.311	0.103	0.123	0.233	0.277	0.214

Tabel F.4 – Retention times obtained at 45°C with each of the probes tested, for all the 31 samples produced.

45°C Sample	Compound										
	Methane	C6	C7	C8	C9	C10	DCM	TCM	Acet	ETA	THF
St	0.093	0.117	0.156	0.262	0.545	1.303	0.129	0.140	0.245	0.220	0.265
StS1-05	0.070	0.090	0.120	0.200	0.410	0.967	0.103	0.107	0.157	0.273	0.253
StS1-10	0.087	0.109	0.137	0.219	0.441	1.075	0.112	0.121	0.154	0.189	0.177
StS1-20	0.083	0.100	0.132	0.213	0.425	1.002	0.118	0.123	0.225	0.250	0.257
StS2-05	0.074	0.097	0.133	0.230	0.494	1.237	0.110	0.118	0.275	0.337	0.308
StS2-10	0.067	0.080	0.103	0.169	0.342	0.817	0.090	0.097	0.226	0.266	0.248
StS2-20	0.062	0.080	0.109	0.191	0.407	0.993	0.093	0.103	0.224	0.416	0.349
StS3-05	0.067	0.067	0.090	0.142	0.286	0.671	0.077	0.079	0.132	0.147	0.150
StS3-10	0.080	0.108	0.141	0.231	0.480	1.130	0.116	0.126	0.229	0.211	0.250
StS3-20	0.100	0.119	0.158	0.268	0.557	1.343	0.130	0.143	0.189	0.252	0.311
StS4-05	0.073	0.087	0.113	0.183	0.363	0.902	0.104	0.108	0.198	0.237	0.239
StS4-10	0.063	0.077	0.103	0.167	0.336	0.801	0.092	0.094	0.195	0.273	0.322
StS4-20	0.070	0.090	0.127	0.223	0.483	1.196	0.111	0.119	0.559	0.786	0.399
StS5-05	0.070	0.087	0.110	0.177	0.350	0.810	0.093	0.100	0.142	0.209	0.182
StS5-10	0.087	0.107	0.133	0.227	0.463	1.117	0.123	0.127	0.197	0.233	0.230
StS5-20	0.077	0.097	0.133	0.217	0.443	1.070	0.103	0.117	0.167	0.210	0.180
StS6-05	0.083	0.103	0.137	0.227	0.490	1.087	0.117	0.120	0.213	0.260	0.247
StS6-10	0.083	0.100	0.130	0.220	0.447	1.053	0.113	0.117	0.190	0.240	0.220
StS6-20	0.083	0.093	0.130	0.207	0.417	0.977	0.113	0.114	0.207	0.260	0.250
StS7-05	0.093	0.103	0.143	0.249	0.535	1.320	0.146	0.153	0.094	0.543	0.563
StS7-10	0.087	0.098	0.130	0.213	0.436	1.049	0.114	0.127	0.376	0.466	0.480
StS7-20	0.070	0.083	0.109	0.172	0.342	0.779	0.094	0.100	0.160	0.184	0.182
StS8-05	0.080	0.097	0.123	0.193	0.379	0.877	0.105	0.114	0.204	0.194	0.209
StS8-10	0.095	0.113	0.147	0.232	0.459	1.053	0.127	0.134	0.233	0.255	0.230
StS8-20	0.067	0.080	0.100	0.156	0.299	0.670	0.085	0.092	0.112	0.149	0.138
StS9-05	0.070	0.086	0.117	0.197	0.416	1.015	0.105	0.113	0.221	0.373	0.396
StS9-10	0.127	0.167	0.227	0.400	0.860	2.137	0.220	0.220	0.349	0.472	0.465
StS9-20	0.057	0.070	0.097	0.163	0.337	0.803	0.083	0.090	0.140	0.177	0.190
StS10-05	0.087	0.097	0.129	0.210	0.423	1.000	0.110	0.123	0.267	0.473	0.341
StS10-10	0.070	0.083	0.113	0.188	0.383	0.922	0.093	0.097	0.113	0.175	0.158
StS10-20	0.077	0.090	0.117	0.193	0.387	0.927	0.103	0.111	0.207	0.243	0.199

Tabel F.5 – Retention times obtained at 35°C with each of the probes tested, for all the 31 samples produced.

50°C	Compound										
Sample	Methane	C6	C7	C8	C9	C10	DCM	TCM	Acet	ETA	THF
St	0.093	0.113	0.140	0.219	0.419	0.937	0.124	0.129	0.171	0.205	0.220
StS1-05	0.073	0.087	0.110	0.173	0.323	0.717	0.097	0.107	0.157	0.163	0.223
StS1-10	0.073	0.087	0.107	0.160	0.293	0.652	0.091	0.099	0.117	0.139	0.140
StS1-20	0.083	0.096	0.120	0.177	0.322	0.710	0.107	0.113	0.166	0.225	0.194
StS2-05	0.070	0.088	0.117	0.187	0.370	0.855	0.103	0.112	0.208	0.307	0.306
StS2-10	0.067	0.080	0.097	0.147	0.276	0.612	0.090	0.093	0.148	0.183	0.181
StS2-20	0.063	0.080	0.100	0.160	0.316	0.716	0.087	0.094	0.168	0.207	0.233
StS3-05	0.063	0.070	0.087	0.130	0.240	0.527	0.073	0.080	0.124	0.130	0.139
StS3-10	0.074	0.093	0.111	0.167	0.310	0.690	0.114	0.124	0.184	0.175	0.184
StS3-20	0.083	0.093	0.117	0.183	0.347	0.786	0.106	0.110	0.137	0.182	0.180
StS4-05	0.076	0.087	0.107	0.160	0.294	0.661	0.099	0.103	0.172	0.208	0.195
StS4-10	0.063	0.073	0.093	0.140	0.260	0.577	0.084	0.088	0.162	0.210	0.238
StS4-20	0.063	0.080	0.103	0.167	0.332	0.767	0.098	0.097	0.320	0.318	0.274
StS5-05	0.070	0.087	0.103	0.157	0.287	0.623	0.090	0.097	0.130	0.160	0.145
StS5-10	0.087	0.100	0.127	0.200	0.373	0.873	0.113	0.123	0.194	0.220	0.227
StS5-20	0.080	0.097	0.123	0.193	0.377	0.847	0.103	0.113	0.143	0.173	0.167
StS6-05	0.083	0.103	0.123	0.190	0.353	0.790	0.109	0.110	0.173	0.223	0.220
StS6-10	0.083	0.100	0.123	0.187	0.347	0.803	0.107	0.113	0.157	0.220	0.210
StS6-20	0.080	0.093	0.117	0.173	0.317	0.707	0.100	0.112	0.167	0.193	0.180
StS7-05	0.083	0.090	0.117	0.189	0.376	0.873	0.110	0.117	0.084	0.229	0.189
StS7-10	0.083	0.093	0.113	0.177	0.335	0.747	0.106	0.113	0.286	0.358	0.302
StS7-20	0.067	0.082	0.100	0.150	0.267	0.583	0.089	0.093	0.125	0.151	0.153
StS8-05	0.082	0.090	0.113	0.167	0.302	0.652	0.101	0.107	0.155	0.175	0.174
StS8-10	0.097	0.111	0.138	0.202	0.362	0.780	0.121	0.129	0.187	0.202	0.190
StS8-20	0.070	0.079	0.097	0.139	0.249	0.520	0.083	0.090	0.109	0.134	0.132
StS9-05	0.063	0.076	0.096	0.147	0.281	0.638	0.084	0.093	0.182	0.247	0.267
StS9-10	xxx	xxx	xxx	xxx	xxx	xxx	xxx	xxx	xxx	xxx	xxx
StS9-20	0.057	0.070	0.087	0.135	0.259	0.580	0.075	0.083	0.157	0.162	0.194
StS10-05	0.083	0.090	0.113	0.170	0.317	0.700	0.100	0.110	0.199	0.235	0.202
StS10-10	0.073	0.080	0.102	0.157	0.300	0.677	0.087	0.096	0.117	0.156	0.149
StS10-20	0.077	0.087	0.107	0.160	0.300	0.670	0.097	0.103	0.177	0.200	0.167

Tabel F.6 – Retention times obtained at 55°C with each of the probes tested, for all the 31 samples produced.

55°C Sample	Compound										
	Methane	C6	C7	C8	C9	C10	DCM	TCM	Acet	ETA	THF
St	0.095	0.110	0.132	0.201	0.337	0.703	0.117	0.123	0.160	0.194	0.179
StS1-05	0.073	0.087	0.103	0.150	0.260	0.540	0.093	0.097	0.157	0.140	0.173
StS1-10	0.077	0.087	0.103	0.142	0.245	0.502	0.093	0.097	0.116	0.125	0.126
StS1-20	0.083	0.097	0.117	0.163	0.280	0.567	0.105	0.110	0.159	0.163	0.186
StS2-05	0.076	0.090	0.111	0.167	0.309	0.657	0.101	0.103	0.258	0.201	0.269
StS2-10	0.067	0.080	0.093	0.132	0.227	0.463	0.087	0.090	0.135	0.155	0.166
StS2-20	0.063	0.080	0.097	0.143	0.256	0.548	0.087	0.091	0.163	0.185	0.226
StS3-05	0.063	0.067	0.079	0.110	0.188	0.377	0.070	0.073	0.108	0.120	0.112
StS3-10	0.090	0.103	0.123	0.172	0.319	0.640	0.113	0.123	0.167	0.170	0.178
StS3-20	0.086	0.097	0.116	0.167	0.283	0.603	0.113	0.116	0.148	0.170	0.164
StS4-05	0.076	0.087	0.100	0.143	0.243	0.343	0.096	0.100	0.164	0.190	0.186
StS4-10	0.063	0.073	0.090	0.123	0.213	0.440	0.082	0.083	0.127	0.157	0.163
StS4-20	0.060	0.077	0.093	0.140	0.260	0.558	0.087	0.089	0.232	0.247	0.247
StS5-05	0.073	0.087	0.103	0.140	0.237	0.480	0.090	0.093	0.125	0.138	0.135
StS5-10	0.087	0.100	0.123	0.180	0.317	0.660	0.110	0.113	0.163	0.213	0.183
StS5-20	0.080	0.097	0.120	0.177	0.320	0.667	0.100	0.110	0.140	0.165	0.153
StS6-05	0.083	0.100	0.120	0.167	0.310	0.590	0.105	0.107	0.163	0.193	0.213
StS6-10	0.083	0.097	0.117	0.163	0.280	0.587	0.103	0.107	0.143	0.197	0.183
StS6-20	xxx	xxx	xxx	xxx	xxx	xxx	xxx	xxx	xxx	xxx	xxx
StS7-05	0.082	0.087	0.105	0.147	0.250	0.513	0.092	0.100	0.155	0.190	0.177
StS7-10	0.070	0.080	0.097	0.137	0.237	0.493	0.093	0.096	0.214	0.243	0.224
StS7-20	0.063	0.070	0.081	0.110	0.187	0.376	0.073	0.073	0.092	0.113	0.114
StS8-05	0.082	0.090	0.107	0.149	0.247	0.500	0.100	0.103	0.150	0.152	0.149
StS8-10	0.100	0.110	0.132	0.182	0.303	0.605	0.120	0.123	0.157	0.180	0.171
StS8-20	0.070	0.077	0.090	0.124	0.202	0.402	0.083	0.087	0.105	0.116	0.115
StS9-05	0.062	0.073	0.089	0.130	0.227	0.473	0.082	0.087	0.139	0.190	0.215
StS9-10	0.150	0.180	0.220	0.327	0.585	1.254	0.205	0.212	0.342	0.380	0.349
StS9-20	0.057	0.067	0.083	0.120	0.210	0.443	0.073	0.077	0.113	0.127	0.183
StS10-05	0.077	0.083	0.100	0.140	0.239	0.482	0.093	0.093	0.152	0.158	0.148
StS10-10	0.072	0.080	0.101	0.147	0.263	0.547	0.080	0.092	0.109	0.130	0.129
StS10-20	0.073	0.080	0.093	0.132	0.227	0.463	0.087	0.093	0.127	0.142	0.137

Tabel F.7 – Retention times obtained at 60°C with each of the probes tested, for all the 31 samples produced.

60°C	Compound										
Sample	Methane	C6	C7	C8	C9	C10	DCM	TCM	Acet	ETA	THF
St	0.093	0.107	0.123	0.169	0.277	0.534	0.110	0.117	0.157	0.150	0.163
StS1-05	0.073	0.083	0.097	0.133	0.220	0.420	0.087	0.097	0.127	0.133	0.147
StS1-10	0.077	0.087	0.101	0.132	0.207	0.397	0.090	0.093	0.108	0.115	0.109
StS1-20	0.083	0.093	0.110	0.145	0.229	0.429	0.103	0.107	0.142	0.150	0.158
StS2-05	0.077	0.090	0.107	0.150	0.250	0.502	0.099	0.100	0.199	0.190	0.180
StS2-10	0.067	0.080	0.093	0.123	0.197	0.371	0.086	0.087	0.139	0.158	0.146
StS2-20	0.063	0.078	0.090	0.127	0.213	0.421	0.083	0.087	0.129	0.153	0.169
StS3-05	0.060	0.062	0.073	0.093	0.147	0.282	0.063	0.067	0.079	0.093	0.098
StS3-10	0.083	0.093	0.110	0.149	0.237	0.451	0.103	0.107	0.130	0.154	0.156
StS3-20	0.082	0.092	0.107	0.147	0.239	0.463	0.098	0.104	0.126	0.133	0.140
StS4-05	0.071	0.080	0.093	0.121	0.190	0.354	0.088	0.090	0.134	0.147	0.157
StS4-10	0.067	0.073	0.087	0.116	0.182	0.348	0.080	0.083	0.115	0.132	0.140
StS4-20	0.066	0.077	0.090	0.123	0.213	0.423	0.082	0.087	0.185	0.193	0.228
StS5-05	0.070	0.083	0.093	0.127	0.200	0.373	0.090	0.092	0.120	0.133	0.130
StS5-10	0.087	0.097	0.120	0.163	0.263	0.517	0.105	0.107	0.150	0.163	0.173
StS5-20	0.080	0.093	0.113	0.157	0.273	0.543	0.097	0.105	0.130	0.143	0.138
StS6-05	0.083	0.093	0.110	0.150	0.237	0.467	0.103	0.105	0.157	0.163	0.173
StS6-10	0.083	0.093	0.110	0.150	0.237	0.450	0.100	0.103	0.137	0.170	0.157
StS6-20	0.083	0.093	0.107	0.137	0.217	0.407	0.097	0.100	0.143	0.150	0.147
StS7-05	0.083	0.089	0.103	0.137	0.217	0.412	0.093	0.095	0.147	0.158	0.158
StS7-10	0.073	0.087	0.093	0.127	0.200	0.384	0.080	0.091	0.153	0.177	0.169
StS7-20	0.063	0.073	0.083	0.112	0.176	0.328	0.076	0.079	0.099	0.103	0.113
StS8-05	0.083	0.090	0.103	0.137	0.213	0.390	0.097	0.099	0.140	0.137	0.140
StS8-10	0.100	0.110	0.129	0.167	0.262	0.487	0.117	0.122	0.147	0.165	0.159
StS8-20	0.070	0.077	0.087	0.113	0.175	0.319	0.081	0.083	0.098	0.109	0.109
StS9-05	0.063	0.073	0.087	0.117	0.187	0.360	0.080	0.083	0.135	0.143	0.170
StS9-10	0.169	0.199	0.237	0.330	0.555	1.098	0.227	0.235	0.280	0.346	0.333
StS9-20	0.057	0.067	0.080	0.107	0.177	0.340	0.070	0.077	0.097	0.120	0.120
StS10-05	0.077	0.080	0.093	0.123	0.201	0.373	0.088	0.090	0.133	0.134	0.134
StS10-10	0.067	0.070	0.083	0.113	0.187	0.365	0.073	0.080	0.092	0.104	0.107
StS10-20	0.077	0.082	0.091	0.123	0.197	0.370	0.084	0.090	0.117	0.123	0.117

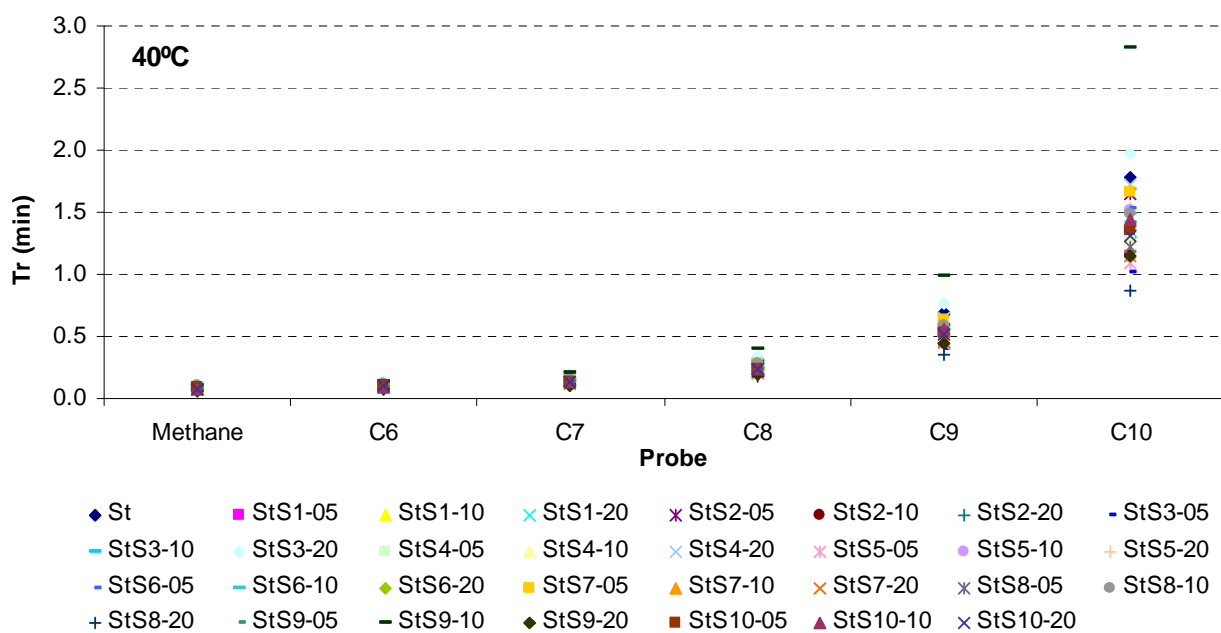


Figure F.1 – Retention times obtained at 40°C with the n-alkanes for the reference samples and the samples sized with each of the sizing agents at each of the incorporation percentages.

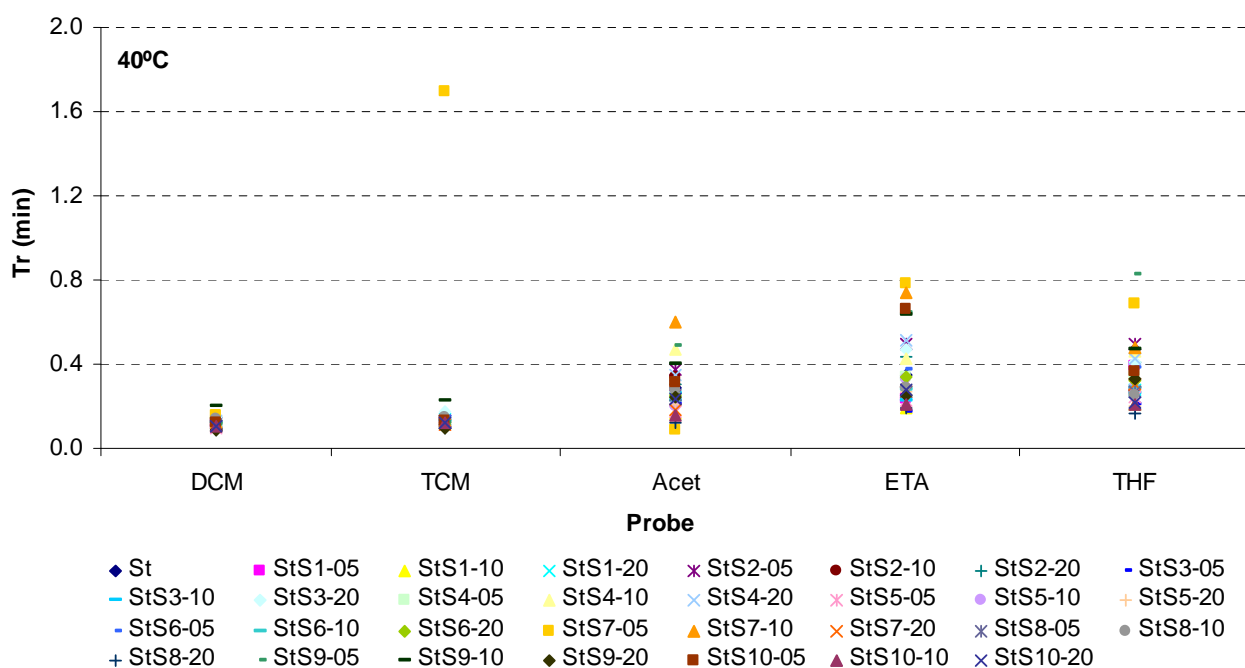


Figure F.2 – Retention times obtained at 40°C with the polar probes for the reference samples and the samples sized with each of the sizing agents at each of the incorporation percentages.

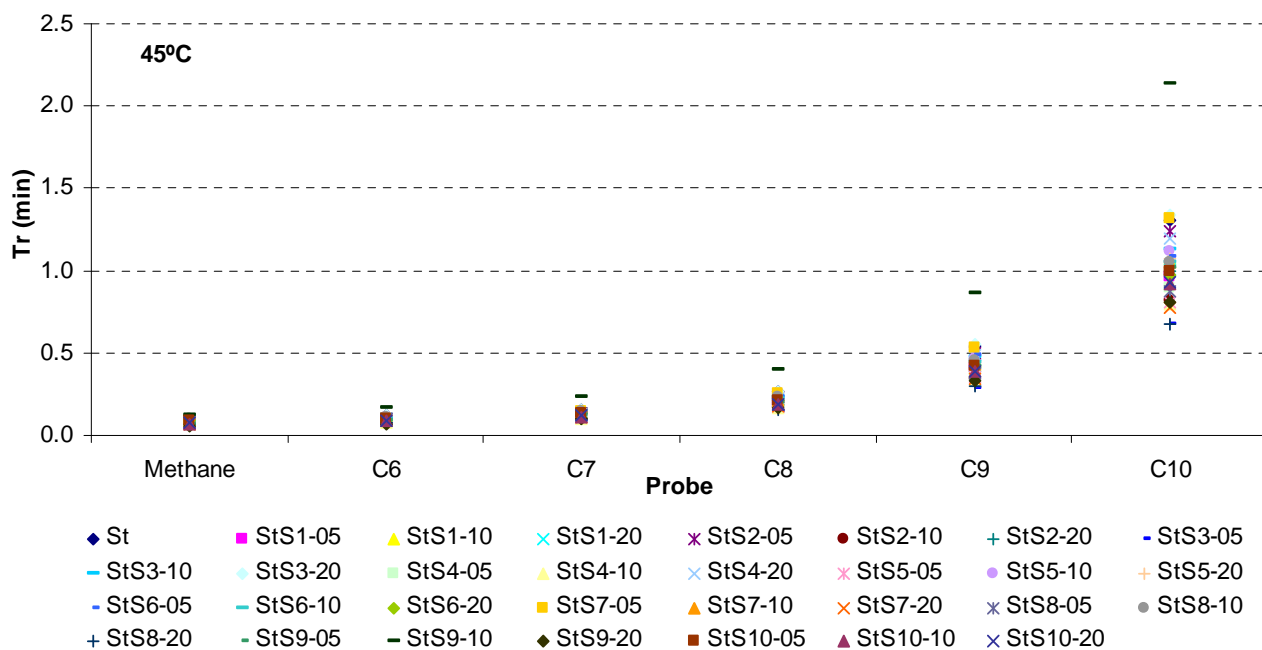


Figure F.3 – Retention times obtained at 40°C with the n-alkanes for the reference samples and the samples sized with each of the sizing agents at each of the incorporation percentages.

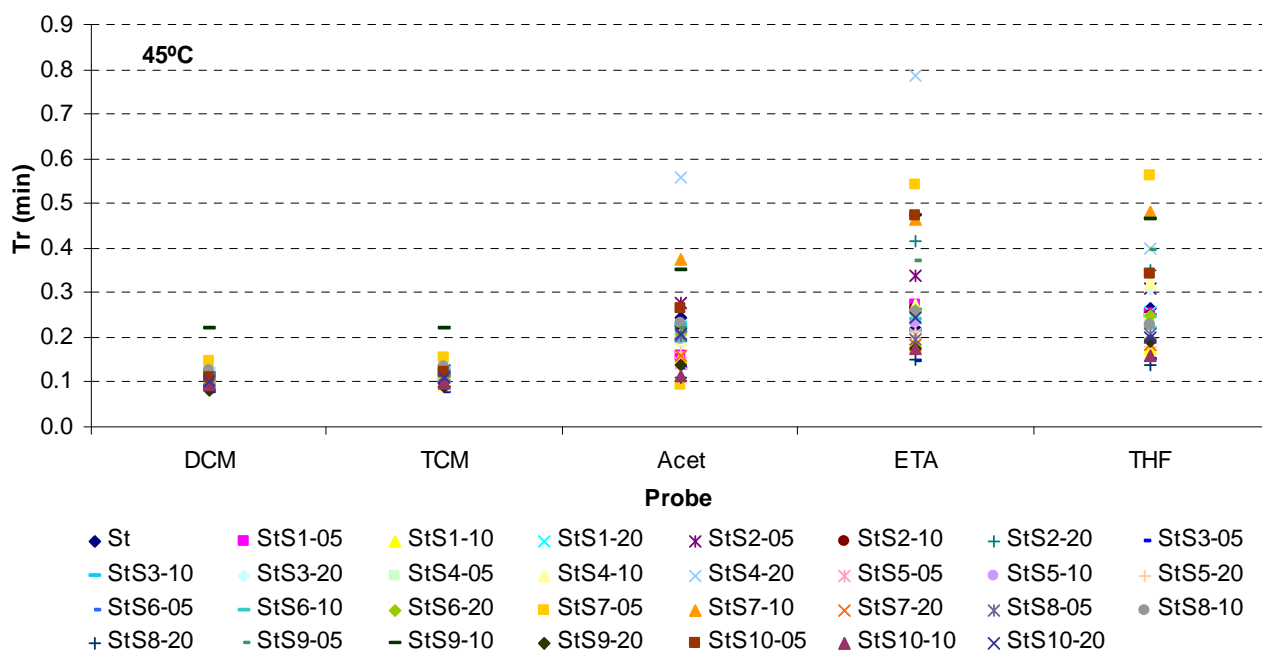


Figure F.4 – Retention times obtained at 40°C with the polar probes for the reference samples and the samples sized with each of the sizing agents at each of the incorporation percentages.

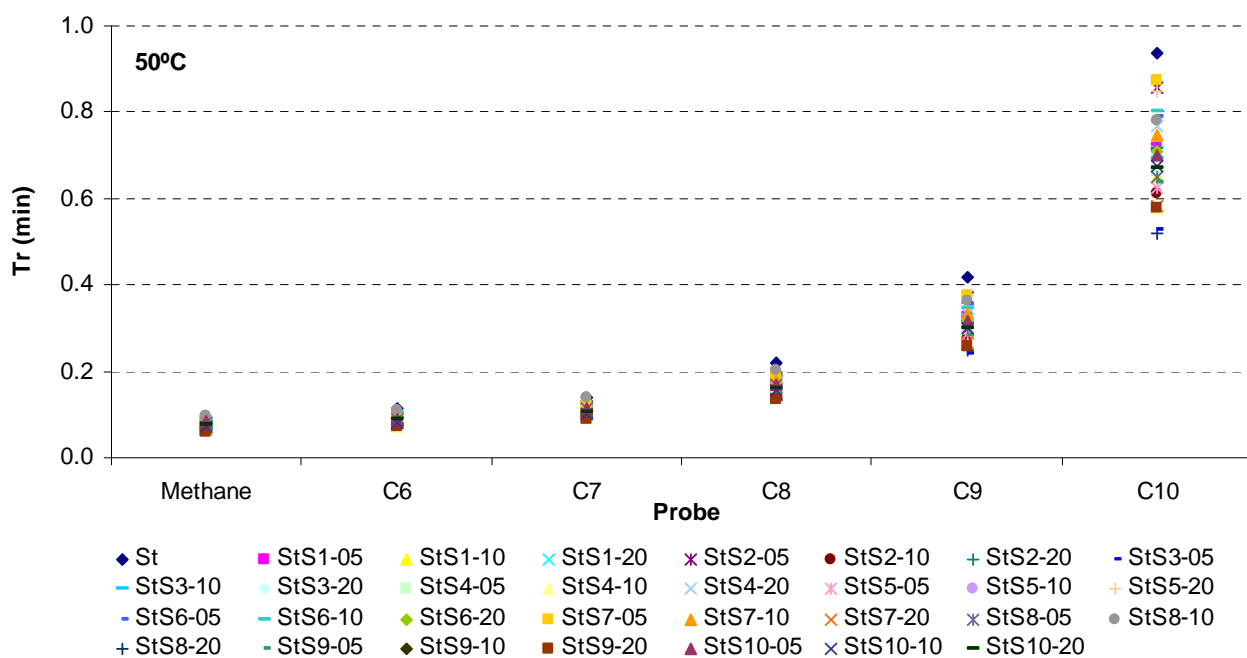


Figure F.5 – Retention times obtained at 40°C with the n-alkanes for the reference samples and the samples sized with each of the sizing agents at each of the incorporation percentages.

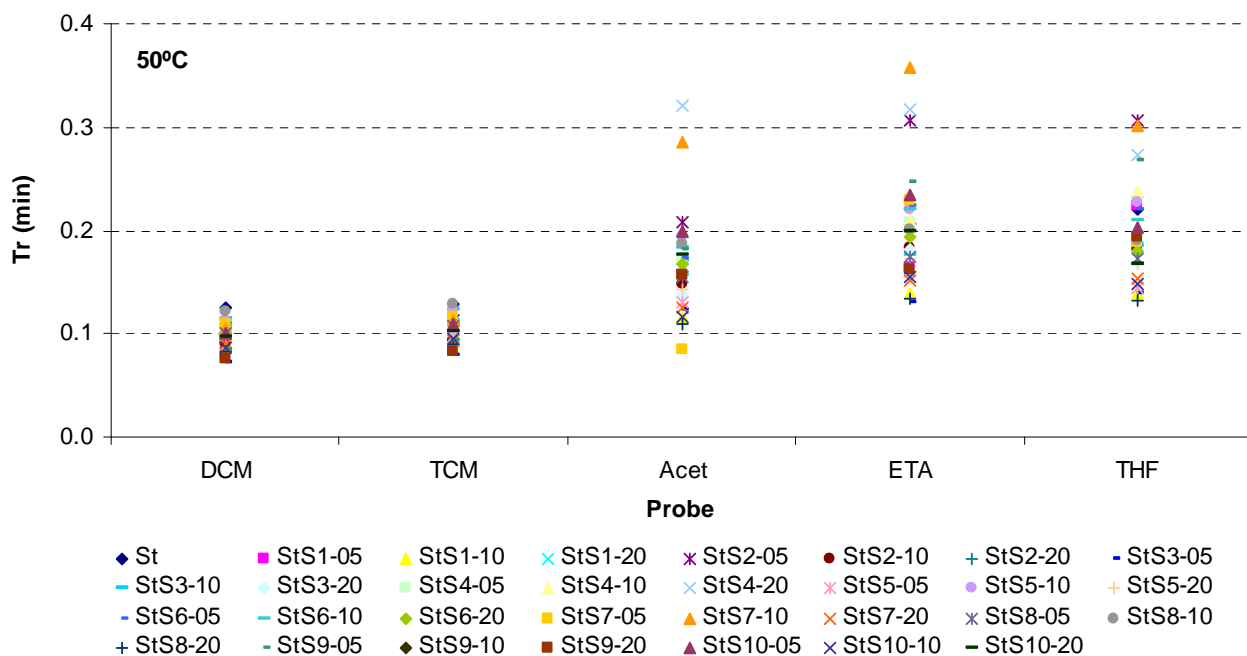


Figure F.6 – Retention times obtained at 40°C with the polar probes for the reference samples and the samples sized with each of the sizing agents at each of the incorporation percentages.

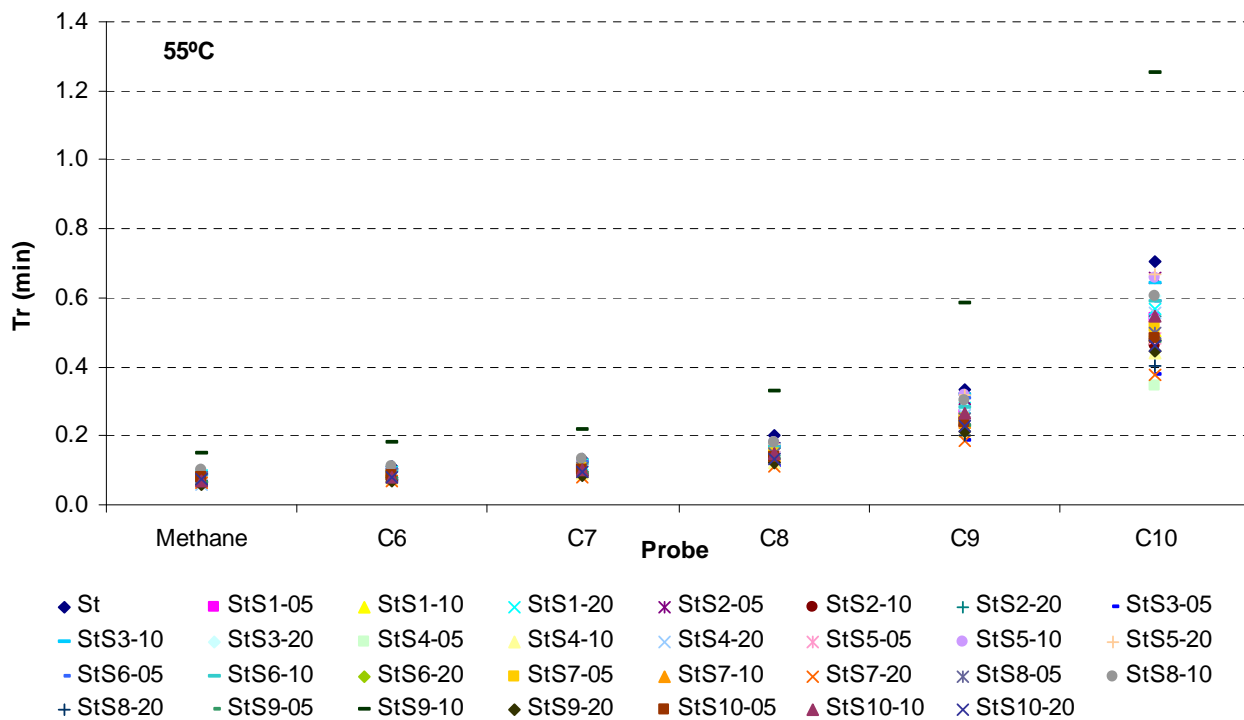


Figure F.7 – Retention times obtained at 40°C with the n-alkanes for the reference samples and the samples sized with each of the sizing agents at each of the incorporation percentages.

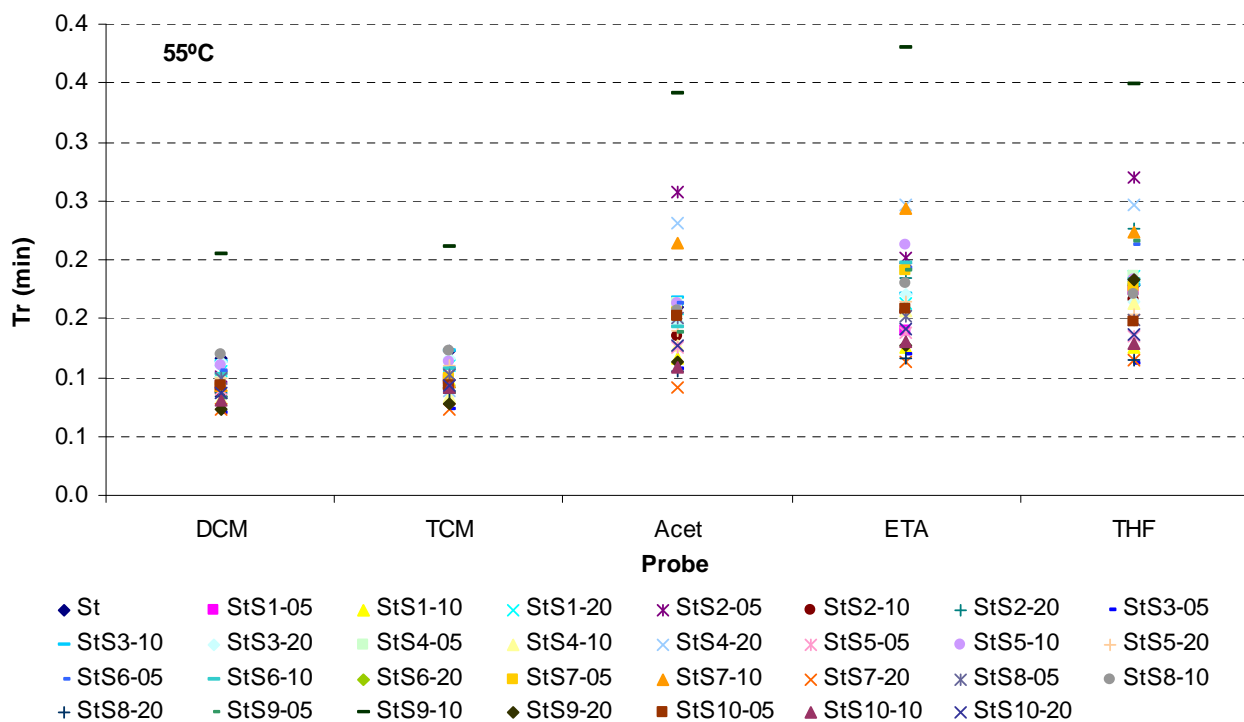


Figure F.8 – Retention times obtained at 40°C with the polar probes for the reference samples and the samples sized with each of the sizing agents at each of the incorporation percentages.

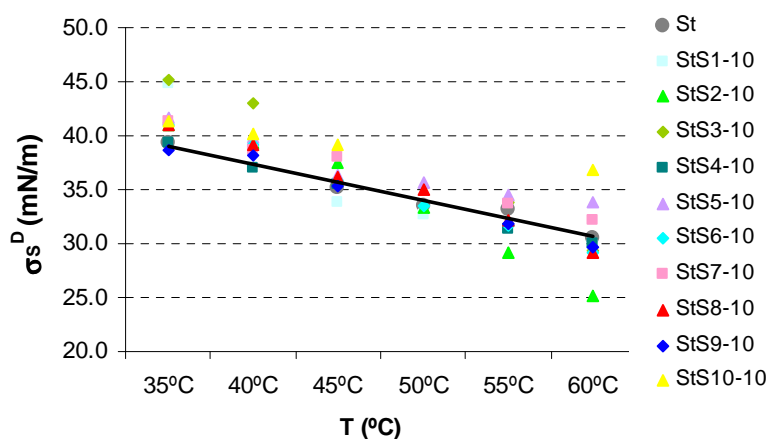


Figure F.9 - Influence of the temperature on the dispersive component of the surface free energy, for the samples sized with 10% incorporation of synthetic sizing agents (the straight line indicates the behavior of sample St).

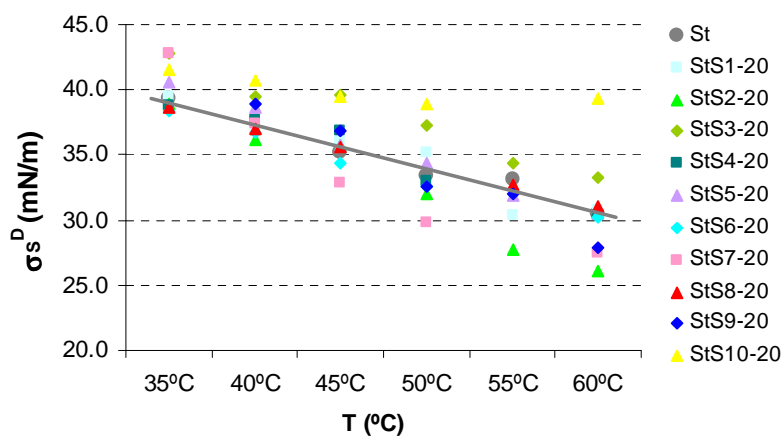


Figure F.10 - Influence of the temperature on the dispersive component of the surface free energy, for the samples sized with 20% incorporation of synthetic sizing agents (the straight line indicates the behavior of sample St).

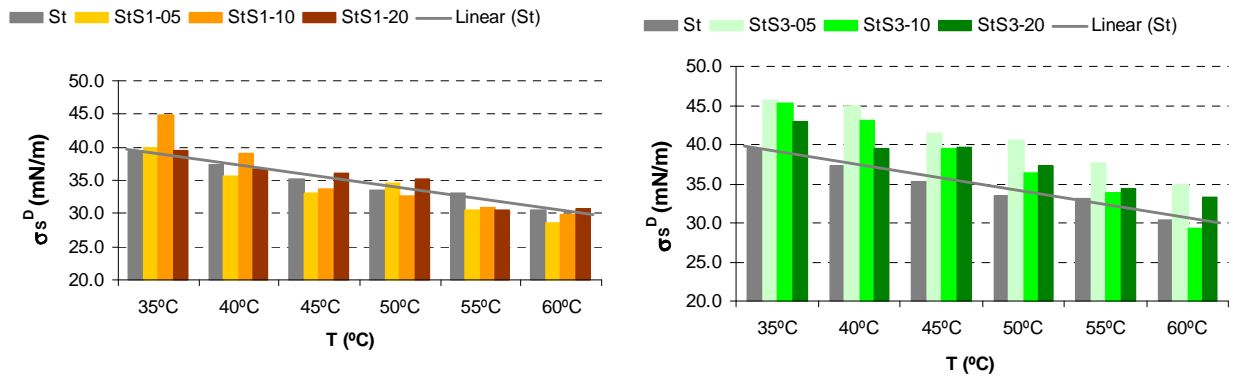


Figure F.11 - Variation of σ_s^D with concentration and temperature for the samples sized with the surface sizing agents S1 and S3 (St sample is also included, as reference).

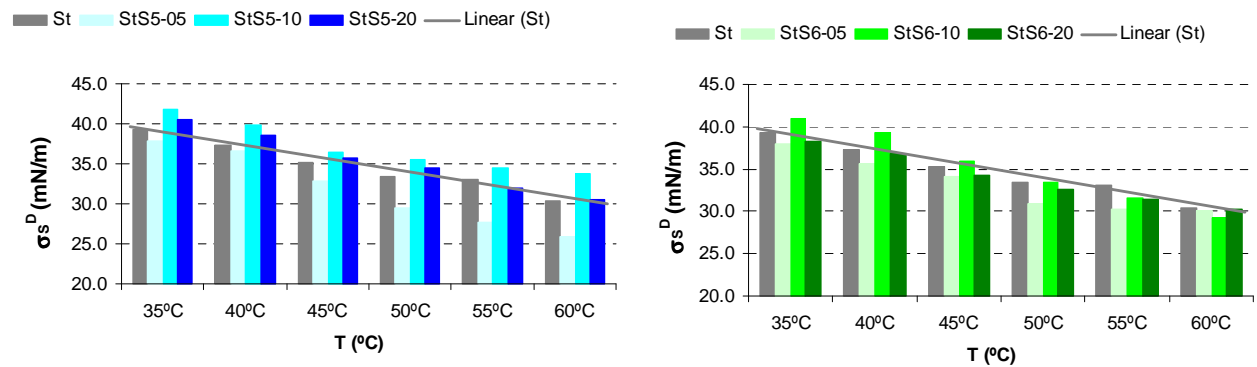


Figure F.12 - Variation of σ_s^D with concentration and temperature for the samples sized with the surface sizing agents S5 and S6 (St sample is also included, as reference).

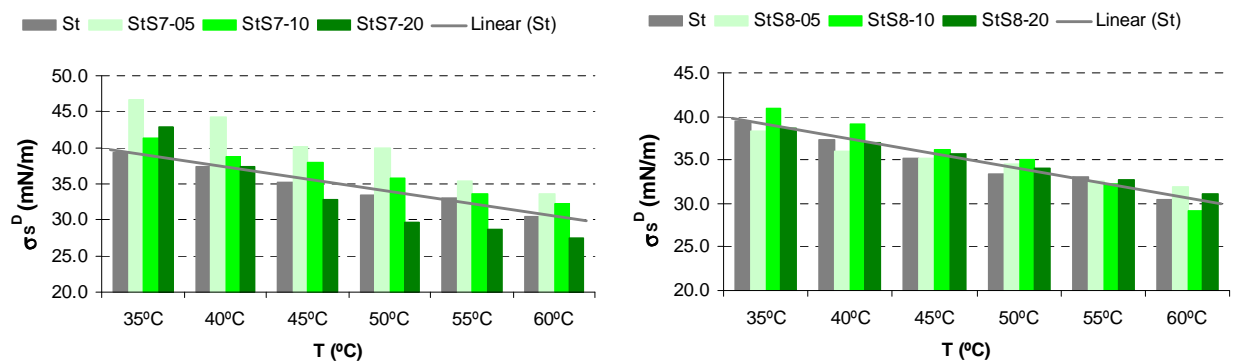


Figure F.13 - Variation of σ_s^D with concentration and temperature for the samples sized with the surface sizing agents S7 and S8 (St sample is also included, as reference).

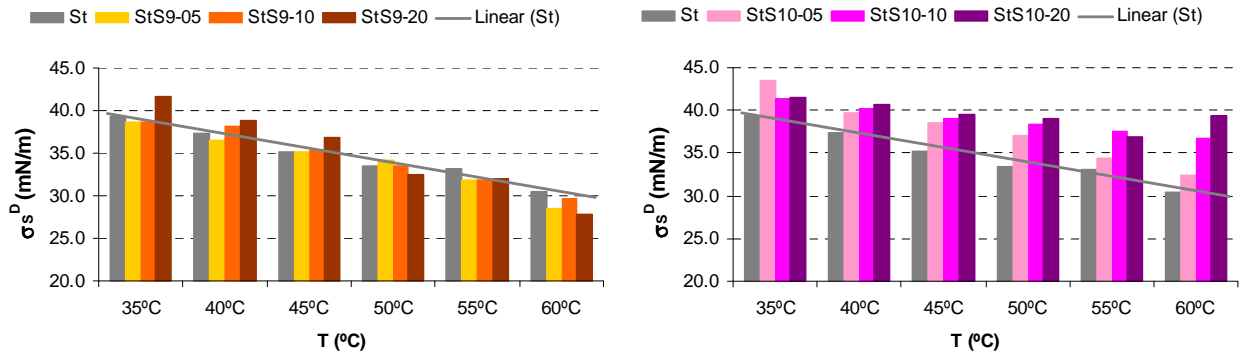


Figure F.14 - Variation of σ_s^D with concentration and temperature for the samples sized with the surface sizing agents S9 and S10 (St sample is also included, as reference).

Table F.8 – Values of σ_s^D obtained through the contact angle measurements and through the extrapolation of the correlations achieved from the IGC experiments.

Sample	σ_s^D	
	Contact Angle	IGC (Extrapolated for 21°C)
St	38.68	43.76
StS1-05	38.89	44.56
StS1-10	40.32	50.34
StS1-20	38.17	44.37
StS2-05	40.49	42.29
StS2-10	39.54	51.74
StS2-20	41.15	47.01
StS3-05	41.75	52.34
StS3-10	40.13	54.46
StS3-20	41.3	48.83
StS4-05	38.38	41.7
StS4-10	38.79	44.37
StS4-20	38.82	44.26
StS5-05	36.14	45.37
StS5-10	29.08	45.45
StS5-20	27.92	46.26
StS6-05	39.82	42.13
StS6-10	39.74	47.83
StS6-20	39.38	42.85
StS7-05	39.56	54.01
StS7-10	39.92	46.27
StS7-20	38.78	49.14
StS8-05	38.28	41.25
StS8-10	37.8	47.75
StS8-20	38.34	42.84
StS9-05	41.1	44.19
StS9-10	40.37	44.53
StS9-20	40.26	49.08
StS10-05	42.51	48.54
StS10-10	38.62	43.59
StS10-20	38.35	45.15

Table F.9 – K_a and K_b Values achieved for each of the 31 samples tested, and corresponding determination coefficient.

Sample	K_a	K_b	r^2
St	0.312	0.557	0.997
StS1-05	0.301	0.702	0.990
StS1-10	0.361	0.163	0.963
StS1-20	0.160	1.247	0.957
StS2-05	0.313	0.743	0.996
StS2-10	0.261	2.190	0.919
StS2-20	0.772	1.853	0.992
StS3-05	0.108	2.048	0.856
StS3-10	0.286	1.455	0.971
StS3-20	0.438	1.006	0.994
StS4-05	0.188	1.115	0.916
StS4-10	0.462	1.241	0.992
StS4-20	0.668	1.186	0.995
StS5-05	0.444	0.843	0.995
StS5-10	0.266	0.369	0.977
StS5-20	0.320	0.448	0.905
StS6-05	0.159	1.395	0.969
StS6-10	0.168	0.853	0.939
StS6-20	0.263	0.665	0.975
StS7-05	0.603	2.943	0.991
StS7-10	0.306	2.913	0.921
StS7-20	0.342	1.814	0,9701
StS8-05	0.315	0.189	0.990
StS8-10	0.235	1.245	0.983
StS8-20	0.188	0.245	0.982
StS9-05	0.596	1.239	0.991
StS9-10	0.344	1.252	0.995
StS9-20	0.454	0.564	0.990
StS10-05	0.515	1.854	0.907
StS10-10	0.131	1.140	0.940
StS10-20	0.169	0.754	0.979

APPENDIX G

PRINTING QUALITY PARAMETERS

Tabel G.1 - – Optical Density values for color Black, Cyan, Magenta and Yellow .colors, measured for each of the 31 samples produced.

Sample	Optical density			
	Black	Cyan	Magenta	Yellow
St	2.50 ± 0.054	1.17 ± 0.014	1.13 ± 0.014	1.03 ± 0.013
StS1-05	2.61 ± 0.030	1.19 ± 0.005	1.15 ± 0.009	1.04 ± 0.006
StS1-10	2.63 ± 0.048	1.19 ± 0.012	1.13 ± 0.012	1.02 ± 0.003
StS1-20	2.73 ± 0.011	1.18 ± 0.010	1.14 ± 0.011	1.03 ± 0.006
StS2-05	2.61 ± 0.018	1.19 ± 0.009	1.16 ± 0.005	1.05 ± 0.003
StS2-10	2.68 ± 0.021	1.20 ± 0.008	1.16 ± 0.013	1.05 ± 0.005
StS2-20	2.82 ± 0.011	1.16 ± 0.013	1.12 ± 0.005	0.99 ± 0.006
StS3-05	2.64 ± 0.013	1.18 ± 0.011	1.15 ± 0.012	1.01 ± 0.013
StS3-10	2.62 ± 0.023	1.16 ± 0.015	1.15 ± 0.010	1.05 ± 0.000
StS3-20	2.69 ± 0.032	1.18 ± 0.014	1.12 ± 0.003	0.99 ± 0.010
StS4-05	2.79 ± 0.015	1.11 ± 0.023	1.08 ± 0.018	0.99 ± 0.009
StS4-10	2.65 ± 0.038	1.26 ± 0.008	1.21 ± 0.013	1.08 ± 0.008
StS4-20	2.54 ± 0.026	1.22 ± 0.019	1.18 ± 0.012	1.06 ± 0.011
StS5-05	2.43 ± 0.023	1.17 ± 0.011	1.13 ± 0.012	1.04 ± 0.006
StS5-10	2.78 ± 0.035	1.14 ± 0.012	1.13 ± 0.011	1.01 ± 0.008
StS5-20	2.69 ± 0.019	1.12 ± 0.012	1.10 ± 0.003	1.01 ± 0.006
StS6-05	2.43 ± 0.034	1.19 ± 0.003	1.14 ± 0.008	1.04 ± 0.009
StS6-10	2.79 ± 0.028	1.13 ± 0.019	1.10 ± 0.029	0.95 ± 0.014
StS6-20	2.81 ± 0.024	1.16 ± 0.013	1.12 ± 0.013	0.97 ± 0.009
StS7-05	2.48 ± 0.051	1.20 ± 0.014	1.15 ± 0.003	1.04 ± 0.011
StS7-10	2.69 ± 0.025	1.20 ± 0.015	1.14 ± 0.019	1.02 ± 0.006
StS7-20	2.65 ± 0.038	1.17 ± 0.012	1.12 ± 0.010	0.98 ± 0.008
StS8-05	2.57 ± 0.034	1.11 ± 0.028	1.10 ± 0.011	1.01 ± 0.013
StS8-10	2.60 ± 0.024	1.11 ± 0.005	1.10 ± 0.008	1.00 ± 0.006
StS8-20	2.73 ± 0.032	1.19 ± 0.008	1.12 ± 0.006	1.00 ± 0.006
StS9-05	2.60 ± 0.013	1.19 ± 0.006	1.16 ± 0.013	1.06 ± 0.009
StS9-10	2.59 ± 0.019	1.15 ± 0.008	1.12 ± 0.011	1.02 ± 0.012
StS9-20	2.67 ± 0.030	1.19 ± 0.008	1.16 ± 0.014	1.04 ± 0.006
StS10-05	2.74 ± 0.035	1.11 ± 0.015	1.10 ± 0.015	0.95 ± 0.018
StS10-10	2.62 ± 0.022	1.18 ± 0.011	1.16 ± 0.009	1.04 ± 0.006
StS10-20	2.67 ± 0.026	1.15 ± 0.005	1.11 ± 0.009	1.01 ± 0.008

Tabel G. 2 – Gamut Area and Line quality parameters obtained for each of the 31 samples produced.

Sample	Gamut Area	Line Quality		
		Plain (mm ²)	Borderlength (mm)	Roughness
St	7569.45 ± 91.54	5.54 ± 0.015	9.46 ± 0.27	0.06 ± 0.002
StS1-05	7563.77 ± 72.55	5.52 ± 0.019	9.64 ± 0.34	0.06 ± 0.009
StS1-10	7485.95 ± 103.11	5.50 ± 0.005	9.60 ± 0.10	0.06 ± 0.004
StS1-20	7550.32 ± 196.96	5.50 ± 0.014	9.54 ± 0.14	0.06 ± 0.006
StS2-05	7746.98 ± 147.27	5.53 ± 0.004	9.87 ± 0.29	0.06 ± 0.001
StS2-10	7723.42 ± 126.13	5.54 ± 0.001	9.79 ± 0.17	0.07 ± 0.005
StS2-20	6926.56 ± 113.30	5.55 ± 0.007	10.23 ± 0.08	0.07 ± 0.003
StS3-05	6834.42 ± 1065.50	5.62 ± 0.015	10.24 ± 0.06	0.07 ± 0.002
StS3-10	7791.64 ± 45.95	5.56 ± 0.003	9.52 ± 0.24	0.06 ± 0.002
StS3-20	7966.59 ± 409.83	5.53 ± 0.014	9.41 ± 0.79	0.06 ± 0.017
StS4-05	6634.12 ± 97.61	5.57 ± 0.010	10.21 ± 0.07	0.07 ± 0.001
StS4-10	7769.95 ± 119.77	5.58 ± 0.004	9.62 ± 0.17	0.06 ± 0.001
StS4-20	7484.79 ± 163.47	5.56 ± 0.005	9.80 ± 0.11	0.06 ± 0.005
StS5-05	7598.57 ± 20.64	5.49 ± 0.018	9.79 ± 0.36	0.07 ± 0.002
StS5-10	6913.01 ± 199.41	5.54 ± 0.018	10.17 ± 0.05	0.07 ± 0.005
StS5-20	6658.75 ± 20.53	5.55 ± 0.016	10.25 ± 0.14	0.07 ± 0.004
StS6-05	7580.85 ± 301.86	5.52 ± 0.011	9.72 ± 0.21	0.07 ± 0.008
StS6-10	7322.57 ± 602.76	5.51 ± 0.014	9.14 ± 0.42	0.05 ± 0.008
StS6-20	7548.51 ± 799.04	5.52 ± 0.013	8.89 ± 0.60	0.05 ± 0.004
StS7-05	7600.97 ± 29.75	5.52 ± 0.018	9.98 ± 0.21	0.07 ± 0.005
StS7-10	7053.12 ± 909.00	5.53 ± 0.038	9.59 ± 0.19	0.06 ± 0.008
StS7-20	7902.79 ± 243.08	5.55 ± 0.003	9.14 ± 0.48	0.06 ± 0.003
StS8-05	7503.76 ± 104.82	5.48 ± 0.020	9.51 ± 0.33	0.05 ± 0.009
StS8-10	7493.00 ± 337.20	5.49 ± 0.017	9.60 ± 0.32	0.06 ± 0.013
StS8-20	7851.94 ± 360.46	5.51 ± 0.004	9.43 ± 0.50	0.05 ± 0.012
StS9-05	7660.04 ± 30.62	5.50 ± 0.023	9.45 ± 0.04	0.06 ± 0.003
StS9-10	7498.09 ± 14.66	5.50 ± 0.003	9.74 ± 0.34	0.06 ± 0.001
StS9-20	7408.69 ± 214.86	5.57 ± 0.011	9.90 ± 0.14	0.07 ± 0.001
StS10-05	6159.29 ± 61.76	5.58 ± 0.015	10.36 ± 0.15	0.07 ± 0.010
StS10-10	7604.18 ± 222.20	5.52 ± 0.018	9.97 ± 0.70	0.07 ± 0.008
StS10-20	7321.36 ± 167.33	5.50 ± 0.006	9.70 ± 0.24	0.06 ± 0.004

